Fakultät für Medizin

Abteilung für diagnostische und interventionelle Neuroradiologie

Graded degeneration of cortical networks and medial temporal lobe dysconnectivity: Brain network dysfunctions in Alzheimer's disease

Lorenzo Pasquini

Vollständiger Abdruck der von der Fakultät für Medizin der Technischen Universität München zur Erlangung des akademischen Grades eines

Doctor of Philosophy (Ph.D.)

genehmigten Dissertation.

Vorsitzende/r: Univ.-Prof. Dr. Arthur Konnerth

Betreuer/in: Univ.-Prof. Dr. Claus Zimmer

Prüfer der Dissertation:

1. Univ.-Prof. Dr. Johann Förstl
2. Priv.-Doz. Dr. Markus Ploner
3. Univ.-Prof. Dr. Michael Ewers

Die Dissertation wurde am 06.06.2016 bei der Fakultät für Medizin der Technischen Universität München eingereicht und durch die Fakultät für Medizin am 07.09.2016 angenommen.

Acknowledgements

To begin, I would like to express my gratitude to my supervisors Prof. Dr. Claus Zimmer and Dr. Christian Sorg for their guidance, patience and encouragement throughout these intense years of my PhD. In particular, I would like to thank Christian for his passion and trust, for the freedom granted, and for the never ending discussions. Beside my advisors, I would also like to thank the TUM Medical Graduate Center for the outstanding support and teaching, and my mentors Prof. Dr. Hans Förstl and Prof. Dr. Stefan Förster for their insightful comments and encouragement. Moreover, I wish to express my sincere gratitude to the German Academic Foundation (Studienstiftung des deutschen Volkes), for the generous support and outstanding exchange opportunities during the last two years of my PhD.

A special thanks and a big hug goes to my colleagues and friends at the TUM-NIC for the stimulating collaborations and the amazing time outside research. I would also like to thank the participants and patients of the studies, the clinical staff and technical assistants that made the research projects of my Thesis possible.

Last but not least, my gratitude goes to my family and beloved ones: my parents, siblings, to “nur hayeti” and friends, for their love and for being part of my life.

P. Ovidi Nasonis Metamorphoseon libri quindecim

Liber sextus – Arachne

‘Mentis inops longaque venis confecta senecta,

et nimium vixisse diu nocet. audiat istas,

si qua tibi nurus est, si qua est tibi filia, voces.

consilii satis est in me mihi, neve monendo

profecisse putes, eadem est sententia nobis.

cur non ipsa venit? cur haec certamina vitat?’

tum dea ‘venit!’ ait formamque removit anilem

Palladaque exhibuit.

To “Nonna Tina” - In beloved memory of my grandmother

INDEX

List of publications included in the Thesis

Following four articles are part of the Thesis.

List of publications, reprinted with permission from:

1. Myers N, **Pasquini L**, Gottler J, Grimmer T, Koch K, Ortner M, Neitzel J, Muhlau M, Forster S, Kurz A, Forstl H, Zimmer C, Wohlschlager AM, Riedl V, Drzezga A, Sorg C (2014) Within-patient correspondence of amyloid-beta and intrinsic network connectivity in Alzheimer's disease. Brain 137, 2052-2064.
2. **Pasquini L**, Scherr M, Tahmasian M, Meng C, Myers NE, Ortner M, Muhlau M, Kurz A, Forstl H, Zimmer C, Grimmer T, Wohlschlager AM, Riedl V, Sorg C (2014) Link between hippocampus' raised local and eased global intrinsic connectivity in AD. Alzheimer's and Dementia 11, 475-484.
3. Tahmasian M, **Pasquini L**, Scherr M, Meng C, Förster S, Mulej Bratec S, Shi K, Yakushev I, Schwaiger M, Grimmer T, Diehl-Schmid J, Rield V, Sorg C, Drzezga A (2015) The lower hippocampus global connectivity, the higher its local metabolism in Alzheimer's disease. Neurology 84, 1956-1963.
4. **Pasquini L**, Scherr M, Tahmasian M, Myers N, Ortner M, Kurz A, Förstl H, Zimmer C, Grimmer T, Akhrif A, Wohlschläger AM, Riedl V, Sorg C (2016) Increased intrinsic activity of medial-temporal lobe subregions is associated with decreased cortical thickness of medial-parietal areas in patients with Alzheimer's disease dementia. Journal of Alzheimer's Disease.

ABSTRACT

Neurodegenerative diseases target intrinsic functional connectivity (iFC) brain networks. The default mode network (DMN) is particularly targeted in Alzheimer's disease (AD), where dementia is preceded by amyloid-β pathology, tau pathology and atrophy of the medial temporal lobes (MTL). Here, I investigated two distinct aspects of brain network dysfunction, particularly affecting the DMN, in AD: *(i)* amyloid-β-associated graded degeneration of cortical networks and *(ii)* MTL dysconnectivity-associated MTL hyperactivity. In order to map structural, functional and molecular correlates of brain network dysfunction, I used multi-modal neuroimaging data from considerable cross-sectional samples of cognitively healthy subjects and patients across stages of the AD continuum.

Amyloid-β associated graded degeneration of cortical networks was investigated via amyloid-β and intrinsic brain network imaging of patients with mild cognitive impairment and cognitively healthy subjects. Within-subject voxel-wise correlations were used to derive measures for global and local correspondence between amyloid-β load and iFC. In patients, we found a positive global correspondence between amyloid-β pathology and iFC. This global correspondence was highest in the DMN and gradually decreased in other cognitive and primary sensory networks. At the local level, patients showed a negative correspondence between amyloid-β pathology and iFC, particularly within high connectivity nodes of heteromodal intrinsic brain networks. Gradual global correspondence across distinct brain networks, suggests that amyloid-β accumulates from connectivity nodes of the DMN to the periphery and to other brain networks, with gradients in iFC being the driving force of the pathophysiological process. The local negative correspondence within connectivity nodes of distinct brain networks, suggests a detrimental effect of amyloid-β pathology on circuit activity of neuronal assemblies as shown in animal models of AD.

The association between MTL dysconnectivity and MTL hyperactivity at rest, was explored via imaging of glucose metabolism, intrinsic activity and brain structure across stages of the AD continuum. First findings revealed progressively increased local iFC within the hippocampus in patients. Increased local iFC within the hippocampus correlated with global functional dysconnectivity of the hippocampus within the DMN and impaired memory. These findings were extended by further results, in which patients showed reduced iFC between the hippocampus and the precuneus, two major connectivity nodes of the DMN. Critically, in patients with AD, hippocampus-precuneus iFC negatively correlated with hippocampal glucose metabolism. Finally, I explored whether these findings of AD-related MTL hyperactivity at rest affect distinct MTL subregions, and whether MTL hyperactivity is linked with structural degeneration of medial parietal connectivity nodes of the DMN. Intrinsic activity of several MTL subregions was increased in AD and correlated with structural atrophy of medial parietal connectivity nodes of the DMN as the precuneus and posterior cingulate. More precisely, hyperactivity at rest negatively correlated with ipsilateral cortical degeneration and with impaired cognitive performance. Overall, these findings support a mechanistic link between MTL hyperactivity in patients and both functional and structural dysconnectivity of the MTL from medial parietal connectivity nodes of the DMN. The association between MTL hyperactivity at rest, MTL dysconnectivity, and impaired cognitive performance supports a dysfunctional nature of aberrant MTL hyperactivity.

In conclusion, the findings presented in this Thesis contribute to a deeper understanding of large-scale brain network dysfunction in AD, and suggest a link between amyloid-β pathology, MTL dysconnectivity and aberrant MTL hyperactivity in AD. Interventions targeting network degradation and MTL hyperactivity, may hold the key to improve life quality of patients and prevent degenerative processes already at preclinical disease stages.

KEYWORDS

Alzheimer's disease, amyloid-β, default mode network, dysconnectivity, clinical neuroimaging, intrinsic brain activity, intrinsic functional connectivity, medial temporal lobe, mild cognitive impairment, network degeneration.

LIST OF ABBREVIATIONS

AD = Alzheimer's disease

BOLD = blood-oxygenation-level-dependent signal

CA = cornu ammonis

DG = dentate gyrus

DMN = default mode network

DTI = diffusion tensor imaging

FDG = 18F-fluorodeoxyglucose

IBN = intrinsic brain networks

IFC = intrinsic functional connectivity

FMRI = functional magnetic resonance imaging

MCI = mild cognitive impairment

MRI = magnetic resonance imaging

MTL = medial temporal lobe

PET = positron emission tomography

PIB = Pittsburgh Compound-B

Rs-fMRI = resting-state functional magnetic resonance imaging

1. Introduction

1.1. Motivation and content of the Thesis

With the demographical and epidemiological transition of the last century, Alzheimer's disease (AD) has acquired enormous interest among researchers and the public community. The increasing AD prevalence worldwide and the associated emotional and economic costs for families and health care systems (1) have highlighted the need for a better understanding of the neurodegenerative processes involved, in order to develop new preventative measures and innovative biomarkers aimed at tackling this devastating disease. In particular, recent works provide strong support for a brain network-based degenerative process in AD. This thesis explores two aspects of brain network dysfunction in AD: *(i)* amyloid-β-associated graded degeneration of cortical networks and *(ii)* medial temporal lobe (MTL) dysconnectivity-associated MTL hyperactivity.

1.2. Alzheimer's disease: General background

AD is a neurodegenerative disease characterized by neuropathological depositions of amyloid-β plaques and neurofibrillary tangles (introduced more in detail later on) and clinically by progressive dementia and behavioral deficits (2). Dementia syndromes are characterized by specific patterns of cognitive deficits, preventing the patient to live independently. The symptomatic hallmark of AD is the increasing impairment of declarative memory, particularly of episodic and semantic memory (1). Further cognitive deficits of AD include progressive impairments of executive functions, attention, and planning. Behavioral deficits include affective syndromes such as depressive or anxiety-related syndromes, states of confusion, and changes of impulsivity, sleep, circadian rhythms, and vegetative functions (1).

Current AD treatments aim to decrease the severity of symptoms and cognitive decline. Treatments include medicaments such as cholinesterase inhibitors and regulators of glutamatergic activity (N-methyl-D-Aspartate receptor antagonists), as well as psychosocial interventions including cognitive, emotional and behavioral therapies. No curative approach is currently available, albeit novel therapeutical strategies aim at stopping the neurodegenerative process, while promising clinical trials are testing the efficacy of new medicaments targeting neuroinflammatory processes, amyloid-β immunization and network dysfunction (3,4). AD research has identified both genetic risk factors as the *APOE* gene and modifiable risk factors. Findings suggest that primary prevention should involve interventions that increase cognitive reserve and target risk factors for vascular disease, including diabetes, midlife hypertension, midlife obesity, smoking, and physical inactivity (5).

1.2.1. Epidemiology of dementia and Alzheimer's disease

AD is the most frequent neurodegenerative disorder and the most common form of dementia, accounting for 50-60% of all cases (2). In individuals aged 60-64 years, the prevalence of dementia is below 1%, but shows an almost exponential increase with age: in people aged 85 years or more, the prevalence rises up to 24-33% in the Western world (6). Changing demographics due to population aging and the ongoing epidemiological transition pose dementia as a major public health issue in several low and middle income countries, with similar or even higher estimates for dementia prevalence as compared to high income countries (6). Recent estimates by the World Health Organization expect the number of patients with dementia worldwide to reach 115 million by 2050 (5).

In terms of economic burden, the total estimated worldwide costs of dementia were US$ 604 billion in 2010. In high-income countries, informal care (45%) and formal social care (40%) account for the majority of costs, while the proportionate contribution of direct medical costs (15%) is much lower. In low and middle income countries, direct social care costs are small; the majority of costs are predominated by informal care costs (i.e. unpaid care provided by families) (5).

In conclusion, AD accounts for most cases of dementia and presents a huge burden of disease worldwide in terms of disease prevalence, disease incidence, care dependence and mortality. AD is characterized by a high economic and emotional impact on families, caregivers and communities. Patients and familiars have to face stigma and social exclusion, particularly in low resource settings. A better understanding of the pathophysiological mechanisms underpinning this disease is critical to successfully tackle this world-wide epidemic.

1.2.2. The continuum of Alzheimer's disease

AD reflects the end stage of a continuum of biological and clinical phenomena (7). Longitudinal data including imaging and biofluid markers of AD, suggest that neuropathological changes occur several years before first cognitive symptoms arise and are detectable in cognitively healthy subjects, which are hence at a preclinical stage of AD and bear a higher risk of developing AD dementia later on (8). A clinical group at higher risk of developing AD are patients with mild cognitive impairment (MCI). MCI is a syndrome defined as cognitive decline greater than expected for an individual's age and education level but that does not interfere notably with activities of daily life (9). Prevalence ranges from 3% to 19% in adults older than 65 years and more than half progress to dementia within 5 years. In particular, the amnestic subtype has a high risk of

progression to AD and could constitute a prodromal AD stage particularly in presence of AD typical biomarkers (9,10).

DSM-IV criteria for diagnosis of AD include gradual onset and continuing decline of impairments in social and occupational functioning; impairments in memory and other cognitive domains; and exclusion of other psychiatric, neurological or systemic disease causing cognitive deficits (11). More precise classification criteria for AD have been developed by the National Institute of Neurological and Communicative Disorders and Stroke and the Alzheimer's Disease and Related Disorders Association (NINCDS-ADRDA) and include diverse criterion, varying from neuroimaging and biofluid markers to cognitive symptoms, allowing for a more accurate diagnosis of AD.

(i) Probable AD dementia: Criteria for dementia - including cognitive symptoms and disruption of daily life functions - are met, and information from neuroimaging or cerebral-spinal-fluid biomarkers is unavailable or positive. For a probable AD diagnosis, certainty is increased by evidence of either amyloid-β deposition (detected though neuroimaging or biofluid markers of amyloid-β pathology) or neuronal injury (biofluid markers of tangles pathology, neuroimaging of glucose metabolism, or structural neuroimaging).

(ii) Possible AD dementia: Patients show an atypical clinical course but both types of biomarkers are present (i.e. amyloid-β deposition and neuronal injury).

(iii) Dementia unlikely due to Alzheimer's disease: Patients show atypical clinical syndromes for AD or an alternative diagnosis is available. Both biomarkers for amyloid-β deposition and neuronal injury are negative (12).

Psychiatric interviews and neuroimaging are used to differentiate probable AD and other forms of dementia (as vascular dementia or Lewy-body dementia). However, *post-mortem* histopathology is still considered the golden diagnostic standard. Please refer to Box 1 for a short summary of used clinical terms throughout the Thesis.

Box 1. The continuum of AD.

- **Preclinical AD:** cognitively healthy subjects with presence of AD biomarkers.
- **MCI:** cognitive decline greater than expected for an individual's age and education level but that does not interfere notably with activities of daily life. The **amnestic subtype** has a high risk of progression to AD and could constitute a **prodromal AD** stage particularly in presence of AD typical biomarkers.
- **Probable AD dementia:** Cognitive symptoms of **AD-dementia** are met; certainty is increased by presence of AD biomarkers. Patients with **AD** and **AD-dementia** are recurrent terms used to designate this group.

1.2.3. Pathological hallmarks of Alzheimer's disease

Histopathological hallmarks of AD are amyloid-β plaques and neurofibrillary tangles (2), with recent evidence indicating that both deposits appear several years before first cognitive symptoms arise (13) and spread in the brain following a specific spatial-temporal pattern (14,15). The overwhelming presence of both deposits in AD has led to the formulation of the *"amyloid cascade hypothesis"* and the *"tau hypothesis"* of AD, with both hypotheses assigning a pivotal role to the respective protein in disease pathogenesis.

(I) Amyloid-β plaques:

Plaques are extracellular filaments composed mainly of amyloid-β fragments. Amyloid-β is a protein composed by 40-42 amino acids and is generated by the proteolytic cleavage of the much larger amyloid precursor protein, a trans-membrane protein of uncertain function (16). The enzymes β- and γ-secretase are responsible for the extracellular N and the trans-membrane C termini of the amyloid precursor protein, while a third enzyme α-secretase is responsible for the cleavage (16). Mutations of the amyloid precursor protein gene (on Chromosome 21) and of genes involved in the expression of the secretase as the presenilin gene family have been linked to the accumulation of amyloid-β and play a significant role in the development of familial AD.

Amyloid-β plaques deposition follows a specific spatial-temporal pattern with initial deposits observed in basal portions of the isocortex several decades before first symptoms arise (14,15). Along stages of AD, amyloid-β pathology spreads to the rest of the isocortex and to limbic areas, finally targeting subcortical areas and the brainstem at very advanced stages of the disease (15). The overwhelming presence of amyloid-β along AD progression has led to the formulation of the "*amyloid cascade hypothesis"* (17), which postulates that an aberrant clearance of amyloid-β is essential for the neurodegenerative process occurring in AD. However, it is unclear which mechanism underlie aberrant clearance of amyloid-β and the eventual plaques deposition.

Intriguingly, an intimate relationship has been observed between amyloid-β and neuronal activity, with amyloid-β influencing neuronal activity and vice-versa. On the one hand, amyloid-β has been shown to affect transmitter release and neuronal structures such as spines and synapses that are critically involved in neuronal signaling (4). Moreover, in the mouse model, amyloid-β has been shown to induce neuronal dysfunction by both silencing and hyper-activating set of neurons

and by impairing long term potentiation (4,18–20), the main electrophysiological signal underpinning memory consolidation. This finding suggests that amyloid-β might accelerate excitotoxicity through excessive or aberrant neuronal firing (4). On the other hand, production of amyloid-β has been observed after sustained activity of neurons and after neuronal stimulation (18). These findings are in line with those in human brain imaging, showing that amyloid-β plaque deposition is most prominent in a set of brain regions showing elevated metabolic activity and aerobic glycolysis, supporting a relationship between patterns of neuronal activity throughout life and the topography of amyloid-β deposition in AD (18).

(II) Neurofibrillary tangles:

Neurofibrillary tangles are composed by intracellular hyperphosphorylated tau proteins, which affect microtubule organization and hence cellular transport. Tau also spreads anatomically in an orderly fashion that is frequently denoted with the ordinal staging scheme proposed by Braak and colleagues (19). The earliest of these stages (Braak Stages I–II) occurs in 80% of all individuals by age 60 (20). This early distribution of tau occurring in the transentorhinal cortex of the MTLs likely precedes the emergence of fibrillar amyloid-β burden. In those individuals who are on the pathological trajectory of AD, this initial distribution is propagated to include limbic and neighboring temporal neocortex (Braak III–IV and higher), a propagation that is thought to mark the transition from asymptomatic to symptomatic pathology (20–22). The underlying biological evolution of tau pathology is not completely understood, but recent work in transgenic animals suggests that tau may propagate transynaptically (23,24), and that the widespread cortical pattern of tau spreading may be influenced by connectivity (25). However, there is also evidence of tau spreading via diffusion to more proximal locations, such as the adjacent inferior temporal cortices,

as described by Braak (19) and of early tau deposition in subcortical brain stem nuclei as the nuclei raphe (26). Strikingly, tau accumulation leads to synaptic dysfunction, glial activation, and eventually neuronal loss. Tau pathology is far better associated with age-at-onset and cognitive decline than amyloid-β accumulation (27). However, tau has been suggested to be part of the normal aging process, exacerbated by the rise of amyloid-β pathology in AD (8,28,29). Recent models of AD pathophysiology, suggest that amyloid-β increases the accumulation of tau aggregates and in particular accelerates the spread of tau out of the MTL into the neocortex through local diffusion and perhaps via transynaptic spread across neural networks, leading to neurodegeneration and eventually cognitive decline (see Figure 1) (8,29).

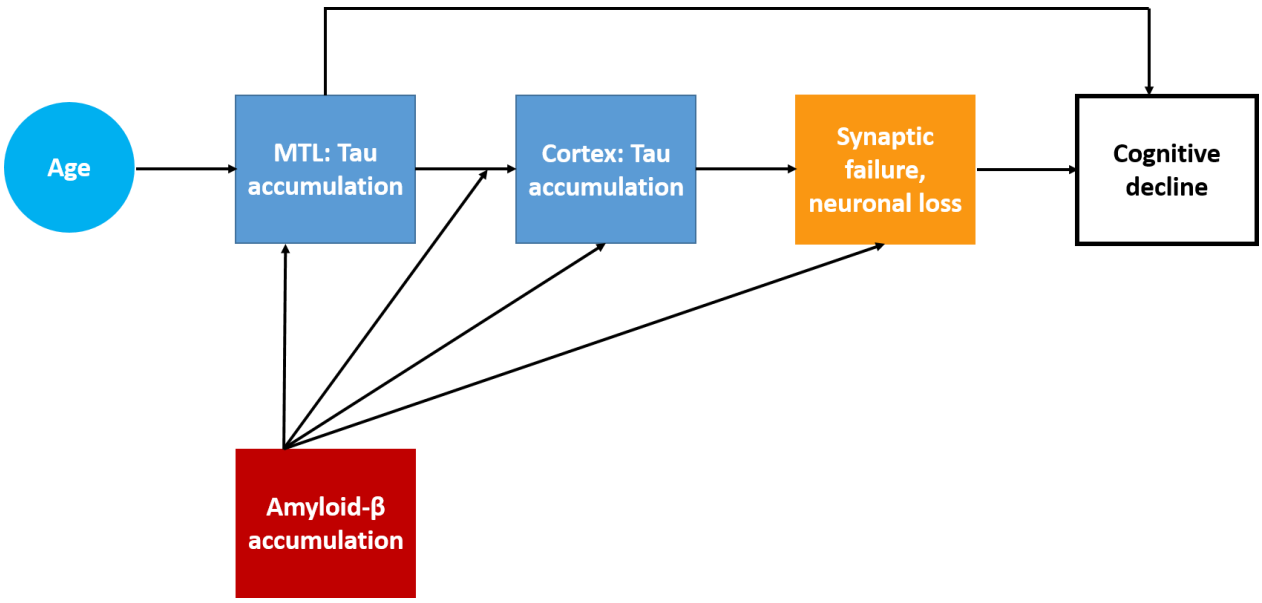

Figure 1. Amyloid-β facilitates MTL tau pathology and its cortical spread. MTL tau pathology is age related. MTL = medial temporal lobe. Modified from Sorg and Grothe, 2015.

1.3. Clinical neuroimaging in Alzheimer's disease

The advent of new powerful imaging technologies has recently empowered the research community to unravel the structure and function of the human brain *in-vivo* and to disentangle pathological mechanisms in several diseases including AD. The following section will shortly introduce clinical neuroimaging techniques, the associated underlying physiological brain signal and focus on relevant findings in AD. For a short summary of the techniques and related terms used throughout the Thesis please refer to Box 2.

(I) Positron emission tomography:

Positron emission tomography (PET) is a molecular imaging technique based on the detection of pairs of gamma rays emitted indirectly by a positron-emitting radionuclide tracer, which is introduced into the body on a biologically active molecule. Current use of PET-tracers in both research and medical praxis include imaging of amyloid-β pathology and glucose metabolism of the brain, while their application to tau pathology is still under development.

Glucose metabolism in the brain is often visualized through 18F-fluorodeoxyglucose (FDG) PET, a glucose analogue with positron-emitting radioactive isotope fluorine-18. Brain tissue consumes glucose via slow aerobic glycolysis in the neurons and via fast anaerobic glycolysis in the astrocytes in order to produce energy (30). Glucose is the main source of brain energy and glucose metabolism is tightly coupled to local synaptic activity. Specifically, the energy-demanding synaptic activity of a neuron increases glucose uptake into surrounding glial cells which act as energy carriers by transferring lactate to the neurons. The glucose metabolism measured through FDG-PET is hence believed to reflect local neuronal activity. FDG-PET studies robustly identified patterns of hypometabolism in the temporal, parietal and posterior cingulate cortex of

patients with AD, with a specificity and sensitivity for AD of 93% (2). Such patterns of hypometabolism are believed to partially reflect the ongoing neurodegenerative process related to tau pathology (31). Other brain regions as the cerebellum and the visual cortex remain relatively spared by metabolic alterations, while controversial findings have been reported for the hippocampus and MTLs (32,33). Both hypometabolism and hypermetabolism have been reported for these regions, and such differential findings seem to differ depending on methods applied (such as partial volume correction) and stage of patients involved in the study.

Labelling of amyloid-β pathology in the living human brain can be performed through several tracers including Pittsburgh Compound-B (PIB) and Florbetapir (F-AV-45). Cortical areas known to contain large amounts of amyloid-β plaques in AD showed comparable PIB and F-AV-45 retention in patients. Brain regions showing high levels of amyloid-β burden include lateral and medial parietal areas, such as the precuneus and the posterior cingulate cortex, but also frontal and temporal brain regions (34). Several studies have investigated the association between amyloid-β pathology and brain metabolism measured via PET tracers (35–37).

FDG and PIB have been used in order to distinguish different neurodegenerative diseases and for early detection of AD, respectively (13,38,39). Consistent links have been established between amyloid-β load and glucose hypometabolism (40), and in particular global amyloid-β load rather than local amyloid-β burden seems to be linked to local cortical glucose hypometabolism (35).

(II) Structural magnetic resonance imaging:

Magnetic resonance imaging (MRI) is a medical imaging technique which measures changes in magnetic properties of atomic nuclei induced by the application of an oscillating magnetic field. The magnetic field oscillates at the resonance frequency of the nuclei, usually hydrogen, and can be used to visualize detailed internal structures of the human body (41). In particular, structural MRI can be used to visualize soft tissue such as gray and withe matter in the human brain. Structural MRI has been extensively used to visualize and follow atrophic patterns in the brain of patients with AD and those at risk of developing AD. Patterns of atrophy are believed to reflect ongoing tau related neurodegeneration (31). Atrophy can be quantified by estimating changes in volumetry and cortical thickness of concerned regions via automatic and manual segmentation procedures (42–44). Voxel-based morphometry is an additional technique used to estimate white matter and gray matter density within a voxel and has also been widely used to investigate gray matter atrophy and white matter degeneration in AD (45,46). Structural MRI findings are in line with the first atrophic changes in AD, occurring in the MTL, including the hippocampus and the entorhinal cortex, and in medial and lateral parietal cortex, including the precuneus and posterior cingulate cortex (34,47). In particular, atrophy of the MTLs and related subfields such as the dentate gyrus have been followed in longitudinal approaches and might offer some diagnostic value (44). Finally, diffusion tensor imaging (DTI), which detects aspects of water diffusion, has been extensively used to measure integrity of white matter bundles in AD. DTI studies have shown degeneration of all major fiber tracts, in particular of the cingulum bundle, a set of fibers connecting the MTLs with medial parietal areas (48,49). Intriguingly, recent high-resolution DTI studies were able to visualize degeneration of the perforant pathway, the main entrance pathway from the entorhinal cortex into the hippocampus and one of the earliest sites showing tau pathology and extensive degeneration in AD (50,51).

(III) Functional magnetic resonance imaging:

Functional Magnetic Resonance Imaging (fMRI) can be used to measure brain activity via the blood-oxygenation-level-dependent (BOLD) signal (41). The BOLD signal can be measured due to different magnetic properties of oxygenated and deoxygenated hemoglobin. The BOLD signal is essentially reflecting the haemodynamic response, the quick transport of glucose and oxygen from cerebral blood to brain tissue in order to support neurotransmitter recycling and sustained neuronal firing (41). Simultaneous electrophysiological recordings and fMRI acquisition in the visual cortex of monkeys provide evidence that local field potentials best predict fMRI responses. These findings indicate that the BOLD signal primarily measures the synaptic input and processing of neuronal information within a region (52).

Task fMRI is used to map brain regions activated during a specific task, by correlating the time course of the task with the BOLD signal in the brain. However, the brain is active also at rest, which can be detected by measuring ongoing slow fluctuations in the BOLD signal below 0.1 Hz (53,54). Such intrinsic brain activity can be assessed via resting-state fMRI (rs-fMRI), where the participant is left in the scanner free from any tasks or specific stimuli – usually with their eyes closed – for about six to ten minutes. While the nature of the signal is still under investigation and not the main scope of this Thesis, a short summary on the physiological underpinnings of intrinsic brain activity assessed via rs-fMRI is provided at the end of the introduction under Box 3.

Synchronized intrinsic BOLD activity of distant brain regions has been used to derive patterns of intrinsic functional connectivity (iFC), denominated as intrinsic brain networks (iBN) (55). IBN are robust over species, cognitive states, developmental stages and partially overlap with known structural and anatomical connections (53,55). Several sets of functional iBNs have been

identified that show a high degree of overlap with activation maps from task-fMRI, suggesting that iBNs underpin human brain function (53,55). In the following section, a specific network extremely relevant for AD will be presented: the default mode network (DMN).

Box 2. Clinical neuroimaging in AD.

- **PET:** molecular imaging technique used to track levels of **glucose hypometabolism** (**FDG-PET**) related to ongoing neurodegeneration and **amyloid-β plaques** deposition (e.g. **PIB-PET**) in AD.
- **Structural MRI:** medical imaging technique applying an oscillating magnetic field in order to visualize **gray** and **withe matter** of the human brain. It is used to quantify both gray and white matter **atrophy** levels and related neurodegenerative processes in AD. **DTI** is an additional technique that can be used to visualize **white matter bundles** and quantify its **degeneration** in AD.
- **FMRI:** medical imaging technique used to measure **brain activity** by assessing the **BOLD** signal, hence the quick transport of glucose and oxygen in the blood to activated brain areas. **Task fMRI** assesses brain activity during a **specific task**. **Resting-state fMRI** measures **intrinsic brain activity** by assessing **ongoing fluctuations of the BOLD signal below 0.1 Hz.**
- **IBN:** intrinsic brain network, **correlated resting-state activity** of distant brain regions used to derive patterns of **iFC**. The **DMN** is an **iBN** particularly targeted in AD.

1.3.1. The default mode network and Alzheimer's disease

The default mode network (DMN) is an iBN composed of the medial prefrontal cortex, the MTLs (including the hippocampal formation) and areas of the medial and lateral parietal cortices, including the posterior cingulate and precuneus (56,57). The DMN is characterized by deactivation during external stimuli and goal directed behavior and has been consistently associated with internal mental states such as mnemonic processes, future planning and daydreaming (56–58).

Intriguingly, the DMN shows a striking overlap with characteristic pathological changes taking place in AD. Glucose hypometabolism, amyloid-β load and atrophy are extensively found within key connectivity nodes of the DMN including the precuneus, posterior cingulate cortex and MTLs. AD also impacts functional integrity of the DMN, with several studies reporting decreased iFC within the DMN in patients with AD or at risk of developing AD. More precisely, studies provide evidence for decreased iFC between medial parietal areas, such as the posterior cingulate and precuneus, and MTL areas, such as the hippocampal formation (32,59–62).

1.3.2. The medial temporal lobe and neuroimaging in Alzheimer's disease

The MTLs are characterized by the hippocampal-entorhinal system, which subserves navigation and memory functions via highly coordinated oscillatory dynamics among subregions (63). The hippocampal-entorhinal system includes a main excitatory feedforward loop of subregions, starting from lower layers of the entorhinal cortex (EC) to dentate gyrus (DG), cornu ammonis (CA) 3, CA1, and finally to upper layers of the EC (64). As introduced in the aforementioned section, this loop interacts extensively with several cortical systems along the longitudinal axis of the MTL (65,66), whereas one of these two systems is mainly constituted by posterior cingulate cortex and precuneus i.e., medial parietal cortices (67).

Characteristic MTL pathophysiology in AD is characterized by tau-based pathological changes, structural degradation and substantial cell loss; while amyloid-β-based pathology is less prominent – at least in early stages of the disease (14,28). Tau based pathological changes and substantial cell loss start typically in the transition zone between EC and adjacent temporal cortices, then spread to limbic and later to cortical regions (19). Start of first clinical symptoms such as impaired memory commonly follow first MTL alterations (14).

MTL activity, particularly in the hippocampus, is paradoxically increased in disease stages of MCI, most notably during memory processes (68). Such increased hippocampus activation during memory processing is associated with cortical thinning in parietal lobes (69). Since both hyperactivity and memory performance normalize after anti-epileptic medication, activity increases seem to be dysfunctional (70). Beyond memory-related activity, intrinsic activity within the MTL (including local iFC and amplitude of low frequency fluctuations of the BOLD resting-state signal), is progressively increased in MCI and AD. Increased intrinsic activity and iFC within the MTL is linked with impaired memory function and with functional dysconnectivity of the MTL from medial parietal connectivity nodes of the DMN (61,62,68,71,72).

1.3.3. *"Network degeneration hypothesis"* in Alzheimer's disease

Several lines of evidence suggest that neurodegenerative diseases progress along the boundaries of brain networks and essentially reflect brain network dysfunction. Pathological findings in rodent models of neurodegenerative diseases and in *post-mortem* brains of patients provide evidence that misfolded proteins aggregate within small, selectively vulnerable neuronal populations, resulting in the progressive dismantling of synapses, neuronal circuits and networks already at very early stages of the disease (17,73). Synapses falter, and damage spreads to new

regions with known anatomical connections to the sites of earlier injury, accompanied by worsening clinical deficits (17). Neuroimaging studies support such a link between neurodegeneration and network dysfunction, as exemplified by characteristic amyloid-β deposition, glucose hypometabolism, structural and functional alterations within the DMN in AD (56). In a neuroimaging study including patients with AD, frontotemporal degeneration, semantic dementia and progressive non-fluent aphasia, Seeley and colleagues were able to show that syndrome-associated regional degeneration patterns reflect distinct human neural network architectures in healthy subjects (73). Such overwhelming correspondence between network dysfunction and neuropathology have led to the proposal of the "*network degeneration hypothesis of neurodegenerative diseases*", with several competing mechanisms including nodal stress, transneuronal spread, trophic failure and shared vulnerability attempting to explain network-based disease patterning (74). Importantly, such a model deepens our understanding of neurodegenerative processes, opening innovative possibilities for effective diagnostic tools and therapies.

(I) Amyloid-β-associated "graded network degeneration hypothesis" of Alzheimer's disease.

Amyloid-β pathology is known to disturb network function, both at the cellular and the large-scale brain level. Amyloid-β is known to dysregulate glutamatergic and GABAergic activity attenuating synaptic transmission. Moreover, both epileptiform activity and non-convulsive seizures have been observed at the neuronal circuit level (4). At the large-scale brain level, amyloid-β plaque load shows a striking overlap with the DMN, where connectivity nodes undergo early functional alterations in AD, eventually affecting also the DMN's periphery and other cognitive and primary sensory networks later on (56). The "*graded network degeneration hypothesis"* of AD suggests that due to high processing burden, connectivity nodes of the DMN are among the earliest

sites to suffer from amyloid-β dependent neuropathology in AD, which shifts from there to the network periphery and to other cognitive and primary networks later on, with large-scale iFC being the driving force of the pathophysiological process (75).

(II) The "MTL dysconnectivity hypothesis" of Alzheimer's disease.

As introduced in the previous sections, several lines of evidence suggest that activity changes of the MTL in AD and in subjects at risk for AD during both task conditions and at rest are of a dysfunctional nature. In particular, MTL hyperactivity has been shown to relate to both structural and functional dysconnectivity of the MTL from medial parietal connectivity nodes of the DMN. This finding suggests a link between degradation of DMN connectivity nodes and aberrant MTL hyperactivity in AD. The *"MTL dysconnectivity hypothesis"* postulates that in AD, aberrant hyperactivity in the MTL and resulting cognitive impairments are mechanistically linked to MTL dysconnectivity from medial parietal connectivity nodes of the DMN. However, it is currently unclear to what extent aberrant patterns of MTL activity are related to local pathological changes or large-scale network degradation. Future works are needed to unravel the directionality of pathological effects.

Box 3. The brain's intrinsic activity.

Intrinsic dynamic fluctuations of neuronal activity underlie brain function (64) and harmonics are known to exist between the brain's fluctuating rhythms (76). Interaction between different oscillatory rhythms introduces a structured quality to the activity of the brain (77), constraining the naturally stochastic firing of individual neurons (78). Higher frequency oscillations are "nested" within lower frequencies (79), suggesting that fast local computations of widely distributed neuronal assemblies are functionally integrated through slow long-range neuronal communication via a network of structural connections (80). Simultaneous recordings have provided evidence for a temporal relationship between spontaneous BOLD fluctuations at ~ 0.1 Hz and an array of electrophysiological recordings, including infraslow local field potentials (81) and cross-frequency amplitude modulation of gamma and theta waves (82). While such findings support a meaningful role of "resting-state" activity in sustaining long-range functional connections, additional research is needed in order to dissociate genuine neuronal sources of the signal from non-physiological artifacts and vascular contributions (83).

2. Experimental aims and presentation of the articles

The following published articles reflect my effort to elucidate two distinct aspects of brain network dysfunction in AD: *(i)* amyloid-β-associated graded degeneration of cortical networks and *(ii)* MTL dysconnectivity-associated MTL hyperactivity. First, we investigated whether a global correspondence exists between amyloid-β pathology and iFC across several iBNs in AD. We hypothesized that in patients, amyloid-β would aggregate in areas with high iFC on a within-network basis. Further, we hypothesized amyloid-β associated local network dysfunction among functional connectivity nodes of distinct iBNs. Second, we investigated whether a correspondence exists between MTL hyperactivity at rest and MTL dysconnectivity in AD. We consistently found MTL hyperactivity in patients, which was associated with memory impairments and both functional and structural dysconnectivity of the MTLs from key connectivity nodes of the DMN. The four cross-sectional studies applied multi-modal neuroimaging methods and included analysis of brain structure (MRI), brain activity (resting-state fMRI, FDG-PET) and brain amyloid-β pathology load (PIB-PET) from considerable samples of patients with AD-dementia, patients with MCI and age-matched cognitively healthy subjects.

(I) Project 1: Within-patient correspondence of amyloid-β and intrinsic network connectivity in Alzheimer's disease.

Myers N, **Pasquini L**, Gottler J, Grimmer T, Koch K, Ortner M, Neitzel J, Muhlau M, Forster S, Kurz A, Forstl H, Zimmer C, Wohlschlager AM, Riedl V, Drzezga A, Sorg C. Brain 2014, 137, 2052-2064.

The *"graded network degeneration hypothesis"* postulates that disease specific pathological hallmarks affect specific brain networks in neurodegenerative diseases. More

precisely, pathology spreads along network boundaries, from key connectivity nodes to the network's periphery and to other networks in the progression of the disease. In AD, a striking overlap exists between the spatial distribution of amyloid-β pathology and the spatial distribution of iFC in healthy subjects. In order to investigate a correspondence between amyloid-β pathology and iFC, we compared spatial patterns of amyloid-β plaques and iFC of several iBN in amyloid-β positive patients with MCI (n = 24) and aged-matched cognitively healthy subjects (n = 16). We acquired rs-fMRI data to derive sets of iBN including the DMN and PIB-PET data to derive spatial maps of amyloid-β load. Subsequently, we used within-subject global voxel-wise spatial correlation to derive a global measure of amyloid-β/iFC correspondence, and a searchlight approach to associate amyloid-β pathology and iFC at the local level. At the global network level, amyloid-β was positively associated with iFC. This correspondence was particularly prominent in the DMN and with progressively decreased correspondence from higher cognitive to primary sensory networks. At the local level, we found a negative correspondence between amyloid-β pathology and iFC, particularly affecting high connectivity nodes of distinct heteromodal iBNs including the DMN. These findings suggest that amyloid-β pathology accumulates from connectivity nodes of the DMN to the periphery and to other brain networks, with gradients in iFC being the driving force of the pathophysiological process. Strikingly, our analysis unraveled a negative correspondence between amyloid-β pathology and iFC, possibly reflecting the deleterious action of amyloid-β pathology on activity of neuronal assemblies, as observed in the animal model.

Contribution:

For this paper, I was substantially involved at the level of data analysis and interpretation. Importantly, my involvement was critical in the execution of additional analyses and in the final drafting and article revision during the major revision process. First, findings of altered iFC across groups for the relevant iBNs had to be entirely replicated using the more recent preprocessing and

analysis software version SPM8 instead of SPM5, which included replicating the whole preprocessing and analysis pipeline for functional data. Moreover, I performed additional analyses investigating the level of atrophy from structural MRI data and the presence of head movement artifacts in rs-fMRI data. I performed voxel based morphometry analyses to assess the level of gray matter atrophy within regions of the DMN. Head movement was assessed after realignment of functional data, which was comparable across groups and did not affect our findings.

(II) Project 2: Link between hippocampus' raised local and eased global intrinsic connectivity in AD.

Pasquini L, Scherr M, Tahmasian M, Meng C, Myers NE, Ortner M, Muhlau M, Kurz A, Forstl H, Zimmer C, Grimmer T, Wohlschlager AM, Riedl V, Sorg C. Alzheimer's and Dementia 2014, 11, 475-484.

Several lines of evidence suggest an association between dysfunctional patterns of MTL hyperactivity during memory tasks and MTL dysconnectivity from medial parietal connectivity nodes of the DMN in AD. In order to elucidate whether a correspondence also exists between MTL hyperactivity at rest and MTL dysconnectivity from medial parietal connectivity nodes of the DMN, we acquired partial-brain and whole-brain rs-fMRI data in patients with AD (n = 21), MCI (n = 22) and aged-matched healthy cognitively subjects (n = 22). Independent component analysis was used to derive patterns of global iFC for the DMN and local iFC for the hippocampus, from whole-brain and partial-brain data respectively. Analyses were corrected for atrophy and head-movement artifacts. Group comparisons revealed progressively increased levels of local iFC in the hippocampus of patients with MCI and AD. Local iFC increases within the hippocampus correlated

with global functional dysconnectivity of the hippocampus within the DMN and impaired memory. These findings support a mechanistic link between MTL dysconnectivity, dysfunctional MTL hyperactivity and impaired memory along the AD continuum, as proposed by the *"MTL dysconnectivity hypothesis"*.

Contribution:

This project was critical in the development of my research questions regarding the *"MTL dysconnectivity hypothesis"* and served as a basis for the following projects. In this article, I was involved at all levels of analysis including quality control of functional and structural data, design and execution of preprocessing pipelines, including head motion correction of functional data, and independent component analysis of whole-brain as partial-brain rs-fMRI data. Finally, I primarily contributed in drafting the manuscript and during the major revision process.

(III) Project 3: The lower hippocampus global connectivity, the higher its local metabolism in Alzheimer's disease.

Tahmasian M, **Pasquini L**, Scherr M, Meng C, Förster S, Mulej Bratec S, Shi K, Yakushev I, Schwaiger M, Grimmer T, Diehl-Schmid J, Rield V, Sorg C, Drzezga A. Neurology 2015, 84, 1956-1963.

Following the research line of the previously presented article, in this project we aimed at linking hippocampal local activity with hippocampal functional dysconnectivity from medial parietal areas. We acquired simultaneously rs-fMRI and FDG-PET data in patients with AD (n = 40), MCI (n = 21) and healthy cognitive age matched subjects (n = 26). We used a seed-based approach to derive iFC between the hippocampus and the precuneus and related this measure to

hippocampal local activity measured via glucose metabolism from FDG-PET data. Analyses were corrected for atrophy, age, gender and partial volume effects. IFC between hippocampus and precuneus was decreased in patients with MCI and AD. In patients, glucose metabolism was reduced in the precuneus, but did not change in the hippocampus. Critically, in patients with AD, iFC between hippocampus and precuneus correlated negatively with hippocampal glucose metabolism. These findings provided additional evidence for a mechanistic link between MTL dysconnectivity form medial parietal connectivity nodes of the DMN and aberrant patterns of MTL hyperactivity in AD.

Contribution:

The research question of this article was the natural result of the preceding project and reflects the common effort of our research group to explore a correspondence between MTL hyperactivity at rest and MTL dysconnectivity. This effort involved an intensive collaboration between Dr. Tahmasian M. and me at several levels. Such collaboration was characterized by regular meetings, journal clubs and intensive teamwork. Our close cooperation resulted in common contributions to conception and execution of the projects, analysis and interpretation of the data, alongside the drafting and revision of the articles. More specifically, I was particularly involved in collecting and sharing relevant literature, in the conceptualization and design of the preprocessing pipeline of functional resting-state fMRI data, in the writing of scripts performing quality control within the seed-based approach (particularly in regard to head movement artifacts and signal to noise ratio assessment) and in the critical revision of the article for intellectual content during the submission and publication process.

(IV) Project 4: Increased intrinsic activity of medial-temporal lobe subregions is associated with decreased cortical thickness of medial-parietal areas in patients with Alzheimer's disease dementia

Pasquini L, Scherr M, Tahmasian M, Myers N, Ortner M, Kurz A, Förstl H, Zimmer C, Grimmer T, Akhrif A, Wohlschläger AM, Riedl V, Sorg C. Journal of Alzheimer's Disease 2016.

In this final project I aimed at extending previous findings. I explored whether, in AD, MTL hyperactivity at rest affects distinct MTL subregions and whether MTL hyperactivity is linked with structural degeneration of medial parietal connectivity nodes of the DMN. We acquired rs-fMRI and structural MRI data from patients with AD (n = 21), patients with MCI (n = 22) and aged-matched cognitively healthy subjects (n = 22). I used automatic segmentation algorithms to segment the medial parietal cortex and the MTL into regions of interest. I then calculated the power spectrum of the BOLD signal to investigate changes in intrinsic activity of several MTL subregions and cortical thickness of medial parietal areas to derive a measure of structural degeneration of key DMN connectivity nodes. Analyses were corrected for atrophy and head-movement artifacts. Intrinsic activity of several MTL subregions was increased in AD and correlated with structural atrophy of medial parietal areas of the DMN, such as the precuneus and posterior cingulate. More precisely, hyperactivity at rest negatively correlated with ipsilateral cortical degeneration and with impaired cognitive performance. This findings offer additional support for the proposed mechanistic link between MTL dysconnectivity, dysfunctional MTL hyperactivity and impaired memory in AD.

Contribution:

In a final attempt to elucidate the *"MTL dysconnectivity hypothesis"* in AD, in this article we aimed at finding structural correlates of MTL hyperactivity at rest and investigated whether

specific MTL subregions were selectively characterized by aberrant patterns of MTL hyperactivity. Besides routine quality controls of functional and structural MRI data, this project required extensive computational skills with different computational neuroimaging software. In particular, in this project I performed the segmentation pipeline for MTL subregions and parietal regions-of-interest which involved an intensive confrontation with the software Freesurfer. Moreover, I was primarily involved in writing and applying in home MATLAB-scripts for the computation of MTL subregional power spectrum density of BOLD low frequency fluctuations, our proxy for intrinsic activity. Finally, I primarily contributed in drafting the manuscript and during the major revision process.

3. Discussion

Multimodal-neuroimaging in cross-sectional studies involving patients with AD, patients with MCI and aged-matched cognitively healthy controls, allowed me to investigate two variants of large-scale brain network dysfunction in AD: *(i)* amyloid-β-associated graded degeneration of cortical networks and *(ii)* MTL dysconnectivity-associated MTL hyperactivity. In the next section key findings are summarized and contextualized; a model of network degeneration in AD is presented; limitations, future perspectives and final considerations on the development of neuroimaging biomarkers are discussed.

3.1. Key findings and contextualization

In the first study, we investigated amyloid-β-associated graded degeneration of cortical networks in AD, by assessing the level of correspondence between amyloid-β load and iFC among amyloid-β positive patients with MCI and aged matched healthy cognitive subjects. At the global network level, we found a positive correspondence between amyloid-β pathology and iFC primarily for the DMN, with decreasing correspondence among other cognitive and primary sensory networks. At the local network level, we observed a negative association between amyloid-β pathology and iFC primarily affecting key connectivity nodes of hetermododal iBNs, including the DMN. The positive global correspondence is in line with established findings reporting a striking spatial overlap between the DMN and patterns of amyloid-β deposition (34) and with several neuroimaging studies supporting amyloid-β-associated network degradation in AD (73,74,84,85). Importantly, the positive global correspondence supports the *"graded network degeneration hypothesis"*, where amyloid-β pathology accumulates from connectivity nodes of the DMN to the periphery and to other brain networks, with gradients in iFC being the driving force

of the pathophysiological process. Strikingly, our analysis unraveled a negative local correspondence between amyloid-β pathology and iFC, possibly reflecting the detrimental action of amyloid-β pathology on circuit activity of neuronal assemblies. Such findings are in line with findings from animal models of AD, which describe a deleterious action of amyloid-β pathology on activity of circuit function and local network organization (4,86,87).

The remaining three studies provide evidence for aberrant patterns of MTL hyperactivity at rest in AD. MTL hyperactivity at rest was associated with MTL functional and structural dysconnectivity from medial parietal connectivity nodes of the DMN and impaired cognitive functions. More precisely, the three studies revealed:

- Progressively increased local iFC within the hippocampus across stages of AD. Increased local iFC within the hippocampus correlated with both global functional dysconnectivity of the hippocampus within the DMN and impaired cognitive performance.
- Decreased iFC between hippocampus and precuneus in patients with MCI and AD. In patients, glucose metabolism was reduced in the precuneus, but did not change in the hippocampus. Critically, in patients with AD, iFC between hippocampus and precuneus correlated negatively with hippocampal glucose metabolism.
- Increased intrinsic activity of several MTL subregions in AD. Hyperactivity of MTL subregions correlated with structural atrophy of medial parietal areas of the DMN as the precuneus and posterior cingulate. More precisely, hyperactivity at rest negatively correlated with ipsilateral cortical degeneration and with impaired cognitive performance.

These results are in line with findings of hippocampal hyperactivity during both task conditions and at rest in patients with AD and at risk for AD, which have also been related to both functional and structural dysconnectivity from key medial parietal areas of the DMN (34,68,69,71). In patients with MCI, hippocampal hyperactivity during task conditions and related cognitive performance have been shown to normalize after antiepileptic medication, providing additional support for a dysfunctional nature of hyperactivity patterns in the MTL (70). Remarkably, similar neuroimaging findings of MTL hyperactivity at rest have been reported in subjects with medial temporal lobe epilepsy (88). Evidence suggests that hippocampal structural and functional dysconnectivity is a process occurring early in AD and involving both long-range tracts (e.g. the cingulum bundle connecting the posterior cingulate to the MTL) (49) but also short-range connections (e.g. the perforant pathway, the major cortical afferent connecting the hippocampus to the EC) (50,51). In conclusion, our findings are in line with the *"MTL dysconnectivity hypothesis"* of AD, suggesting a mechanistic link between MTL dysconnectivity, aberrant patterns of MTL activity during both task conditions and at rest, and impaired memory in AD.

3.2. Linking amyloid-β-associated graded degeneration of cortical networks, MTL dysconnectivity and MTL hyperactivity

We have provided evidence for two variants of network dysfunction in AD: *(i)* amyloid-β-associated graded degeneration of cortical networks and *(ii)* MTL dysconnectivity-associated MTL hyperactivity. However, how do both processes relate to each other? We postulate that amyloid-β accumulates several years before first symptoms arise, with iFC being the driving force of the pathophysiological process (73,74,89). In parallel with amyloid-β accumulation, amyloid-β pathology exerts a deleterious impact on local neuronal populations, affecting both long-range and

short-range iFC of iBNs (86,89). Such circuit dysfunction leads to MTL dysconnectivity from connectivity nodes of the DMN where amyloid-β accumulates early on, including the cingulate cortex and basal portions of the temporal cortex (14). Progressive MTL dysconnectivity might contribute to disinhibition of the EC-hippocampus circuit and misbalanced circuit activity (64), resulting in MTL hyperactivity during both task conditions and at rest and eventually contributing to the typical amnestic impairments in AD (32,61,62,68–71). Tau pathology has been associated with epileptic activity both in animal models and in patients with status epilepticus (90–92). MTL circuit hyperexcitability and hyperactivity could be the driving force facilitating tau accumulation and related neurodegeneration subsequently spreading to neocortical areas (8,14) (Figure 2; H-I. Amyloid-β mediated MTL dysconnectivity hypothesis; a. Long-range, b. Short-range). However, such a model needs additional validation. In particular, the exact phenomenology and chain of events is at the moment unclear: Are aberrant MTL activity patterns taking place as a direct result of amyloid-β pathophysiology driving MTL dysconnectivity from connectivity nodes of the DMN? Alternatively, is MTL hyperactivity induced by local tau accumulation and related neurodegeneration, which is preceding aforementioned circuit dysfunction? Is hence MTL hyperactivity resulting from circuit dysconnectivity or from imbalanced activity due to local pathology? MTL hyperactivity could result from the deleterious impact of tau pathology on activity of neuronal populations in the MTL (90–92). The synergistic action of tau pathology and MTL hyperactivity could subsequently trigger neurodegenerative processes leading to MTL dysconnectivity (49–51). Short-range and long-range MTL structural and functional dysconnectivity would be followed by tau spread and neurodegeneration to neocortical areas highly connected to the MTL as the temporal and cingulate cortices (8,14) (Figure 2; H-II. Tau mediated MTL dysconnectivity hypothesis; a. Long-range, b. Short-range). However, one should note that both models are probably not exclusive but rather complementary mechanisms involved in the

neurodegenerative process. In order to assess whether dependency and causality exist, additional research is needed in order to shed light on the chain of events in the pathophysiological process. In particular, longitudinal studies including recently available tau tracers and translational approaches including multimodal recordings in animal models may prove particularly useful.

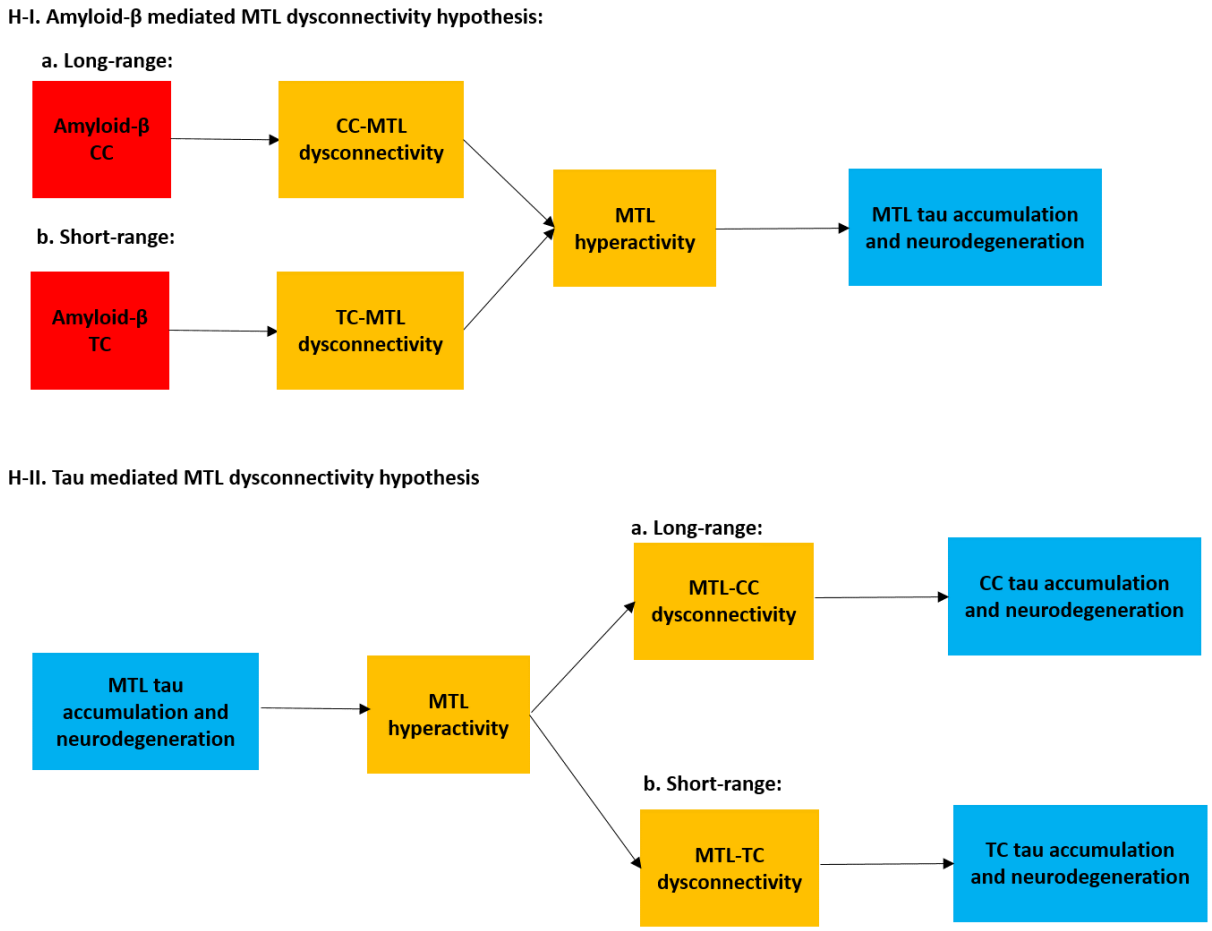

Figure 2. The amyloid-β and tau mediated MTL dysconnectivity hypotheses in AD. Panel A: Amyloid-β mediated MTL dysconnectivity hypothesis. Amyloid-β accumulates in connectivity nodes of the DMN including the CC and the TC, with iFC being the driving force of the pathophysiological process. In parallel, amyloid-β exerts a deleterious impact on local neuronal assemblies, driving long-range CC-MTL (H-I. a) and short-range TC-MTL (H-II. b) dysconnectivity. MTL dysconnectivity results in disinhibition-like changes of the EC-hippocampus circuit, resulting

in MTL hyperactivity. Finally, MTL hyperactivity facilitates MTL tau accumulation and neurodegeneration. **Panel B:** Tau mediated MTL dysconnectivity hypothesis. MTL tau accumulation and degeneration exerts a deleterious impact on neuronal activity of the MTL, driving MTL hyperactivity patterns. The synergistic action of tau pathology and MTL hyperactivity trigger neurodegenerative processes leading to MTL dysconnectivity. Long-range (H-II. a) and short-range MTL (H-II. b) structural and functional dysconnectivity is followed by tau spread and neurodegeneration to highly connected neocortical areas including the CC and TC. AD = Alzheimer's disease; CC = cingulate cortex; DMN = default mode network; EC = entorhinal cortex; MTL = medial temporal lobe; TC = temporal cortex.

3.3. Limitations and future perspectives

Two main limitations advise caution in the interpretation of results and indicate promising avenues for future research perspectives. First, all four studies are of cross-sectional nature, hence no causal inference can be concluded. Longitudinal studies involving large cohorts of amyloid-β positive and negative healthy adults are necessary in order to clearly understand the chain of events in the pathophysiological process. Such studies should optimally involve multi-modal imaging modalities mapping changes in brain structure, metabolism, function and include imaging of both amyloid-β and tau accumulation (93). Moreover, longitudinal clinical neuroimaging studies would profit enormously if framed within randomized control trials, with the inclusion of interventions bearing a high potential for AD treatment. Such interventions could include therapies against neuroinflammatory processes, amyloid-β immunization and network dysfunction (3,4,94). But also neuro-enhancing strategies involving psychological and behavioral therapies should be considered (95). In particular, such studies would help to unravel directionality of effects, e.g. dependence of MTL hyperactivity patterns from amyloid-β pathology within connectivity nodes of the DMN, and help to map the impact of interventions on degenerative brain processes.

Secondly, our currently poor understanding of the cellular signals underlying the neuroimaging measures needs to be clarified before certain conclusions on the biological nature of pathophysiological processes in AD can be made. While a striking correspondence exists between findings relating AD pathophysiology with electrophysiological signals in animal models and corresponding accepted proxies in human neuroimaging, additional translational research is urgently needed in order to assess correspondence of signal across different species and imaging-levels. In particular, translational research would enormously profit from multimodal imaging in animal models of AD, including electrophysiological recordings and neuroimaging techniques as PET, MRI and fMRI.

3.4. Towards the development of neuroimaging biomarkers in AD

Neuroimaging has been repeatedly praised for holding promising potential in the establishment of effective and innovative biomarkers, which could be of use in the diagnosis of several psychiatric and neurological diseases including AD. The research community is extensively working on the development of multimodal neuroimaging biomarkers and their application in: *(i)* early diagnosis and prevention of AD; *(ii)* the differential diagnosis between AD and other major neurodegenerative diseases, including fronto-temporal degeneration and Lewy body dementia; *(iii)* monitoring brain changes during AD progression and evaluation of medical interventions (96).

The ideal dementia diagnostic biomarker should encompass the following properties: be highly sensitive and specific, reliable, detect several features of the neuropathological process, time-efficient and easy to use, non-invasive, and inexpensive (96). A strategy has been recently proposed that could allow diagnostic AD biomarkers from research to be translated into routine clinical practice (97). This strategy would consist of five phases: *(i)* identify potential biomarkers;

(ii) estimate sensitivity and specificity of the biomarkers; *(iii)* assess the capacity of the biomarker to detect preclinical disease stages; *(iv)* determine operating characteristics of the biomarker-based test in a care population; *(v)* estimate the reduction in mortality, morbidity and disability achieved through the biomarker. While the first two phases have already been widely achieved, two major barriers need to be assessed in order to proceed. First, future efforts should focus on the development of reliable and robust preclinical neuroimaging markers, by inclusion of an optimal combination of several imaging modalities derived from retrospective and longitudinal studies. Future developments may profit enormously from ongoing technical improvements that increase the spatial and temporal resolution of neuroimaging modalities (e.g. multiband fMRI) (98) and by the development of quantitative physiological imaging (e.g. quantitative fMRI) (99). Secondly, strategies implementing clinical neuroimaging in primary and specialized care are urgently needed. In particular, the cost effectiveness of neuroimaging in the clinical setting needs to be assessed by the public health community (96). Dementia, hence also AD, is increasingly a world-wide public health issue, also in low and middle income countries where the general population lacks access to advanced diagnostic technologies (6). Alternative forms of diagnosis based on cognitive and neurological tests (e.g. testing frontal release signs), or biomarkers as macular amyloidosis and blood fluids should be considered (100–102).

3.5. Conclusion

The aim of this Thesis was to investigate two variants of brain network dysfunction underlying AD pathophysiology: *(i)* amyloid-β-associated graded degeneration of cortical networks and *(ii)* MTL dysconnectivity-associated MTL hyperactivity. We found a positive correspondence between iFC and amyloid-β load at the global network level. Such global

correspondence was highest in the DMN, and gradually decreased in other cognitive and primary sensory networks. This finding suggests that amyloid-β pathology accumulates from key connectivity nodes of the DMN to the periphery and secondly across network boundaries to other cognitive and primary sensory networks, following gradients of iFC. Moreover, at the local level we found a negative correspondence between amyloid-β pathology and iFC within connectivity nodes of heteromodal brain networks, potentially reflecting the deleterious effects of amyloid-β on circuit activity of neuronal assemblies. When focusing our attention on the MTL, we used several multimodal neuroimaging measures and consistently found evidence for MTL hyperactivity in patients. MTL hyperactivity was consistently associated with MTL functional and structural dysconnectivity from medial parietal connectivity nodes of the DMN. The link between MTL hyperactivity and impaired cognitive performance, together with MTL structural and functional dysconnectivity from medial parietal connectivity nodes of the DMN, suggest a dysfunctional nature of aberrant MTL activity levels. We contextualize our findings within a model in which amyloid-β pathology exerts a deleterious action on short-range and long-range neuronal circuits, driving MTL dysconnectivity. MTL dysconnectivity leads to network dysfunction and to aberrant MTL hyperactivity patterns both under task conditions and rest, underlying the mnemonic deficits in AD. MTL hyperactivity might act as a catalyzer driving tau accumulation and related neurodegeneration in the MTL, subsequently spreading to the rest of the brain. Interventions targeting network degeneration and MTL hyperactivity ma hold the key to improve the quality of life of patients and prevent degenerative processes already at preclinical disease stages.

4. References

1. Hodges JR. Alzheimer's centennial legacy: origins, landmarks and the current status of knowledge concerning cognitive aspects. Brain J Neurol. 2006 Nov;129(Pt 11):2811–22.

2. Blennow K, de Leon MJ, Zetterberg H. Alzheimer's disease. Lancet Lond Engl. 2006 Jul 29;368(9533):387–403.

3. Huang Y, Mucke L. Alzheimer mechanisms and therapeutic strategies. Cell. 2012 Mar 16;148(6):1204–22.

4. Palop JJ, Mucke L. Amyloid-beta-induced neuronal dysfunction in Alzheimer's disease: from synapses toward neural networks. Nat Neurosci. 2010 Jul;13(7):812–8.

5. World Health Organization. Dementia, a Public Health Priority [Internet]. 2012. Available from: http://www.who.int/mental_health/publications/dementia_report_2012/en/

6. Ferri CP, Prince M, Brayne C, Brodaty H, Fratiglioni L, Ganguli M, et al. Global prevalence of dementia: a Delphi consensus study. Lancet Lond Engl. 2005 Dec 17;366(9503):2112–7.

7. McKhann G, Drachman D, Folstein M, Katzman R, Price D, Stadlan EM. Clinical diagnosis of Alzheimer's disease: report of the NINCDS-ADRDA Work Group under the auspices of Department of Health and Human Services Task Force on Alzheimer's Disease. Neurology. 1984 Jul;34(7):939–44.

8. Sperling R, Mormino E, Johnson K. The evolution of preclinical Alzheimer's disease: implications for prevention trials. Neuron. 2014 Nov 5;84(3):608–22.

9. Gauthier S, Reisberg B, Zaudig M, Petersen RC, Ritchie K, Broich K, et al. Mild cognitive impairment. Lancet Lond Engl. 2006 Apr 15;367(9518):1262–70.

10. Dubois B, Feldman HH, Jacova C, Dekosky ST, Barberger-Gateau P, Cummings J, et al. Research criteria for the diagnosis of Alzheimer's disease: revising the NINCDS-ADRDA criteria. Lancet Neurol. 2007 Aug;6(8):734–46.

11. American Psychiatric Association. Diagnostic and statistical manual of mental disorders: DSM-IV-TR. 4th Edition Text revision ed. Washington, DC: American Psychiatric Association;

12. McKhann GM, Knopman DS, Chertkow H, Hyman BT, Jack CR, Kawas CH, et al. The diagnosis of dementia due to Alzheimer's disease: recommendations from the National Institute on Aging-Alzheimer's Association workgroups on diagnostic guidelines for Alzheimer's disease. Alzheimers Dement J Alzheimers Assoc. 2011 May;7(3):263–9.

13. Bateman RJ, Xiong C, Benzinger TLS, Fagan AM, Goate A, Fox NC, et al. Clinical and biomarker changes in dominantly inherited Alzheimer's disease. N Engl J Med. 2012 Aug 30;367(9):795–804.

14. Braak H, Braak E. Neuropathological stageing of Alzheimer-related changes. Acta Neuropathol (Berl). 1991;82(4):239–59.

15. Thal DR, Rüb U, Orantes M, Braak H. Phases of A beta-deposition in the human brain and its relevance for the development of AD. Neurology. 2002 Jun 25;58(12):1791–800.

16. Goedert M, Spillantini MG. A century of Alzheimer's disease. Science. 2006 Nov 3;314(5800):777–81.

17. Hardy J, Selkoe DJ. The amyloid hypothesis of Alzheimer's disease: progress and problems on the road to therapeutics. Science. 2002 Jul 19;297(5580):353–6.

18. Bero AW, Yan P, Roh JH, Cirrito JR, Stewart FR, Raichle ME, et al. Neuronal activity regulates the regional vulnerability to amyloid-β deposition. Nat Neurosci. 2011 Jun;14(6):750–6.

19. Braak H, Alafuzoff I, Arzberger T, Kretzschmar H, Del Tredici K. Staging of Alzheimer disease-associated neurofibrillary pathology using paraffin sections and immunocytochemistry. Acta Neuropathol (Berl). 2006 Oct;112(4):389–404.

20. Nelson PT, Alafuzoff I, Bigio EH, Bouras C, Braak H, Cairns NJ, et al. Correlation of Alzheimer disease neuropathologic changes with cognitive status: a review of the literature. J Neuropathol Exp Neurol. 2012 May;71(5):362–81.

21. Hyman BT, Phelps CH, Beach TG, Bigio EH, Cairns NJ, Carrillo MC, et al. National Institute on Aging-Alzheimer's Association guidelines for the neuropathologic assessment of Alzheimer's disease. Alzheimers Dement J Alzheimers Assoc. 2012 Jan;8(1):1–13.

22. Price JL, Morris JC. Tangles and plaques in nondemented aging and "preclinical" Alzheimer's disease. Ann Neurol. 1999 Mar;45(3):358–68.

23. de Calignon A, Polydoro M, Suárez-Calvet M, William C, Adamowicz DH, Kopeikina KJ, et al. Propagation of tau pathology in a model of early Alzheimer's disease. Neuron. 2012 Feb 23;73(4):685–97.

24. Liu L, Drouet V, Wu JW, Witter MP, Small SA, Clelland C, et al. Trans-synaptic spread of tau pathology in vivo. PloS One. 2012;7(2):e31302.

25. Ahmed Z, Cooper J, Murray TK, Garn K, McNaughton E, Clarke H, et al. A novel in vivo model of tau propagation with rapid and progressive neurofibrillary tangle pathology: the pattern of spread is determined by connectivity, not proximity. Acta Neuropathol (Berl). 2014 May;127(5):667–83.

26. Rüb U, Del Tredici K, Schultz C, Thal DR, Braak E, Braak H. The evolution of Alzheimer's disease-related cytoskeletal pathology in the human raphe nuclei. Neuropathol Appl Neurobiol. 2000 Dec;26(6):553–67.

27. Murray AD, Staff RT, McNeil CJ, Salarirad S, Ahearn TS, Mustafa N, et al. The balance between cognitive reserve and brain imaging biomarkers of cerebrovascular and Alzheimer's diseases. Brain J Neurol. 2011 Dec;134(Pt 12):3687–96.

28. Crary JF, Trojanowski JQ, Schneider JA, Abisambra JF, Abner EL, Alafuzoff I, et al. Primary age-related tauopathy (PART): a common pathology associated with human aging. Acta Neuropathol (Berl). 2014 Dec;128(6):755–66.

29. Sorg C, Grothe MJ. The complex link between amyloid and neuronal dysfunction in Alzheimer's disease. Brain J Neurol. 2015 Dec;138(Pt 12):3472–5.

30. Magistretti PJ. Cellular bases of functional brain imaging: insights from neuron-glia metabolic coupling. Brain Res. 2000 Dec 15;886(1-2):108–12.

31. Jack CR, Holtzman DM. Biomarker modeling of Alzheimer's disease. Neuron. 2013 Dec 18;80(6):1347–58.

32. Tahmasian M, Pasquini L, Scherr M, Meng C, Förster S, Mulej Bratec S, et al. The lower hippocampus global connectivity, the higher its local metabolism in Alzheimer disease. Neurology. 2015 May 12;84(19):1956–63.

33. Mosconi L. Brain glucose metabolism in the early and specific diagnosis of Alzheimer's disease. FDG-PET studies in MCI and AD. Eur J Nucl Med Mol Imaging. 2005 Apr;32(4):486–510.

34. Buckner RL, Snyder AZ, Shannon BJ, LaRossa G, Sachs R, Fotenos AF, et al. Molecular, structural, and functional characterization of Alzheimer's disease: evidence for a relationship between default activity, amyloid, and memory. J Neurosci Off J Soc Neurosci. 2005 Aug 24;25(34):7709–17.

35. Altmann A, Ng B, Landau SM, Jagust WJ, Greicius MD, Alzheimer's Disease Neuroimaging Initiative. Regional brain hypometabolism is unrelated to regional amyloid plaque burden. Brain J Neurol. 2015 Dec;138(Pt 12):3734–46.

36. Drzezga A, Grimmer T, Henriksen G, Stangier I, Perneczky R, Diehl-Schmid J, et al. Imaging of amyloid plaques and cerebral glucose metabolism in semantic dementia and Alzheimer's disease. NeuroImage. 2008 Jan 15;39(2):619–33.

37. Johnson KA, Fox NC, Sperling RA, Klunk WE. Brain imaging in Alzheimer disease. Cold Spring Harb Perspect Med. 2012 Apr;2(4):a006213.

38. Rabinovici GD, Rosen HJ, Alkalay A, Kornak J, Furst AJ, Agarwal N, et al. Amyloid vs FDG-PET in the differential diagnosis of AD and FTLD. Neurology. 2011 Dec 6;77(23):2034–42.

39. Jack CR, Knopman DS, Jagust WJ, Petersen RC, Weiner MW, Aisen PS, et al. Tracking pathophysiological processes in Alzheimer's disease: an updated hypothetical model of dynamic biomarkers. Lancet Neurol. 2013 Feb;12(2):207–16.

40. Cohen AD, Price JC, Weissfeld LA, James J, Rosario BL, Bi W, et al. Basal Cerebral Metabolism May Modulate the Cognitive Effects of Aβ in Mild Cognitive Impairment: An Example of Brain Reserve. J Neurosci Off J Soc Neurosci. 2009 Nov 25;29(47):14770.

41. Huettel SA, Song AW, McCarthy G. Functional Magnetic Resonance Imaging. 2nd ed. Sunderland, Massachusetts U.S.A.: Sinauer Associates; 2004.

42. Fischl B, Dale AM. Measuring the thickness of the human cerebral cortex from magnetic resonance images. Proc Natl Acad Sci U S A. 2000 Sep 26;97(20):11050–5.

43. Van Leemput K, Bakkour A, Benner T, Wiggins G, Wald LL, Augustinack J, et al. Automated segmentation of hippocampal subfields from ultra-high resolution in vivo MRI. Hippocampus. 2009 Jun;19(6):549–57.

44. de Flores R, La Joie R, Chételat G. Structural imaging of hippocampal subfields in healthy aging and Alzheimer's disease. Neuroscience. 2015 Nov 19;309:29–50.

45. Li J, Pan P, Huang R, Shang H. A meta-analysis of voxel-based morphometry studies of white matter volume alterations in Alzheimer's disease. Neurosci Biobehav Rev. 2012 Feb;36(2):757–63.

46. Busatto GF, Diniz BS, Zanetti MV. Voxel-based morphometry in Alzheimer's disease. Expert Rev Neurother. 2008 Nov;8(11):1691–702.

47. Small SA, Schobel SA, Buxton RB, Witter MP, Barnes CA. A pathophysiological framework of hippocampal dysfunction in ageing and disease. Nat Rev Neurosci. 2011 Oct;12(10):585–601.

48. Stěpán-Buksakowska I, Keller J, Laczó J, Rulseh A, Hort J, Lisý J, et al. Diffusion tensor imaging in Alzheimer disease and mild cognitive impairment. Neurol Neurochir Pol. 2012 Oct;46(5):462–71.

49. Villain N, Fouquet M, Baron J-C, Mézenge F, Landeau B, de La Sayette V, et al. Sequential relationships between grey matter and white matter atrophy and brain metabolic abnormalities in early Alzheimer's disease. Brain J Neurol. 2010 Nov;133(11):3301–14.

50. Hyman BT, Van Hoesen GW, Damasio AR, Barnes CL. Alzheimer's disease: cell-specific pathology isolates the hippocampal formation. Science. 1984 Sep 14;225(4667):1168–70.

51. Yassa MA, Muftuler LT, Stark CEL. Ultrahigh-resolution microstructural diffusion tensor imaging reveals perforant path degradation in aged humans in vivo. Proc Natl Acad Sci U S A. 2010 Jul 13;107(28):12687–91.

52. Logothetis NK. The neural basis of the blood-oxygen-level-dependent functional magnetic resonance imaging signal. Philos Trans R Soc Lond B Biol Sci. 2002 Aug 29;357(1424):1003–37.

53. Smith SM, Fox PT, Miller KL, Glahn DC, Fox PM, Mackay CE, et al. Correspondence of the brain's functional architecture during activation and rest. Proc Natl Acad Sci U S A. 2009 Aug 4;106(31):13040–5.

54. Raichle ME. The restless brain: how intrinsic activity organizes brain function. Philos Trans R Soc Lond B Biol Sci. 2015 May 19;370(1668).

55. Allen EA, Erhardt EB, Damaraju E, Gruner W, Segall JM, Silva RF, et al. A baseline for the multivariate comparison of resting-state networks. Front Syst Neurosci. 2011;5:2.

56. Buckner RL, Andrews-Hanna JR, Schacter DL. The brain's default network: anatomy, function, and relevance to disease. Ann N Y Acad Sci. 2008 Mar;1124:1–38.

57. Andrews-Hanna JR, Reidler JS, Sepulcre J, Poulin R, Buckner RL. Functional-anatomic fractionation of the brain's default network. Neuron. 2010 Feb 25;65(4):550–62.

58. Christoff K, Gordon AM, Smallwood J, Smith R, Schooler JW. Experience sampling during fMRI reveals default network and executive system contributions to mind wandering. Proc Natl Acad Sci U S A. 2009 May 26;106(21):8719–24.

59. Sorg C, Riedl V, Mühlau M, Calhoun VD, Eichele T, Läer L, et al. Selective changes of resting-state networks in individuals at risk for Alzheimer's disease. Proc Natl Acad Sci U S A. 2007 Nov 20;104(47):18760–5.

60. Drzezga A, Becker JA, Van Dijk KRA, Sreenivasan A, Talukdar T, Sullivan C, et al. Neuronal dysfunction and disconnection of cortical hubs in non-demented subjects with elevated amyloid burden. Brain J Neurol. 2011 Jun;134(Pt 6):1635–46.

61. Pasquini L, Scherr M, Tahmasian M, Myers NE, Ortner M, Kurz A, et al. Increased Intrinsic Activity of Medial-Temporal Lobe Subregions is Associated with Decreased Cortical Thickness of Medial-Parietal Areas in Patients with Alzheimer's Disease Dementia. J Alzheimers Dis JAD. 2016 Jan 21;51(1):313–26.

62. Pasquini L, Scherr M, Tahmasian M, Meng C, Myers NE, Ortner M, et al. Link between hippocampus' raised local and eased global intrinsic connectivity in AD. Alzheimers Dement J Alzheimers Assoc. 2015 May;11(5):475–84.

63. Harris KD, Csicsvari J, Hirase H, Dragoi G, Buzsáki G. Organization of cell assemblies in the hippocampus. Nature. 2003 Jul 31;424(6948):552–6.

64. Buzsaki G. Rhythms of the Brain. 1st ed. 198 Madison Avenue, New York, New York 10016: Oxford University Press; 2006.

65. Qin S, Duan X, Supekar K, Chen H, Chen T, Menon V. Large-scale intrinsic functional network organization along the long axis of the human medial temporal lobe. Brain Struct Funct. 2015 Sep 3;

66. Robinson JL, Barron DS, Kirby LAJ, Bottenhorn KL, Hill AC, Murphy JE, et al. Neurofunctional topography of the human hippocampus. Hum Brain Mapp. 2015 Dec;36(12):5018–37.

67. Libby LA, Ekstrom AD, Ragland JD, Ranganath C. Differential connectivity of perirhinal and parahippocampal cortices within human hippocampal subregions revealed by high-resolution functional imaging. J Neurosci Off J Soc Neurosci. 2012 May 9;32(19):6550–60.

68. Das SR, Pluta J, Mancuso L, Kliot D, Orozco S, Dickerson BC, et al. Increased functional connectivity within medial temporal lobe in mild cognitive impairment. Hippocampus. 2013 Jan;23(1):1–6.

69. Putcha D, Brickhouse M, O'Keefe K, Sullivan C, Rentz D, Marshall G, et al. Hippocampal hyperactivation associated with cortical thinning in Alzheimer's disease signature regions in non-demented elderly adults. J Neurosci Off J Soc Neurosci. 2011 Nov 30;31(48):17680–8.

70. Bakker A, Krauss GL, Albert MS, Speck CL, Jones LR, Stark CE, et al. Reduction of hippocampal hyperactivity improves cognition in amnestic mild cognitive impairment. Neuron. 2012 May 10;74(3):467–74.

71. Gour N, Ranjeva J-P, Ceccaldi M, Confort-Gouny S, Barbeau E, Soulier E, et al. Basal functional connectivity within the anterior temporal network is associated with performance on declarative memory tasks. NeuroImage. 2011 Sep 15;58(2):687–97.

72. Wang Z, Yan C, Zhao C, Qi Z, Zhou W, Lu J, et al. Spatial patterns of intrinsic brain activity in mild cognitive impairment and Alzheimer's disease: a resting-state functional MRI study. Hum Brain Mapp. 2011 Oct;32(10):1720–40.

73. Seeley WW, Crawford RK, Zhou J, Miller BL, Greicius MD. Neurodegenerative diseases target large-scale human brain networks. Neuron. 2009 Apr 16;62(1):42–52.

74. Zhou J, Gennatas ED, Kramer JH, Miller BL, Seeley WW. Predicting regional neurodegeneration from the healthy brain functional connectome. Neuron. 2012 Mar 22;73(6):1216–27.

75. Jones DT, Knopman DS, Gunter JL, Graff-Radford J, Vemuri P, Boeve BF, et al. Cascading network failure across the Alzheimer's disease spectrum. Brain J Neurol. 2016 Feb;139(Pt 2):547–62.

76. Carhart-Harris RL, Leech R, Hellyer PJ, Shanahan M, Feilding A, Tagliazucchi E, et al. The entropic brain: a theory of conscious states informed by neuroimaging research with psychedelic drugs. Front Hum Neurosci. 2014;8:20.

77. Rumsey CC, Abbott LF. Equalization of synaptic efficacy by activity- and timing-dependent synaptic plasticity. J Neurophysiol. 2004 May;91(5):2273–80.

78. Deco G, Rolls ET, Romo R. Stochastic dynamics as a principle of brain function. Prog Neurobiol. 2009 May;88(1):1–16.

79. Jensen O, Colgin LL. Cross-frequency coupling between neuronal oscillations. Trends Cogn Sci. 2007 Jul;11(7):267–9.

80. Ganzetti M, Mantini D. Functional connectivity and oscillatory neuronal activity in the resting human brain. Neuroscience. 2013 Jun;240:297–309.

81. Pan W-J, Thompson GJ, Magnuson ME, Jaeger D, Keilholz S. Infraslow LFP correlates to resting-state fMRI BOLD signals. NeuroImage. 2013 Jul 1;74:288–97.

82. Foster BL, Parvizi J. Resting oscillations and cross-frequency coupling in the human posteromedial cortex. NeuroImage. 2012 Mar;60(1):384–91.

83. Ekstrom A. How and when the fMRI BOLD signal relates to underlying neural activity: the danger in dissociation. Brain Res Rev. 2010 Mar;62(2):233–44.

84. Lim HK, Nebes R, Snitz B, Cohen A, Mathis C, Price J, et al. Regional amyloid burden and intrinsic connectivity networks in cognitively normal elderly subjects. Brain J Neurol. 2014 Dec;137(Pt 12):3327–38.

85. He Y, Chen Z, Evans A. Structural insights into aberrant topological patterns of large-scale cortical networks in Alzheimer's disease. J Neurosci Off J Soc Neurosci. 2008 Apr 30;28(18):4756–66.

86. Busche MA, Eichhoff G, Adelsberger H, Abramowski D, Wiederhold K-H, Haass C, et al. Clusters of hyperactive neurons near amyloid plaques in a mouse model of Alzheimer's disease. Science. 2008 Sep 19;321(5896):1686–9.

87. Busche MA, Chen X, Henning HA, Reichwald J, Staufenbiel M, Sakmann B, et al. Critical role of soluble amyloid-β for early hippocampal hyperactivity in a mouse model of Alzheimer's disease. Proc Natl Acad Sci U S A. 2012 May 29;109(22):8740–5.

88. Zhang Z, Lu G, Zhong Y, Tan Q, Chen H, Liao W, et al. fMRI study of mesial temporal lobe epilepsy using amplitude of low-frequency fluctuation analysis. Hum Brain Mapp. 2010 Dec;31(12):1851–61.

89. Myers N, Pasquini L, Göttler J, Grimmer T, Koch K, Ortner M, et al. Within-patient correspondence of amyloid-β and intrinsic network connectivity in Alzheimer's disease. Brain J Neurol. 2014 Jul;137(Pt 7):2052–64.

90. Palop JJ, Chin J, Roberson ED, Wang J, Thwin MT, Bien-Ly N, et al. Aberrant excitatory neuronal activity and compensatory remodeling of inhibitory hippocampal circuits in mouse models of Alzheimer's disease. Neuron. 2007 Sep 6;55(5):697–711.

91. Monti G, Tondelli M, Giovannini G, Bedin R, Nichelli PF, Trenti T, et al. Cerebrospinal fluid tau proteins in status epilepticus. Epilepsy Behav EB. 2015 Aug;49:150–4.

92. DeVos SL, Goncharoff DK, Chen G, Kebodeaux CS, Yamada K, Stewart FR, et al. Antisense reduction of tau in adult mice protects against seizures. J Neurosci Off J Soc Neurosci. 2013 Jul 31;33(31):12887–97.

93. Villemagne VL, Okamura N. Tau imaging in the study of ageing, Alzheimer's disease, and other neurodegenerative conditions. Curr Opin Neurobiol. 2016 Feb;36:43–51.

94. Perry D, Sperling R, Katz R, Berry D, Dilts D, Hanna D, et al. Building a roadmap for developing combination therapies for Alzheimer's disease. Expert Rev Neurother. 2015 Mar;15(3):327–33.

95. Kelly ME, Loughrey D, Lawlor BA, Robertson IH, Walsh C, Brennan S. The impact of cognitive training and mental stimulation on cognitive and everyday functioning of healthy older adults: a systematic review and meta-analysis. Ageing Res Rev. 2014 May;15:28–43.

96. Teipel S, Drzezga A, Grothe MJ, Barthel H, Chételat G, Schuff N, et al. Multimodal imaging in Alzheimer's disease: validity and usefulness for early detection. Lancet Neurol. 2015 Oct;14(10):1037–53.

97. The Lancet Neurology null. Bringing forward the diagnosis of Alzheimer's disease. Lancet Neurol. 2014 Oct;13(10):961.

98. Moeller S, Yacoub E, Olman CA, Auerbach E, Strupp J, Harel N, et al. Multiband multislice GE-EPI at 7 tesla, with 16-fold acceleration using partial parallel imaging with application to high spatial and temporal whole-brain fMRI. Magn Reson Med. 2010 May;63(5):1144–53.

99. Pike GB. Quantitative functional MRI: concepts, issues and future challenges. NeuroImage. 2012 Aug 15;62(2):1234–40.

100. Murphy RR, Abner EL, Jicha GA. Frontal release signs predict future decline in subjects with intact cognition and mild cognitive impairment. Alzheimers Dement J Alzheimers Assoc. 2015 Jul 1;11(7):P785.

101. Ikram MK, Cheung CY, Wong TY, Chen CPLH. Retinal pathology as biomarker for cognitive impairment and Alzheimer's disease. J Neurol Neurosurg Psychiatry. 2012 Sep;83(9):917–22.

102. Kiddle SJ, Sattlecker M, Proitsi P, Simmons A, Westman E, Bazenet C, et al. Candidate blood proteome markers of Alzheimer's disease onset and progression: a systematic review and replication study. J Alzheimers Dis JAD. 2014;38(3):515–31.

doi:10.1093/brain/awu103 Brain 2014: 137; 2052–2064 | 2052

BRAIN
A JOURNAL OF NEUROLOGY

Within-patient correspondence of amyloid-β and intrinsic network connectivity in Alzheimer's disease

Nicholas Myers,[1,2,3] Lorenzo Pasquini,[1,2] Jens Göttler,[1,2] Timo Grimmer,[4] Kathrin Koch,[1,2] Marion Ortner,[4] Julia Neitzel,[1,2] Mark Mühlau,[2,5] Stefan Förster,[2,6] Alexander Kurz,[4] Hans Förstl,[4] Claus Zimmer,[1] Afra M. Wohlschläger,[1,2] Valentin Riedl,[1,2,6] Alexander Drzezga[6,7,*] and Christian Sorg[1,2,4,*]

1 Department of Neuroradiology, Technische Universität München, Ismaningerstr. 22, 81675 Munich, Germany
2 TUM-Neuroimaging Centre, Technische Universität München, Ismaningerstr. 22, 81675 Munich, Germany
3 Department of Experimental Psychology, Oxford University, 9 South Parks Road, Oxford OX1 3UD, UK
4 Department of Psychiatry, Technische Universität München, Ismaningerstr. 22, 81675 Munich, Germany
5 Department of Neurology of Klinikum rechts der Isar, Technische Universität München, Ismaningerstr. 22, 81675 Munich, Germany
6 Department of Nuclear Medicine, Technische Universität München, Ismaningerstr. 22, 81675 Munich, Germany
7 Department of Nuclear Medicine, University of Cologne, Kerpener Straße 62, 50937 Köln, Germany

*These authors contributed equally to this work.

Correspondence to: Nicholas Myers,
Department of Experimental Psychology,
Oxford University, 9 South Parks Road,
Oxford OX1 3UD, UK
E-mail: nicholas.myers@psy.ox.ac.uk

There is striking overlap between the spatial distribution of amyloid-β pathology in patients with Alzheimer's disease and the spatial distribution of high intrinsic functional connectivity in healthy persons. This overlap suggests a mechanistic link between amyloid-β and intrinsic connectivity, and indeed there is evidence in patients for the detrimental effects of amyloid-β plaque accumulation on intrinsic connectivity in areas of high connectivity in heteromodal hubs, and particularly in the default mode network. However, the observed spatial extent of amyloid-β exceeds these tightly circumscribed areas, suggesting that previous studies may have underestimated the negative impact of amyloid-β on intrinsic connectivity. We hypothesized that the known positive baseline correlation between patterns of amyloid-β and intrinsic connectivity may mask the larger extent of the negative effects of amyloid-β on connectivity. Crucially, a test of this hypothesis requires the within-patient comparison of intrinsic connectivity and amyloid-β distributions. Here we compared spatial patterns of amyloid-β-plaques (measured by Pittsburgh compound B positron emission tomography) and intrinsic functional connectivity (measured by resting-state functional magnetic resonance imaging) in patients with prodromal Alzheimer's disease via spatial correlations in intrinsic networks covering fronto-parietal heteromodal cortices. At the global network level, we found that amyloid-β and intrinsic connectivity patterns were positively correlated in the default mode and several fronto-parietal attention networks, confirming that amyloid-β aggregates in areas of high intrinsic connectivity on a within-network basis. Further, we saw an internetwork gradient of the magnitude of correlation that depended on network plaque-load. After accounting for this globally positive correlation, local amyloid-β-plaque concentration in regions of high connectivity co-varied negatively with intrinsic connectivity, indicating that amyloid-β pathology adversely reduces connectivity anywhere in an affected network as a function of local amyloid-β-plaque concentration.

Received December 10, 2013. Revised March 3, 2014. Accepted March 15, 2014. Advance Access publication April 26, 2014

The local negative association between amyloid-β and intrinsic connectivity was much more pronounced than conventional group comparisons of intrinsic connectivity would suggest. Our findings indicate that the negative impact of amyloid-β on intrinsic connectivity in heteromodal networks is underestimated by conventional analyses. Moreover, our results provide first within-patient evidence for correspondent patterns of amyloid-β and intrinsic connectivity, with the distribution of amyloid-β pathology following functional connectivity gradients within and across intrinsic networks.

Keywords: Alzheimer's disease; amyloid-β plaques; intrinsic connectivity; resting-state functional MRI; PiB-PET

Abbreviations: ATN = attention network; DMN = default mode network; PiB = Pittsburgh compound B

Introduction

Alzheimer's disease is tightly associated with amyloid-β pathology. Aberrant clearance of amyloid-β precursor protein is thought to be a critical initial event in the disease's pathogenesis, leading to amyloid-β peptide accumulation and plaque formation 20 to 30 years before cognitive symptoms arise (Selkoe, 2002; Jack *et al*., 2010; Bateman *et al*., 2012). Typically, the deposition of plaques has been associated with the default mode network (DMN; Buckner *et al*., 2005; Sperling *et al*., 2009), a set of frontal and parietal midline structures with high metabolic activity that are coupled through high intrinsic functional connectivity (i.e. synchronous ongoing activity, where regions that are more strongly synchronized will exhibit higher connectivity). This association is mostly due to the apparent spatial overlap between the DMN and the average deposition of amyloid across the cortex (e.g. Buckner *et al*., 2005, 2009; Vlassenko *et al*., 2010; Mormino *et al*., 2011). The overlap has led to the proposal that in Alzheimer's disease; (i) amyloid-β-dependent neurodegeneration progresses along network boundaries, spreading to functionally connected areas rather than to spatially contiguous but less connected neighbours (He *et al*., 2008; Seeley *et al*., 2009; Bero *et al*., 2012; Zhou *et al*., 2012); and that (ii) amyloid-β pathology is accelerated by local stress caused by a lifetime of increased metabolism and intrinsic activity and connectivity (Greicius *et al*., 2004; Buckner *et al*., 2005, 2009; Bero *et al*., 2011; Drzezga *et al*., 2011). Given the widespread and well-known distribution of amyloid-β outside the DMN (Lehmann *et al*., 2013*a*, *b*; Sepulcre *et al*., 2013), and the well-characterized deficits in functional connectivity of other intrinsic networks covering heteromodal areas (Sorg *et al*., 2007; Brier *et al*., 2012; Li *et al*., 2012; see also Sorg *et al*., 2012), the latter point has been reformulated in a model that supposes effects of amyloid-β in hetermodal (i.e. fronto-parietal) functional networks in general (Jagust and Mormino, 2011). However, this revised model has not been empirically validated.

Critically, the observed spatial overlap implies two concurrent relationships between amyloid-β pathology and intrinsic connectivity. On the one hand, animal studies have linked amyloid-β to reduced intrinsic activity and connectivity (Busche *et al*., 2008; Bero *et al*., 2011), a finding that has been repeatedly corroborated in the human DMN (Sheline *et al*., 2010; Mormino *et al*., 2011; for a review see Sheline and Raichle, 2013). On the other hand, the spatial overlap also suggests the possibility of a more graded 'positive' relationship: wherever intrinsic connectivity is high, amyloid-β pathology tends to be high as well. This has been established for the spatial distribution of amyloid-β and intrinsic connectivity across subjects (Buckner *et al*., 2009; Drzezga *et al*., 2011; Bero *et al*., 2012), but should also apply intra-individually. However, most studies to date have observed these two relationships in isolation. This could have led to an overlooked confound: assume Patient X with particularly high lifetime (or baseline) intrinsic connectivity is prone to stronger amyloid-β plaque accumulation. In turn, the stronger accumulation leads to an increased reduction in connectivity. Compared to Patient Y with lower baseline connectivity (resulting in less plaque accumulation, with a less severe impact on connectivity), the higher baseline connectivity in Patient X could confound measures of that patient's amyloid-β-induced connectivity 'reduction', making them appear less severe than they are. By ignoring the initial positive baseline correlation between amyloid-β pathology and intrinsic connectivity, previous studies therefore may have underestimated the resulting 'negative' impact of amyloid-β on connectivity. As a consequence, connectivity reductions in amyloid-β-positive cohorts may only be robust enough to be noticeable once the accumulation is already substantial. This argument also applies to different brain areas: high lifetime connectivity in region X (compared to region Y) increases amyloid-β plaque accumulation, leading to a larger connectivity reduction (that is nevertheless masked by higher baseline connectivity). On average, the DMN seems to show the highest amyloid-β aggregation, making it the network in which amyloid-β-related connectivity reduction is easiest to detect. This could therefore lead to an overemphasis of this network in studying Alzheimer's disease, even though other networks are also affected.

Here, we addressed both of these issues using a novel methodological approach that for the first time attempts to disentangle the positive and negative relationship between amyloid-β and intrinsic connectivity within the same patient cohort. To this end, we used multimodal imaging that estimated regional plaque load [via Pittsburgh Compound B (PiB)-PET] and intrinsic connectivity (via resting-state functional MRI) in patients with prodromal Alzheimer's disease harbouring significant amyloid-β-plaque pathology and in healthy controls. The use of within-patient statistics was central to our approach for two reasons: for one, it would otherwise be impossible to disentangle negative and positive relationships. Additionally, it allowed us to confirm previous studies done in animal models (e.g. Bero *et al*., 2011, 2012) or using intrinsic connectivity estimates from healthy controls (e.g. Buckner *et al*., 2009, Seeley *et al*., 2009, Zhou *et al*., 2012) that may not necessarily replicate in patients (Huang and Mucke, 2012). In addition, we recruited a control group of healthy

persons without significant amyloid-β-plaque pathology. Although our within-subject approach does not strictly require a control group, we wanted to ensure that any effects do in fact depend on amyloid-β pathology. In the patient group, we found that the distributions of amyloid-β plaques and intrinsic networks within a number of heteromodal fronto-parietal networks are positively correlated, confirming a relationship that had previously been established only for the DMN. Critically, by taking this positive relationship into account, we found that our approach led to a substantial increase in the sensitivity of detecting the negative impact of amyloid-β pathology on intrinsic connectivity, compared to conventional group comparisons of connectivity.

Methods and materials

Participants

Twenty-four patients (10 female, age range 50–83 years) diagnosed with prodromal Alzheimer's disease (using standard diagnostic criteria, see below) and 16 healthy controls (nine female, age range 57–75 years) participated in the study (Table 1). All participants provided informed consent in accordance with the Human Research Committee guidelines of the Klinikum Rechts der Isar, Technische Universität, München. Patients were recruited from the Memory Clinic of the Department of Psychiatry, and controls by word-of-mouth advertising. Examination of every participant included medical history, neurological examination, informant interview (Morris, 1993), neuropsychological assessment by the neuropsychological assessment battery of the Consortium to Establish a Registry for Alzheimer's disease (CERAD, Morris *et al*., 1989), structural MRI and PiB-PET. Prodromal Alzheimer's disease has recently been defined by the coincidence of both mild cognitive impairment and the presence of at least one of five supportive biological signs for Alzheimer's disease, such as medial temporal lobe atrophy or significant PiB uptake (Dubois *et al*., 2007). Criteria for mild cognitive impairment include reported and neuropsychologically assessed cognitive impairments, largely intact activities of daily living, and excluded dementia (Gauthier *et al*., 2006). Patients in our study met criteria for mild cognitive impairment and demonstrated significant cortical PiB-uptake (i.e. they were PiB-positive). We used a cut-off for 'high' or 'low' neocortical standardized uptake value ratios of 1.15, consistent with cut-off values used in previous PiB-PET studies (Drzezga *et al*., 2011). Patients with high PiB binding (i.e. standardized uptake ratio $\geqslant$1.15) were classified as PiB-positive and those with standardized uptake ratio $<$1.15 were classified as PiB-negative, which was an inclusion criterion for healthy control subjects (see Supplementary material and Supplementary Fig. 4). Standardized PiB-uptake is measured for a pre-established large cortical volume of interest including lateral prefrontal, parietal, and temporal areas and the retrosplenial cortex (Hedden *et al*., 2009; Drzezga *et al*., 2011). Exclusion criteria for entry into the study were other neurological, psychiatric or systemic diseases (e.g. stroke, depression, alcoholism), or clinically remarkable structural MRI (e.g. stroke lesions) potentially related to cognitive impairment. Fifteen patients and eight healthy control subjects were treated for hypertension (beta-blockers, ACE-inhibitors, and calcium channel blockers), and seven patients and five healthy control subjects were treated for hypercholesterolaemia (statins). Two patients had diabetes mellitus, four patients received antidepressant medication (mirtazapine, citalopram), and no patient received cholinesterase inhibitors.

All participants underwent both MRI and PET imaging sessions. The MRI session included structural MRI and resting-state functional MRI acquisition. PET and MRI sessions were conducted within 3.7 (±2.5) months for patients, and within 8 (±3.1) months for healthy controls. One patient and four control participants were excluded from further analysis because of corrupted PET data, resulting in all analyses being conducted on 23 patients and 12 healthy control participants.

Table 1 Demographic and clinical-neuropsychological data

	Groups	
	Patients	Controls
n	23	12
Age	69.3 (7.4)	63.8 (5.15)*
Gender (F/M)	9/14	9/5
CDR global	0.5 (0)	0 (0)*
CDR-SB	1.6 (0.5)	0 (0)*
CERAD total	66.3 (10.8)	88.1 (6.8)*

CDR = Clinical Dementia Rating; CDR-SB = CDR sum of boxes; CERAD = neuropsychological assessment battery of the Consortium to Establish a Registry for Alzheimer's disease; CERAD-total = summary of CERAD subtests; group comparisons: χ^2 (gender), two-sample *t*-test (age, CDR global, CDR-SB, CERAD-total).
*Significant group difference with $P < 0.05$.

Pittsburgh Compound B-positron emission tomography imaging and data analysis

PET-imaging with *N*-methyl-^{11}C-2-(4-methylaminophenyl)-6-hydroxybenzothiazole (Pittsburgh Compound B) and data analysis followed standard protocols as described in a previous study (Mosconi *et al*., 2008). All participants were injected with 370 MBq ^{11}C-PiB at rest before entering the scanner 30 min later. Forty minutes post-injection, three 10-min frames of data acquisition were started and later summed into a single frame (40–70 min). Acquisition was performed using a Siemens ECAT HR+ PET scanner (CTI) in 3D mode and a transmission scan was carried out subsequently to allow for later attenuation correction.

The first step of imaging data analysis consisted of image reconstruction, correction of dead time, scatter and attenuation. Statistical parametric mapping software (SPM 5, Wellcome Department of Cognitive Neurology, London, UK) was used for image realignment, transformation into standard stereotactic space (MNI PET template), smoothing and statistical analysis (Mosconi *et al*., 2008). For the spatial transformation of PiB data, standardized uptake value images (40–70 min post injection) were co-registered to each individual's volumetric MRI and then

automatically spatially normalized to the MNI-template in SPM5 using warping parameters derived from previous individual structural MRI normalization (Mosconi *et al*., 2008). For each subject, all voxel values were normalized to the cerebellar vermis. Additionally, images were smoothed (Gaussian kernel of 10 mm × 10 mm × 10 mm) for the group comparisons. For the regression and searchlight analyses, we used unsmoothed PET images. Whole brain voxel-wise group comparisons (two-sample *t*-test) were performed with a threshold of $P < 0.0001$ uncorrected and k = 100.

Magnetic resonance imaging data acquisition and analysis

MRI was performed on a 3 T whole body MR scanner (Achieva) using an 8-channel phased-array head coil. For co-registration, T_1-weighted anatomical data were obtained from each participant using a MPRAGE sequence (echo time = 4 ms, repetition time = 9 ms, inversion time = 100 ms, flip angle = 5°, field of view = 240 × 240 mm^2, matrix = 240 × 240, 170 slices, voxel size = 1 × 1 × 1 mm^3). Functional MRI data were collected using a gradient echo echo planar imaging sequence (echo time = 35 ms, repetition time = 2000 ms, flip angle = 82°, field of view = 220 × 220 mm^2, matrix = 80 × 80, 32 slices, slice thickness = 4 mm, and 0 mm interslice gap, 300 volumes).

For each participant the first three functional scans of each functional MRI session were discarded because of magnetization effects. SPM5 (Wellcome Department of Cognitive Neurology, London) was used for data preprocessing. First, we used affine coregistration (to the first image) to motion-correct the resting-state functional MRI data. We observed no excessive head motion (i.e. cumulative translation or rotation >3 mm or 3° and mean point-to-point translation or rotation >0.15 mm or 0.1°). Framewise displacement (Power *et al*., 2012) or the root-mean-square of translational parameters (Van Dijk *et al*., 2012) were not different between groups ($P > 0.05$, two-sample *t*-tests). Further, groups yielded no significant differences in signal-to-noise ratio of functional MRI data ($P > 0.05$). The high-resolution structural image was coregistered to the mean functional MRI image (using affine registration), and normalized to a template in the stereotactic space of the Montreal Neurological Institute (MNI) with the 'segment' function (SPM5), which uses an iterative combination of non-linear registration and cortical segmentation (Ashburner and Friston, 2005). Normalization was then applied to the functional images before smoothing with an 8 × 8 × 8 mm^3 Gaussian kernel.

As described previously (Sorg *et al*., 2013), the preprocessed data were decomposed into spatially independent components reflecting intrinsic networks in a group-independent component analysis framework (Calhoun *et al*., 2001), which is implemented in the GIFT software (http://icatb.sourceforge.net). Our independent component analysis approach consisted of a series of well-established analysis steps (Kiviniemi *et al*., 2003; Erhardt *et al*., 2011). We estimated data dimensionality using a minimum description length criterion, which gave an estimate of 35 components (the mean of all individual dimensionality estimates). Data from all participants were temporally concatenated into one data set. The estimation of independent component analysis across both groups was in line with previous research (e.g. Filippini *et al*., 2009) and ensured a better correspondence of network maps between groups. Concatenated data were reduced by two-step principal component analysis to reduce computational burden. Principal component analysis was followed by independent component analysis with the infomax-algorithm. We ran 40 independent component analyses (ICASSO) to ensure stability of the estimated components. This results in a set of averaged group components, which are then back-reconstructed into single-subject space. For each subject, each component was represented as a combination of a network time course and a spatial map of *z*-scores. The *z*-map reflects the component's functional connectivity pattern (i.e. the mixing weights) across the brain. Voxels whose time courses are highly correlated with the component time course receive high connectivity *z*-scores, whereas voxels that are not part of the network have *z*-scores near 0.

Following previous findings of aberrant medial and lateral heteromodal frontoparietal networks in early Alzheimer's disease (Sorg *et al*., 2007, 2009; Neufang *et al*., 2011; Agosta *et al*., 2012), the DMN and so-called attentional networks were of *a priori* interest (Allen *et al*., 2011). To automatically select networks of interest, we applied multiple spatial regression analyses of the 35 independent components on masks derived from a previous study (Allen *et al*., 2011): the anterior and posterior DMN [aDMN IC 25, pDMN IC 53 of Allen *et al*. (2011)], attentional networks (ATN; right ATN IC 60, left ATN IC 34, dorsal ATN IC 72, salience network SN IC 55), and, as a control, a network around the primary auditory cortex (pAN; IC 17). Masks were generated with the WFU-Pickatlas (http://www.fmri.wfubmc.edu/).

To evaluate statistically the spatial z-maps of selected components, we calculated voxel-wise one-sample *t*-tests on participants' reconstructed spatial maps for each group, using SPM5 ($P < 0.05$, family wise error (FWE) corrected at cluster level, voxel-level height threshold $P < 0.001$). To analyse group differences, corresponding spatial z-maps were entered into two-sample *t*-tests, restricted to appropriate one-sample *t*-test masks ($P < 0.01$ uncorrected, calculated prior to group comparison) across all subjects ($P < 0.05$, FWE cluster level, voxel-level height threshold $P < 0.001$). As a more conservative test of group differences, for each subject and network we also identified all network voxels (as voxels with a connectivity z-score >1) and calculated the median (log-transformed) z-score across the entire network. Resulting network connectivity scores were then submitted to two-way mixed-effects ANOVA with factors group and network.

Multimodal analyses

Figure 1 gives an overview of our multimodal analysis approach. In a first step, we analysed the extent of PiB-uptake in the different intrinsic networks. For each subject and network, we identified all voxels belonging to the network (i.e. with a *z*-scored connectivity weight of ⩾1 in the individual back-projected maps). We then calculated (for each subject) the median PiB-uptake across all

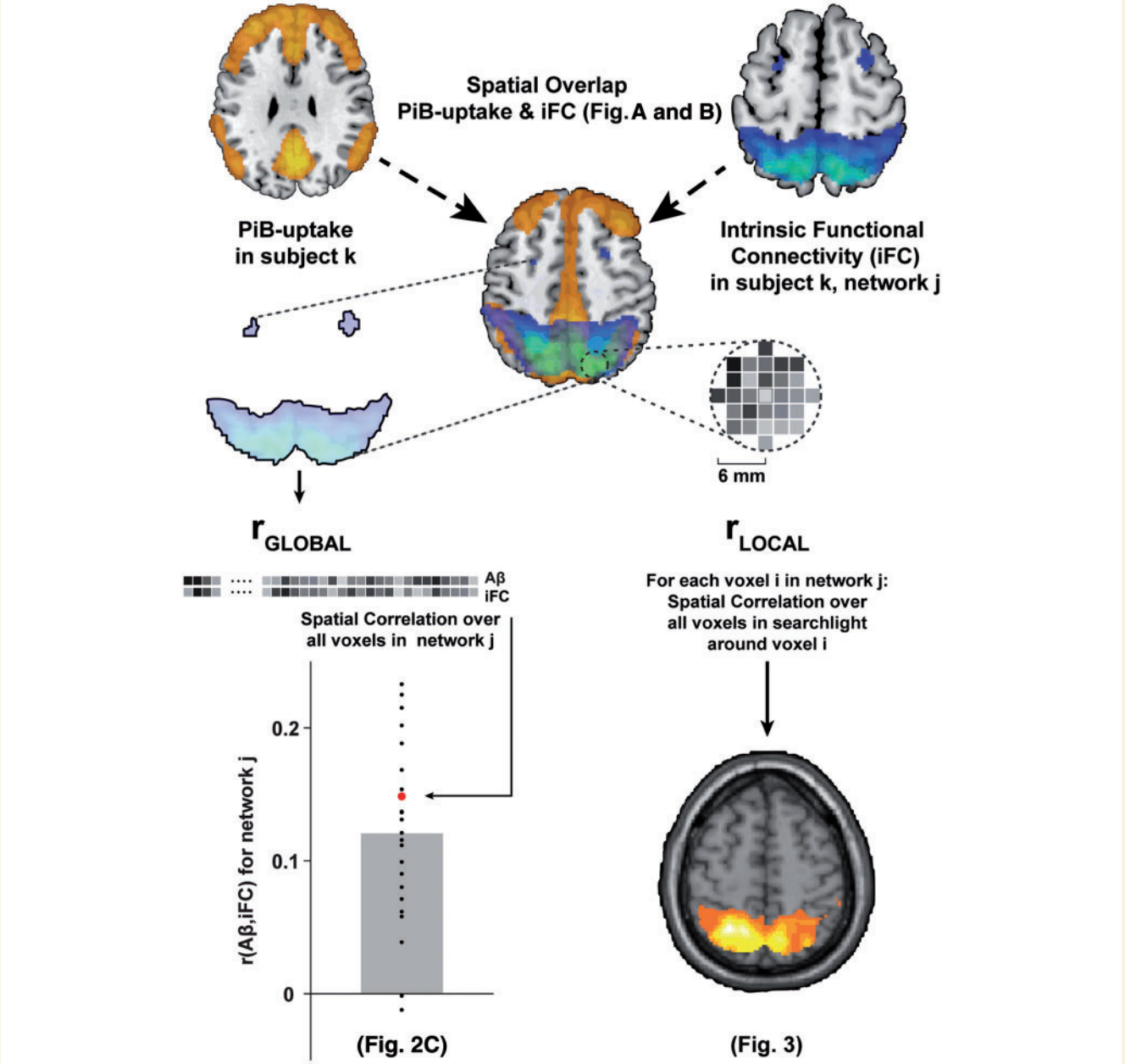

Figure 1 Overview of analysis approach. For each individual, voxel-wise PiB-uptake was determined as a measure of amyloid plaque density. For each intrinsic network j (as determined by resting-state functional MRI and independent component analysis independent component analysis) in each individual k, we identified the voxels belonging to that network (*top right*) and extracted the intrinsic functional connectivity (iFC) values of those (~10 000) voxels. We also extracted that individual's PiB-uptake values for the same voxels. To determine average plaque load in each network, we then calculated the median PiB-uptake (shown in Fig. 2A and B). We then calculated global and local correlations between both modalities across the entire network and confined to neighbouring voxels. To determine the global spatial correlation between intrinsic functional connectivity and PiB-uptake, we calculated the Pearson correlation coefficient across all selected voxels in the network (r_{GLOBAL}, *bottom left* and Fig. 2C). After correcting for r_{GLOBAL} (via orthogonalization, see 'Materials and methods' section), we then used a searchlight approach to calculate local spatial correlation in the neighborhood surrounding each voxel in the network (r_{LOCAL}, *bottom right* and Fig. 3). Aβ = amyloid-β.

voxels in the network. To control for the potential effects of network-wise grey matter density, age or gender, we then regressed these variables out of the median PiB data (Supplementary material, Supplementary Fig. 2 and Supplementary Table 8). For each network and separately for each group, we fit to the median PiB values a linear model consisting of three regressors: median grey matter density (in that network), age and gender. None of the three covariates had a notable effect on PiB-uptake (or on r_{GLOBAL} or r_{LOCAL}, see below). We subtracted model-predicted PiB values from the real data to obtain residuals that were independent of

the three covariates. These residual PiB values were evaluated with a mixed between- and within-subject effects ANOVA (with factors group (patient/control) and network) and *post hoc* two-sample *t*-tests.

Next, we tested for spatial correlations between PiB-uptake and network connectivity across the entire network (r_{GLOBAL}). Again, for each subject and network we identified network voxels as all voxels with a connectivity z-score >1. For all voxels, we extracted PiB-uptake and connectivity values. We log-transformed connectivity values to reduce the skew in their distribution, which was induced by including only values >1 (although analyses using untransformed connectivity values gave qualitatively and statistically comparable results). For each subject and network, we calculated the Pearson correlation coefficient between PiB-uptake and connectivity *z*-values, and Fisher-transformed the resulting r-values. The resulting r_{GLOBAL} values were again (as with PiB-uptake, above) corrected for grey matter density, age, and gender, and the residuals were submitted to a mixed-effects ANOVA and *post hoc* *t*-tests (as above).

To investigate the local impact of amyloid-β pathology on intrinsic connectivity, we used local spatial correlations between PiB-uptake and connectivity (r_{LOCAL}) via a searchlight approach. Searchlight approaches (Kriegeskorte *et al*., 2006) are multivariate analysis methods that step through all voxels of interest in sequence (in our case, all voxels in a given network) and examine voxel values in a 'searchlight' region of interest surrounding the current voxel. The measure of interest is then recorded in that voxel, resulting in a spatial map of local multivariate measures. We again identified the same set of voxels for each subject and network. As for this analysis we were explicitly interested in local variability between PiB-uptake and connectivity that was not already accounted for by the global positive correlation (r_{GLOBAL}), we first decorrelated PiB-uptake and connectivity values across the whole network. To this end (see Supplementary Fig. 3), we used Gram-Schmidt orthogonalization to decorrelate PiB uptake with respect to connectivity *z*-values across the entire network (ensuring a network correlation of 0). This approach has been used to remove zero-lag correlations when connectivity is calculated in magnetoencephalographic data (see Brookes *et al*., 2011; Hipp *et al*., 2012). As orthogonalization is an asymmetric operation (modifying one vector while leaving the other unchanged), we repeated the orthogonalization and subsequent searchlight analysis, but this time decorrelating connectivity *z*-values with respect to PiB-uptake. The searchlight results of the two analyses were then averaged.

Next, for each voxel in the network, we identified all voxels in its immediate neighbourhood (i.e. within a 6-mm radius, typically ~100 voxels). To avoid unreliable estimates of r_{LOCAL} at network boundaries, all voxels with less than 25 voxels in their neighborhood were skipped. Then we calculated the Pearson correlation between PiB-uptake and connectivity *z*-values in that neighbourhood, and recorded the (Fisher-transformed) correlation coefficient in the neighbourhood's central voxel, resulting in a spatial map of r_{LOCAL} values for each subject and network. For each group and network, we submitted these maps to one-sample *t*-tests using SPM. In addition, for each subject and network we extracted the median r_{LOCAL} value across all voxels, and submitted the corrected values (after regressing out covariates of no interest) to a mixed-effects ANOVA and *post hoc* *t*-tests (as above).

Results

Reduced intrinsic connectivity in the default mode and right attention networks in patients with prodromal Alzheimer's disease

Using independent component analysis of resting-state functional MRI data, we identified six fronto-parietal heteromodal networks (Fig. 2 and Supplementary Fig. 1). These networks included the posterior and anterior DMN, the left, right and dorsal attention networks (all covering the lateral parietal and prefrontal cortex), and the fronto-limbic salience network, covering the insula and anterior cingulate cortex. As a control, we also selected a primary sensory network (the primary auditory network). Group comparisons revealed regionally reduced *z*-scored connectivity values in the prodromal Alzheimer's disease group (two-sample *t*-tests, $P < 0.05$ FWE cluster corrected for multiple comparisons) only in posterior parietal regions of the posterior DMN and right attention networks, replicating previous results (e.g. Sorg *et al*., 2007; see Supplementary Fig. 1).

Pittsburgh Compound B uptake in prodromal Alzheimer's disease extends to lateral fronto-parietal attention network

In patients with prodromal Alzheimer's disease, we found significantly increased PiB-uptake (compared to controls) in a large number of cortical regions, including areas of the DMN, but extending to the lateral parietal and frontal lobes (Fig. 2A), corresponding well with characteristic distribution patterns previously described in patients with Alzheimer's disease and mild cognitive impairment (Drzezga *et al*., 2011).

Next, we tested quantitatively how PiB-uptake overlaps with intrinsic connectivity networks. We extracted the median PiB-uptake in each of these networks. After correcting for grey matter density, age and gender, we compared the network-wise PiB-uptake between prodromal Alzheimer's disease and control subjects (with ANOVA and two-sample *t*-tests). As already suggested by visual inspection (Fig. 2A), the patient group had significantly increased PiB-uptake [Fig. 2B: main effect of group across seven networks, $F(1,33) = 23.94$, $P < 10^{-4}$]. Importantly, patients showed a gradient of plaque deposition across networks [$F(6,132) = 3.83$, $P = 0.001$], with the highest PiB-uptake in the posterior DMN [significantly increased compared to left ATN and right ATN, all $t(22) > 3.12$, corrected $P < 0.035$], and strong trends compared to anterior DMN [$t(22) = 2.95$, corrected $P = 0.052$], and to posterior auditory cortex network [$t(22) = 2.77$, corrected $P = 0.078$].

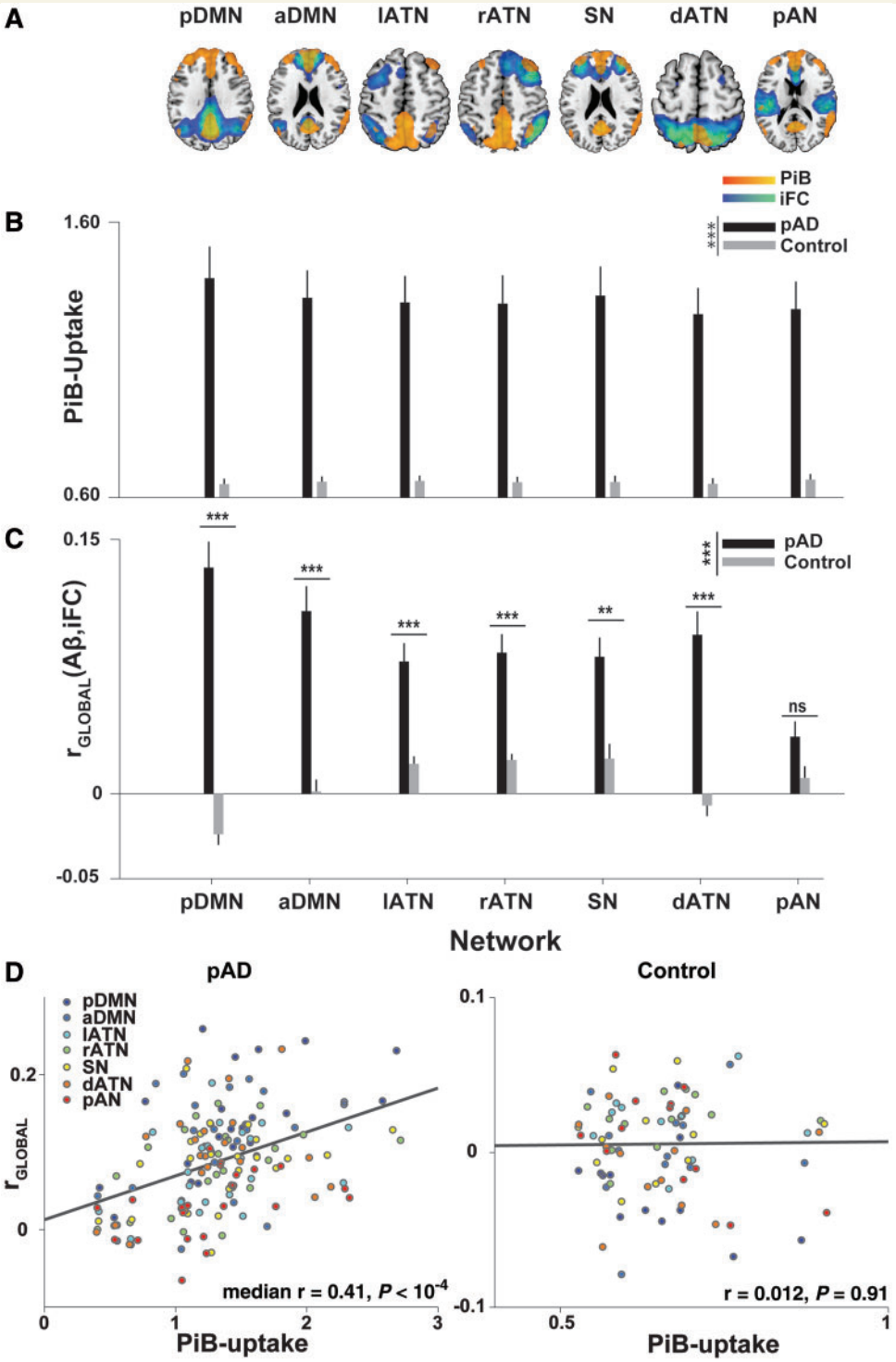

Figure 2 Amyloid-β deposition is increased in a number of heteromodal networks and correlates with intrinsic functional connectivity. (**A**) Each image shows a group-level intrinsic functional connectivity (iFC) network map (cold colours) at a FWE-corrected threshold of $P < 0.05$, superimposed on the group-level difference map in amyloid-β deposition (warm colors), thresholded at $P < 0.0001$, minimum cluster extent of 100 voxels. The pattern of amyloid-β (Aβ) deposition overlaps noticeably with a number of fronto-parietal networks (lATN = left lateral frontoparietal ATN; rATN = right frontoparietal ATN; dATN = posterior parietal dorsal ATN; SN = salience network) besides the DMN [split into a posterior (pDMN) and anterior (aDMN) component], and even with regions of primary sensory cortex, such as the primary auditory network (pAN). Notably, in some networks amyloid-β plaque deposition appears limited to network hubs (as in the left ATN and dorsal ATN, where frontal network regions lack significant amyloid-β burden at the group level). (**B**) Patients showed significantly increased PiB-uptake in all tested networks [main effect of group across seven networks, $F(1,33) = 22.11$, $P < 10^{-4}$]. There was also a main effect of network that interacted with group [main effect of network for patient group, $F(6,132) = 5.37$, $P < 10^{-4}$],

(continued)

Spatial patterns of Pittsburgh compound B uptake correlate positively with those of intrinsic connectivity in default mode and attention networks

After confirming the presence of amyloid-β-pathology in a number of fronto-parietal networks, we examined the relationship between amyloid-β-pathology and intrinsic connectivity. For each network and subject, we calculated the spatial correlation coefficient between PiB-uptake and connectivity-reflecting z-values over all network voxels, i.e. $r_{GLOBALiFC}$ [amyloid-β, intrinsic functional connectivity (iFC)] (see Supplementary Fig. 5 for a representative scatterplot of voxel-wise PiB-uptake against connectivity in one patient). For each network (except the auditory network, posterior AN), we found a modest but robust positive correlation between amyloid-β and connectivity in patients [Fig. 2C, main effect of group, $P < 10^{-7}$, mean correlation coefficients ranging from 0.134 (posterior DMN) to 0.078 (left ATN), corrected $P < 0.002$ in all networks except for the auditory network, mean $r = 0.034$, $t(33) = 2.26$, non-significant]. Correlations in the control group did not deviate from 0 (mean $r < \pm 0.024$, $P = 0.136$).

In analogy to the observed gradient in PiB-uptake across networks (Fig. 2A and B), we found a gradient of r_{GLOBAL} across networks [$F(6,132) = 10.72$, $P < 10^{-7}$] as the six default and attention networks showed a stronger r_{GLOBAL} than the auditory network [all $t(22) > 3.45$, corrected $P < 0.014$]. r_{GLOBAL} was also stronger in the pDMN than in any of the other networks except the aDMN [all $t(22) > 3.31$, corrected $P < 0.019$, paired t-test between posterior DMN and anterior DMN, $t(22) = 1.81$, uncorrected $P = 0.084$]. Finally, average PiB-uptake was positively correlated with r_{GLOBAL} in patients, but not in controls (Fig. 2D, posterior DMN in patients, $r = 0.64$, $P < 0.01$, median $r = 0.47$ for patients, median $r = 0.06$ for control subjects). In contrast, r_{GLOBAL} did not correlate with mean intrinsic connectivity in any network of either group (all uncorrected $P > 0.12$), indicating that the correlation was mainly driven by variability in PiB-uptake.

In network cores of higher connectivity, amyloid-β pathology has a negative impact on functional connectivity

Next we focused on the concomitant 'negative' impact of amyloid-β load in local network regions: specifically, after accounting for the variability in amyloid-β-pathology that is attributable to r_{GLOBAL}, the neurotoxic effects of higher pathology should lead to a 'relative decrease' in intrinsic connectivity, especially in network cores with high connectivity (where amyloid-β pathology presumably has been accumulating for longer; Bero *et al.*, 2012). To account for the diluting effects of r_{GLOBAL}, we regressed out the impact of intrinsic connectivity on plaque deposition at the whole-network level and used a searchlight approach to calculate the local spatial correlation of the residuals around each voxel (see Fig. 1); we called this measure r_{LOCAL}(Aβ,iFC) to indicate that here we calculated correlations in small (6-mm radius), homogeneous neighbourhoods around each voxel (in every network and subject), yielding a local measure of amyloid-β pathology impact that could potentially vary 'within' networks.

In patients (Fig. 3A), all networks except for the pAN showed significant negative r_{LOCAL} across large parts of the network, peaking in network cores. For example, in the dorsal attention network (Fig. 3A), r_{LOCAL} was significantly below zero in the superior parietal core of the network, but not strongly negative in peripheral regions such as the frontal eye fields (compare to network distribution in Fig. 2A or Supplementary Fig. 1). r_{LOCAL} did not deviate from 0 in the control group (Fig. 3A). In addition to comparing voxel-wise maps, we also examined the median r_{LOCAL} values across all voxels in a network (Fig. 3B). r_{LOCAL} was significantly below 0 for all networks [all $t(22) < -6.73$, corrected $P < 10^{-5}$] except the auditory network [$t(22) = -0.04$]. Direct comparisons between patients and controls revealed a strong main effect of group [$F(1,33) = 44.21$, $P < 10^{-6}$, all $t(33) < -3.65$, corrected $P < 0.006$], with the exception of the posterior auditory network, which showed no difference in median r_{LOCAL} [$t(33) = 0.68$, non-significant]. As suggested by the spatial distribution of r_{LOCAL} in Fig. 3A, we also found a correlation between PiB-uptake and r_{LOCAL}. In other words, local regions with higher amyloid-β pathology overall (where plaques have presumably been accumulating

Figure 2 Continued
indicating that there is a gradient of amyloid-β deposition across networks in patients. (**C**) A number of networks in the patient group exhibited a positive network-wide correlation between voxel-wise intrinsic functional connectivity and voxel-wise PiB-uptake (i.e. r_{GLOBAL}), indicating that voxels in the network core (i.e. voxels with high intrinsic functional connectivity) were burdened with higher amyloid-β deposition than the network periphery (voxels with low intrinsic functional connectivity). This correlation was modest in magnitude but consistently positive [main effect of group, $F(1,33) = 47.19$, $P < 10^{-7}$, t-tests of Fisher-transformed Pearson correlation coefficients against control group, all $t(33) > 3.61$, Bonferroni-corrected $P < 0.01$, except for the auditory network, $t(33) = 1.87$, non-significant]. Correlations in the control group were negligible. There was a gradient of correlation strength across networks as the six default and attention networks showed a stronger correlation than the posterior auditory network. Also, the amyloid-β–intrinsic functional connectivity correlation was stronger in the posterior DMN than in any of the other networks except the anterior DMN. Error bars indicate standard error of the mean. $***P < 0.001$, $**P < 0.01$, $*P < 0.05$, all Bonferroni-corrected, ns = not significant. (**D**) Median PiB-uptake is positively correlated with r_{GLOBAL} in patients (*left*), but not in controls (*right*). Each point in the scatter plot represents one network in one individual, with network identity denoted by colour. The regression lines are derived from a linear fit across all individuals and networks in each group. Nevertheless, correlations were also performed separately for each network.

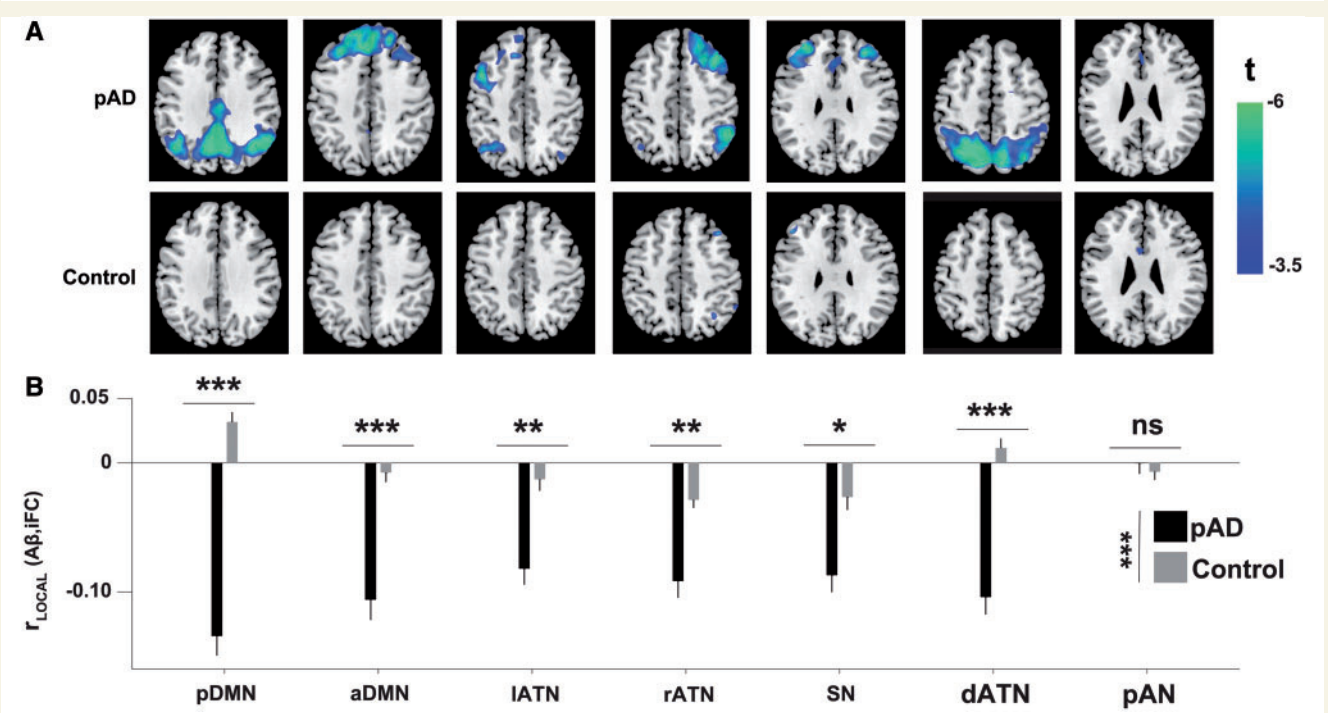

Figure 3 Local negative impact of amyloid-β on intrinsic connectivity. (**A**) Searchlight analysis demonstrated negative correlations between amyloid-β plaques (Aβ) and intrinsic functional connectivity (iFC) in small neighbourhoods with generally homogeneous connectivity strength. After accounting for the impact of intrinsic functional connectivity on PiB-uptake across an entire network (i.e. r_{GLOBAL} described in Figs 1B and 2) through orthogonalization, we calculated at each network voxel the local amyloid-β–intrinsic functional connectivity (Aβ,iFC) correlation r_{LOCAL} across surrounding voxels in a 6-mm radius. For each group, we submitted the subject-level maps of correlation coefficients to *t*-tests, using FWE to correct for multiple comparisons. In the prodromal AD group (*top*), all networks except for the auditory network (pAN) showed significant negative r_{LOCAL} across large parts of the networks, focusing on network hubs. There were no such correlations in the control group (*bottom*). Colour scale indicates *t*-statistics at the group level. A *t*-value of 3.5 corresponds to $P = 0.001$, uncorrected. (**B**) In patients, median r_{LOCAL} values were significantly below 0 for all networks except the auditory network. The control group showed no significant correlations. Hence, direct comparisons between patients and controls revealed a strong main effect of group [$F(1,33) = 43.25$, $P < 10^{-6}$, all $t(33) < -3.17$, corrected $P < 0.025$], with the exception of the auditory network, which showed no difference in median r_{LOCAL} [$t(33) = 0.54$, ns]. Error bars indicate standard error of the mean. a/pDMN = anterior/posterior DMN; l/r/dATN = left/right/dorsal ATN; SN = salience network.

for longer and may have had a stronger connectivity-reducing effect on neurons) also exhibit a stronger negative impact of amyloid-β pathology on connectivity (Supplementary Fig. 3). Together, our results show that after accounting for the globally positive relationship between amyloid-β and intrinsic connectivity, local neighbourhoods exhibit a strong negative influence of plaques on connectivity, even in networks where typical estimates do not yet indicate connectivity reductions (see Supplementary Fig. 1 and Supplementary Tables 1–7 for direct comparisons of connectivity between groups).

Control analyses

Finally, we tested whether either differences in group size or any methodological steps (such as orthogonalization of PiB-uptake and intrinsic connectivity) could have influenced our results. To control for the difference in group size, we used a subsampling approach that repeatedly selects a random subgroup of patients, matched in size with the control group, and re-computed statistics for this smaller, matched data set (Supplementary material and Supplementary Table 9). All relevant comparisons remained significant (with the exception of r_{GLOBAL} and r_{LOCAL} in the salience network and left ATN, and r_{LOCAL} in right ATN, which nevertheless are highly significant at an uncorrected threshold). Further, control analyses (e.g. concerning orthogonalization, see Supplementary material and Supplementary Fig. 3) showed that negative r_{LOCAL} does not depend on specific steps of our analysis approach.

Discussion

In patients with prodromal Alzheimer's disease, spatial correlations revealed two distinct effects of PiB-uptake on intrinsic connectivity within individual persons and in several heteromodal intrinsic networks. First, at the global network level, patterns of amyloid-β plaques correspond spatially with patterns of connectivity, with the highest correlation in networks carrying the highest plaque load. Second, at the local network level, plaques are negatively associated with connectivity, especially in regions of high connectivity. These results extend previous findings by demonstrating the

negative impact of amyloid-β pathology on intrinsic connectivity beyond the DMN and by showing a general pattern of correlations between plaques and connectivity within and across intrinsic networks.

In heteromodal intrinsic networks, patterns of plaques correspond with patterns of intrinsic connectivity

In several heteromodal fronto-parietal networks, including the DMN and lateral attention networks, we found within-patient spatial correlations between amyloid plaque distributions and intrinsic connectivity (Fig. 2C). We had anticipated this outcome, based on previous findings (at the group level) of positive correlations centred on the DMN (Buckner *et al*., 2009). This finding was specific for heteromodal networks, as we saw no effect in the primary auditory network (Fig. 2C). The dissociation between heteromodal and primary networks is in line with findings that primary sensory and sensorimotor regions are relatively spared in earlier stages of Alzheimer's disease (Braak and Braak, 1991). In all of the networks exhibiting a significant spatial correlation, patients with prodromal Alzheimer's disease had significant plaque load (Fig. 2A and B), with the highest load in the posterior DMN. Generally, the correlation between plaques and connectivity was higher in networks of higher median plaque load (Fig. 2C and D). Inclusion of control variables confirmed that these findings were not influenced by grey matter atrophy, age, or gender, and that they were specific to heteromodal networks, since we did not find comparable results in the primary auditory network (Fig. 2).

Our observations are in line with recent results by Drzezga *et al*. (2011), who found that patterns of both plaques and hubness (i.e. the average connectivity of any one region or voxel to the rest of the brain, irrespective of network boundaries; see also Buckner *et al*., 2005, 2009) overlap in patients with significant plaque load. These studies focused on effects in the DMN, as their methodological approach did not differentiate between networks and therefore emphasized areas with the highest hubness, which tend to be in the DMN. Here, we extended these studies by confirming that the plaque/connectivity correlation exists at the level of individual intrinsic heteromodal networks beyond the DMN, and by showing that it does not rely on network-unspecific hubness. Our finding provides strong evidence for the previously stated hypothesis (Jagust and Mormino, 2011) that high levels of connectivity in heteromodal areas are associated with increased levels of amyloid-β pathology, potentially due to nodal stress incurred by a lifetime of increased intrinsic activity (Bero *et al*., 2011).

Accounting for network level plaque–connectivity correlations reveals the widely distributed negative impact of amyloid-β pathology on intrinsic connectivity

After accounting for global plaque-connectivity correlations across a network, we found negative correlations (r_{LOCAL}, in small neighbourhoods of ~100 voxels) between the local plaque distribution and intrinsic connectivity in several heteromodal networks, particularly in regions of high intrinsic connectivity (Fig. 3). These negative correlations were stronger in networks of high plaque load (Supplementary Fig. 3), suggesting a detrimental impact of amyloid-β pathology on intrinsic connectivity. This finding is in line with results of previous studies, which found intersubject correlations between amyloid-β load and intrinsic connectivity in the DMN in individuals with significant plaque pathology (Hedden *et al*., 2009; Sheline *et al*., 2010; Mormino *et al*., 2011).

Our results extend these findings in two ways. First, we showed the negative impact of pathology on connectivity within single patients, instead of across patients. Second, we found significant results in heteromodal networks beyond the DMN. With respect to the latter point, our approach appears to be more sensitive than conventional methods used to detect connectivity reductions (Supplementary Fig. 1). Although our spatial correlation approach revealed strong and widespread effects in several networks, simple group comparisons of voxel-wise connectivity found reduced connectivity only in the posterior DMN and the right attention network (Supplementary Fig. 1). Control analyses (Supplementary Fig. 3 and Supplementary material) confirmed that removing the globally positive whole-network baseline correlation between plaques and connectivity is critical for this increase in sensitivity. Approaches that neglect baseline plaque/connectivity correlations potentially underestimate disease effects on intrinsic connectivity. Given that significant PiB-uptake is measurable in the DMN even in early preclinical stages of Alzheimer's disease (Jack *et al*., 2010; Bateman *et al*., 2012), where conventional measures of connectivity do not report robust connectivity reductions, the method presented here may help detect early, subtle reductions in connectivity. Future studies or reanalyses are necessary to test these suggestions.

Gradients of plaques along intrinsic connectivity across and within networks furnish an extended network degeneration model for Alzheimer's disease

Our results suggest a view of Alzheimer's disease that goes beyond previous models that focus on both the DMN and its associated amyloid-β-plaque accumulation while ignoring other intrinsic networks and the complex relationship between connectivity-mediated amyloid-β-increases on a network scale and local amyloid-β-mediated connectivity decreases. Although we confirmed that PiB-uptake and its effects on intrinsic connectivity were strongest in the posterior DMN (as measured both by r_{GLOBAL} and r_{LOCAL}; Figs 2 and 3), we focused on the well-known but somewhat neglected finding that, even in prodromal Alzheimer's disease, amyloid-β-plaques accumulate outside the DMN (Fig. 2A and B). We found that PiB-uptake was higher in the network core, where network connectivity (and, presumably, neural activity and metabolism) is higher than in the periphery. A speculative model (Fig. 4) summarizes our results and illustrates the graded (but temporally overlapping) effects of amyloid-β-pathology across networks (that are strongest in the posterior DMN, but robust in other networks as well).

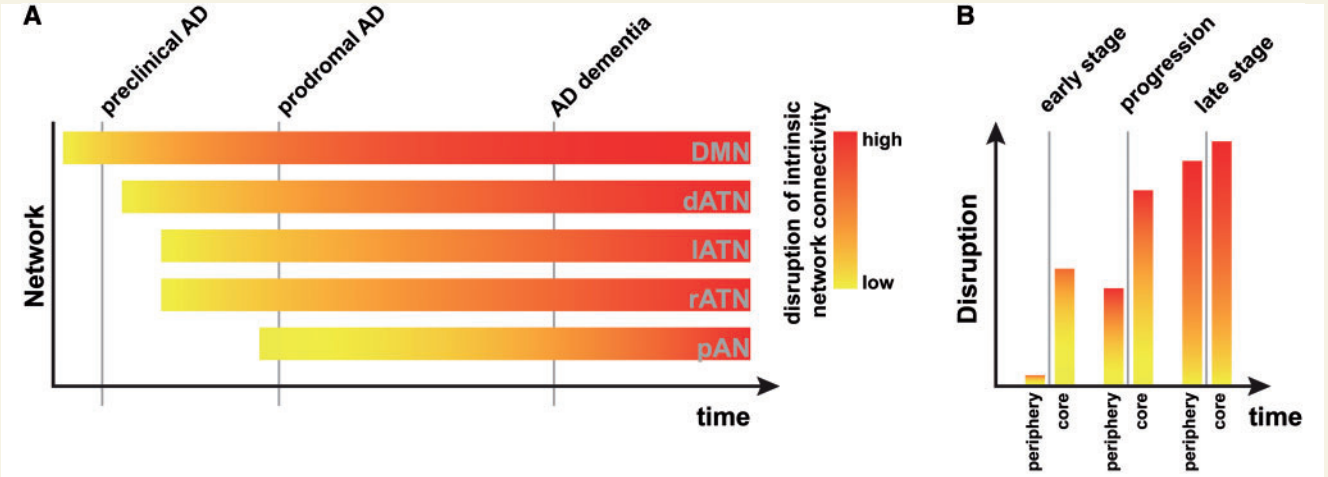

Figure 4 Proposed model of graded network degeneration. Graded network degeneration hypothesis of amyloid-β propagation in Alzheimer's disease (AD). *Left*: In spite of a predominant focus on amyoid-β pathology accumulation and spread along intrinsic connectivity in the DMN [*top* bar, with colour indicating the (putatively amyloid-related) connectivity decrease over time], amyloid-β plaques are also found in other cortical regions that typically have lower resting-state metabolism and connectivity than the DMN (e.g. left and right ATNs). In an average person with prodromal Alzheimer's disease, amyloid-β pathology deposition and connectivity-based spread will start in the DMN, followed in close succession by a number of other heteromodal networks, leading to a cross-network gradient (i.e. along the vertical grey lines cutting across networks). We propose that the same principle is at work 'within' networks (*right*), where the network core will accumulate amyloid-β and show signs of disruption sooner than areas in the periphery.

We propose that the within-network effects of amyloid-β-pathology will be similar in all affected networks (but possibly shifted in time depending on how early amyloid-β plaques aggregate in a particular network).

One speculative explanation for our findings is that in general, plaque accumulation follows connectivity (leading to the positive correlation). In addition, wherever plaque load is high, plaques have been accumulating longer, and have exerted a negative influence on local intrinsic activity and connectivity for longer. Viewed in this light, our findings are in line with animal and computational studies linking amyloid-β pathology to increased connectivity in early stages (i.e. increased r_{GLOBAL}) and decreased connectivity (i.e. negative r_{LOCAL}) in later stages of Alzheimer's disease (Bero *et al.*, 2012; de Haan *et al.*, 2012). In contrast with many previous models that describe the temporal staging of Alzheimer's disease as a fixed progression, our model acknowledges that some brain networks (and areas within those networks) will be affected by pathology before others. A hub within a network that was affected early on might already show neural effects reminiscent of late Alzheimer's disease, while at the same time another network might show only the neural effects associated with early Alzheimer's disease.

Importance of within-patient spatial correlations between Pittsburgh compound B uptake and connectivity scores

In contrast to previous studies, which tested amyloid-β-propagation models in healthy controls and compared them with patient atrophy data (Buckner *et al.*, 2009; Seeley *et al.*, 2009; Raj *et al.*, 2012; Zhou *et al.*, 2012), or which correlated amyloid-β plaques with DMN connectivity across subjects (Drzezga *et al.*, 2011), here we developed a methodological frame that allowed us to analyse the within-subject relationship between amyloid-β pathology and functional connectivity. Although the importance of animal models and connectivity measures in healthy subjects is unquestionable, it is essential to transfer findings from disease models to patients. For instance, mouse models show clear differences in amyloid-β aggregation and clearance compared with patients, and the effect of amyloid-β plaques on cognition is not necessarily comparable (Hall and Roberson, 2012; Huang and Mucke, 2012). By looking at within-subject-correlations, we can reduce the possibility that third variables (such as disease state in general) are mediating the correlation between amyloid-β and intrinsic connectivity. More importantly, it allows us to estimate the impact amyloid-β has had on functional connectivity at the single subject and single-network level. This increase in sensitivity compared to conventional measures of intrinsic connectivity may facilitate earlier detection of the functional impact of amyloid accumulation in incipient disease. In future studies, it may additionally help to differentiate patients with prodromal Alzheimer's disease from patients whose mild cognitive impairment was caused by another form of neurodegeneration. The correct differential diagnosis is an essential component of developing more sensitive biomarkers for the earliest stages of Alzheimer's disease. Nevertheless, this study was cross-sectional, and examined only the prodromal stage of Alzheimer's disease. Longitudinal studies are required to examine more carefully the temporal progression of network impairments that our model proposes, and to test whether the relationship between amyloid-β-pathology and intrinsic connectivity holds in later stages of the disease.

Conclusion and outlook

In this study, we show evidence that amyloid-β-plaques accumulating in medial and lateral heteromodal fronto-parietal networks in prodromal Alzheimer's disease have a robust impact on intrinsic functional connectivity at the local scale, and that their accumulation focuses on network cores and declines toward the periphery of networks. These results led us to an extension of the network degeneration hypothesis. It supposes that amyloid-β deposition and functional impairment spread by the same mechanism in many networks, but that the onset is graded such that it affects the DMN more strongly than others, and affects cores more strongly than (and possibly before) peripheries. Since our model predicts that the same mechanism governs amyloid-β-related neurodegeneration, irrespective of the affected network, it should also apply to other variants of Alzheimer's disease, such as posterior cortical atrophy or logopenic primary progressive aphasia (Lehmann *et al*., 2013*a*, *b*). In this framework, amyloid-β pathology would spread out by the same mechanism, but begin in different networks. Future studies examining this possibility could help in the development of mechanistic accounts of neurodegeneration.

Acknowledgements

The authors declare no commercial or other conflicts of interest. They also wish to thank Magdolna Tardy and Josette Höhn for assistance with data collection.

Funding

C.S. is supported by the Kommission für Klinische Forschung (KKF) of the Klinikum Rechts der Isar der Technischen Universität München grant 8765162, and German Federal Ministry of Education and Research (BMBF) grant 01ER0803. A.M.W. is supported by the BMBF grant 01EV0710. V.R. is supported by the KKF grant 8762754. N.M. is supported by the Wellcome Trust grant CQRTDY0.

Supplementary material

Supplementary material is available at *Brain* online.

References

Agosta F, Pievani M, Geroldi C, Copetti M, Frisoni GB, Filippi M. Resting state fMRI in Alzheimer's disease: beyond the default mode network. Neurobiol Aging 2012; 33: 1564–78.

Allen EA, Erhardt EB, Damaraju E, Gruner W, Segall JM, Silva RF, et al. A baseline for the multivariate comparison of resting-state networks. Front Syst Neurosci 2011; 5: 2.

Ashburner J, Friston KJ. Unified segmentation. Neuroimage 2005; 26: 839–51.

Bateman RJ, Xiong C, Benzinger TLS, Fagan AM, Goate A, Fox NC, et al. Clinical and biomarker changes in dominantly inherited Alzheimer's disease. N Engl J Med 2012; 367: 795–804.

Bero AW, Bauer AQ, Stewart FR, White BR, Cirrito JR, Raichle ME, et al. Bidirectional relationship between functional connectivity and amyloid-β deposition in mouse brain. J Neurosci 2012; 32: 4334–40.

Bero AW, Yan P, Roh JH, Cirrito JR, Stewart FR, Raichle ME, et al. Neuronal activity regulates the regional vulnerability to amyloid-β deposition. Nat Neurosci 2011; 14: 750–6.

Braak H, Braak E. Neuropathological stageing of Alzheimer-related changes. Acta Neuropathol 1991; 82: 239–59.

Brier MR, Thomas JB, Snyder AZ, Benzinger TL, Zhang D, Raichle ME, et al. Loss of intranetwork and internetwork resting state functional connections with Alzheimer's disease progression. J Neurosci 2012; 32: 8890–9.

Brookes MJ, Woolrich M, Luckhoo H, Price D, Hale JR, Stephenson MC, et al. Investigating the electrophysiological basis of resting state networks using magnetoencephalography. Proc Natl Acad Sci USA 2011; 108: 16783–8.

Buckner RL, Sepulcre J, Talukdar T, Krienen FM, Liu H, Hedden T, et al. Cortical hubs revealed by intrinsic functional connectivity: mapping, assessment of stability, and relation to Alzheimer's disease. J Neurosci 2009; 29: 1860–73.

Buckner RL, Snyder AZ, Shannon BJ, LaRossa G, Sachs R, Fotenos AF, et al. Molecular, structural, and functional characterization of Alzheimer's disease: evidence for a relationship between default activity, amyloid, and memory. J Neurosci 2005; 25: 7709–17.

Busche MA, Eichhoff G, Adelsberger H, Abramowski D, Wiederhold KH, Haass C, et al. Clusters of hyperactive neurons near amyloid plaques in a mouse model of Alzheimer's disease. Science 2008; 321: 1686–9.

Calhoun VD, Adalı T, Pearlson GD, Pekar JJ. Spatial and temporal independent component analysis of functional MRI data containing a pair of task-related waveforms. Hum Brain Mapp 2001; 13: 43–53.

de Haan W, Mott K, van Straaten ECW, Scheltens P, Stam CJ. Activity dependent degeneration explains hub vulnerability in Alzheimer's disease. PLoS Comput Biol 2012; 8: e1002582.

Drzezga A, Becker JA, Van Dijk KRA, Sreenivasan A, Talukdar T, Sullivan C, et al. Neuronal dysfunction and disconnection of cortical hubs in non-demented subjects with elevated amyloid burden. Brain 2011; 134: 1635–46.

Dubois B, Feldman HH, Jacova C, DeKosky ST, Barberger-Gateau P, Cummings J, et al. Research criteria for the diagnosis of Alzheimer's disease: revising the NINCDS–ADRDA criteria. Lancet Neurol 2007; 6: 734–46.

Erhardt EB, Rachakonda S, Bedrick EJ, Allen EA, Adali T, Calhoun VD. Comparison of multi-subject ICA methods for analysis of fMRI data. Hum Brain Mapp 2011; 32: 2075–95.

Filippini N, MacIntosh BJ, Hough MG, Goodwin GM, Frisoni GB, Smith SM, et al. Distinct patterns of brain activity in young carriers of the APOE-4 allele. Proc Natl Acad Sci USA 2009; 106: 7209–14.

Gauthier S, Reisberg B, Zaudig M, Petersen RC, Ritchie K, Broich K, et al. Mild cognitive impairment. Lancet 2006; 367: 1262–70.

Greicius MD, Srivastava G, Reiss AL, Menon V. Default-mode network activity distinguishes Alzheimer's disease from healthy aging: evidence from functional MRI. Proc Natl Acad Sci USA 2004; 101: 4637–42.

Hall AM, Roberson ED. Mouse models of Alzheimer's disease. Brain Res Bull 2012; 88: 3–12.

He Y, Chen Z, Evans A. Structural insights into aberrant topological patterns of large-scale cortical networks in Alzheimer's disease. J Neurosci 2008; 28: 4756–66.

Hedden T, Van Dijk KRA, Becker JA, Mehta A, Sperling RA, Johnson KA, et al. Disruption of functional connectivity in clinically normal older adults harboring amyloid burden. J Neurosci 2009; 29: 12686–94.

Hipp JF, Hawellek DJ, Corbetta M, Siegel M, Engel AK. Large-scale cortical correlation structure of spontaneous oscillatory activity. Nat Neurosci 2012; 15: 884–90.

Huang Y, Mucke L. Alzheimer mechanisms and therapeutic strategies. Cell 2012; 148: 1204–22.

Jack CR Jr, Knopman DS, Jagust WJ, Shaw LM, Aisen PS, Weiner MW, et al. Hypothetical model of dynamic biomarkers of the Alzheimer's pathological cascade. Lancet Neurol 2010; 9: 119–28.

Jagust WJ, Mormino EC. Lifespan brain activity, β-amyloid, and Alzheimer's disease. Trends Cogn Sci 2011; 15: 520–6.

Kiviniemi V, Kantola J-H, Jauhiainen J, Hyvärinen A, Tervonen O. Independent component analysis of nondeterministic fMRI signal sources. Neuroimage 2003; 19: 253–60.

Kriegeskorte N, Goebel R, Bandettini P. Information-based functional brain mapping. Proc Natl Acad Sci USA 2006; 103: 3863–8.

Lehmann M, Ghosh PM, Madison C, Laforce R, Corbetta-Rastelli C, Weiner MW, et al. Diverging patterns of amyloid deposition and hypometabolism in clinical variants of probable Alzheimer's disease. Brain 2013a; 136: 844–58.

Lehmann M, Madison CM, Ghosh PM, Seeley WW, Mormino E, Greicius MD, et al. Intrinsic connectivity networks in healthy subjects explain clinical variability in Alzheimer's disease. Proc Natl Acad Sci USA 2013b; 110: 11606–11.

Li R, Wu X, Fleisher AS, Reiman EM, Chen K, Yao L. Attention-related networks in Alzheimer's disease: a resting functional MRI study. Hum Brain Mapp 2012; 33: 1076–88.

Mormino EC, Smiljic A, Hayenga AO, Onami SH, Greicius MD, Rabinovici GD, et al. Relationships between beta-amyloid and functional connectivity in different components of the default mode network in aging. Cereb Cortex 2011; 21: 2399–407.

Morris JC. The Clinical Dementia Rating (CDR): current version and scoring rules. Neurology 1993; 43: 2412–14.

Morris JC, Heyman A, Mohs RC, Hughes JP. The consortium to establish a registry for Alzheimer's disease (CERAD): I. clinical and neuropsychological assessment of Alzheimer's disease. Neurology 1989; 39: 1159–65.

Mosconi L, Tsui WH, Herholz K, Pupi A, Drzezga A, Lucignani G, et al. Multicenter standardized 18F-FDG PET diagnosis of mild cognitive impairment, Alzheimer's disease, and other dementias. J Nucl Med 2008; 49: 390–8.

Neufang S, Akhrif A, Riedl V, Förstl H, Kurz A, Zimmer C, et al. Disconnection of frontal and parietal areas contributes to impaired attention in very early Alzheimer's disease. J Alzheimers Dis 2011; 25: 309–21.

Power JD, Barnes KA, Snyder AZ, Schlaggar BL, Petersen SE. Spurious but systematic correlations in functional connectivity MRI networks arise from subject motion. Neuroimage 2012; 59: 2142–54.

Raj A, Kuceyeski A, Weiner M. A network diffusion model of disease progression in dementia. Neuron 2012; 73: 1204–15.

Seeley WW, Crawford RK, Zhou J, Miller BL, Greicius MD. Neurodegenerative diseases target large-scale human brain networks. Neuron 2009; 62: 42–52.

Selkoe DJ. Alzheimer's disease is a synaptic failure. Science 2002; 298: 789–91.

Sepulcre J, Sabuncu MR, Becker A, Sperling R. *In vivo* characterization of the early states of the amyloid-beta network. Brain 2013; 136: 2239–52.

Sheline YI, Raichle ME. Resting state functional connectivity in preclinical Alzheimer's disease. Biol Psychiatry 2013; 74: 340–7.

Sheline YI, Raichle ME, Snyder AZ, Morris JC, Head D, Wang S, et al. Amyloid plaques disrupt resting state default mode network connectivity in cognitively normal elderly. Biol Psychiatry 2010; 67: 584–7.

Sorg C, Manoliu A, Neufang S, Myers N, Peters H, Schwerthoffer D, et al. Increased intrinsic brain activity in the striatum reflects symptom dimensions in schizophrenia. Schizophr Bull 2013; 39: 387–95.

Sorg C, Myers N, Redel P, Bublak P, Riedl V, Manoliu A, et al. Asymmetric loss of parietal activity causes spatial bias in prodromal and mild Alzheimer's disease. Biol Psychiatry 2012; 71: 798–804.

Sorg C, Riedl V, Mühlau M, Calhoun VD, Eichele T, Laer L, et al. Selective changes of resting-state networks in individuals at risk for Alzheimer's disease. Proc Natl Acad Sci USA 2007; 104: 18760–5.

Sorg C, Riedl V, Perneczky R, Kurz A, Wohlschläger AM. Impact of Alzheimer's disease on the functional connectivity of spontaneous brain activity. Curr Alzheimer Res 2009; 6: 541–53.

Sperling RA, LaViolette PS, O'Keefe K, O'Brien J, Rentz DM, Pihlajamaki M, et al. Amyloid deposition is associated with impaired default network function in older persons without dementia. Neuron 2009; 63: 178–88.

Van Dijk KRA, Sabuncu MR, Buckner RL. The influence of head motion on intrinsic functional connectivity MRI. Neuroimage 2012; 59: 431–8.

Vlassenko AG, Vaishnavi SN, Couture L, Sacco D, Shannon BJ, Mach RH, et al. Spatial correlation between brain aerobic glycolysis and amyloid-β (Aβ) deposition. Proc Natl Acad Sci USA 2010; 107: 17763–7.

Zhou J, Gennatas ED, Kramer JH, Miller BL, Seeley WW. Predicting regional neurodegeneration from the healthy brain functional connectome. Neuron 2012; 73: 1216–27.

Supplemental Materials for

"Within-patient correspondence of amyloid-β and intrinsic network connectivity in Alzheimer's disease"

by Myers et al.

Supplemental Methods

Analysis of Gray Matter Differences (voxel-based morphometry)

Control Analysis Accounting for Differences in Group Size

Supplemental Results (including Supplemental Figures):

- Frontoparietal heteromodal intrinsic networks in healthy controls and patients (including ***Fig. S1*** Comparison of global and local network intrinsic connectivity)
- Gray matter differences in patients (including ***Fig. S2*** Voxel-based morphometry shows that group differences in gray matter density are restricted mainly to medial temporal regions)
- Control analyses of r_{LOCAL} accounting for orthogonalization procedure (including ***Fig. S3*** Supplemental and control analyses of r_{LOCAL})
- Control Analysis Accounting for Differences in Group Size
- Mean standardized uptake value (SUV) for PiB-PET (including ***Fig. S4*** Mean standardized uptake value for large cortical volume of interest)
- Illustration of voxel-wise correlation between PiB-uptake and connectivity (including ***Fig. S5*** Example scatterplot illustrating voxel-wise correlation between PiB-uptake and connectivity)

Supplemental Tables

- Tables S1-7: Intrinsic network peak activity and group differences
- Table S8: Gray Matter Differences between Groups
- Table S9: Results of Subsampling Analysis

Supplemental Methods

Analysis of Gray Matter Differences (using voxel-based morphometry, VBM)

We were interested in whether reductions in gray matter volume in our networks of interest in the patient group could have a potentially confounding effect on our results. As described recently (Sorg et al., 2013), we used the VBM8 toolbox (http://dbm.neuro.uni-jena.de/vbm.html) to analyze brain structure. T1-weighted images were corrected for bias-field inhomogeneity, registered using linear (12-parameter affine) and nonlinear transformations, and tissue-classified into gray matter (GM), white matter (WM), and cerebro-spinal fluid (CSF) within the same generative model (Ashburner and Friston, 2005). The resulting GM images were modulated to account for volume changes resulting from the normalization process. Here, we only considered non-linear volume changes so that further analyses did not have to account for differences in head size. Finally images were smoothed with a Gaussian kernel of 8mm (FWHM). For group comparisons, voxel-wise two-sample t-tests were performed. We applied a height threshold (voxel level) of 0.001, uncorrected. Volumes of global GM and WM and of intrinsic networks of interest were derived from the first segmentation process.

Control Analysis Accounting for Differences in Group Size

The control group in our study was noticeably smaller than our patient group. To test whether differences in group sizes could affect our results, we conducting a subsampling analysis that tests for differences when group sizes are matched. For a given analysis (e.g., an ANOVA testing PiB-uptake between groups and across networks), after correcting for gray matter density, age, and gender, we randomly selected a number of patients equal to the number of controls. We then calculated statistics (e.g., F statistics and the corresponding p-values). Since this analysis was based on a random selection of patients, we repeated the sampling and analysis step 1000 times, and evaluated the results by calculating median p-values across the 1000 repetitions, as well as the frequency of finding a significant effect.

Supplemental Results

Fronto-parietal heteromodal intrinsic networks in healthy controls and patients

To investigate group differences in intrinsic functional connectivity for each network at global level, we extracted the median connectivity z-value across all network voxels. We used ANOVAs and post-hoc t-tests to compare these average z-values between groups (see Fig. S1a). While the modestly significant main effect of group indicated an overall reduction in connectivity in the patient group ($F_{1,33} = 4.29$, $p = 0.046$), no network-specific comparisons survived Bonferroni correction for 7 tests (all $t_{33} < 2.29$, all corrected $p > 0.20$). Without correction, only the right attention network (rATN) showed a decrease in connectivity ($t_{33} = 2.29$, $p = 0.029$).

Furthermore, we used conventional voxel-wise two-sample t-tests to test for reductions in intrinsic connectivity in the patient group, compared to controls. We found significant reductions only in two regions: connectivity z-values in the posterior DMN was reduced in the right precuneus, and for the right attention network in the right inferior parietal lobule. We found no other significant group differences (see Supplementary Tables S1-7 and Fig. S1b below).

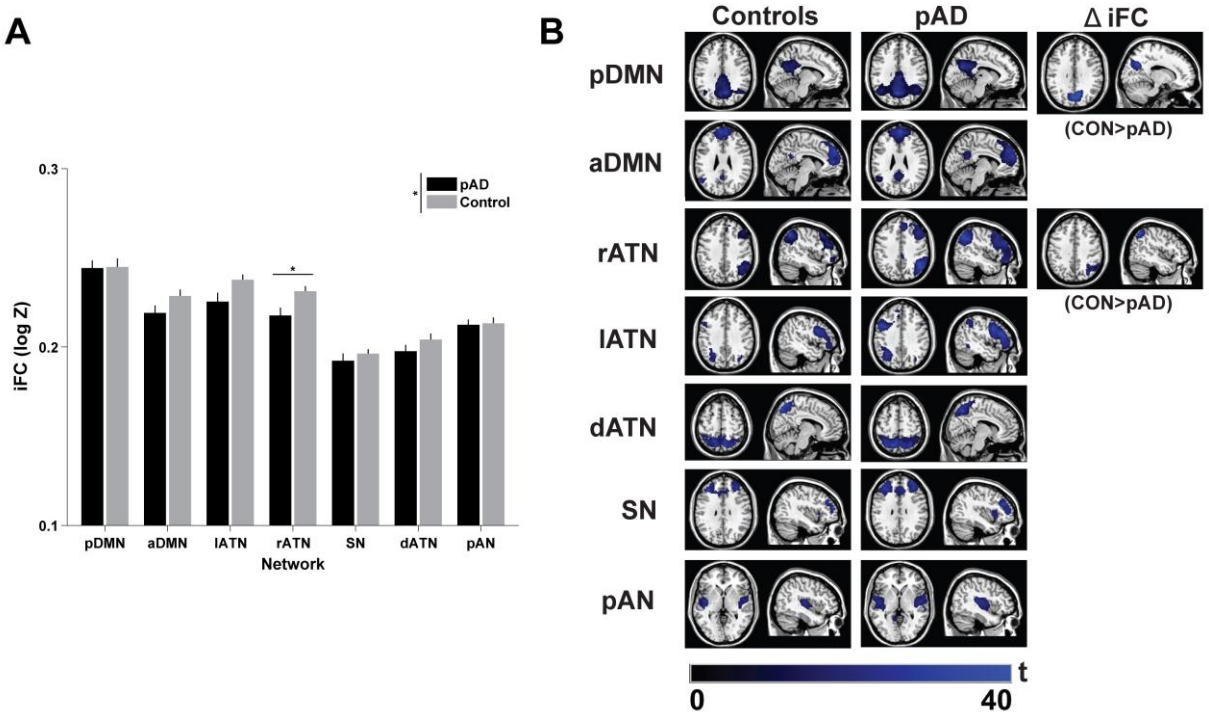

Figure S1. Comparison of global and local network connectivity z-values. **(A)** Global intrinsic connectivity (i.e. the median connectivity z-value of all voxels in the network) was not substantially decreased in patients, compared to controls. **(B)** Results of resting-state functional MRI of patients and controls. Intrinsic connectivity networks characterized by spatial patterns of functional connectivity of resting-state brain activity for patients and controls (SPMs of 1-sample t-tests for each network; p<0.05 FWE corrected at cluster level). Right column: SPMs showing locally decreased connectivity z-values in patients (two-sided two-sample t-tests; p<0.05 FWE cluster level, for illustration purposes, p<0.05, k=10). All SPMs are projected onto a single subject anatomical T1-weighted image. iFC: intrinsic functional connectivity, DMN: default mode network, p: posterior, a: anterior, ATN: attention network, r: right, l: left, d: dorsal, SN: salience network, pAN: primary auditory network. Colorscale indicates t statistics of one-sample (or two-sample, in the right column) t-tests.

Gray matter differences in patients

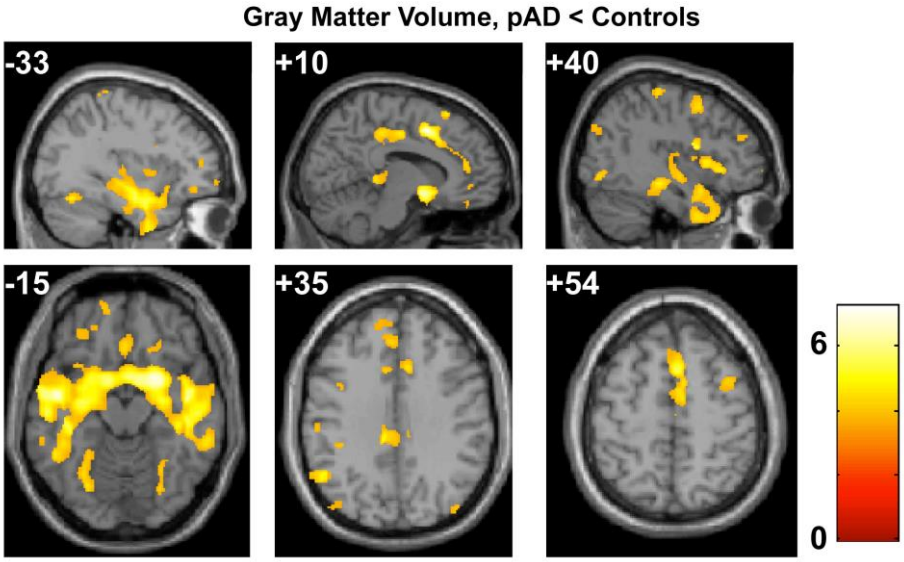

Figure S2. Voxel-based morphometry shows that group differences in gray matter density are restricted mainly to medial temporal regions. Plotted is a map of the t-test contrasting patient and control groups, thresholded at p < 0.001, uncorrected for multiple comparisons. The majority of group differences is restricted to the medial and lateral anterior temporal lobes, extending into the amygdala, ventral striatum, and anterior cingulate. Notably, there are only sparse GM differences in the lateral parietal and prefrontal cortex, as well as the posterior default mode regions

overlapping with DMN and attention networks (also indicated in supplemental table S8).

Control Analyses of r_{LOCAL} accounting for orthogonalization procedure

In addition to the searchlight analyses described in the main text, we performed a control analysis to ensure that the orthogonalization step (which accounted for the effects of r_{GLOBAL}) did not lead to any bias towards negative correlations. We calculated r_{LOCAL} for one subject and network for neighboring voxels (Fig. S3b, as in the analyses shown in Fig. 3) and for matched numbers of voxels sampled randomly from the entire network (Fig. S3b, bottom panel). In the shuffled dataset, the average r_{LOCAL} was close to 0, confirming that orthogonalization did not bias the analysis.

To further illustrate its necessity, we also calculated r_{LOCAL} for all subjects in one network (pDMN) with and without orthogonalization (Fig. S3c). Without orthogonalization, we found no strong positive or negative r_{LOCAL} anywhere in the network. Likewise, subtracting r_{GLOBAL} from (the uncorrected) r_{LOCAL} led only to a small negative correlation in the center of the pDMN. This demonstrates that the proper correction for r_{GLOBAL} was necessary to reveal the local effects.

In a last step, we tested whether there was a relationship between the absolute level of PiB-uptake and the impact it has on r_{LOCAL} (Fig. S3a). Here, for each network and subject, we used linear regression of PiB-uptake on r_{LOCAL} across all network voxels. As before, we submitted the resulting regression weights to two-way mixed-effects ANOVA. We found that in regions with high PiB-uptake, amyloid-β also tended to have a stronger effect on intrinsic connectivity (i.e. r_{LOCAL} was more negative, as measured by linear regression). This effect was significant for all networks except pAN and dATN (main effect group, $F_{1,33} = 34.86$, $p < 10^{-5}$, network-wise t-tests between MCI and controls, all $t_{33} < -3.27$, corrected $p < 0.018$, dATN, $t_{33} = -2.61$, $p = 0.094$, pAN, $t_{33} = -1.99$, $p = 0.393$).

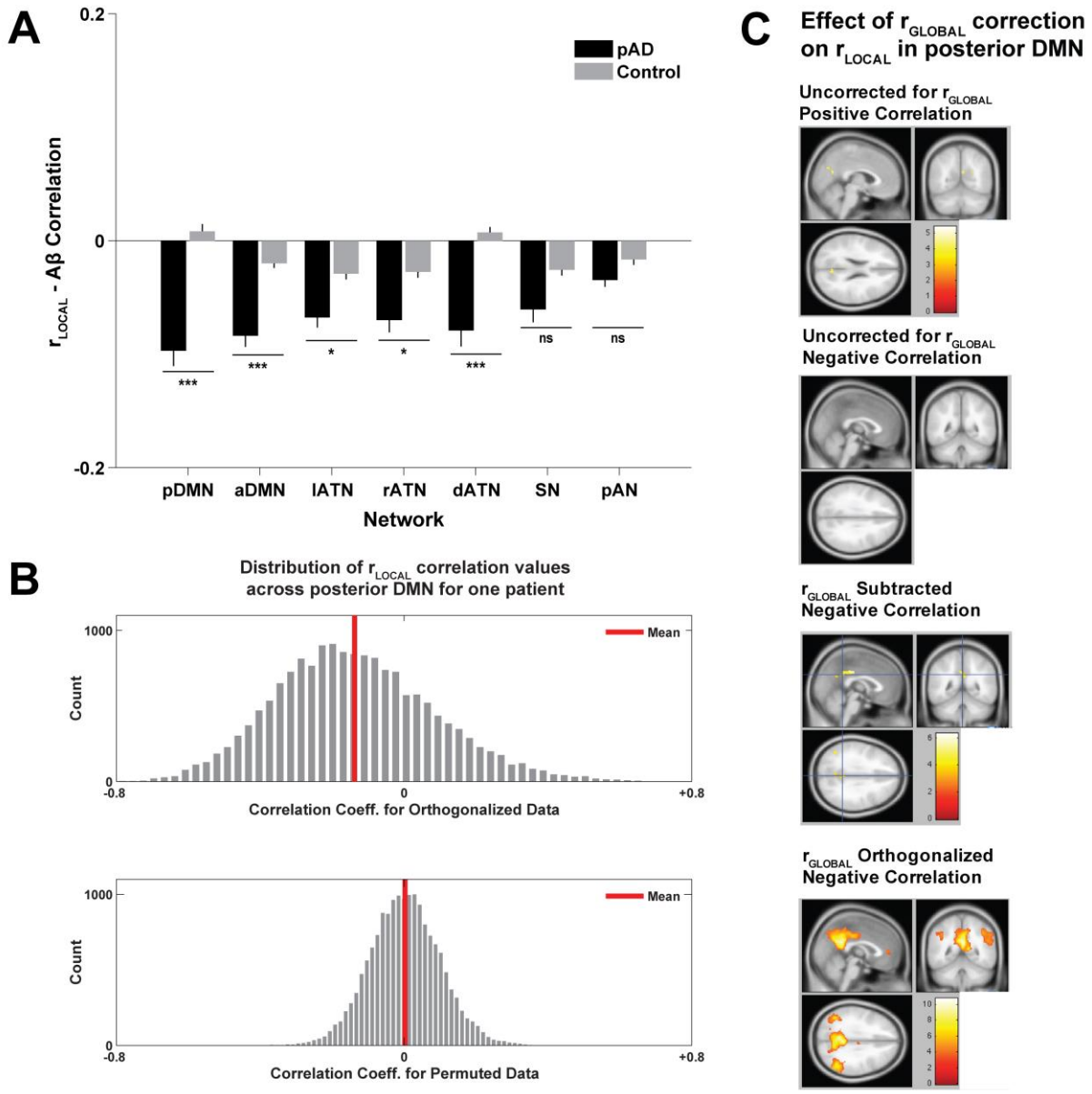

Figure S3. Supplemental and Control Analyses of r_{LOCAL}. **(A)** Negative impact of amyloid-β on intrinsic connectivity is most pronounced in high-PiB regions. After calculating r_{LOCAL} (see Fig. 1&3) in every network voxel, we used linear regression to estimate the correlation between voxel-wise PiB-uptake and r_{LOCAL}. The resulting regression coefficient quantifies how much the local negative impact of PiB on connectivity z-values depends on overall PiB levels in that neighborhood. These regression coefficients, estimated separately for every subject and network, were then submitted to mixed-effects ANOVAs and post-hoc t-tests. **(B)** Control Analysis of the Effect of Orthogonalization. To ensure that orthogonalizing intrinsic connectivity z-values and PiB-uptake across the entire network did not lead to a bias towards negative correlations, we calculated r_{LOCAL} for one subject for neighboring voxels (top panel, as in the analyses shown in Fig. 3) and for matched numbers of voxels

sampled randomly from the entire network (bottom panel). In the shuffled dataset, the distribution of r_{LOCAL} was centered on 0, confirming that orthogonalization did not bias the analysis. **(C)** Effect of orthogonalization on r_{LOCAL} at the group level in one network. For the pDMN, we calculated the average local PiB-uptake/connectivity z-values correlation before and after accounting for r_{GLOBAL} through orthogonalization. Top panels show no significant (positive or negative) local correlations in the pDMN, across the pAD group. Subtracting r_{GLOBAL} from r_{LOCAL} (bottom left panel) led to a small negative correlation in the posterior cingulate. However, this negative correlation was significantly stronger after orthogonalizing across the network (bottom right panel). Maps show t-statistics from a one-sample t-test (thresholded at $p<0.001$, uncorrected) on the Fisher-transformed local correlation values (calculated at the single subject level). Color scale of the t-maps is indicated next to each panel, except for the top right, which showed no suprathreshold voxels.

Control Analysis Accounting for Differences in Group Size

The table below (S9) details the effects of reducing the patient group size (via subsampling) to match the size of the control group. Each column shows the statistical outcome of between-group comparisons across all networks (first column, main effect of group in a mixed-model ANOVA with factors group and network) or in a single network (two-sample t-test). For each outcome measure (PiB-uptake, r_{GLOBAL}, and median r_{LOCAL}, in different rows), we ran statistics on 1000 random subsamplings of the patient group (each time matching the size of the control group). On each random subsampling and statistical test (ANOVA or t-test), we calculated a p-value, generating 1000 p-values for each comparison. Shown are the median p-values (top rows) and the percentage of significant tests ($p<0.05$) out of the 1000 subsamplings. For t-tests, we show Bonferroni-corrected values (corrected for 7 networks), along with uncorrected values underneath. Most comparisons that are significant in the main text remain significant (and for the control network, pAN, r_{GLOBAL} and r_{LOCAL} are still not significant, as expected). The only exceptions are r_{GLOBAL} and r_{LOCAL} in two networks (lATN and SN), and r_{LOCAL} in one network (rATN). These, however, are highly significant (median $p<0.01$) at the uncorrected level.

Mean standardized uptake value (SUV) for PiB-PET.

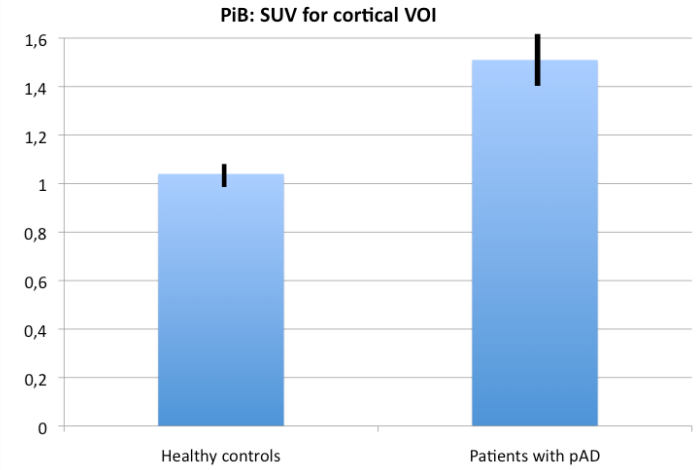

Figure S4. Mean standardized uptake value (SUV) for large cortical volume of interest (VOI). Mean PiB-uptake scores within pre-established large cortical volume of interest (VOI) including lateral prefrontal, parietal, and temporal areas and the retrosplenial cortex were used to define PiB-positivity and -negativity (Hedden et. al, 2009, Drzega et al., 2011). Cut-off for 'high (i.e. PiB-positive)' or 'low (i.e. PiB-negative)' neocortical standardized uptake value (SUV) ratios was 1.15 (Hedden et al, 2009, Drzezga et al., 2011). Patients were PiB-positive and healthy controls were PiB-negative.

Illustration of voxel-wise correlation between PiB-uptake and connectivity.

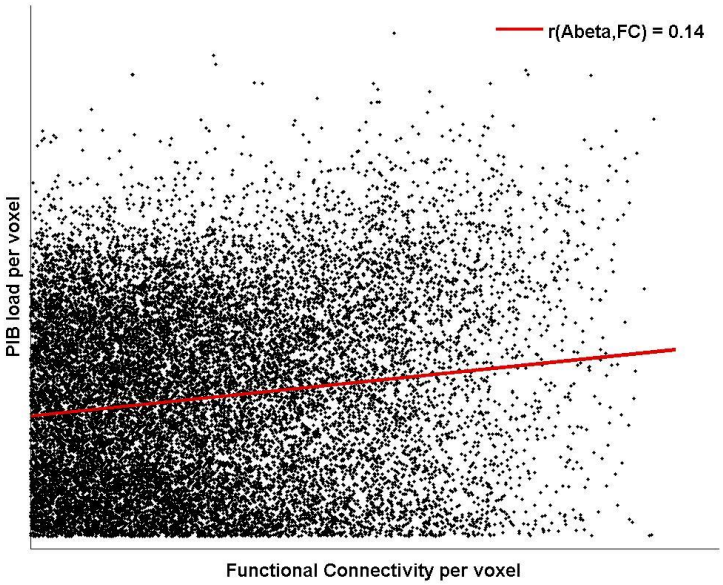

Figure S5. Example scatterplot illustrating voxel-wise correlation between PiB-uptake and connectivity. The plot shows all voxels taken from the posterior DMN of one patient (black dots). As can be seen, there is a modest positive correlation (Pearson r = 0.14, red line).

Supplemental Tables

Tables S1-7: Intrinsic network peak activity and group differences.

Table S1.

Posterior Default Mode Network						
Anatomical region	L/R	cluster	Z-score	T-score	p-value	MNI (x;y;z)
Controls, one-sample-t-test						
Precuneus	L	6195	>8	39.71	<0.001	-6;-66;28
Precuneus	R		>8	34.98	<0.001	8;-62;32
Posterior Cingulate Cortex	R		6.58	16.56	<0.001	2;-32;36
Posterior Cingulate Cortex	L		6.85	18.86	<0.001	-4;-44;32
Inferior Parietal Lobule	R		7.61	27.78	<0.001	40;-62;34
Inferior Parietal Lobule	L	521	5.20	8.99	0.018	-42;-60;28
Anterior Medial Prefrontal Cortex	R	4	5.14	8.78	0.025	6;48;2
Patients, one-sample-t-test						
Precuneus	L	11051	>8	36.86	<0.001	-4;-68;32
Precuneus	R		>8	29.73	<0.001	6;-66;34
Posterior Cingulate Cortex	R		>8	26.28	<0.001	4;-44;24
Posterior Cingulate Cortex	L		>8	25.72	<0.001	-2;-56;30
Inferior Parietal Lobule	L		>8	19.82	<0.001	-40;-62;38
Inferior Parietal Lobule	R		7.01	13.40	<0.001	48;-60;28
Anterior Medial Prefrontal Cortex	L	10	5.19	7.28	0.015	-6;48;4
Controls>Patients, two-sample-t-test						
Precuneus	R	24	4.14	4.69	0.022	8;-66;32

Table S2.

Anterior Default Mode Network						
Anatomical region	L/R	cluster	Z-score	T-score	p-value	MNI (x;y;z)
Controls, one-sample-t-test						
Superior Medial Gyrus	L	5395	7.25	22.99	<0.001	-6;52;36
Superior Medial Gyrus	R		6.71	17.65	<0.001	6;52;30
Pregenual Anterior Cingulate Cortex	L		7.07	21.02	<0.001	-4;50;12
Pregenual Anterior Cingulate Cortex	R		5.84	11.86	<0.001	10;40;28
Angular Gyrus	L	309	6.75	17.97	<0.001	-54;-60;30
Posterior Cingualte Cortex	L/R	182	5.93	12.30	<0.001	+/- 2;-54;24
Patients, one-sample-t-test						
Superior Medial Gyrus	R	7771	>8	27.75	<0.001	8;56;20
Superior Medial Gyrus	L		>8	22.18	<0.001	-6;44;36
Pregenual Anterior Cingulate Cortex	L/R		7.42	15.48	<0.001	0;42;12
Posterior Cingualte Cortex	L	861	6.94	13.09	<0.001	-2;-52;32
Angular Gyrus	L	395	6.17	10.06	<0.001	-52;-58;28

Table S3.

Right Attention Network						
Anatomical region	L/R	cluster	Z-score	T-score	p-value	MNI (x;y;z)
Controls, one-sample-t-test						
Inferior Parietal Lobule	R	2234	>8	40.74	<0.001	44;-58;46
Middle Frontal Gyrus	R	2003	7.50	26.18	<0.001	44;20;48
Superior Frontal Gyrus	R	930	7.04	20.71	<0.001	22;60;6
Medial Frontal Gyrus	R	345	5.70	11.15	0.001	10;44;40
Cerebellum	L	52	5.47	10.09	0.004	-10;-80;-30
Patients, one-sample-t-test						
Middle Frontal Gyrus	R	7633	7.63	16.74	<0.001	36;16;48
Superior Frontal Gyrus	R		6.48	11.17	<0.001	16;34;60
Medial Frontal Gyrus	R		6.93	13.02	<0.001	10;34;38
Inferior Parietal Lobule	R	2899	>8	21.04	<0.001	52;-56;50
Cerebellum	L	1068	7.05	13.57	<0.001	-34;-72;-44
Controls>Patients, two-sample-t-test						
Inferior Parietal Lobule	R	19	4.15	4.70	0.044	50;-58;50

Table S4.

Left Attention Network						
Anatomical region	L/R	cluster	Z-score	T-score	p-value	MNI (x;y;z)
Controls, one-sample-t-test						
Inferior Parietal Lobule (Angular Gyrus)	L	1715	7.25	22.87	<0.001	-52;-56;42
Middle Frontal Gyrus	L	575	7.14	21.74	<0.001	-38;28;46
Superior Frontal Gyrus	L		5.95	12.43	<0.001	-24;16;66
Inferior Frontal Gyrus	L	236	5.81	11.66	<0.001	-48;36;-16
Inferior Parietal Lobule (Angular Gyrus)	R	44	5.43	9.90	<0.001	60;-44;38
Patients, one-sample-t-test						
Inferior Parietal Lobule (Angular Gyrus)	L	2864	>8	22.54	<0.001	-46;-62;52
Superior and Middle Frontal Gyrus	L	1755	7.45	15.68	<0.001	-42;20;48
Inferior Frontal Gyrus	L	579	6.83	12.58	<0.001	-40;46;-16
Inferior Parietal Lobule (Angular Gyrus)	R	903	>8	19.62	<0.001	56;-58;40
Cerebellum	R	960	6.64	11.80	<0.001	38;-64;-40

Table S5.

Dorsal Attention Network						
Anatomical region	L/R	cluster	Z-score	T-score	p-value	MNI (x;y;z)
Controls, one-sample-t-test						
Superior and Inferior Parietal Lobule	L	5849	7.64	28.15	<0.001	-30;-56;48
Precuneus	L		7.28	23.34	<0.001	-12;-72;46
Precuneus	R		7.45	25.45	<0.001	12;-72;50
Superior and Inferior Parietal Lobule	R		7.24	22.93	<0.001	22;-72;50
Patients, one-sample-t-test						
Superior and Inferior Parietal Lobule	R	9743	>8	27.08	<0.001	24;-70;52
Precuneus	R		>8	22.97	<0.001	8;-64;50
Superior and Inferior Parietal Lobule	L		>8	22.92	<0.001	-26;-64;54
Precuneus	L		>8	19.88	<0.001	-4;-52;62

Table S6.

Salience Network						
Anatomical region	L/R	cluster	Z-score	T-score	p-value	MNI (x;y;z)
Controls, one-sample-t-test						
Middle and Superior Frontal Gyrus	L	2094	7.23	22.81	<0.001	-36;36;32
Anterior Cingulate Cortex	R		6.13	13.48	<0.001	8;32;20
Middle and Superior Frontal Gyrus	R	1045	6.50	16.00	<0.001	32;40;28
Insula Lobe	L	239	6.73	17.77	<0.001	-32;16;10
Superior Orbital Gyrus	R	88	5.69	11.07	0.001	24;50;0
Insula Lobe	R	53	5.82	11.72	0.001	32;18;-8
Patients, one-sample-t-test						
Middle and Superior Frontal Gyrus	R	6851	7.84	18.24	<0.001	30;48;22
Middle and Superior Frontal Gyrus	L		7.77	17.69	<0.001	-26;48;14
Anterior Cingulate Cortex	R		6.47	11.14	<0.001	6;32;32
Insula Lobe	L		6.84	12.63	<0.001	-32;12;6
Insula Lobe	R	329	5.76	8.77	0.001	36;24;-2

Table S7.

Primary Auditory Network						
Anatomical region	L/R	cluster	Z-score	T-score	p-value	MNI (x;y;z)
Controls, one-sample-t-test						
Insula/Superior Temporal Gyrus	R	1894	7.38	24.52	<0.001	-42;-20;12
Insula/Superior Temporal Gyrus	L	1462	7.11	21.41	<0.001	44;-20;8
Anterior Cingulate Cortex	L/R	294	5.93	12.31	<0.001	0;20;16
Patients, one-sample-t-test						
Insula/Superior Temporal Gyrus	L	3791	>8	19.87	<0.001	-54;-30;8
Insula/Superior Temporal Gyrus	R	3067	>8	20.50	<0.001	60;-16;12
Anterior Cingulate Cortex	L/R	1370	7.09	14.62	<0.001	0;24;30

One-sample-t-tests are thresholded at p<0.05 FWE corrected. Clusters of the two-sample-t-test are FWE corrected.

Table S8: Gray Matter Differences between Groups.

Anatomical region	L/R	cluster	Z-score	T-score	p-value	x (MNI)	y	z
Controls > pAD, two-sample-t-test								
cingulate gyrus	R	13458	5.71	7.25	<0.001	10	8	46
superior / medial temporal gyrus	R	56041	5.55	6.95	<0.001	56	-24	-5
postcentral gyrus	R	878	4.52	5.24	<0.001	45	-25	63
superior frontal gyrus	R	799	4.22	4.81	<0.001	30	58	1
superior parietal lobule	L	258	4.21	4.79	<0.001	-15	-63	69
postcentral gyrus	L	434	4.19	4.77	<0.001	-44	-18	61
middle frontal gyrus	R	362	4.16	4.72	<0.001	36	42	22
superior frontal gyrus	R	472	4	4.5	<0.001	18	45	45
angular gyrus	L	385	4	4.49	<0.001	-46	-79	30
superior orbitofrontal gyrus	R	907	3.94	4.41	<0.001	18	34	-26
superior frontal gyrus	R	186	3.85	4.29	<0.001	20	57	27
fusiform gyrus	R	314	3.85	4.29	<0.001	27	-73	-17
middle temporal gyrus	R	513	3.69	4.08	<0.001	44	-82	33
superior frontal gyrus	R	147	3.66	4.04	<0.001	15	62	-9
inferior frontal gyrus	R	278	3.61	3.98	<0.001	57	14	9
superior temporal gyrus	R	148	3.55	3.89	<0.001	56	-27	16
middle occipital gyrus	L	185	3.54	3.88	<0.001	-30	-81	18
precentral gyrus	R	81	3.51	3.85	<0.001	48	-16	39

precuneus	R	67	3.48	3.8	<0.001	10	-54	22
middle occipital gyrus	R	226	3.48	3.8	<0.001	20	-96	6
cuneus	L	56	3.46	3.79	<0.001	-14	-100	19
cerebellum	R	260	3.41	3.72	<0.001	20	-79	-47
precuneus	L	71	3.37	3.66	<0.001	-6	-55	27

Table S9. Results of Subsampling Analysis

	main effect	pDMN	aDMN	lATN	rATN	SN	dATN	pAN
PiB								
median p (corr.)	<0.001	0.003	0.002	0.003	0.004	0.003	0.002	0.003
% < 0.05 (corr.)	100%	99.8%	100%	99.7%	98.4%	99.3%	100%	99.6%
r_{GLOBAL}								
median p (corr.)	<0.001	<0.001	0.002	0.012	0.006	0.024	<0.001	0.594
% < 0.05 (corr.)	100%	100%	100%	85.7%	94.4%	65.9%	100%	10.8%
median p (uncorr.)		<0.001	<0.001	<0.001	<0.001	0.004	<0.001	0.080
% < 0.05 (uncorr.)		100%	100%	100%	100%	98.9%	100%	36.7%
r_{LOCAL}								
median p (corr.)	<0.001	<0.001	0.006	0.018	0.027	0.065	<0.001	0.999
% < 0.05 (corr.)	100%	100%	93.3%	73.5%	65.3%	42.5%	100%	0%
median p (uncorr.)		<0.001	0.001	0.003	0.004	0.009	<0.001	0.550
% < 0.05 (uncorr.)		100%	100%	99.7%	98.5%	91.2%	100%	0%

Supplemental References

Ashburner, J., and Friston, K.J. (2005). Unified segmentation. *NeuroImage 26*, 839–851.

Drzezga, A., Becker, J.A., Van Dijk, K.R.A., Sreenivasan, A., Talukdar, T., Sullivan, C., Schultz, A.P., Sepulcre, J., Putcha, D., and Greve, D. (2011). Neuronal dysfunction and disconnection of cortical hubs in non-demented subjects with elevated amyloid burden. *Brain 134*, 1635–1646.

Hedden, T., Van Dijk, K.R.A., Becker, J.A., Mehta, A., Sperling, R.A., Johnson, K.A., et al. (2009). Disruption of functional connectivity in clinically normal older adults harboring amyloid burden. *Journal of Neuroscience 29*, 12686–12694.

Sorg, C., Manoliu, A., Neufang, S., Myers, N., Peters, H., Schwerthöffer, D., et al. (2013). Increased intrinsic brain activity in the striatum reflects symptom dimensions in schizophrenia. *Schizophrenia Bulletin 39*, 387–395.

Alzheimer's & Dementia 11 (2015) 475-484

Link between hippocampus' raised local and eased global intrinsic connectivity in AD

Lorenzo Pasquini[a,b], Martin Scherr[b,c], Masoud Tahmasian[a,b,d], Chun Meng[a], Nicholas E. Myers[b,e], Marion Ortner[f], Mark Mühlau[b,g], Alexander Kurz[f], Hans Förstl[f], Claus Zimmer[a], Timo Grimmer[f], Afra M. Wohlschläger[a,b], Valentin Riedl[a,b,d], Christian Sorg[a,b,f,*]

[a]*Department of Neuroradiology, Technische Universität München, Munich, Germany*
[b]*TUM-Neuroimaging Center, Technische Universität München, Munich, Germany*
[c]*Department of Neurology, Christian Doppler Klinik, Paracelsus Medical University Salzburg, Salzburg, Austria*
[d]*Department of Nuclear Medicine, Technische Universität München, Munich, Germany*
[e]*Department of Experimental Psychology, Oxford University, Oxford, United Kingdom*
[f]*Department of Psychiatry, Technische Universität München, Munich, Germany*
[g]*Department of Neurology of Klinikum rechts der Isar, Technische Universität München, Munich, Germany*

Abstract

Background: The hippocampus (HP) is part of the default mode network (DMN), and both are key targets of Alzheimer's disease (AD). Because of widespread network degeneration, it has been suggested that increasing HP disconnection from the DMN may lead to progressive disinhibition of intra-HP synchronized activity.

Methods: To analyze HP local (i.e., within HP) and global (i.e., within DMN) intrinsic functional connectivity (local/global intrinsic functional connectivity [iFC]), healthy controls and patients with mild cognitive impairment and AD dementia were assessed by spatial high and normal resolution resting-state functional magnetic resonance imaging.

Results: Although patients' parietal local-iFC was reduced and positively correlated with reduced global-iFC within the DMN, HP local connectivity was progressively increased and negatively correlated with HP decreased global connectivity. Increased intra-HP connectivity was associated with impaired memory.

Conclusion: Our result demonstrates a link between increased local and reduced global hippocampal connectivity in AD. Increased intra-HP synchrony may contribute to distinct symptoms such as memory impairment or more speculatively epileptic seizure.

Keywords: Alzheimer's disease; Mild cognitive impairment; Default mode network; Hippocampus; Intrinsic functional connectivity; Synchrony; High-resolution resting-state fMRI; Independent component analysis

1. Introduction

The medial temporal lobes (MTL), including the hippocampus (HP), are key targets of Alzheimer's disease (AD) [1,2]. Beyond atrophy, aberrant local activity and global connectivity have been observed in the HP [3], but their relationship is poorly understood.

Global connectivity changes, i.e., aberrant HP connectivity with extra-MTL regions, target mainly the default mode network (DMN). The DMN is characterized by intrinsic functional connectivity (iFC; synchronized ongoing activity) among prefrontal, parietal, and temporal midline structures, including the HP [4,5]. The DMN is affected by amyloid-plaque deposition in prodromal stages of AD [6,7] and appears to show selective deficits in both neuronal activity and iFC in AD dementia and mild cognitive impairment (MCI; a high-risk state for AD) [8–12]. Particularly, iFC of the HP to the parietal DMN is

Disclosure Statement: The authors declare no competing financial interests.
*Corresponding author. Tel.: +49-89-4140-4665.
E-mail address: c.sorg@lrz.tum.de

1552-5260/$ - see front matter
http://dx.doi.org/10.1016/j.jalz.2014.02.007

already strongly disrupted in very early AD [9,10,13–15]. Paradoxically, local HP activity during memory tasks is consistently increased in individuals at-risk for AD such as MCI or cognitively normal Apolipoprotein E (*APOE*) ε4 carriers [3,16–19]. In patients with AD-dementia, HP activity is decreased, creating an inverse U-shaped function of memory-related HP activity. Contrary to the idea that HP hyperactivity in MCI is beneficial, a recent study found antiepileptics to suppress HP hyperactivity during memory performance in MCI and to reduce memory deficits [20]. This result suggests that HP hyperactivity contributes to HP-dependent memory deficits, rather than compensating for them. Furthermore, HP hyperactivity seems to be linked to overall disrupted network health, supporting the idea of a large-scale pattern of neurodegeneration reflective of AD-pathology [20,21].

In line with such network degeneration, it has been suggested that global HP disconnection may disinhibit local HP activity arising from trisynaptic intra-HP loops [13,22]. This model implies that beyond memory-related activity, the synchrony of ongoing intra-HP activity might be increased in MCI. Such an increase may depend on correspondingly decreased global iFC of the HP within the DMN, and it might grow with progressive disease severity due to progressive HP disconnection. Furthermore, increased intra-HP synchrony might reflect memory deficits in patients. Recently, Das and colleagues reported initial evidence for this hypothesis [13]. They found that local iFC between the HP and adjacent entorhinal cortex increased in MCI (see also [23]). Simultaneously, the overall MTL intrinsic connectivity within the DMN was reduced. However, it was not shown whether local and global connectivity changes are related to each other, whether any of the observed changes had functional consequences for memory, and, importantly, which trajectory of changes takes place beyond MCI.

In this study, we tested these more specific predictions of the HP disconnection hypothesis. We assessed healthy controls (HC) and patients with MCI and AD dementia with resting-state functional magnetic resonance imaging (rs-fMRI) indicating blood-oxygenation-level-dependent signals (BOLD). Independent component analysis (ICA) of fMRI data was used to identify statistically independent spatial patterns of coherent activity in a data-driven, spatially unbiased way. Individual spatial z-maps, which reflect patterns of coactivity, were used as surrogate for iFC and constitute the study's main outcome measure [9,24]. To increase spatial resolution of z-maps and to test for anatomical specificity of potential local iFC increases, additional spatial high-resolution rs-fMRI was applied focused on the HP and retrosplenial parietal cortex. Following previous results, we expected to delineate four regional subsystems within the DMN via local iFC patterns (from here on referred to as "DMN subsystems"), namely the anterior HP (aHP), posterior HP (pHP), precuneus (PrC), and posterior cingulate cortex (PCC) [23,25,26]. We defined local-iFC as iFC-maps derived from the partial-brain high-resolution scan, reflecting only connectivity within the DMN regions covered by its limited field-of-view (FoV). Global-iFC, in contrast, was defined by iFC-maps derived from the whole-brain scans, therefore reflecting connectivity to the rest of the cortex as well. Maps of local- and global-iFC were cross-validated for different methodological approaches, compared across groups, and correlated among each other and with memory scores.

2. Materials and methods

2.1. Subjects

Twenty-two HC (16 females, aged 56–85 years), 22 patients with MCI (11 females, aged 48–80 years) and 21 patients with AD dementia (13 females, aged 57–83 years) participated in this study (Table 1). All subjects provided informed consent in accordance with the Human Research Committee guidelines of the Klinikum rechts der Isar, Technische Universität München. Patients were recruited from the Memory Clinic of the Department of Psychiatry and HC by word-of-mouth advertising. Examination of every participant included medical history, neurological examination, informant interview (Clinical Dementia Rating, CDR) [27], neuropsychological assessment (Consortium to Establish a Registry for AD [CERAD] battery) [27], structural MRI, and blood tests (for patients only). Patients with

Table 1
Demographic and neuropsychological data

	AD (n = 21)	MCI (n = 22)	HC (n = 22)	*F*	*P* value
Age (y)	72.3 (8.6)	65.3 (8.7)	66.3 (9.0)	7.00	.16
Education (years of school)	9.3 (1.6)	9.9 (1.7)	10.1 (1.7)	0.94	.40
% Female	61.9	50.0	72.7	–	.31
CERAD					
Verbal fluency	10.9 (4.9)	15.7 (5.6)	23.3 (1.7)	31.33	.001
Boston naming test	11.4 (3.7)	14.0 (1.1)	14.9 (0.3)	11.15	.001
Word list learning	10.6 (3.0)	16.3 (3.4)	24.2 (2.1)	87.82	.001
Constructional praxis	8.4 (1.9)	9.9 (1.2)	10.8 (0.6)	12.36	.001
World list delayed recall	1.9 (1.6)	4.0 (2.6)	9.1 (1.2)	56.10	.001
World list recognition	7.7 (1.7)	8.0 (1.6)	9.9 (0.3)	9.07	.001

Abbreviations: AD, Alzheimer's disease; MCI, mild cognitive impairment; HC, healthy controls; group comparisons: analysis of variance for all measures except gender (Kruskal-Wallis test); CERAD, Consortium to Establish a Registry for Alzheimer's Disease.

MCI (CDR-global = 0.5) met the criteria for MCI including reported and neuropsychologically assessed cognitive impairments, largely intact activities of daily living, and excluded dementia [28]. Patients with AD dementia fulfilled the criteria for mild dementia (CDR-global = 1) and the National Institute of Neurological and Communicative Disorders and Stroke and the Alzheimer's Disease and Related Disorders Association criteria for AD [29]. Study exclusion criteria were other neurological, psychiatric, or systemic diseases (e.g., stroke, depression, alcoholism) or clinically remarkable structural MRI (e.g., stroke lesions) potentially related to cognitive impairment. Nine patients with AD/eight patients with MCI/six healthy controls were treated for hypertension (beta-blockers, ACE-inhibitors, and calcium channel blockers), 4/5/3 for hypercholesterolemia (statins), 2/2/0 had diabetes mellitus, 6/3/0 received antidepressant medication (mirtazapine, citalopram), and 21/0/0 received cholinesterase inhibitors.

2.2. MRI data acquisition

All subjects underwent structural MRI and 10 min of whole- and partial-brain rs-fMRI, respectively. For rs-fMRI, subjects were instructed to keep their eyes closed and not to fall asleep. We verified that subjects stayed awake by interrogating via intercom immediately after each scan. MRI was performed on a 3 T MRI scanner using a eight-channel phased-array head coil (Achieva, Philips, the Netherlands). T1-weighted anatomical data were obtained by using a magnetization-prepared rapid acquisition gradient echo sequence (TE = 4 ms, TR = 9 ms, TI = 100 ms, flip angle = 5°, FoV = 240 × 240 mm^2, matrix = 240 × 240, 170 slices, voxel size = 1 × 1 × 1 mm^3). Whole-brain rs-fMRI used a gradient echo planar imaging sequence (TE = 35 ms; TR = 2000 ms; flip angle = 82°; FoV = 220 × 220 mm^2; matrix = 80 × 80; 32 slices; slice thickness = 4 mm; 0 mm interslice gap). Partial-brain rs-fMRI of high spatial resolution used a gradient echo planar imaging sequence (TE = 35 ms; TR = 2000 ms; flip angle = 82°; FoV = 220 × 196.4 mm^2; matrix = 112 × 96; 26 slices; slice thickness = 2 mm; 0.2 mm interslice gap) and was centered on HP and PCC. To cover optimally both the HP and PCC, the FoV orientation of the partial-brain rs-fMRI scan was individually adapted (Fig. 1A).

2.3. FMRI data analysis

FMRI data analysis was performed as described previously [30] and in detail in the Supplementary Material. Briefly, after discarding first three volumes of each fMRI run, data were motion corrected, normalized into stereotactic Montreal Neurological Institute (MNI) space (isotropic voxel size whole/partial-brain fMRI 3 × 3 × 3/1 × 1 × 1.5 mm^3), and spatially smoothed (8 × 8 × 8/3 × 3 × 3 mm^3 Gaussian kernel for whole-/partial brain rs-fMRI data). To control for motion-induced artifacts, point-to-point head motion and mean head motion were estimated for each subject [31,32]. Excessive head-motion (cumulative translation or rotation > 3 mm or 3° and mean point-to-point translation or rotation > 0.15 mm or 0.1°) was applied as an exclusion criterion. ANOVA and t-tests between groups yielded no significant differences between groups regarding translational and rotational movements of any direction as well as the signal-to-noise ratio of fMRI data ($P > .05$) (Supplementary Table 1).

Preprocessed whole- and partial-brain rs-fMRI data were decomposed by identical procedures based on group-ICA using GIFT-software (http://icatb.sourceforge.net). For partial-brain imaging data, the volume of analysis was restricted to a partial-brain volume in the temporo-parietal lobes, which was defined by the maximal temporo-parietal overlap of all subjects' partial-brain rs-fMRI volumes. ICs-of-interest reflecting the DMN and DMN subsystems were selected for whole-brain data by the use of a DMN-template derived from [33] and for partial-brain data by visual inspection. For each subject, this procedure resulted in two spatial z-maps reflecting the global-iFC pattern of the anterior and posterior DMN, and four z-maps reflecting local-iFC of aHP, pHP, PrC, and PCC, which together were main outcome measures of the study.

Finally, simple univariate statistical analyses including one-sample t-tests (to evaluate group specific maps), one-way ANOVA (for group comparison), and Pearson's correlation (link between regionally averaged local- and global-iFC, and memory performance) were performed. To estimate the effect of structural changes in DMN subsystems on local-iFC, additional voxel-based morphometry (VBM) was performed (supplement methods), and regional gray matter volumes were used as covariates in corresponding second-level analyses.

Several control analyses were performed, which are described in detail in the supplement. To control effects of subjective bias (i.e., visual inspection), imaging procedure (i.e., partial- vs. whole-brain imaging), and the model order of ICA (i.e., component number) on the detection of temporo-parietal DMN subsystems, additional ICAs were performed, once on whole-brain fMRI data but restricted to partial-brain volume, once on partial-brain data but with different component number. To estimate the effect of different smoothing kernels on the DMN subsystem decomposition, preprocessing with kernels of different dimensions was performed. To control potential effects of head movement on group differences particularly in hippocampal subsystems, frame censoring via despiking and the additional inclusion of movement parameter as covariate-of-no-interest into group comparisons were performed.

3. Results

3.1. Demographic and neuropsychological scores

Healthy controls and patients did not differ for age, gender, and education. Patients had reduced performance

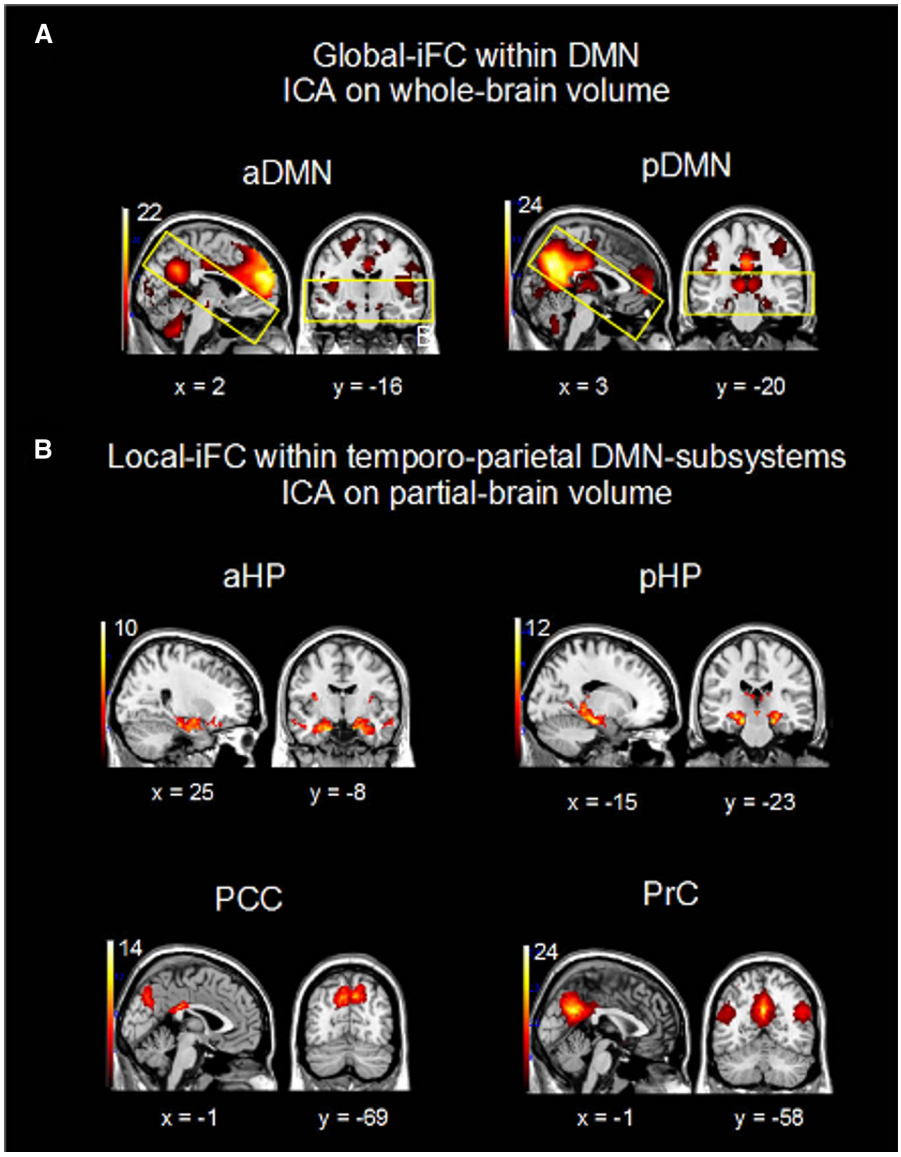

Fig. 1. Global- and local intrinsic functional connectivity (iFC) of the default mode network (DMN) and selected temporo-parietal subsystems. (A) Spatial patterns of global-iFC within the anterior and posterior DMN were derived from independent component analysis (ICA) of whole-brain resting-state functional magnetic resonance imaging (rs-fMRI) data (one-sample t-tests of back-reconstructed IC patterns from patients with mild cognitive impairment [MCI], Alzheimer's disease [AD] dementia, and healthy controls, $P < .05$, cluster level family wise error [FWE] corrected). Yellow lines indicate the field-of-view of spatial high-resolution partial brain rs-fMRI covering temporo-parietal DMN subsystems of interest. (B) Spatial patterns of local-iFC within temporo-parietal DMN subsystems were derived from ICA of partial-brain rs-fMRI data, restricted to the temporo-parietal brain volume of (A) ($P < .05$, FWE cluster level). Color scales represent t-values; maps are superimposed on a single subject T1-weighted structural image. Abbreviations: a/pDMN, anterior/posterior default mode network; aHP, anterior hippocampus, pHP, posterior hippocampus, PrC, precuneus, PCC, posterior cingulate cortex.

scores in most CERAD subtests, in particular for delayed-recall performance (analysis of variance [ANOVA], $P = .001$) (Table 1).

3.2. *Patients' local-iFC was progressively increased in the hippocampus but decreased in the retrosplenial cortex*

We identified four DMN subsystems centered on aHP, pHP, PCC, and PrC, respectively (one-sample t-tests across all subjects, $P < .05$ FWE cluster level; Fig. 1B, Supplementary Table 2). DMN subsystems were in line with previous findings [23,25,26] and consistent across different approaches (Supplementary Materials and Supplementary Fig. 3). A comparison of DMN subsystems across groups revealed that local-iFC within the aHP subsystem was progressively increased in the hippocampus in patients with MCI and AD dementia (ANOVA, post hoc two-sample t-tests; $P < .05$, FWE cluster level, Fig. 2, Supplementary Table 3). Control analyses demonstrated that this finding was not influenced by movement artifacts (Supplementary Fig. 5 and 6). For the PCC subsystem, local-iFC was unchanged in MCI but reduced in its

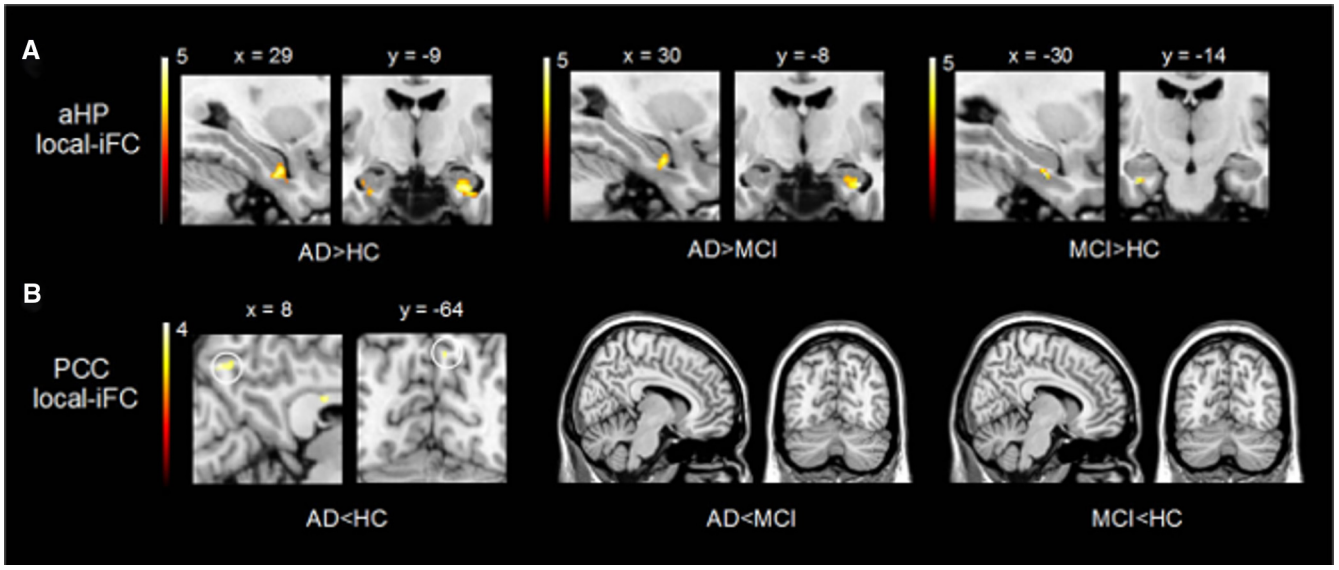

Fig. 2. Aberrant local-iFC in patients' hippocampus and retrosplenial cortex. One-way analysis of variance (ANOVA) of local intrinsic functional connectivity (iFC) maps and correspondent post hoc t-tests, $P < .05$ family wise error (FWE) cluster corrected. (A) For the default mode network (DMN) subsystem centered on the anterior hippocampus (aHP, see panel B of Fig. 1), progressively increased local-iFC was found in the hippocampus of patients with mild cognitive impairment (MCI) and Alzheimer's disease (AD) dementia. (B) Patients with AD dementia show decreased local-iFC in the precuneal part of the DMN subsystem centered on the PCC compared with healthy controls (PCC, see panel B of Fig. 1). No group differences for local-iFC were found in DMN subsystems centered on the posterior hippocampus and precuneus. Color scales represent t-values; maps are superimposed on a single subject T1-weighted structural image. Abbreviations: DMN, default mode network; aHP, anterior hippocampus; PCC, posterior cingulate cortex.

precuneal part in patients with AD dementia. For pHP and PrC subsystems, groups did not differ. To evaluate the effect of gray matter changes and the relationship with global-iFC, local-iFC changes in patients with dementia were further analyzed.

Voxelwise VBM-analysis revealed atrophy in medial and lateral temporal and parietal areas in patients with AD-dementia, with spatial pattern matching previous findings [34] (two-sample t-test, $P < .05$; Supplementary Fig. 1). Regional gray matter volumes of the aHP and PCC subsystems were reduced in patients (two-sample t-test, $P < .05$; Supplementary Fig. 2). We added regional volumes of local-iFC patterns as a nuisance covariate in two-sample t-tests for group differences in local-iFC (Supplementary Fig. 2). After adding these regional brain volumes as covariates, patients' local-iFC increases in the aHP subsystem remained significant, whereas no differences in local-iFC in the PCC subsystem were found anymore.

3.3. Link between patients' aberrant local- and global-iFC changes in the hippocampus and retrosplenial cortex

Next we analyzed the relationship between local- and global-iFC of DMN subsystems. We identified anterior and posterior DMN (a/pDMN) for all subjects, with spatial patterns matching previous results [11] (one-sample t-test across all subjects, $P < .05$ FWE cluster level; Fig. 1A, Supplementary Table 2). Then, we replicated previous findings of reduced global-iFC, once within the aDMN in the anterior hippocampus, once within the pDMN in the precuneus in patients with AD dementia compared with healthy controls (two-sample t-test, $P < .05$, FWE cluster level; Fig. 3A). These decreases overlapped spatially with the changes in local-iFC in the aHP and PCC subsystems (Fig. 3B and C). Furthermore, across patients with AD dementia and across all subjects, average local-iFC in the aHP (Fig. 2) correlated negatively with averaged hippocampal global-iFC in the aDMN (Fig. 3D; $P < .05$). Conversely, local-iFC in the PCC subsystem (Fig. 2) correlated positively with averaged retrosplenial global-iFC in the pDMN, again across demented patients only and all subjects (Fig. 3E; $P < .05$).

3.4. Increased hippocampal local-iFC is associated with impaired delayed recall

Finally, we found that averaged local-iFC of the aHP negatively correlated with delayed-recall scores for both all subjects and patients with dementia only ($P < .05$; Fig. 4). To test whether negative correlation across all subjects is driven by patients with dementia, we performed analysis of covariance of recall scores with group (dementia, nondementia) as categorical variable and local-iFC as continuous covariate. We found significant effect of group ($P < .001$), indicating that negative association between local-iFC in the hippocampus and delayed recall is specific for patients with AD dementia.

4. Discussion

To analyze local and global intrinsic functional connectivity of the hippocampus in early AD, we assessed healthy controls and patients with MCI and AD dementia by spatial

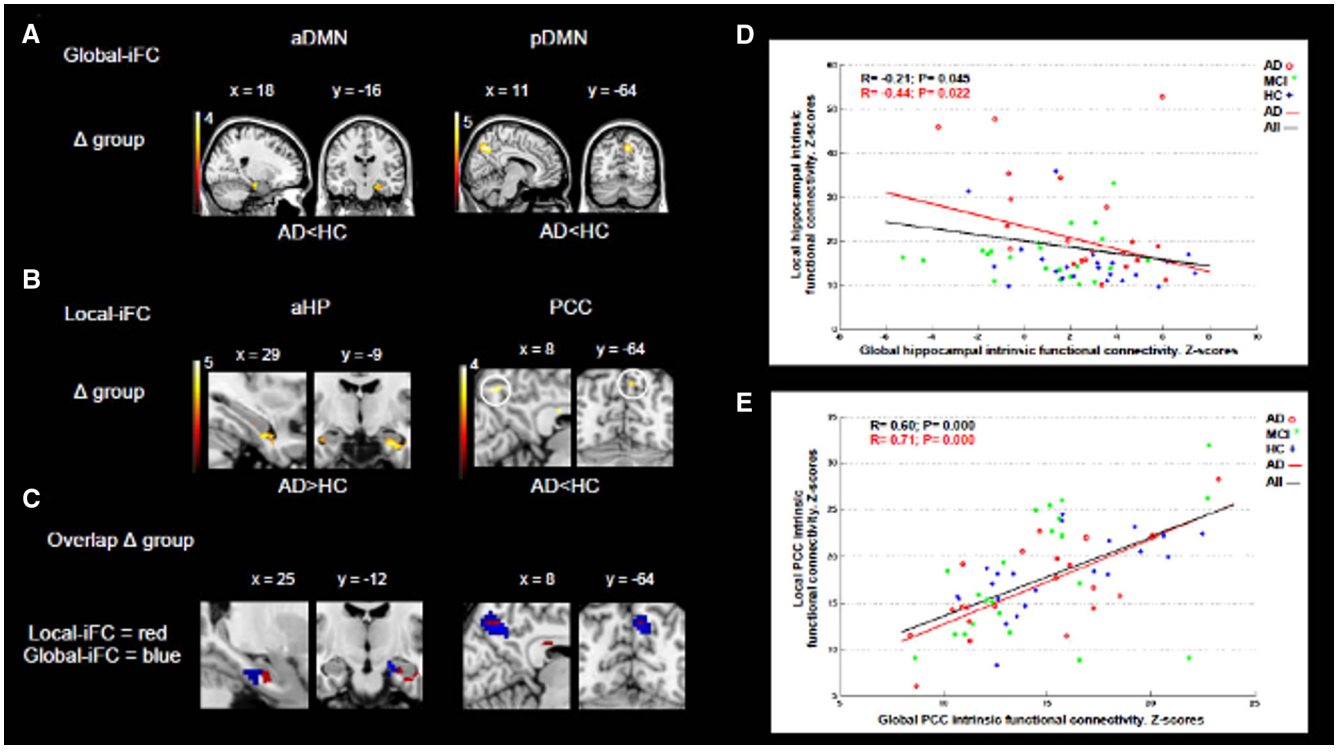

Fig. 3. Relationship between global- and local intrinsic functional connectivity (iFC) in the hippocampus and retrosplenial cortex of Alzheimer's disease (AD). (A) Decreased hippocampal global-iFC within the anterior default mode network (DMN) and decreased retrosplenial global-iFC within the posterior DMN in patients with AD dementia compared with controls (two-sample t-test, $P < .05$, FWE corrected cluster level). (B) In patients with AD compared with healthy controls, local-iFC within the hippocampus is increased, whereas local-iFC within retrosplenial cortex is decreased ($P < .05$, FWE corrected cluster level). (C) Regional overlap of local- and global-iFC changes in the hippocampus and retrosplenial cortex. (D) In the hippocampus, local-iFC correlates negatively with global-iFC within the anterior DMN in all subjects and for patients with AD only (Pearson's correlation, $P < .05$). (E) In the retrosplenial cortex, local-iFC correlates positively with global-iFC within the posterior DMN in all subjects and for patients with AD only (Pearson's correlation, $P < .05$). Color scales represent t-values. Abbreviations: aDMN, pDMN anterior and posterior default mode network; aHP, anterior hippocampus; PCC, posterior cingulate cortex.

high- and normal-resolution rs-fMRI and analyzed imaging data by the use of ICA. We found progressively increased local-iFC within the hippocampus across all patient groups, which negatively correlated with hippocampal global-iFC decrease. In contrast, local-iFC within the retrosplenial cortex was reduced and correlated positively with global-iFC within the DMN. Furthermore, increased local-iFC within the HP was associated with patients' memory impairment. This result provides first evidence for specific and progressive local-iFC increases within the HP in AD that link with global-iFC disruptions and memory deficits. Our data suggest that global disconnection of the hippocampus might be a potential factor for increased intrahippocampal synchrony in AD, which in turn may contribute to different symptoms, such as memory impairment.

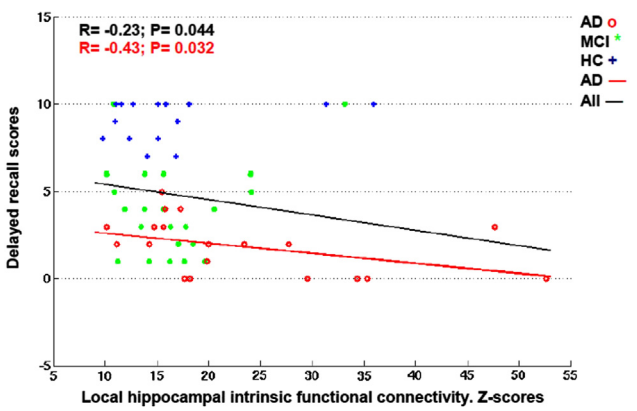

Fig. 4. Association between hippocampal local intrinsic functional connectivity (iFC) and delayed-recall performance. Anterior hippocampus (aHP) local-iFC correlates negatively with delayed-recall scores derived from Consortium to Establish a Registry for Alzheimer's Disease (CERAD) test battery, both across all subjects and for patients with Alzheimer's disease (AD) only (Pearson's correlation, $P < .05$).

4.1. Intrahippocampal intrinsic functional connectivity in AD

4.1.1. Progressive local-iFC increases within the hippocampus are negatively associated with reduced global-iFC in early AD

Progressively increased local-iFC was found in the hippocampus of patients with MCI and AD dementia (Fig. 2A, Supplementary Table 3). Increase of local-iFC was specific for the HP, because local-iFC within the retrosplenial cortex was reduced (Fig. 2). Local-iFC increases were independent of both movement artifacts (Supplementary Fig. 5 and 6) and hippocampus atrophy,

with the latter suggesting the functional nature of changes (Supplementary Fig. 2). Importantly, increased local-iFC in the hippocampus was associated with decreased global-iFC within the DMN (Fig. 3A-D), suggesting a relationship between increased BOLD intrahippocampus synchrony and disrupted intrinsic connectivity of the hippocampus in the DMN in AD. A reasonable model is that progressive global disconnection of the hippocampus might be associated with the increased disinhibition of intrahippocampal loops across dentate gyrus, CA3, CA1, and subiculum, resulting in the elevated synchrony of hippocampal circuit activity [13,22,35]. This model is supported by two of our findings: the regional specificity of local-iFC increases in the hippocampus (verified by an unbiased, data-driven approach) (Fig. 2A, Supplementary Fig. 2, Fig. 3B,C; Supplementary Table 3) and the hippocampus-specific negative correlation between local- and global-iFC (Fig. 3D).

One should note that in addition to global hippocampus disconnection, hippocampus-specific pathology induced by AD likely contributes to increased intrahippocampal connectivity. For instance, recent rodent studies have shown amyloid-β plaque induced hyperactivity within the hippocampus [36–38]; tau-pathology, which affects the hippocampus very early in AD [2], is associated with local network hyperexcitabilty in mice correspondent with seizure frequency [39]. These data suggest that local hippocampal pathology is potentially relevant for increased local-iFC. As a further point to consider, such local pathology may also contribute to global hippocampus disconnectivity. Like previous studies [8,9] we found reduced global-iFC of the hippocampus within the DMN that is linked with aberrant local-iFC. Beyond AD-induced changes within the DMN [4,16,21], intrahippocampal changes may additionally contribute to global hippocampus dysconnectivity (Fig. 3). Taken together, our data suggest that among other factors, reduced hippocampal global connectivity may contribute to progressively increased intra-HP synchrony.

4.1.2. *Progressive local-iFC increases within the hippocampus and impaired memory*

We found progressive increases in hippocampal local-iFC from healthy elderly to MCI to mild AD. Increased hippocampus local-iFC in MCI corresponds with previous findings of increased hippocampus activity during memory tasks in MCI [3,17,18]. However, the continued increase of local-iFC into mild AD stands in contrast with the "inverse U-shaped" trajectory of hippocampal activation during memory encoding, where hippocampus hyperactivation was found only in MCI [3,17]. Recent results from Bakker et al. [20] suggest that this encoding-associated HP hyperactivity in MCI might be due to impending neuronal failure rather than to beneficial compensatory mechanisms. They found that the treatment of MCI patients with antiepileptics reduced HP hyperactivation and increased memory performance. How do the linear increase in local-iFC and the nonlinear trajectory of declining memory activation in mild AD fit together? We speculate that increasing HP disconnection from cortical circuits might play a critical role [3,13,21]. Increasing disconnection leads to increased HP intrinsic activity. Successful memory encoding, in turn, requires HP to coordinate with cortical circuits particularly in the DMN [40]. In MCI with mild HP disconnection, communication between HP and cortex still takes place, resulting in HP hyperactivation during encoding. However, in mild dementia with advanced HP disconnection, connectivity between HP and cortex is severely reduced, resulting in hippocampal hypoactivation compared with healthy elderly. In line with this model, we found moderate memory impairment in MCI but almost total impairment in patients. Furthermore, HP local-iFC correlated with memory impairment (Fig. 4, Table 1). To validate this model, future studies combining rs- and task-fMRI in subjects ranging from healthy elderly to mild AD are necessary.

4.1.3. *Clinical implications of increased intra-HP synchrony beyond impaired memory*

An intriguing aspect of the current finding is its correspondence with results from patients with MTL-epilepsy [41,42]. Previous studies of patients with MTL-epilepsy that recorded rs-fMRI in the interictal period found that regions of seizure activity (particularly in the hippocampus) are characterized by both increased regional BOLD homogeneity and decreased global-iFC within the DMN [41,42]. These results correspond with the changes in local- and global-iFC observed here (Fig. 2, 3). This correspondence suggests that the increased intrahippocampal BOLD synchrony might indicate risk for MTL-seizure in AD (Fig. 2A, 3B-D). Furthermore, the progressive increase of local-iFC in the hippocampus from MCI to AD dementia corresponds well with the progressive increase of seizure risk with progressive symptom severity [43]. Global MTL disconnection might contribute to the increased seizure risk in AD via increased synchrony of intrahippocampal activity. This large-scale mechanism may add to known microscale mechanisms of the eleptogenic potential of amyloid pathology [37,38].

4.2. *Parietal iFC. Methodological issues*

4.2.1. *Reduced local-iFC within the retrosplenial cortex corresponds positively with reduced global-iFC in patients with AD*

For the retrosplenial cortex, we found reduced local-iFC in the precuneus of patients with AD dementia (Fig. 2B, Supplementary Table 3). This finding corresponds with a previous result of reduced regional homogeneity of retrosplenial BOLD activity in patients with AD [44]. In the same DMN subsystem centered on the PCC, we found progressive atrophy (Supplementary Fig. 2, 3); when including regional brain volumes as an additional covariate into group comparisons, we did not find group differences for local-iFC anymore

(Supplementary Fig. 2). This effect of regional atrophy indicates that observed functional retrosplenial changes depend on structural changes. Additionally, we found a strong association between retrosplenial local- and global-iFC changes in terms of both an almost perfect regional overlap (Fig. 3A-C) and a positive correlation concerning local- and global-iFC (Fig. 3E). These results suggest that retrosplenial disruptions of local- and global-iFC and structural atrophy are present in early AD and related among each other. Importantly, despite consistent global-iFC disruption, local-iFC changes of the hippocampus and retrosplenial cortex differ significantly for sign, i.e., local-iFC is increased for the HP and decreased for the retrosplenial cortex (Fig. 2). This inconsistency suggests that distinct microstructure (i.e., allocortex versus neocortex) together with loss of inhibition (i.e., based on HP disconnection) might be critical for AD's effects on local connectivity.

4.2.2. Methodological issues

This study focused on regional clusters of local-iFC within the DMN. Because only few studies have focused on such DMN subsystems, there is no established way to detect them. We combined data-driven spatial ICA with partial-brain rs-fMRI. Partial-brain fMRI allows for increasing the spatial resolution of the BOLD-signal, while ICA allows for detecting DMN subsystem in a way that is independent of any a priori spatial hypothesis [45]. We identified four temporo-parietal clusters of local-iFC (Supplementary Fig. 1), which we interpreted as DMN subsystems for the following reasons: (i) The identified clusters overlap with the DMN (Fig. 3A-C). (ii) iFC of subsystems was identified with ICA, a standard method to determine iFC in rs-fMRI data [24]. (iii) Previous studies have demonstrated the existence of DMN subsystems matching those we found [4,11,23,25,26,46,47]. For example, Margulies and colleagues used rs-fMRI and seed-based iFC analysis to detect PrC- and PCC-centered iFC-maps resembling the DMN subsystems of this study [26]. Gour et al. used an ICA approach similar to ours to find an anterior hippocampal network, matching perfectly the aHP network of our study [23]. Finally (iv), the identified subsystems were consistent across subjects (group-ICA including all subjects, i.e., controls and patients) and independent from both fMRI imaging techniques and ICA parameters (Supplementary Fig 3, Supplementary Table 2).

4.3. Conclusion

The current results provide first evidence for a link between hippocampus' progressively increased local and decreased global intrinsic connectivity in AD, and indicate that hippocampal hyperactivity may contribute to memory deficits in AD.

Acknowledgments

This work was supported by the German Federal Ministry of Education and Research (BMBF 01EV0710 to A.M.W., 01ER0803 to C.S.), the Alzheimer Forschung Initiative (AFI 08860 to V.R., 12819 to C.S.), the Wellcome Trust (to N.E.M.), and the Kommission für Klinische Forschung of the Klinikum rechts der Isar der Technischen Universität München (KKF 8765162 to C.S.).
We are grateful to the participants of the study and the staff of the Department of Psychiatry and Neuroradiology for their help in recruitment and data collection.

Supplementary data

Supplementary data related to this article can be found at http://dx.doi.org/10.1016/j.jalz.2014.02.007.

RESEARCH IN CONTEXT

1. Systematic review: While in AD dementia hippocampus (HP) activity during memory is decreased, local HP activity is paradoxically increased in MCI, creating an inverse-U-shaped function (for review Sperling 2010). Contrary to the idea of beneficial HP hyperactivity, antiepileptics suppress HP hyperactivity and improve memory performance in MCI (Bakker 2012). Furthermore, memory-related HP hyperactivity links with cortical atrophy, suggesting HP disconnection to modulate HP activity (Putcha 2011).
2. Interpretation: Beyond memory-related activity, we found in patients with MCI and dementia progressively increased synchrony of ongoing within-HP activity that is linked with reduced global HP connectivity and impaired memory. Data support the view that global HP disconnection may disinhibit local HP activity arising from trisynaptic intra-HP loops. Increased HP synchrony may contribute to distinct symptoms such as memory impairment or epileptic seizure.
3. Future direction: What is the link between increasing ongoing HP synchrony and inverse-U-shaped function of memory-related HP activity in AD? Might HP synchrony be a specific target to treat HP dysfunction in AD?

References

[1] Blennow K, de Leon MJ, Zetterberg H. Alzheimer's disease. Lancet 2006;368:387–403.
[2] Braak H, Braak E. Neuropathological stageing of Alzheimer-related changes. Acta Neuropathol 1991;82:239–59.
[3] Sperling RA, Dickerson BC, Pihlajamaki M, Vannini P, LaViolette PS, Vitolo OV, et al. Functional alterations in memory networks in early Alzheimer's disease. Neuromolecular Med 2010;12:27–43.

[4] Buckner RL, Andrews-Hanna JR, Schacter DL. The brain's default network: anatomy, function, and relevance to disease. Ann N Y Acad Sci 2008;1124:1–38.
[5] Greicius MD, Krasnow B, Reiss AL, Menon V. Functional connectivity in the resting brain: a network analysis of the default mode hypothesis. Proc Natl Acad Sci U S A 2003;100:253–8.
[6] Drzezga A, Becker JA, Van Dijk KR, Sreenivasan A, Talukdar T, Sullivan C, et al. Neuronal dysfunction and disconnection of cortical hubs in non-demented subjects with elevated amyloid burden. Brain 2011;134:1635–46.
[7] Sheline YI, Raichle ME. Resting state functional connectivity in preclinical Alzheimer's disease. Biol Psychiatry 2013;74:340–7.
[8] Greicius MD, Srivastava G, Reiss AL, Menon V. Default-mode network activity distinguishes Alzheimer's disease from healthy aging: evidence from functional MRI. Proc Natl Acad Sci U S A 2004; 101:4637–42.
[9] Sorg C, Riedl V, Muhlau M, Calhoun VD, Eichele T, Laer L, et al. Selective changes of resting-state networks in individuals at risk for Alzheimer's disease. Proc Natl Acad Sci U S A 2007;104:18760–5.
[10] Sorg C, Riedl V, Perneczky R, Kurz A, Wohlschlager AM. Impact of Alzheimer's disease on the functional connectivity of spontaneous brain activity. Curr Alzheimer Res 2009;6:541–53.
[11] Damoiseaux JS, Prater KE, Miller BL, Greicius MD. Functional connectivity tracks clinical deterioration in Alzheimer's disease. Neurobiol Aging 2012;33:828.e19–30.
[12] Agosta F, Pievani M, Geroldi C, Copetti M, Frisoni GB, Filippi M. Resting state fMRI in Alzheimer's disease: beyond the default mode network. Neurobiol Aging 2012;33:1564–78.
[13] Das SR, Pluta J, Mancuso L, Kliot D, Orozco S, Dickerson BC, et al. Increased functional connectivity within medial temporal lobe in mild cognitive impairment. Hippocampus 2013;23:1–6.
[14] Wang L, Zang Y, He Y, Liang M, Zhang X, Tian L, et al. Changes in hippocampal connectivity in the early stages of Alzheimer's disease: evidence from resting state fMRI. Neuroimage 2006;31:496–504.
[15] Kim J, Kim YH, Lee JH. Hippocampus-precuneus functional connectivity as an early sign of Alzheimer's disease: a preliminary study using structural and functional magnetic resonance imaging data. Brain Res 2013;1495:18–29.
[16] Celone KA, Calhoun VD, Dickerson BC, Atri A, Chua EF, Miller SL, et al. Alterations in memory networks in mild cognitive impairment and Alzheimer's disease: an independent component analysis. J Neurosci 2006;26:10222–31.
[17] Dickerson BC, Salat DH, Bates JF, Atiya M, Killiany RJ, Greve DN, et al. Medial temporal lobe function and structure in mild cognitive impairment. Ann Neurol 2004;56:27–35.
[18] Dickerson BC, Salat DH, Greve DN, Chua EF, Rand-Giovannetti E, Rentz DM, et al. Increased hippocampal activation in mild cognitive impairment compared to normal aging and AD. Neurology 2005; 65:404–11.
[19] Filippini N, MacIntosh BJ, Hough MG, Goodwin GM, Frisoni GB, Smith SM, et al. Distinct patterns of brain activity in young carriers of the APOE-epsilon4 allele. Proc Natl Acad Sci U S A 2009; 106:7209–14.
[20] Bakker A, Krauss GL, Albert MS, Speck CL, Jones LR, Stark CE, et al. Reduction of hippocampal hyperactivity improves cognition in amnestic mild cognitive impairment. Neuron 2012;74:467–74.
[21] Putcha D, Brickhouse M, O'Keefe K, Sullivan C, Rentz D, Marshall G, et al. Hippocampal hyperactivation associated with cortical thinning in Alzheimer's disease signature regions in non-demented elderly adults. J Neurosci 2011;31:17680–8.
[22] Yassa MA, Muftuler LT, Stark CE. Ultrahigh-resolution microstructural diffusion tensor imaging reveals perforant path degradation in aged humans in vivo. Proc Natl Acad Sci U S A 2010;107:12687–91.
[23] Gour N, Ranjeva JP, Ceccaldi M, Confort-Gouny S, Barbeau E, Soulier E, et al. Basal functional connectivity within the anterior temporal network is associated with performance on declarative memory tasks. Neuroimage 2011;58:687–97.
[24] Fox MD, Raichle ME. Spontaneous fluctuations in brain activity observed with functional magnetic resonance imaging. Nat Rev Neurosci 2007;8:700–11.
[25] Kahn I, Andrews-Hanna JR, Vincent JL, Snyder AZ, Buckner RL. Distinct cortical anatomy linked to subregions of the medial temporal lobe revealed by intrinsic functional connectivity. J Neurophysiol 2008;100:129–39.
[26] Margulies DS, Vincent JL, Kelly C, Lohmann G, Uddin LQ, Biswal BB, et al. Precuneus shares intrinsic functional architecture in humans and monkeys. Proc Natl Acad Sci U S A 2009; 106:20069–74.
[27] Morris JC, Edland S, Clark C, Galasko D, Koss E, Mohs R, et al. The consortium to establish a registry for Alzheimer's disease (CERAD). Part IV. Rates of cognitive change in the longitudinal assessment of probable Alzheimer's disease. Neurology 1993; 43:2457–65.
[28] Gauthier S, Reisberg B, Zaudig M, Petersen RC, Ritchie K, Broich K, et al. Mild cognitive impairment. Lancet 2006;367:1262–70.
[29] McKhann G, Drachman D, Folstein M, Katzman R, Price D, Stadlan EM. Clinical diagnosis of Alzheimer's disease: report of the NINCDS-ADRDA Work Group under the auspices of Department of Health and Human Services Task Force on Alzheimer's Disease. Neurology 1984;34:939–44.
[30] Sorg C, Manoliu A, Neufang S, Myers N, Peters H, Schwerthoffer D, et al. Increased intrinsic brain activity in the striatum reflects symptom dimensions in schizophrenia. Schizophr Bull 2013;39:387–95.
[31] Power JD, Barnes KA, Snyder AZ, Schlaggar BL, Petersen SE. Spurious but systematic correlations in functional connectivity MRI networks arise from subject motion. Neuroimage 2012;59:2142–54.
[32] Van Dijk KR, Sabuncu MR, Buckner RL. The influence of head motion on intrinsic functional connectivity MRI. Neuroimage 2012; 59:431–8.
[33] Allen EA, Erhardt EB, Damaraju E, Gruner W, Segall JM, Silva RF, et al. A baseline for the multivariate comparison of resting-state networks. Front Syst Neurosci 2011;5:2.
[34] Derflinger S, Sorg C, Gaser C, Myers N, Arsic M, Kurz A, et al. Grey-matter atrophy in Alzheimer's disease is asymmetric but not lateralized. J Alzheimers Dis 2011;25:347–57.
[35] Hyman BT, Van Hoesen GW, Damasio AR, Barnes CL. Alzheimer's disease: cell-specific pathology isolates the hippocampal formation. Science 1984;225:1168–70.
[36] Busche MA, Chen X, Henning HA, Reichwald J, Staufenbiel M, Sakmann B, et al. Critical role of soluble amyloid-beta for early hippocampal hyperactivity in a mouse model of Alzheimer's disease. Proc Natl Acad Sci U S A 2012;109:8740–5.
[37] Palop JJ, Mucke L. Amyloid-beta-induced neuronal dysfunction in Alzheimer's disease: from synapses toward neural networks. Nat Neurosci 2010;13:812–8.
[38] Palop JJ, Mucke L. Epilepsy and cognitive impairments in Alzheimer disease. Arch Neurol 2009;66:435–40.
[39] DeVos SL, Goncharoff DK, Chen G, Kebodeaux CS, Yamada K, Stewart FR, et al. Antisense reduction of tau in adult mice protects against seizures. J Neurosci 2013;33:12887–97.
[40] Eichenbaum H, Yonelinas AP, Ranganath C. The medial temporal lobe and recognition memory. Annu Rev Neurosci 2007;30:123–52.
[41] Pittau F, Grova C, Moeller F, Dubeau F, Gotman J. Patterns of altered functional connectivity in mesial temporal lobe epilepsy. Epilepsia 2012;53:1013–23.
[42] Zeng H, Pizarro R, Nair VA, La C, Prabhakaran V. Alterations in regional homogeneity of resting-state brain activity in mesial temporal lobe epilepsy. Epilepsia 2013;54:658–66.
[43] Friedman D, Honig LS, Scarmeas N. Seizures and epilepsy in Alzheimer's disease. CNS Neurosci Ther 2012;18:285–94.
[44] Zhang Z, Liu Y, Jiang T, Zhou B, An N, Dai H, et al. Altered spontaneous activity in Alzheimer's disease and mild cognitive impairment revealed by Regional Homogeneity. Neuroimage 2012; 59:1429–40.

[45] Calhoun VD, Liu J, Adali T. A review of group ICA for fMRI data and ICA for joint inference of imaging, genetic, and ERP data. Neuroimage 2009;45:S163–72.
[46] Zarei M, Beckmann CF, Binnewijzend MA, Schoonheim MM, Oghabian MA, Sanz-Arigita EJ, et al. Functional segmentation of the hippocampus in the healthy human brain and in Alzheimer's disease. Neuroimage 2012;66C:28–35.
[47] Andrews-Hanna JR, Reidler JS, Sepulcre J, Poulin R, Buckner RL. Functional-anatomic fractionation of the brain's default network. Neuron 2010;65:550–62.

Supplementary Material for

"Link between hippocampus' raised local and eased global intrinsic connectivity in AD"

by Lorenzo Pasquini[1,5], Martin Scherr [5,7], Masoud Tahmasian[1,3,5], Chun Meng[1], Nick Myers[5,6], Marion Ortner[2], Mark Mühlau[4,5], Alexander Kurz[2], Hans Förstl[2], Claus Zimmer[1], Timo Grimmer[2], Afra M. Wohlschläger[1,5], Valentin Riedl[1,3,5], Christian Sorg*[1,2,5].

Supplementary Methods: 3

- FMRI data analysis
- Control analyses
- Voxel-based morphometry (VBM)

Supplementary Results: 1

- Consistent DMN-subsystems in the hippocampus and retrosplenial cortex

Supplementary Discussion: 1

- Methodological issues and limitations

Supplementary Figures: 6

- Whole-brain voxelwise VBM analysis reveals temporo-parietal atrophy in AD
- Impact of atrophy on aberrant local-iFC of DMN-subsystems
- Consistent detection of temporo-parietal DMN subsystems
- Estimating effects of smoothing kernel on both the detection of anterior hippocampus (aHP) local-iFC patterns from whole-brain data and corresponding group differences
- Control for head motion: Progressively increased local-iFC in the aHP along the course of AD with mean head-motion as control variable

- Control for head motion and frame censoring: Progressively increased local-iFC in the aHP along the course of AD using despiked fMRI data

Supplementary Tables: 4

- Parameters of head movement
- Global and local intrinsic functional connectivity of the default mode network and its temporo-parietal subsystems
- Group differences for local-iFC in DMN-subsystems
- Spatial multiple regression coefficients of local-iFC patterns representing DMN-subsystems derived from different analysis approaches

Supplementary Methods

FMRI data analysis.

Preprocessing. For each rs-fMRI run, the first three volumes were discarded to account for magnetization effects. SPM5 (Wellcome Department of Cognitive Neurology, London) was used for motion correction, spatial normalization into the stereotactic space of the Montreal Neurological Institute (MNI) (isotropic voxel size whole/partial-brain fMRI 3x3x3/1x1x1.5 mm^3) and spatial smoothing (whole-/partial brain rs-fMRI: 8x8x8/3x3x3 mm^3 Gaussian kernel). To control for motion-induced artifacts, point-to-point head motion and mean head motion were estimated for each subject [1, 2]. Excessive head motion (cumulative translation or rotation > 3 mm or 3° and mean point-to-point translation or rotation > 0.15 mm or 0.1°) was applied as an exclusion criterion. ANOVA and t-tests between groups yielded no significant differences between groups regarding translational and rotational movements of any direction as well as signal-to-noise ratio of fMRI data ($p > 0.05$) (Tab. S1). Before volumes were entered into independent component analysis (ICA), voxel-wise z-transformation on time course data $y_{ijk}(t)$ was applied by subtracting the mean $\langle y_{ijk} \rangle$ and dividing by the standard deviation σ_{ijk} ($\hat{y}_{ijk}(t) = (y_{ijk}(t) - \langle y_{ijk} \rangle) / \sigma_{ijk}$, t time, i,j,k directions in space) [3]. The sensitivity of the multivariate ICA algorithm for correlation of variance between voxels, i.e. functional connectivity, was thereby rendered independent of the original BOLD signal magnitude across subjects.

ICA and network selection. To analyze global-iFC, we performed standard group-ICA approach on whole-brain rs-fMRI data. Subsequently, to identify the DMN, we used a template-based network selection procedure as described previously [3], whereas the DMN-template was derived from a previous study identifying intrinsic connectivity networks in a sample of more than 600 healthy controls [4]. Specifically,

preprocessed whole-brain rs-fMRI data of all subjects were decomposed into 40 spatial independent components within a group-ICA framework [5], which is based on the infomax-algorithm and implemented in the GIFT-software (http://icatb.sourceforge.net). Dimensionality estimation was performed by using the minimum description length criteria and resulted in 40 components representing the mean of all individual estimates. Data were concatenated and reduced by two-step principal component analysis (PCA), followed by independent component estimation with the infomax-algorithm. We subsequently ran 40 ICA (ICASSO) to ensure stability of the estimated components [6]. This results in a set of averaged group components, which are then back reconstructed into single subject space. To select those components reflecting the DMN in an automated way, we applied spatial regression analysis of the 40 independent components onto a mask containing the DMN. The mask was generated by merging templates of DMN-components of a previous study by Allen and colleagues [4]. Two ICs with highest correlation coefficients were selected to represent the anterior and posterior DMN. Before we entered individual's spatial maps into second-level statistics we reintegrated the initially calculated scaling factor σ_{ijk} into the data by voxel-wise multiplication in order to preserve each individual's profile of variance magnitude while leaving the normalized timecourse component unchanged. For each subject, our procedure resulted in two spatial z-maps as main outcome measures reflecting spatial global-iFC pattern of the anterior and posterior DMN.

To analyze local-iFC and particularly to identify temporo-parietal DMN-subsystems via local-iFC, we performed the identical ICA approach as just described but on partial-brain rs-fMRI data. Since the orientation of the temporo-parietal field-of-view of partial brain imaging was adapted for each subject, we defined a consistent

temporo-parietal partial-brain volume (PBV) by the maximal overlap of all subjects' partial-brain rs-fMRI volumes. This PVB was used for further analyses concerning local-iFC. After ICA of partial-brain rs-fMRI data, we identified by visual inspection 4 DMN-subsystems, respectively centered on the aHP, pHP, PrC, and PCC.

Statistical analysis across subjects. To evaluate statistically spatial z-maps reflecting global- and local-iFC of the DMN and DMN-subsystems, we used voxelwise one-sample t-tests ($p<0.05$, family wise error (FWE) correction for multiple testing at cluster level). Comparisons across groups were performed by voxelwise one-way-ANOVA and corresponding post-hoc t-tests ($p<0.05$ FWE cluster level) with and without covariates of regional brain volumes defined by voxel-based morphometry (VBM) analysis (see below). These comparisons were restricted to spatial masks of corresponding one-sample t-tests defined at liberal threshold ($p<0.001$ uncorrected).

To test the relationship of local-iFC of DMN-subsystem with both global-iFC and memory, we correlated averaged z-scores of local-iFC with averaged global-iFC z-scores and delayed recall CERAD scores, respectively, by the use of Pearson's correlation ($p<0.05$). Averaged z-scores of global-iFC for the aDMN and pDMN, respectively, were extracted from masks of the hippocampus/parahippocampus and retrosplenial cortex, which were derived from the WFU-PickAtlas (www.ansir.wfubmc.edu).

Voxel-based morphometry (VBM) of structural MRI data.

To evaluate the influence of regional atrophy on functional results, we used the VBM8 toolbox (http://dbm.neuro.uni-jena.de/vbm.html) to analyze brain structure as described recently [3]. T1-weighted images were corrected for bias-field inhomogeneity, registered using linear (12-parameter affine) and non-linear

transformations, and tissue-classified into gray matter (GM), white matter (WM), and cerebro-spinal fluid (CSF) within the same generative model [7]. The resulting GM images were modulated to account for volume changes resulting from the normalization process. Here, we only considered non-linear volume changes so that further analyses did not have to account for differences in head size. Finally images were smoothed with a Gaussian kernel of 8mm (FWHM). For group comparisons, two-sample t-tests were performed for averaged regional brain volumes restricted to regions of interest ($p<0.05$). Regional volumes of GM were derived from the first segmentation process and region of interests based on results of the fMRI data analysis. Finally, voxel-wise ANOVA and post-hoc t-tests were performed at whole brain level and restricted to regions of interest ($p<0.05$, FWE corrected). Results of voxel-wise group comparison in VBM are shown in Fig. S1.

Control analyses

To control our main findings for potential confounding effects, we performed extensive control analyses.

Consistent detection of temporoparietal DMN subsystems. To control for effects of subjective bias (i.e. visual inspection), field-of-view (i.e. partial- vs. whole-brain imaging), and model order of ICA (i.e. component number), additional ICAs were performed once on whole-brain fMRI data but restricted to PVB, once on partial-brain data but with different model order. For the analysis of whole-brain data restricted to PVB, we chose 40 components for ICA in order to be consistent with used ICA model order of above described approaches. For the analysis of partial-brain data, we chose 70 components; model order around 70 components has been demonstrated to reveal most robust ICs in rs-fMRI data analysis [8]. Again we selected for each analysis the

correspondent four DMN-subsystems by visual inspection. By this means, for each subject and each of the two additional ICA-approaches, we extracted four spatial z-maps as components-of-interest reflecting the local-iFC pattern of the aHP-, pHP-, PrC-, and PCC-subsystem of the DMN. To confirm the consistency of selected components based on our initial approach (partial-brain rs-fMRI, ICA with 40 components), we cross-validated each selected component by calculating its spatial fit with all the other components of the two control analyses, respectively, via spatial regression analysis as implemented in the GIFT toolbox. Results of this analysis are shown in Figure S3 and Tab. S4.

Estimating effects of smoothing kernel. The increase of spatial resolution of partial-brain high-resolution rs-fMRI requires the use of smaller smoothing kernels for data smoothing, to preserve advantages of increased spatial resolution. Therefore, we used 3x3x3 mm^3 smoothing kernel for partial-brain data in contrast to the use of 8x8x8 mm^3 kernel for whole-brain data. However, smaller kernels may influence the detection of iFC pattern. To estimate the effect of different smoothing kernels on DMN subsystem decomposition, preprocessing with kernels of different dimensions (3x3x3 mm^3 / 8x8x8 mm^3) was performed in whole-brain data. Since our study was focused on hippocampal DMN subsystems, we used ICA of model order 70, which allowed for the robust detection of hippocampal subsystems in whole-brain data and therefore for comparison with results based on partial-brain data (see Fig. S4 upper part). Results are shown in Fig. S4. Furthermore, to estimate the effect of smoothing kernels not only on the detection of DMN subsystems but also on group differences for these subsystems, we performed corresponding group comparisons for subsystems. Results, which are presented in Figure S4 for the aHP system, indicate

that the increase of spatial resolution is critical for the detection of group differences in aHP local-iFC.

Control for head movement. Previous studies in rs-fMRI [1, 2] demonstrated that even when study groups were not different for head movement parameters, group differences iFC may be due to movement artifacts. To control potential effects of head movement on group differences particularly in hippocampal subsystems, frame censoring via despiking and the additional inclusion of movement parameter as co-variate-of-no-interest into group comparisons was performed. In more detail, to estimate whether individual head motion affects our main finding of progressively increased local-iFC in the aHP subsystems in AD and MCI patients, mean head motion parameters were added as additional co-variate-of-no-interest in ANOVA of group comparisons. Group differences did not substantially differ from previous findings, which were not controlled for head motion (Figure S5).

There is ongoing discussion which frame censoring method might be optimal to remove head movement artifacts from resting-state fMRI data [1, 2, 9-12]. We decided for a despiking procedure that is implemented by the ArtRepair toolbox in SPM (http://cibsr.stanford.edu/tools/human-brain-project/artrepair-software.html). This decision was made for two reasons: first, despiking has been suggested and successfully used for the control of movement artifacts in previous studies [1, 13]. Second, our group-ICA approach on fMRI data needs volume time series of equal length across subjects; despiking removes movement related “spikes” from fMRI data and replaces them by linearly interpolated data from immediately preceding and following scans, thus preserving the length of image time series. After inclusion of despiking in our preprocessing pipeline for partial-brain rs-fMRI data, we applied ICA on despiked data as described previously. We found almost identical

temporoparietal DMN subsystems as presented in Fig. 1 (see Fig. S6A for aHP subsystem). Group comparisons for local-iFC in the aHP subsystem derived from despiked data, provided largely identical results as analyses with undespiked data, namely progressively increased local functional connectivity in the hippocampus along the course of Alzheimer's disease (see Fig. S6B). This result provides evidence that the main finding of our study is not confounded by head motion.

Supplementary Results:

Consistent DMN-subsystems in the hippocampus and retrosplenial cortex.

As expected, we identified four DMN-subsystems centered on aHP, pHP, PCC, and PrC, respectively, (one-sample t-tests across all subjects, $p<0.05$ FWE cluster level; Fig. 1B, Tab. S1), matching previous findings [14-16]. DMN-subsystems were spatially consistent with those identified by control analyses, indicating validity of the partial-brain ICA approach (Fig. S3).

More specifically, beyond the approach based on ICA of partial-brain fMRI with 40 components, two additional ICAs were performed, once on whole-brain fMRI data but restricted to PVB (i.e. partial brain volume of maximal overlap of FOV of partial-brain fMRI across subjects), once on partial-brain data but with different model order (i.e. 70 components). For each approach, visual inspection of ICs revealed aHP-, pHP-, PCC-, and PrC-subsystems (one-sample t-tests across all subjects, $p<0.05$ FWE cluster level; Fig. S3B, Tab. S2). To control for effects of subjective bias (i.e. visual inspection), imaging procedure (partial- vs. whole-brain imaging), and ICA (i.e. choice of model order), cross-validation of DMN-subsystem maps was performed by multiple spatial regression procedure (implemented in the GIFT toolbox). Multiple regressions revealed consistent spatial patterns of DMN-subsystems across different approaches (Tab. S4). For example spatial regression of the aHP-pattern, which was derived from ICA of partial-brain fMRI data with 40 components, on all ICs, which were derived from ICA of partial-brain fMRI data with 70 components, revealed a regression coefficient of 0.62 for the corresponding aHP pattern (Tab. S4); regression coefficients of all other ICs were below 0.09.

Concerning between-group comparisons of DMN-subsystems, we reported only results from the approach based on the ICA of partial-brain fMRI with 40

components. Group-comparisons, which were based on the ICA of restricted whole-brain fMRI data, did not reveal differences between groups, indicating that increased spatial resolution of imaging data is necessary to detect AD effects on DMN-subsystems (see also Fig. S6). Group-comparisons, which were based on ICA of partial-brain data with 70 components, revealed almost identical results like those of the reported approach with 40 components, indicating consistency of findings across different ICA approaches.

Supplementary Discussion:

Methodological issues. Although the current study used partial-brain-fMRI, one should note that our ICA-based approach does not enable analysis of specific subregions of the hippocampus. Such an analysis, which is beyond this study's aim, relies on region-of-interest-based iFC calculation combined with elaborated across-subject normalization [17].

In order to preserve advantages of increased spatial resolution, we used smaller smoothing kernel of 3x3x3 mm^3 when smoothing partial-brain high-resolution rs-fMRI. We found that smaller kernels applied on whole-brain data affected detection of local-iFC patterns of hippocampal subsystems (Fig. S4), suggesting a potential influence of smoothing kernel extent on iFC measuring. This influence might be further modulated by structural changes such as atrophy, which may interact with smoothing kernel extent. For example partial volume effects of atrophy influence BOLD signals in a spatially non-homogeneous way; smoothing kernels of different spatial extent are sensitive for this inhomogeneity; therefore, potential group differences in BOLD-iFC might be due to interactions between atrophy and smoothing kernel extent. Since the hippocampus is strongly affected by atrophy in AD, we cannot exclude that observed group differences in hippocampal local-iFC are influenced by interacting smoothing kernel extent and atrophy, even when control for atrophy alone suggests significantly increased local-iFC in patients (Fig. S2). Further systematic studies on the influence of atrophy and preprocessing (such as smoothing kernel extent) on iFC are necessary.

Limitations. As MCI is an etiologically heterogeneous syndrome [18], it is possible that some of the current MCI patients did not suffer from AD. Although AD is the

most frequent cause underlying MCI [19], results of patients with MCI should be interpreted carefully when linked to early AD.

Finally, patients with dementia were treated with cholinesterase inhibitors, which may influence BOLD activity and consequently correspondent iFC group differences [20]. Even if our results are consistent with both previous findings in dementia and current results for patients with MCI [16, 21-24], they have to be interpreted carefully.

References:

[1] Power JD, Barnes KA, Snyder AZ, Schlaggar BL, Petersen SE. Spurious but systematic correlations in functional connectivity MRI networks arise from subject motion. NeuroImage 2012; 59:2142-54.

[2] Van Dijk KR, Sabuncu MR, Buckner RL. The influence of head motion on intrinsic functional connectivity MRI. NeuroImage 2012; 59:431-8.

[3] Sorg C, Manoliu A, Neufang S, Myers N, Peters H, Schwerthoffer D et al. Increased intrinsic brain activity in the striatum reflects symptom dimensions in schizophrenia. Schizophrenia bulletin 2013; 39:387-95.

[4] Allen EA, Erhardt EB, Damaraju E, Gruner W, Segall JM, Silva RF et al. A baseline for the multivariate comparison of resting-state networks. Frontiers in systems neuroscience 2011; 5:2.

[5] Calhoun VD, Adali T, Pearlson GD, Pekar JJ. A method for making group inferences from functional MRI data using independent component analysis. Human brain mapping 2001; 14:140-51.

[6] Himberg J, Hyvarinen A, Esposito F. Validating the independent components of neuroimaging time series via clustering and visualization. NeuroImage 2004; 22:1214-22.

[7] Ashburner J, Friston KJ. Unified segmentation. NeuroImage 2005; 26:839-51.

[8] Abou-Elseoud A, Starck T, Remes J, Nikkinen J, Tervonen O, Kiviniemi V. The effect of model order selection in group PICA. Human brain mapping 2010; 31:1207-16.

[9] Jo HJ, Gotts SJ, Reynolds RC, Bandettini PA, Martin A, Cox RW et al. Effective Preprocessing Procedures Virtually Eliminate Distance-Dependent Motion Artifacts in Resting State FMRI. J Appl Math 2013;

[10] Power JD, Mitra A, Laumann TO, Snyder AZ, Schlaggar BL, Petersen SE. Methods to detect, characterize, and remove motion artifact in resting state fMRI. NeuroImage 2014; 84:320-41.

[11] Satterthwaite TD, Wolf DH, Loughead J, Ruparel K, Elliott MA, Hakonarson H et al. Impact of in-scanner head motion on multiple measures of functional connectivity: relevance for studies of neurodevelopment in youth. NeuroImage 2012; 60:623-32.

[12] Satterthwaite TD, Elliott MA, Gerraty RT, Ruparel K, Loughead J, Calkins ME et al. An improved framework for confound regression and filtering for control of motion artifact in the preprocessing of resting-state functional connectivity data. NeuroImage 2013; 64:240-56.

[13] Rosso C, Valabregue R, Attal Y, Vargas P, Gaudron M, Baronnet F et al. Contribution of Corticospinal Tract and Functional Connectivity in Hand Motor Impairment after Stroke. PloS one 2013; 8:

[14] Kahn I, Andrews-Hanna JR, Vincent JL, Snyder AZ, Buckner RL. Distinct cortical anatomy linked to subregions of the medial temporal lobe revealed by intrinsic functional connectivity. Journal of neurophysiology 2008; 100:129-39.

[15] Margulies DS, Vincent JL, Kelly C, Lohmann G, Uddin LQ, Biswal BB et al. Precuneus shares intrinsic functional architecture in humans and monkeys. Proceedings of the National Academy of Sciences of the United States of America 2009; 106:20069-74.

[16] Gour N, Ranjeva JP, Ceccaldi M, Confort-Gouny S, Barbeau E, Soulier E et al. Basal functional connectivity within the anterior temporal network is associated with performance on declarative memory tasks. NeuroImage 2011; 58:687-97.

[17] Yassa MA, Stark CE. A quantitative evaluation of cross-participant registration techniques for MRI studies of the medial temporal lobe. NeuroImage 2009; 44:319-27.

[18] Gauthier S, Reisberg B, Zaudig M, Petersen RC, Ritchie K, Broich K et al. Mild cognitive impairment. Lancet 2006; 367:1262-70.

[19] Petersen RC, Smith GE, Waring SC, Ivnik RJ, Tangalos EG, Kokmen E. Mild cognitive impairment: clinical characterization and outcome. Archives of neurology 1999; 56:303-8.

[20] Pa J, Berry AS, Compagnone M, Boccanfuso J, Greenhouse I, Rubens MT et al. Cholinergic enhancement of functional networks in older adults with mild cognitive impairment. Annals of neurology 2013; 73:762-73.

[21] Sperling RA, Dickerson BC, Pihlajamaki M, Vannini P, LaViolette PS, Vitolo OV et al. Functional alterations in memory networks in early Alzheimer's disease. Neuromolecular medicine 2010; 12:27-43.

[22] Zarei M, Beckmann CF, Binnewijzend MA, Schoonheim MM, Oghabian MA, Sanz-Arigita EJ et al. Functional segmentation of the hippocampus in the healthy human brain and in Alzheimer's disease. NeuroImage 2012; 66C:28-35.

[23] Zhang Z, Liu Y, Jiang T, Zhou B, An N, Dai H et al. Altered spontaneous activity in Alzheimer's disease and mild cognitive impairment revealed by Regional Homogeneity. NeuroImage 2012; 59:1429-40.

[24] He Y, Wang L, Zang Y, Tian L, Zhang X, Li K et al. Regional coherence changes in the early stages of Alzheimer's disease: a combined structural and resting-state functional MRI study. NeuroImage 2007; 35:488-500.

Supplementary Figures:

Figure S1:

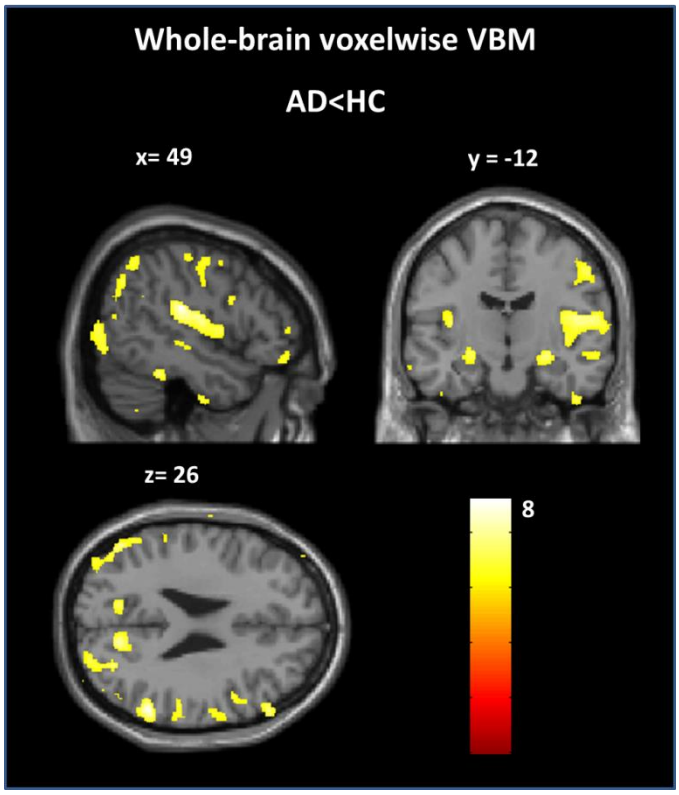

Figure S1. Whole-brain voxelwise VBM analysis reveals temporo-parietal atrophy in AD. Whole-brain voxelwise VBM analysis reveals that patients with AD-dementia have reduced regional grey matter volumes in the medial and lateral temporal lobes and in parietal areas compared to healthy controls (HC) (two-sample t-test, $p<0.05$ FWE cluster corrected). Color scales represent t-values; VBM maps are superimposed on single subject T1-weighted structural image. VBM voxel-based morphometry.

Figure S2:

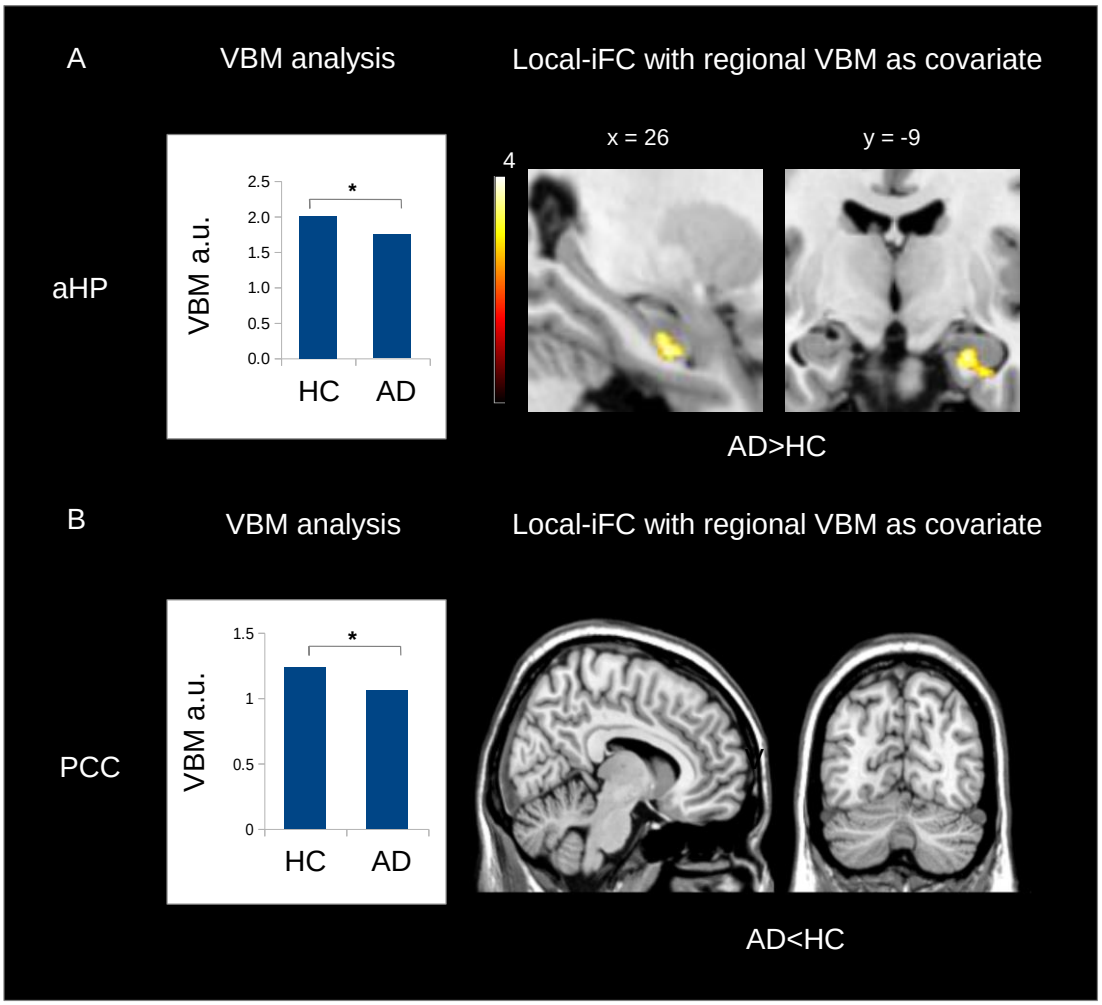

Figure S2. Impact of atrophy on aberrant local-iFC of DMN-subsystems. Regional voxel-based morphometry (VBM) volumes of DMN-subsystems centered on the aHP and PCC were compared across patients with AD dementia and healthy controls (two-sample t-test, $p<0.05$), and added as covariates-of-no-interests in corresponding t-tests for local-iFC ($p<0.05$ FWE cluster corrected). (A) Patients with AD-dementia have reduced regional VBM volumes in the aHP-related DMN-subsystem. When regional volumes were included in the local-iFC analysis as covariate, patients show increased local-iFC within the aHP-related subsystem compared to healthy controls. (B) Patients with AD-dementia have reduced regional VBM volumes in the PCC-related DMN-subsystem. When regional brain volumes were included in the local-iFC analysis as covariate, no group difference for local-iFC is present in the PCC-related DMN-subsystem. Color scales represent t-values. aHP

anterior hippocampus, PCC posterior cingulate cortex, VBM voxel-based morphometry.

Figure S3:

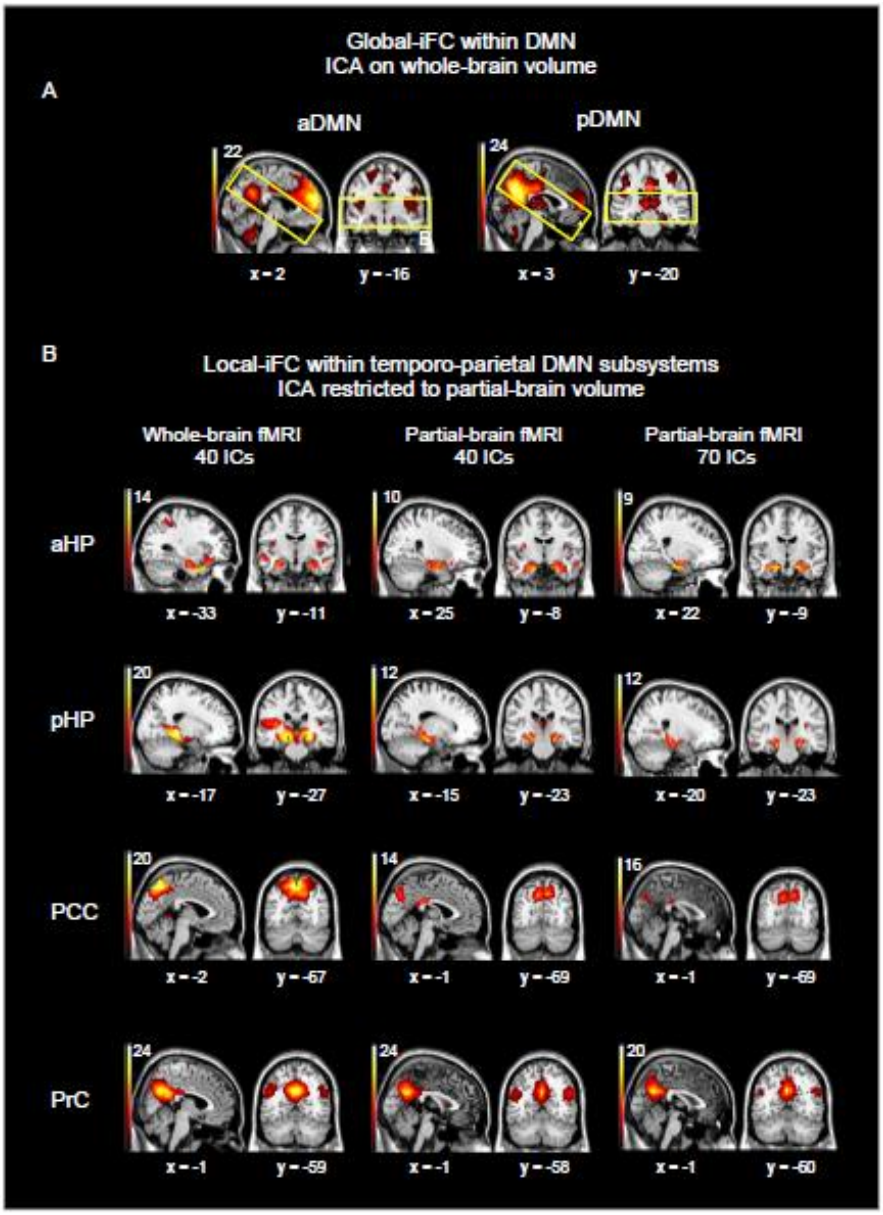

Figure S3. Consistent detection of temporo-parietal default mode network (DMN) subsystems. (A) Spatial patterns of global-iFC within the anterior and posterior DMN were derived from independent component analysis (ICA) of whole-brain rs-fMRI data (one-sample t-tests of back-reconstructed IC patterns from patients with MCI and AD-dementia and healthy controls, $p<0.05$, cluster level family wise error (FWE) corrected). Yellow lines indicate the field-of-view of spatial high-resolution partial brain rs-fMRI covering temporo-parietal DMN-subsystems of interest. (B) Spatial patterns of local-iFC within temporo-parietal DMN subsystems were derived from ICA of whole-brain and partial-brain rs-fMRI data, respectively,

restricted to the temporo-parietal volume of (A) with different ICA model order (40 and 70 components, respectively) (one-sample t-tests, $p<0.05$, FWE cluster level). Color scales represent t-values; maps are superimposed on single subject T1-weighted structural image. aHP anterior hippocampus, pHP posterior hippocampus, PrC, precuneus, PCC posterior cingulate cortex.

Figure S4

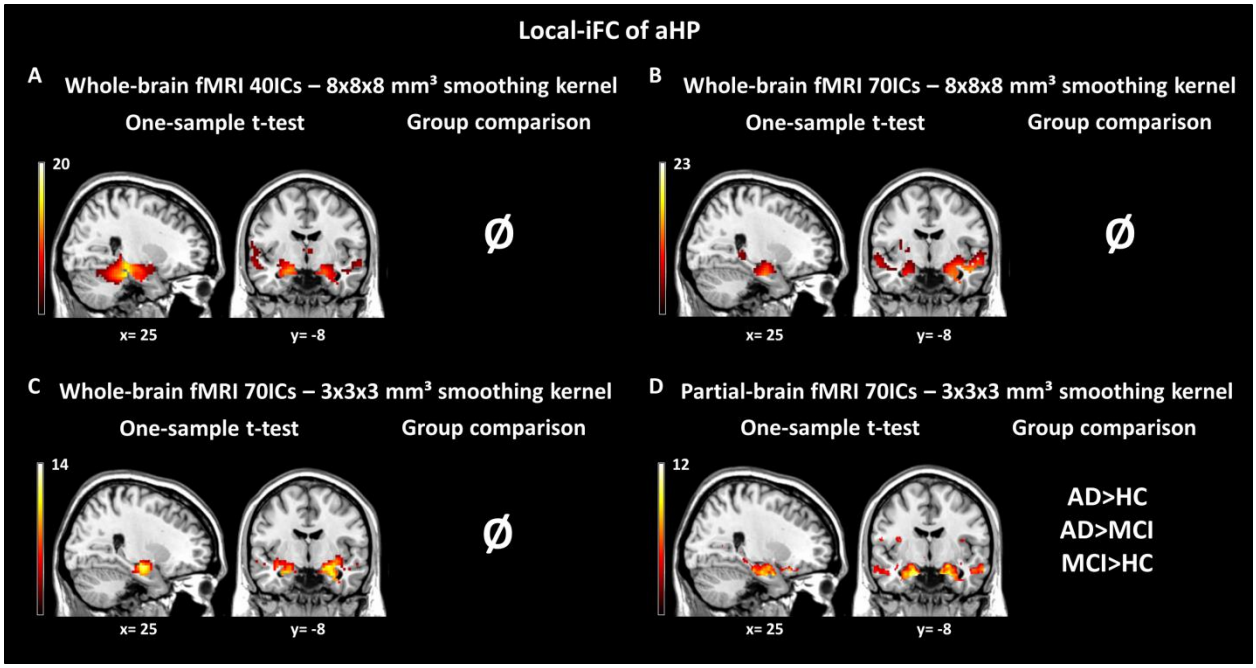

Figure S4. Estimating effects of smoothing kernel on both the detection of anterior hippocampus (aHP) local-iFC patterns from whole-brain data and corresponding group differences. Spatial patterns of aHP local-iFC and related group differences detected by different ICA approaches on whole- (A-C) and partial-brain (D) rs-fMRI data (one-sample t-tests of back-reconstructed IC patterns from patients with MCI and AD-dementia and healthy controls, $p<0.05$, cluster level family wise error (FWE) corrected). A) Spatial pattern of aHP local-iFC derived from ICA of whole-brain rs-fMRI data of model order 40; imaging data were smoothed by an 8x8x8 mm³ kernel. B) Spatial pattern of aHP local-iFC derived from ICA of whole-brain rs-fMRI data of model order 70; imaging data were smoothed by an 8x8x8 mm³ kernel. C) Spatial pattern of aHP local-iFC derived from ICA of model order 70 on whole-brain rs-fMRI; imaging data were smoothed by a 3x3x3 mm³ kernel. D) Spatial pattern of aHP local-iFC derived from ICA of model order 70 on high-resolution partial-brain rs-fMRI; imaging data were smoothed with a 3x3x3 mm³ kernel. Color scales represent t-values; maps are superimposed on a single subject T1-weighted structural image. aHP anterior hippocampus; iFC intrinsic functional connectivity.

Figure S5.

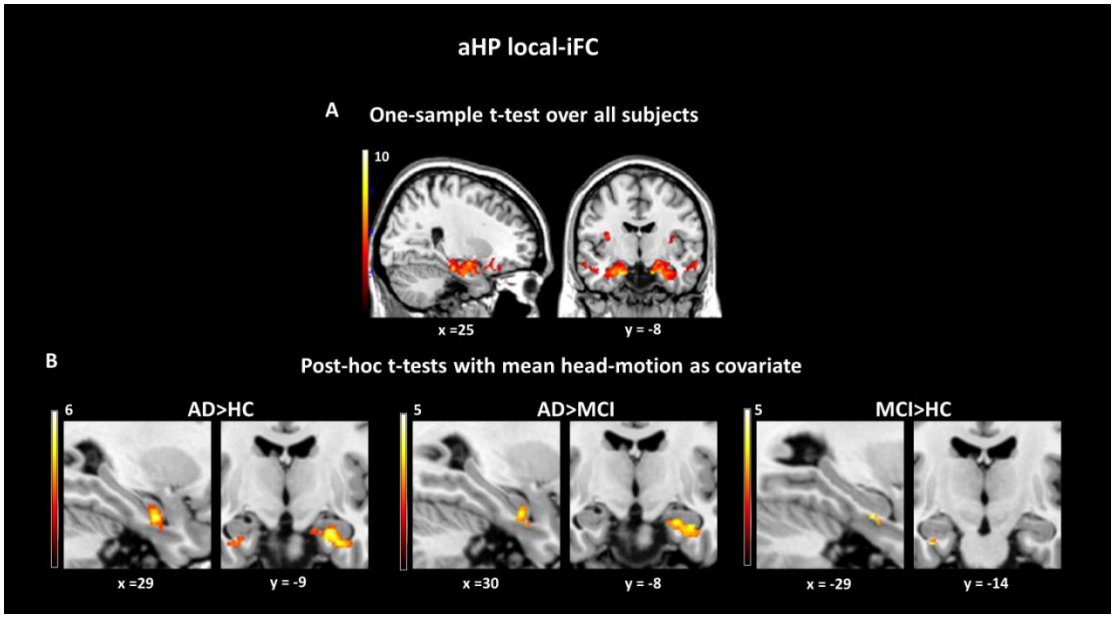

Figure S5. Control for head motion: Progressively increased local-iFC in the aHP along the course of AD with mean head-motion as control variable. A) Spatial pattern of local-iFC of the aHP-subsystem was derived from ICA of partial-brain rs-fMRI data, restricted to the temporo-parietal brain volume (one-sample t-tests of back-reconstructed IC patterns from patients with MCI and AD-dementia and healthy controls including head motion as co-variate-of-no-interest, $p<0.05$, cluster level family wise error (FWE) corrected). B) One-way ANOVA of local-iFC maps and correspondent post-hoc t-tests including head motion as co-variate-of-no-interest ($p<0.05$ FWE cluster corrected). Note chosen slices correspond with slices from Figure 1B and 2A from the manuscript to enable direct comparison of results derived from analyses with and without head motion as co-variate-of-no-interest. Color scales represent t-values; maps are superimposed on a single subject T1-weighted structural image. aHP anterior hippocampus.

Figure S6.

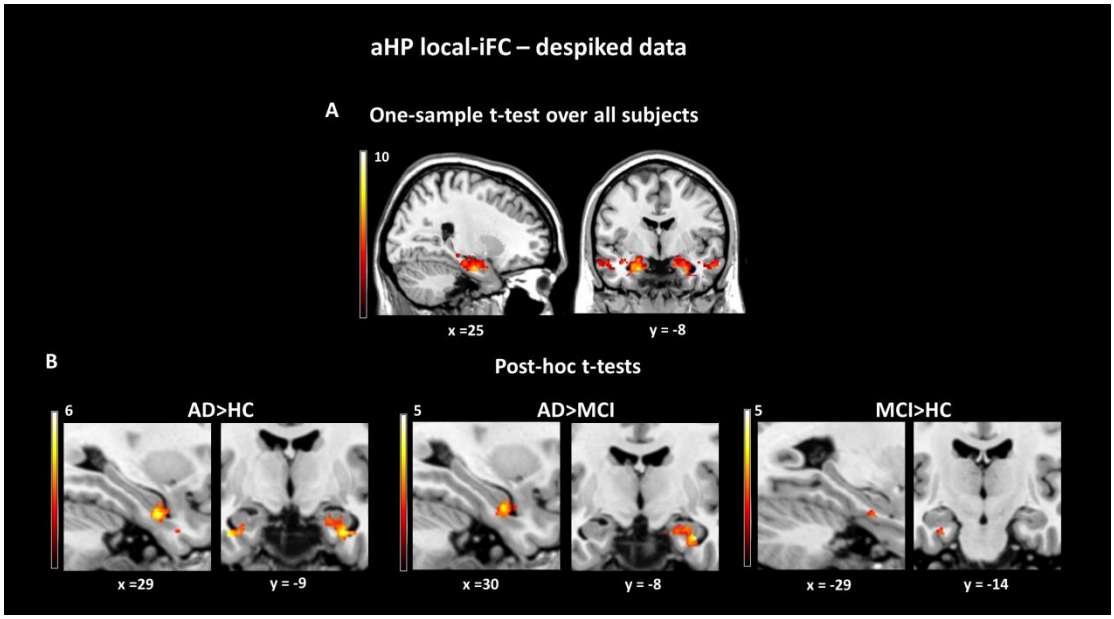

Figure S6. Control for head motion and frame censoring: Progressively increased local-iFC in the aHP along the course of AD using despiked fMRI data. A) Spatial pattern of local-iFC of the aHP-subsystem (derived from ICA of despiked partial-brain rs-fMRI data, restricted to the temporo-parietal brain volume; one-sample t-tests of back-reconstructed IC patterns from patients with MCI and AD-dementia and healthy controls, $p<0.05$, cluster level family wise error (FWE) corrected). B) One-way ANOVA of local-iFC maps and correspondent post-hoc t-tests from despiked data ($p<0.05$ FWE cluster corrected). Note chosen slices correspond with slices from Figure 1B and 2A from the manuscript to enable direct comparison of results in despiked and not-despiked data. Color scales represent t-values; maps are superimposed on a single subject T1-weighted structural image. aHP anterior hippocampus.

Supplementary Tables:

Table S1. Parameters of head movement.

Head motion (mm)	AD (n=21)	MCI (n=22)	HC (n=22)	F	p-value
Mean (SD)	0.08 (0.02)	0.08 (0.04)	0.09 (0.04)	0.06	0.937

Head motion in functional MRI data is measured by averaged root-mean-square (RMS) of translational parameters x, y, and z (mm) for each volume. AD = Alzheimer's disease; MCI = mild cognitive impairment; HC = healthy controls. ANOVA.

Table S2. Global and local intrinsic functional connectivity (iFC) of the default mode network and temporo-parietal DMN-subsystems.

Name	Region	Side	Cluster size (voxels)	peak voxel (x, y, z)	*t* peak voxel	p
Global-iFC in the DMN across all subjects (whole-brain rs-fMRI, ICA with 40 components)						
pDMN	Posterior Cingulate Cortex	L/R	4944	-6; -52; 31	24.59	0.001
	Angular Gyrus	R		33; 23; 25	15.38	0.001
	Angular Gyrus	L		-39; -64; 37	20.01	0.001
	Precuneus	R		9; -52; 25	24.34	0.001
	Orbital Gyrus	R	382	6; 59; -2	10.10	0.001
aDMN	Superior Medial Gyrus	L/R	3204	3; 59; 16	23.22	0.001
	Inferior Frontal Gyrus	R	750	42; 32; -11	7.17	0.001
	Angular Gyrus	L	494	-45; -66; 24	12.40	0.001
	Angular Gyrus	R	169	49; -63; 35	7.15	0.001
	Precuneus	L/R	538	-3; -55; 31	14.01	0.001
	Hippocampus	L	222	-22; -22; -14	5.31	0.001
	Cerebellum	L/R	289	-3; -55; -41	7.82	0.001
Local-iFC in DMN-subsystems across all subjects (partial-brain rs-fMRI, ICA with 40 components)						
pHP	Hippocampus, Parahippocampus	L/R	12385	-17; -22; -17	13.00	0.001
aHP	Hippocampus, Parahippocampus	R	11513	17; -14; -22	12.01	0.001
	Hippocampus, Parahippocampus	L	9779	-20; -7; -26	10.36	0.001
PCC	Precuneus	L/R	14200	11; -65; 32	15.90	0.001
	Posterior Cingulate Cortex	L/R	2435	-3; -29; -28	9.30	0.001
PrC	Precuneus, Posterior	L/R	17439	-1; -59; 28	25.25	0.001

	Cingulate Cortex					
	Angular Gyrus, Mid. Temporal Gyrus	R	4920	49; -61; -28	11.04	0.001
	Angular Gyrus, Mid. Temporal Gyrus	L	5850	-49; -64; 31	9.71	0.001

Results are based on one-sample t-tests, $p<0.05$ FWE cluster level corrected; peak coordinates are based on MNI space. a/pDMN anterior/posterior default mode network, aHP anterior hippocampus, pHP posterior hippocampus, PrC, precuneus, PCC posterior cingulate cortex.

Table S3. Group differences for local-iFC in DMN-subsystems.

DMN-subsystems and group comparison	Region	Side	Cluster size (voxels)	peak voxel (x, y, z)	*t* peak voxel	p
Group comparison without covariate for regional brain volume						
aHP AD>HC	Hippocampus	R	405	26; -11; -22	4.76	0.001
	Hippocampus	L	201	31; -13; -26	4.98	0.008
aHP AD>MCI	Hippocampus	R	306	33; -7; -23	4.57	0.001
aHP MCI>HC	Hippocampus	L	25	-30; -14; -26	4.95	0.039
PCC AD<HC	Precuneus	R	62	9; -65; 44	4.11	0.031
Group comparison including covariate for regional brain volume						
aHP AD>HC	Hippocampus	R	286	26; -11; -22	4.07	0.013

Results are based on ANOVA and corresponding post-hoc t-tests without and with covariates of regional voxel-based morphometry volumes, $p<0.05$ FWE cluster corrected; peak coordinates are based on MNI space. aHP anterior hippocampus, PCC posterior cingulate cortex, AD Alzheimer's disease, MCI mild cognitive impairment, HC healthy control.

Table S4. Spatial multiple regression coefficients of local-iFC patterns representing DMN-subsystems derived from different analysis approaches.

		Whole-brain rs-fMRI ICA model order 40	Partial-brain rs-fMRI ICA model order 70
		Spatial multiple regression coefficients	
Partial-brain rs-fMRI ICA model order 40	aHP	0.31	0.62
	pHP	0.20	0.58
	PCC	0.16	0.78
	PrC	0.57	0.79

Three distinct ICA approaches on rs-fMRI data restricted to a partial-brain-volume (PBV) were performed: partial-brain fMRI/40-model-order ICA, whole-brain fMRI/ 40-model-order ICA, and partial-brain fMRI/70-model-order ICA. Patterns of local-iFC, which were expected for the aHP, pHP, PCC and PrC, were selected for each approach by visual inspection. Consistency of selected patterns across approaches was evaluated by spatial multiple regression analysis. Specifically, selected components of the approach partial-brain rs-fMRI/40-model-order ICA were spatially regressed on all components of the two control approaches, respectively. Regression coefficients for correspondent patterns were presented in the table. All other coefficients were below 0.09, indicating consistency of selected components across imaging and ICA parameter changes. Abbreviations: aHP anterior hippocampus, pHP posterior hippocampus, PCC posterior cingulate cortex, PrC precunes, ICA independent component analysis, rs-fMRI resting state functional magnetic resonance imaging.

Published Ahead of Print on April 15, 2015 as 10.1212/WNL.0000000000001575

The lower hippocampus global connectivity, the higher its local metabolism in Alzheimer disease

Masoud Tahmasian, MD, PhD
Lorenzo Pasquini, MSc
Martin Scherr, MD
Chun Meng, MSc
Stefan Förster, MD
Satja Mulej Bratec, MSc
Kuangyu Shi, PhD
Igor Yakushev, MD
Markus Schwaiger, MD
Timo Grimmer, MD
Janine Diehl-Schmid, MD
Valentin Riedl, MD, PhD
Christian Sorg, MD*
Alexander Drzezga, MD*

Correspondence to Dr. Tahmasian: masoud.tahmasian@lrz.tum.de

ABSTRACT

Objectives: Based on the hippocampus disconnection hypothesis in Alzheimer disease (AD), which postulates that uncoupling from cortical inputs contributes to disinhibition-like changes in hippocampus activity, we suggested that in patients with AD, the more the intrinsic functional connectivity between hippocampus and precuneus is decreased, the higher hippocampal glucose metabolism will be.

Methods: Forty patients with mild AD dementia, 21 patients with mild cognitive impairment, and 26 healthy controls underwent simultaneous PET/MRI measurements on an integrated PET/MR scanner. ^{18}F-fluorodeoxyglucose-PET was used to measure local glucose metabolism as proxy for neural activity, and resting-state functional MRI with seed-based functional connectivity analysis was performed to measure intrinsic functional connectivity as proxy for neural coupling. Group comparisons and correlation analysis were corrected for effects of regional atrophy, partial volume effect, age, and sex.

Results: In both patient groups, intrinsic connectivity between hippocampus and precuneus was significantly reduced. Moreover, in both patient groups, glucose metabolism was reduced in the precuneus (AD < mild cognitive impairment < controls) while unchanged in the hippocampus. Critically, the lower connectivity between hippocampus and precuneus was in patients with AD dementia, the higher was hippocampus metabolism.

Conclusion: Results provide evidence that in patients with AD dementia, stronger decrease of intrinsic connectivity between hippocampus and precuneus is linked with higher intrahippocampal metabolism (probably reflecting higher neuronal activity). These data support the hippocampus disconnection hypothesis, i.e., uncoupling from cortical inputs may contribute to disinhibition-like changes of hippocampal activity with potentially adverse consequences on both intrahippocampal physiology and clinical outcome. *Neurology*® 2015;84:1–8

GLOSSARY

AD = Alzheimer disease; **ANCOVA** = analysis of covariance; **BOLD** = blood oxygen level–dependent; **CDR** = Clinical Dementia Rating; **DMN** = default mode network; **FDG** = ^{18}F-fluorodeoxyglucose; **FDR** = false discovery rate; **FOV** = field of view; **iFC** = intrinsic functional connectivity; **MCI** = mild cognitive impairment; **MP-RAGE** = magnetization-prepared rapid-acquisition gradient echo; **PVC** = partial volume correction; **ROI** = region of interest; **rs-fMRI** = resting-state fMRI; **TUM** = Technische Universität München; **VBM** = voxel-based morphometry.

Hippocampus and retrosplenial cortex are central parts of the default mode network (DMN).[1] The DMN is an intrinsic brain network characterized by synchronous ongoing activity (i.e., intrinsic functional connectivity [iFC]). It is primarily affected in Alzheimer disease (AD) by β-amyloid and tau pathology, atrophy, and reduced iFC.[2–6] For example, β-amyloid pathology is already present in the retrosplenial cortex in the preclinical stages of AD,[4,5] while tau pathology and atrophy start in the transentorhinal region and hippocampus when first clinical symptoms appear.[7] Aberrant hippocampus activity has special characteristics in early AD. First, during

Supplemental data at Neurology.org

*These authors contributed equally to this work.

From the Departments of Neuroradiology (M.T., L.P., M. Scherr, C.M., S.M.B., V.R., C.S.), Nuclear Medicine (M.T., S.F., K.S., I.Y., M. Schwaiger, V.R., C.S., A.D.), and Psychiatry and Psychotherapy (M. Scherr, T.G., J.D.-S., C.S.) of Klinikum rechts der Isar, Technische Universität München; TUM-NIC Neuroimaging Center (M.T., L.P., M. Scherr, C.M., S.F., S.M.B., I.Y., V.R., C.S.), Technische Universität München, Munich; Graduate School of Systemic Neurosciences (C.M., S.M.B.), Ludwig Maximilians University, Munich; Department of Nuclear Medicine (M.T., A.D.), University Hospital of Cologne, Germany; Sleep Disorders Research Center (M.T.), Kermanshah University of Medical Sciences, Iran; and Department of Neurology (M. Scherr), Christian Doppler Clinic, Paracelsus Medical University, Salzburg, Austria.

Go to Neurology.org for full disclosures. Funding information and disclosures deemed relevant by the authors, if any, are provided at the end of the article.

memory processes, hippocampus activity has been demonstrated to be increased in mild cognitive impairment (MCI; a high-risk state for AD) while reduced in AD dementia,[8] with the degree of hyperactivity being linked with the level of structural parietal DMN degradation.[9] Since antiepileptic drugs normalize hippocampus hyperactivity with simultaneous memory improvement, hippocampus hyperactivity may represent an adverse consequence of AD instead of a beneficial compensation.[10] Second, beyond memory-related activity, synchronous ongoing intrahippocampal activity is progressively increased in MCI and AD dementia, with such increased local synchrony being associated with both patients' memory deficits and progressively reduced hippocampus iFC within the DMN.[11,12] Together, these findings suggest that hippocampus uncoupling from its main cortical input system may lead to disinhibition-like changes of intrahippocampal activity ("hippocampus disconnection hypothesis").[11–13] Accordingly, we hypothesized that the more iFC between hippocampus and precuneus is reduced, the higher intrahippocampal glucose metabolism (as a proxy for local hippocampus activity) may be found in patients with AD dementia.

METHODS

Overview. Participants (table) were scanned on an integrated PET/MR scanner using ^{18}F-fluorodeoxyglucose-PET (FDG-PET), resting-state fMRI (rs-fMRI), and structural MRI. FDG-PET was used to measure local glucose metabolism, which reflects local glutamate-dependent synaptic activity,[14,15] seed-based functional connectivity analysis of rs-fMRI data with a seed in the precuneus was used to assess coherent blood oxygen level–dependent (BOLD) activity between hippocampus and precuneus (i.e., functional connectivity between these regions),[16] and voxel-based morphometry (VBM) of structural MRI was used to estimate and control for regional gray matter volumes.[11,16,17] Both the whole hippocampus and precuneus seed were used for further region-of-interest (ROI)-based analysis. Specifically, ROI-averaged values for iFC, FDG metabolism, and VBM values were obtained for all subjects. Analysis of covariance (ANCOVA) was applied for group comparisons of local metabolism and iFC. Partial correlation analysis was performed between local hippocampus metabolism (FDG-PET) and iFC between hippocampus and precuneus (rs-fMRI). All across-subject analyses were controlled for effects of age, sex, regional gray mater volume, and partial volume effects. Further methodologic details and additional confirmatory analyses are presented in appendix e-1 on the *Neurology*® Web site at Neurology.org.

Subjects. Forty-two patients with mild AD dementia, 24 patients with MCI, and 26 healthy controls participated in this study. Patients were recruited from the Memory Clinic of the Department of Psychiatry and Psychotherapy, and healthy controls by word-of-mouth advertising. Examination of every participant included medical history, neurologic examination, informant interview (Clinical Dementia Rating [CDR]),[18] neuropsychological assessment (Consortium to Establish a Registry for Alzheimer's Disease),[19] and blood tests (for patients only). Criteria for MCI (CDR global = 0.5) included reported and neuropsychologically assessed cognitive impairments and largely intact activities of daily living, and excluded dementia.[20] Patients with AD dementia fulfilled criteria for mild dementia (CDR global = 1) and the National Institute of Neurological and Communicative Disorders and Stroke and the Alzheimer's Disease and Related Disorders Association criteria for AD and dementia.[21] Exclusion criteria were other neurologic, psychiatric, or systemic diseases (e.g., stroke, acute depressive episode, substance/drug abuse) or clinically remarkable structural MRI (e.g., cerebrovascular lesions) potentially related to cognitive impairment. Twelve patients with AD dementia/8 patients with MCI/6 healthy controls were treated for hypertension (β-blockers, ACE [angiotensin-converting enzyme] inhibitors, and calcium channel blockers), 10/6/3 for hypercholesterolemia (statins), 2/1/0 had diabetes mellitus, 6/3/0 received antidepressant medication (mirtazapine, citalopram), and 35/0/0 received cholinesterase inhibitors.

Standard protocol approvals, registrations, and patient consents. The study was approved and registered by the medical ethical board of Technische Universität München (TUM) in line with Human Research Committee guidelines of TUM. All subjects provided informed consent in accordance with the standard protocol approvals.

Data acquisition. Scanning was performed on an integrated Siemens Biograph mMR scanner (Siemens, Erlangen, Germany)

Table Demographic and clinical data of participants

	CON (n = 26)	MCI (n = 21)	AD dementia (n = 40)	*p* Value
Age, y, mean (SD)	55.58 (10.21)	66.81 (9.77)	70.83 (8.18)	0.056
Sex, female	9	14	20	0.109
Education, y	10.10 (1.51)	10.02 (1.69)	9.84 (2.03)	0.406
MMSE score, mean (SD)	29.51 (1.02)	26.93 (2.26)	22.03 (4.61)	0.000
CERAD total, mean (SD)	86.10 (8.13)	69.61 (10.44)	53.65 (12.58)	0.000

Abbreviations: AD = Alzheimer disease; CERAD = Consortium to Establish a Registry for Alzheimer's Disease; CON = healthy controls; MCI = mild cognitive impairment; MMSE = Mini-Mental State Examination.
Analysis of variance, $p < 0.05$ as threshold of significance, except of sex (Kruskal-Wallis test).

capable of simultaneously acquiring PET and MRI data using the vendor-supplied 12-channel phase-array head coil. PET images, magnetization-prepared rapid-acquisition gradient echo (MP-RAGE) T1-weighted anatomical images, and T2-weighted echo planar imaging MRI data were acquired using the following scanning parameters. PET: list-mode acquisition, 30 minutes after injection, 15 minutes acquisition time, 128 slices (gap 0.5 mm) covering the whole brain; field of view (FOV) 450 mm; matrix size 192 × 192; voxel size: 3.7 × 2.3 × 2.7 mm. Echo planar imaging: repetition time/echo time/α = 2.000 milliseconds (ms)/30 ms/90°; 35 slices (gap 0.6 mm) aligned to AC/PC covering the whole brain; FOV 192 mm; matrix size 64 × 64; voxel size 3.0 × 3.0 × 3.0 mm. Each measurement consists of 240 acquisitions in interleaved mode with a total scan time of 8 minutes, 08 seconds. MP-RAGE: repetition time/echo time/α = 2.300 ms/2.98 ms/9°; 160 slices (gap 0.5 mm) covering the whole brain; FOV 256 mm; matrix size 256 × 256; voxel size 1.0 × 1.0 × 1.0 mm.[22]

Preprocessing of imaging data. Preprocessing of PET and rs-fMRI data was adapted from previous studies[16,22] and is described in detail in appendix e-1. Briefly, after discarding the first 3 volumes, rs-fMRIs were realigned and coregistered with FDG-PET and T1-weighted images to create subject-specific multimodal datasets. These data were normalized to MNI (Montreal Neurological Institute) space. The rs-fMRI and PET images were resampled to the isotropic voxel size of 3 × 3 × 3 mm.

After smoothing (full width at half maximum gaussian kernel 8 × 8 × 8 mm), rs-fMRI data were intensively controlled for movement-induced artifacts[23] (i.e., excessive head movements, point-to-point translational and rotational movements, temporal signal-to-noise ratio) with no significant differences being found across groups (see appendix e-1).

VBM of structural MRI data was performed as described previously[11,16,17] and in appendix e-1.

rs-fMRI data analysis. For seed-based iFC analysis, we used MarsBaR (http://marsbar.sourceforge.net) to create a spherical ROI in the precuneus with center coordinates (7, −60, 21) and radius of 6 mm (figure 1A). This region was described by Sheline et al.[24] as that part of the DMN with highest levels of β-amyloid plaque load in persons at risk of AD; because of the critical role of β-amyloid pathology in AD, we suggested this region as surrogate for DMN changes in early AD and used it as representative for potential AD-induced iFC changes. After Butterworth bandpass-filtering of all voxel time courses for frequencies from 0.009 to 0.08 Hz, voxel time courses of the seed ROI were extracted and then reduced to ROI-representative time courses by singular value decomposition. We put each time course into the first-level fixed-effects general linear model in SPM8, and iFC analysis was performed for each subject. For each model, additional regressors for global gray matter, white matter, CSF BOLD signal, and 6 movement parameters (translational and rotational movement) were considered as regressors of no interest.

Subsequently, to define iFC of the precuneus with the hippocampus, we restricted our iFC model to a bilateral whole hippocampus mask, which was derived from WFU-PickAtlas (http://fmri.wfubmc.edu/software/PickAtlas, version 2.5.2) (figure 1B). From precuneus and hippocampus ROIs, we extracted and

Figure 1 ROI based on resting-state functional connectivity

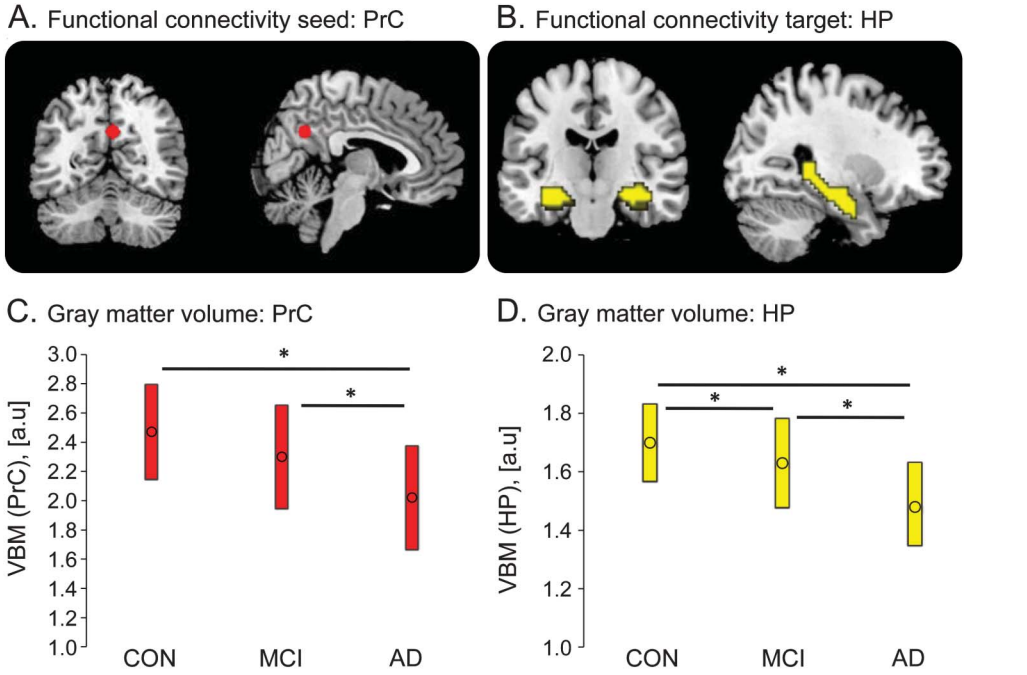

The study focused on the relationship between hippocampal local glucose metabolism and resting-state functional connectivity between precuneus (PrC) and hippocampus (HP) in patients with Alzheimer disease (AD) dementia or mild cognitive impairment (MCI), by the use of region-of-interest (ROI)-based approach. (A) The chosen ROI in the PrC is involved in the earliest stages of AD based on previous studies, and serves as seed for a seed-based functional connectivity analysis. (B) The bilateral whole HP region as a target based on WFU-PickAtlas. (C) Averaged voxel-based morphometry (VBM) revealed volume reductions in patients with AD dementia in the PrC and (D) HP (analysis of variance and post hoc *t* tests, $p < 0.05$). For such structural changes, subsequent analyses in correspondent functional connectivity and local metabolism have been controlled. CON = controls.

averaged values from single-subject iFC maps, FDG metabolism maps, and regional brain volume maps (as described below). Averaged values were fed into further group comparisons and correlation analyses in SPSS version 20 (IBM Corp., Armonk, NY). In the group comparisons, sex, age, and regional gray matter volumes were included as covariates of no interest.

PET data analysis. Preprocessed PET images were scaled by normalization of whole-brain FDG uptake values to cerebellar vermis FDG uptake[25] and were spatially smoothed using a gaussian kernel full-width at half-maximum of 12 mm. To correct FDG-PET data for a potential influence of partial volume effects, correction for partial volume effects (PVC) was performed by the use of segmented individual T1-weighted MRI in gray matter, white matter, and CSF. An algorithm implemented in the PMOD software package (PMOD Technologies Ltd., Adliswil, Switzerland) was applied for PVC, which has been suggested and described previously.[26,27] Afterward, from both ROIs, we extracted and averaged FDG metabolism values from the normalized FDG map of each subject. Group comparisons were performed of values obtained in the ROIs (hippocampus and precuneus) by the use of ANCOVA and corresponding least significant difference post hoc *t* tests including covariates of no interest (sex, age, and gray matter values of precuneus and hippocampus) with a threshold of $p < 0.05$.

Partial correlation analysis. To evaluate the expected relationship between intrahippocampus activity and hippocampus-precuneus iFC, partial correlation analyses were performed for the FDG metabolism in the hippocampus and precuneus and iFC between these regions. Partial correlation is defined here as the relationship between 2 different variables controlled for the influence of another variable such as age, sex, and regional gray matter volume.[28] We performed partial correlation analyses for each patient group separately, controlling for the mentioned covariates of no interest.

Control analyses. To control for critical methodologic steps, we performed additional analyses concerning the effect of PVC of PET data, voxel-wise vs ROI-based correlation between iFC and metabolism, and the effects of global gray matter signal regression (see appendix e-1).

RESULTS

Reduced gray matter volume in precuneus and hippocampus of patients with AD. VBM revealed that gray matter volume of hippocampus ($F_{4,86} = 17.58$, $p < 0.001$) and precuneus ($F_{4,86} = 6.98$, $p < 0.001$) was different across groups (ANCOVA controlled for age and sex, $p < 0.05$). Post hoc tests revealed atrophy for precuneus (controls > AD, $p < 0.001$; MCI > AD, $p = 0.001$) and hippocampus (controls > AD, $p < 0.001$; MCI > AD, $p < 0.001$; and controls > MCI, $p = 0.049$) in patients with AD (figure 1, C and D).

Patients had reduced intrinsic connectivity between precuneus and hippocampus. Restricted to the whole hippocampus region (figure 1B), ANCOVA on averaged iFC values demonstrated iFC difference across groups ($F_{5,86} = 3.40$, $p = 0.038$; controlled for age, sex, and hippocampus volume). Post hoc *t* tests revealed that compared with healthy controls, iFC was reduced for patients with AD dementia ($p = 0.017$) and MCI ($p = 0.043$), and there was no difference between patients with AD dementia and patients with MCI (figure 2A).

Patients had progressive hypometabolism in precuneus but unchanged metabolism in hippocampus. Averaged FDG-PET values were different across groups for the precuneus (ANCOVA, $F_{5,86} = 29.23$, $p < 0.001$) but not for the hippocampus. Post hoc *t* tests revealed progressive decrease of glucose metabolism in the precuneus along patient groups (controls > AD, $p < 0.001$; controls > MCI, $p = 0.006$; and MCI > AD, $p = 0.009$) (figure 2C.a). FDG metabolism in the hippocampus was unchanged across groups (figure 2B.a).

The lower extrahippocampal iFC, the higher hippocampus metabolism in patients with AD dementia. Of note, partial correlation analyses demonstrated that lower precuneus-hippocampus iFC is associated with higher FDG metabolism for the hippocampus, only in patients with AD dementia ($r = -0.275$, $p = 0.050$) (figure 2B.b). For patients with MCI, there was no such correlation ($R = -0.036$, $p = 0.44$). Furthermore, there was no association between iFC and FDG metabolism for the precuneus in both groups ($r = -0.008/0.326$, $p = 0.962/0.174$ for AD/MCI) (figure 2C.b).

Our finding was controlled for different methodologic factors. First, partial correlation between precuneus-hippocampus iFC and hippocampal non-PVC FDG values also demonstrated a similar link between iFC and FDG metabolism in patients with AD dementia ($r = -0.291$, $p = 0.041$) (figure e-1). Second, to confirm the results of the ROI-based approach, we performed a voxel-wise analysis (see methods and appendix e-1), which revealed that higher hippocampus FDG metabolism is linked with lower hippocampal iFC with both the angular gyrus (−48, −64, 40; cluster size = 157, *p* value false discovery rate [FDR]-corrected = 0.028) and the precuneus (0, −49, 52; cluster size = 141, *p* value FDR-corrected = 0.028) (figure e-2). Third, to control the effect of global gray matter regression on the association between hippocampus metabolism and connectivity, we performed alternative preprocessing, which was based on global brain signal regression derived from the white matter and CSF signal as described before.[29,30] We found almost identical results in patients with AD dementia as for the previous analysis based on global gray matter regression, i.e., the lower hippocampus connectivity, the higher its local metabolism ($r = -0.273$, $p = 0.051$; supplement 5 in appendix e-1).

DISCUSSION

To assess the relationship between precuneus-hippocampus iFC and intrahippocampal metabolism in early AD, we used simultaneous

Figure 2 Hippocampus and precuneus: Resting-state functional connectivity, local FDG metabolism, and their relationship in AD

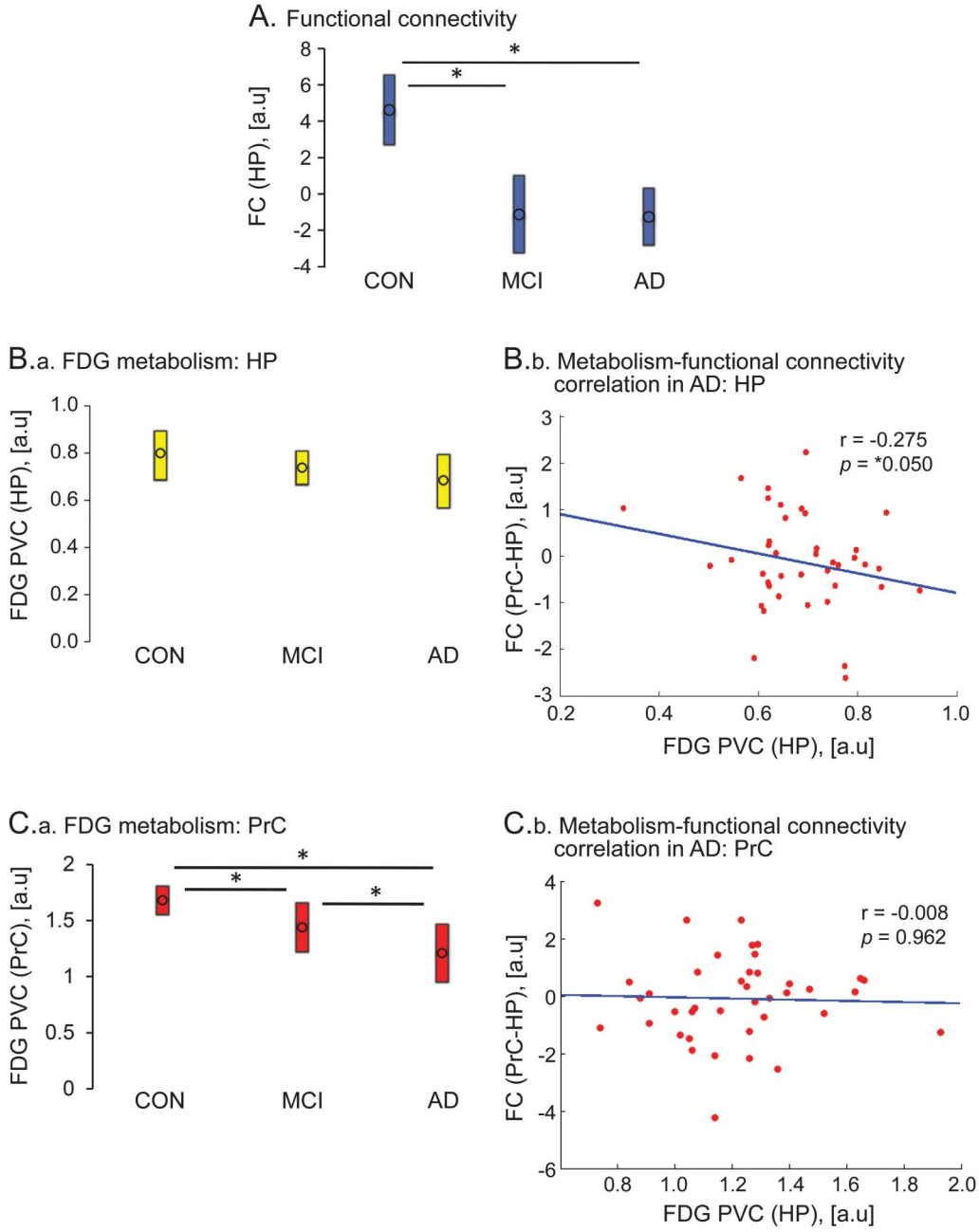

(A) Reduced precuneus (PrC)-hippocampus (HP) functional connectivity (FC) in patients with mild cognitive impairment (MCI) and Alzheimer disease (AD) dementia (ANCOVA and post hoc *t* tests, $p < 0.05$). (B.a) Preserved fluorodeoxyglucose (FDG) metabolism in the HP of patients (ANCOVA, $p < 0.05$). (B.b) The lower PrC-HP FC, the higher HP metabolism in patients with AD dementia (partial correlation with additional covariates of age, sex, HP, and PrC gray matter volume; $p < 0.05$). (C.a) Progressively reduced FDG metabolism in the PrC of patients (ANCOVA, $p < 0.05$). (C.b) Not correlated PrC metabolism and PrC-HP FC in patients with AD dementia (partial correlation with additional variates of age, sex, HP, and PrC gray matter volume; $p < 0.05$). ANCOVA = analysis of covariance; CON = controls; PVC = partial volume correction.

rs-fMRI and FDG-PET in healthy controls and patients with MCI and AD dementia. We found that in patients with AD dementia, lower iFC between hippocampus and precuneus correlated with higher hippocampal metabolism, independent of hippocampal atrophy (figure 2B.b). This result provides evidence that functional disconnectivity of the hippocampus from regions outside the hippocampus is associated with increased intrahippocampal neuronal activity in patients with AD dementia. Complementing our previous findings, functional decoupling from the DMN appears to relate not only to increased synchrony[11] but also to an increased total amount of

hippocampal activity, supporting the hippocampus disconnection hypothesis of AD.

We hypothesized this result because of previously observed association between increased local and decreased global hippocampus resting-state functional connectivity in patients with AD.[11,12] To control for the influence of structural changes on the suggested relationship (figure 1, C and D), we applied a partial correlation approach, which accounts separately for influences of structural changes on local metabolism and global connectivity. Furthermore, neither partial volume effects on PET data (figure e-1) nor voxel-wise vs ROI-based approach (see figure e-2) influenced our finding. Finally, the result was also independent from age and sex for which we controlled our analysis.

While local metabolism was preserved in the hippocampus, patients' metabolism was progressively reduced in the precuneus (figure 2, B.a and C.a). Moreover, patients with AD dementia had atrophy in both hippocampus and precuneus (figure 1, C and D), in line with several previous studies.[31–33] These incongruent patterns of atrophy and metabolism indicate distinctive local activity changes for neocortical and hippocampal regions despite consistent volume reductions. We found reduced iFC between hippocampus and precuneus in both patient groups, in line with previous studies[2,34] (figure 2A). Of note, we observed that reduced hippocampus-precuneus intrinsic connectivity was linked with increased hippocampus metabolism. The observed link between iFC and FDG metabolism was specific for the hippocampus; no such relation was present for the precuneus (figure 2, B.b and C.b). This specificity indicates that in AD, reduced precuneus-hippocampus connectivity is associated with hippocampus metabolism rather than precuneus metabolism. To control whether the link between hippocampus connectivity and metabolism depends on the choice of the precuneus as a seed in the FC analysis, we repeated FC analysis but with the hippocampus as a seed region and found almost identical results (figure e-2). Furthermore, the association between hippocampus connectivity and metabolism was specific for patients with AD dementia, since it was not present in patients with MCI.

The inverse relation between hippocampus connectivity and intrahippocampus activity lends support for the hippocampus disconnection hypothesis.[11–13] This hypothesis states that cortical disconnection leads to disinhibition-like changes of intrahippocampal activity, which is characterized by loop-like glutamate-dependent activity flow from entorhinal cortex to subiculum, dentate gyrus, CA3, CA1, and then back to entorhinal cortex.[35] While disrupted precuneus-hippocampus iFC is a proxy for hippocampal disconnection, hippocampal FDG metabolism may reflect intrahippocampal glutamate-based activity.[14,15] Also in line with the disconnection hypothesis, a previous study found that hippocampal diffusion tensor imaging–based diffusivity (a potential surrogate for hippocampal structural connectivity) is inversely related to hippocampal FDG metabolism.[36] Remarkably, our current results contrast in 2 aspects with our previous finding of progressively increased intrahippocampal synchrony along MCI and AD dementia.[11] First, reduced hippocampus connectivity was found to be inversely linked with increased synchrony in our previous study, while for metabolic activity, we found the same relation but metabolism was not increased in patients relative to healthy controls; this discrepancy between increased synchrony and preserved metabolic activity may indicate that the total amount of glutamate-dependent activity is unchanged but distinctively organized. Second, inverse connectivity-metabolism correlation was found only in patients with AD dementia, while an inverse relationship between global connectivity and local synchrony was also found in patients with MCI previously. In our study, the additional presence of hippocampus atrophy appeared to be a precondition for the inverse connectivity-metabolism relationship. Our findings suggest that such relationship reflects substantial hippocampus reorganization. We speculate whether such atrophy might be due to lasting hypersynchrony of ongoing hippocampus activity. Such hypersynchrony, in turn, might be associated with increased levels of synchronized synaptic glutamate, which is suggested to be detrimental for cellular integrity and therefore relevant for atrophy ("synaptic excitatory toxicity hypothesis"[37,38]). However, one should note that beyond global disconnection, additional other local factors might contribute to impaired hippocampus physiology in AD. For example, a recent rodent study has shown that β-amyloid plaque–induced hyperactivity within the hippocampus[39] and tau pathology, which affects the hippocampus very early in AD,[7] is associated with the local network hyperexcitability in mice correspondent with seizure frequency.[40]

Moreover, across the spectrum of Alzheimer disease, we observed a decline in connectivity and metabolism from cognitively normal to MCI to dementia. Mean levels of metabolism were slightly lower in AD dementia compared to MCI but showing a broader variance (figure 2, B.a). This indicates a general degradation in both parameters with ongoing neurodegeneration. Exclusively within the AD dementia group, we found the negative correlation between hippocampal metabolism and connectivity (figure 2, B.b). This is consistent with the hippocampus disconnection hypothesis but it did not result in an increase of HP metabolism above MCI levels in AD dementia. Furthermore, our findings may be

limited to moderate stages of AD and the observed phenomenon may disappear in later stages of disease.

Taken together, the current study provides evidence that in patients with AD dementia, a stronger decrease of intrinsic connectivity between hippocampus and precuneus is linked with higher intrahippocampal metabolism. Data are consistent with the hippocampus disconnection hypothesis suggesting that cortical uncoupling may contribute to disinhibition-like changes of hippocampus activity—with likely adverse consequences for hippocampus physiology and function.

AUTHOR CONTRIBUTIONS

All authors are fully responsible for the study. M.T., C.S., and A.D. designed the study. M.T., S.F., I.Y., T.G., J.D.-S., V.R., and A.D. recruited subjects and conducted the experiment. M.T., C.M., S.M.B., and K.S. analyzed the data. M. Schwaiger, C.S., and A.D. supervised the experiment. M.T., L.P., M. Scherr, A.D., and C.S. wrote the manuscript.

ACKNOWLEDGMENT

The authors thank all patients and their relatives for their participation in the study. Furthermore, the authors thank the staff of the Departments of Psychiatry and Psychotherapy and also Nuclear Medicine for their help in recruitment and data collection.

STUDY FUNDING

This work was supported by German Federal Ministry of Education and Research (BMBF 01ER0803 to C.S.), German research foundation (DFG) grants (DR 445/4-1 and DR 445/5-2 to A.D. and SFB 824 to M. Schwaiger), the Kommission für Klinische Forschung of the Klinikum Rechts der Isar der Technischen Universität München (KKF 8765162 to C.S.), and the German Academic Exchange service (DAAD) for financial support of M.T.

DISCLOSURE

The authors report no disclosures relevant to the manuscript. Go to Neurology.org for full disclosures.

Received June 16, 2014. Accepted in final form January 28, 2015.

REFERENCES

1. Buckner RL, Andrews-Hanna JR, Schacter DL. The brain's default network: anatomy, function, and relevance to disease. Ann NY Acad Sci 2008;1124:1–38.
2. Sorg C, Riedl V, Muhlau M, et al. Selective changes of resting-state networks in individuals at risk for Alzheimer's disease. Proc Natl Acad Sci USA 2007;104:18760–18765.
3. Greicius MD, Srivastava G, Reiss AL, Menon V. Default-mode network activity distinguishes Alzheimer's disease from healthy aging: evidence from functional MRI. Proc Natl Acad Sci USA 2004;101:4637–4642.
4. Sperling RA, Laviolette PS, O'Keefe K, et al. Amyloid deposition is associated with impaired default network function in older persons without dementia. Neuron 2009;63:178–188.
5. Drzezga A, Becker JA, Van Dijk KR, et al. Neuronal dysfunction and disconnection of cortical hubs in non-demented subjects with elevated amyloid burden. Brain 2011;134:1635–1646.
6. Myers N, Pasquini L, Gottler J, et al. Within-patient correspondence of amyloid-beta and intrinsic network connectivity in Alzheimer's disease. Brain 2014;137:2052–2064.
7. Braak H, Braak E. Neuropathological stageing of Alzheimer-related changes. Acta Neuropathol 1991;82:239–259.
8. Sperling RA, Dickerson BC, Pihlajamaki M, et al. Functional alterations in memory networks in early Alzheimer's disease. Neuromolecular Med 2010;12:27–43.
9. Putcha D, Brickhouse M, O'Keefe K, et al. Hippocampal hyperactivation associated with cortical thinning in Alzheimer's disease signature regions in non-demented elderly adults. J Neurosci 2011;31:17680–17688.
10. Bakker A, Krauss GL, Albert MS, et al. Reduction of hippocampal hyperactivity improves cognition in amnestic mild cognitive impairment. Neuron 2012;74:467–474.
11. Pasquini L, Scherr M, Tahmasian M, et al. Link between hippocampus' raised local and eased global intrinsic connectivity in AD. Alzheimers Dement Epub 2014 Jul 17.
12. Das SR, Pluta J, Mancuso L, et al. Increased functional connectivity within medial temporal lobe in mild cognitive impairment. Hippocampus 2013;23:1–6.
13. Yassa MA, Mattfeld AT, Stark SM, Stark CE. Age-related memory deficits linked to circuit-specific disruptions in the hippocampus. Proc Natl Acad Sci USA 2011;108:8873–8878.
14. Raichle ME, Mintun MA. Brain work and brain imaging. Annu Rev Neurosci 2006;29:449–476.
15. Magistretti PJ, Pellerin L. The contribution of astrocytes to the 18F-2-deoxyglucose signal in PET activation studies. Mol Psychiatry 1996;1:445–452.
16. Tahmasian M, Knight DC, Manoliu A, et al. Aberrant intrinsic connectivity of hippocampus and amygdala overlap in the fronto-insular and dorsomedial-prefrontal cortex in major depressive disorder. Front Hum Neurosci 2013;7:639.
17. Ashburner J, Friston KJ. Unified segmentation. Neuroimage 2005;26:839–851.
18. Gelb DJ, St Laurent RT. Clinical Dementia Rating. Neurology 1994;44:1983–1984.
19. Welsh KA, Butters N, Mohs RC, et al. The Consortium to Establish a Registry for Alzheimer's Disease (CERAD): part V: a normative study of the neuropsychological battery. Neurology 1994;44:609–614.
20. Gauthier S, Reisberg B, Zaudig M, et al. Mild cognitive impairment. Lancet 2006;367:1262–1270.
21. McKhann G, Drachman D, Folstein M, Katzman R, Price D, Stadlan EM. Clinical diagnosis of Alzheimer's disease: report of the NINCDS-ADRDA Work Group under the auspices of Department of Health and Human Services Task Force on Alzheimer's Disease. Neurology 1984;34:939–944.
22. Riedl V, Bienkowska K, Strobel C, et al. Local activity determines functional connectivity in the resting human brain: a simultaneous FDG-PET/fMRI study. J Neurosci 2014;34:6260–6266.
23. Van Dijk KR, Sabuncu MR, Buckner RL. The influence of head motion on intrinsic functional connectivity MRI. Neuroimage 2012;59:431–438.
24. Sheline YI, Raichle ME, Snyder AZ, et al. Amyloid plaques disrupt resting state default mode network connectivity in cognitively normal elderly. Biol Psychiatry 2010;67:584–587.
25. Chetelat G, Desgranges B, Landeau B, et al. Direct voxel-based comparison between grey matter hypometabolism and atrophy in Alzheimer's disease. Brain 2008;131:60–71.
26. Drzezga A, Grimmer T, Henriksen G, et al. Imaging of amyloid plaques and cerebral glucose metabolism in semantic dementia and Alzheimer's disease. Neuroimage 2008;39:619–633.

27. Mevel K, Desgranges B, Baron JC, et al. Detecting hippocampal hypometabolism in mild cognitive impairment using automatic voxel-based approaches. Neuroimage 2007;37:18–25.
28. Marrelec G, Krainik A, Duffau H, et al. Partial correlation for functional brain interactivity investigation in functional MRI. Neuroimage 2006;32:228–237.
29. Behzadi Y, Restom K, Liau J, et al. A component based noise correction method (CompCor) for BOLD and perfusion based fMRI. Neuroimage 2007;37:90–101.
30. Yan CG, Craddock RC, Zuo XN, et al. Standardizing the intrinsic brain: towards robust measurement of inter-individual variation in 1000 functional connectomes. Neuroimage 2013;80:246–262.
31. Samuraki M, Matsunari I, Chen WP, et al. Partial volume effect-corrected FDG PET and grey matter volume loss in patients with mild Alzheimer's disease. Eur J Nucl Med Mol Imaging 2007;34:1658–1669.
32. Ishii K, Sasaki M, Yamaji S, Sakamoto S, Kitagaki H, Mori E. Relatively preserved hippocampal glucose metabolism in mild Alzheimer's disease. Dement Geriatr Cogn Disord 1998;9:317–322.
33. Villain N, Fouquet M, Baron JC, et al. Sequential relationships between grey matter and white matter atrophy and brain metabolic abnormalities in early Alzheimer's disease. Brain 2010;133:3301–3314.
34. Kim J, Kim YH, Lee JH. Hippocampus-precuneus functional connectivity as an early sign of Alzheimer's disease: a preliminary study using structural and functional magnetic resonance imaging data. Brain Res 2013;1495:18–29.
35. Squire LR, Stark CE, Clark RE. The medial temporal lobe. Annu Rev Neurosci 2004;27:279–306.
36. Yakushev I, Schreckenberger M, Muller MJ, et al. Functional implications of hippocampal degeneration in early Alzheimer's disease: a combined DTI and PET study. Eur J Nucl Med Mol Imaging 2011;38:2219–2227.
37. Mackenzie IR, Miller LA. Senile plaques in temporal lobe epilepsy. Acta Neuropathol 1994;87:504–510.
38. Palop JJ, Mucke L. Synaptic depression and aberrant excitatory network activity in Alzheimer's disease: two faces of the same coin? Neuromolecular Med 2010;12:48–55.
39. Busche MA, Chen X, Henning HA, et al. Critical role of soluble amyloid-beta for early hippocampal hyperactivity in a mouse model of Alzheimer's disease. Proc Natl Acad Sci USA 2012;109:8740–8745.
40. DeVos SL, Goncharoff DK, Chen G, et al. Antisense reduction of tau in adult mice protects against seizures. J Neurosci 2013;33:12887–12897.

The lower hippocampus global connectivity, the higher its local metabolism in Alzheimer disease

Masoud Tahmasian, Lorenzo Pasquini, Martin Scherr, et al.

Neurology published online April 15, 2015
DOI 10.1212/WNL.0000000000001575

Appendix e-1

NEUROLOGY/2014/601476

The lower hippocampus global connectivity the higher its local metabolism in Alzheimer's disease

Masoud Tahmasian, Lorenzo Pasquini, Martin Scherr, Chun Meng, Stefan Förster, Satja Mulej Bratec, Kuangyu Shi, Igor Yakushev, Markus Schwaiger, Timo Grimmer, Janine Diehl-Schmid, Valentin Riedl, Christian Sorg, and Alexander Drzezga

Supplement 1: Preprocessing of rs-fMRI and FDG-PET images

PET and rs-fMRI imaging data analysis was adapted from previous studies[16, 22]. First, DICOM images were converted to 3D-NIFTI volumes, and then were preprocessed with SPM8 (Wellcome Trust Center for Neuroimaging, London, UK). Preprocessing encompassed coregistration of the multimodal imaging dataset and preparation of the rs-fMRI EPI time series data for FC analysis separately for each subject. First three images of each subject's EPI-time-series were removed, remaining EPI-images were realigned to this subject's mean EPI-image using 6° rigid-body transformation to correct for head motion during fMRI. Mean FDG-PET image was coregistered to the T1-weighted image using rigid-body transformation, and both images were then coregistered to the mean EPI-image, resulting in a subject-specific coregistered multimodal dataset. Each subject's brain data were then normalized to a standard template provided by the Montreal Neurological Institute (MNI) template using the SPM8 unified segmentation routine. MNI tissue-probability maps of grey matter, white matter, and CSF were warped onto single-subject T1-weighted images and were stored as masks for later use during the FC analysis. To achieve normalized single-subject data, the inverse transformation matrix of the warping process was later applied to T1-weighted, EPI, and PET images, and all EPI and PET images were resampled to an isotropic voxel size of 3x3x3 mm.

Rs-fMRI images were smoothed (FWHM Gaussian kernel 8x8x8mm). Excessive head motion (cumulative motion translation or rotation > 3mm or 3° and mean point-to-point translation or rotation > 0.15mm or 0.1°) was applied as exclusion criterion. 2 patients with AD and 3 with MCI had to be excluded due to excessive movement. Potential movement-induced artifacts across groups were carefully controlled. Firstly, ANOVA for mean point-to-point translation and rotation in any direction ($p > 0.20$) and for tSNR ($p > 0.30$) yielded no significant difference between groups. Secondly, the root mean square (RMS) of the translational head movement parameters was calculated for each subject[23]. ANOVA revealed no significant group differences concerning RMS. Further control for head motion effects was carried out at subject-level iFC analysis.

Supplement 2: Voxel-based morphometry (VBM) of structural MRI data.

To evaluate the influence of regional atrophy on iFC and PET results, we used the VBM8 toolbox (http://dbm.neuro.uni-jena.de/vbm.html) to analyze grey matter volume as described previously[11,16,17]. T1-weighted images were corrected for bias-field inhomogeneity, registered using linear (12-parameter affine) and non-linear transformations, and tissue-classified into gray matter, white matter, and cerebro-spinal fluid within the same generative model. Then, the resulting grey matter images were modulated to account for volume changes that result from the normalization process. We considered non-linear volume changes to control for differences in head size. Afterwards, our images were smoothed with a Gaussian kernel of 8mm (FWHM). Finally, ANOVA was carried out for averaged regional brain volumes restricted to the ROIs (i.e. hippocampus and precuneus) ($p<0.05$) for group comparisons.

Supplement 3:

To control the effect of partial-volume correction (PVC) of FDG-PET data on our findings, all analyses were replicated with non-PVC FDG-PET data, while controlling for age, sex and grey matter volume. The results demonstrated that averaged non-PVC FDG-PET values was different across groups for the precuneus (ANCOVA, $F(5,86)=27,65$, $p<0.001$) and for the hippocampus (ANCOVA, $F(5,86)=6,57$, $p<0.001$). Post-hoc t-tests revealed progressive decrease of non-PVC FDG-PET values in the precuneus across patient groups (CON>AD, $p<0.001$), (CON>MCI, $p=0.004$) and (MCI>AD, $p<0.001$). FDG-metabolism in the hippocampus was decreased in MCI (CON>MCI, $p=0.003$) and increased in AD-dementia group compared to MCI (AD>MCI, $p<0.002$), and finally between controls and AD-dementia there was no difference (CON>AD, $p=0.884$).

Critically, partial correlation analysis demonstrated that lower iFC was associated with higher non-PVC FDG-PET values for the hippocampus in patients with AD-dementia ($r= - 0.291$, $p=0.041$) (Figure e-1 Supplement). For patients with MCI, there was no correlation ($R= - 0.024$, $p=0.46$). This result confirms our main finding that in AD-dementia patients less hippocampus connectivity is associated with higher hippocampus metabolism. In other words, this association is independent of FDG-PET data preprocessing with respect to partial volume effect.

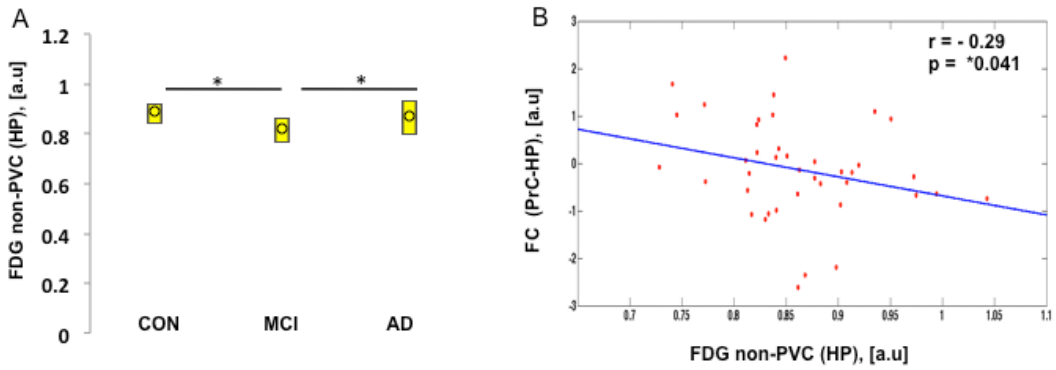

Figure e-1 Supplement: A) Group comparison based on non-partial volume corrected (non-PVC) FDG-PET metabolism of hippocampus; $p<0.05$, B) Lower precuneus (PrC)-hippocampus (HP) functional connectivity is associated with higher non-PVCFDG-PET metabolism of hippocampus in patients with AD-dementia (partial correlation, covariates of no-interest include age, sex, and HP grey matter volume; $p<0.05$).

Supplement 4:

To confirm and extend our findings particularly with respect to the hippocampus disconnection hypothesis, we carried out additional voxel-wise analysis of the association between hippocampal iFC and metabolism using a seed-to-whole brain voxel-wise approach in AD group with seed in the hippocampus. The seed was positioned in the whole bilateral hippocampus derived from WFU-Pickatlas (http://fmri.wfubmc.edu/software/PickAtlas, version 2.5.2) and voxel-wise hippocampus iFC analysis was performed in patients with AD-dementia (details in the methods section of the main text). In particular for across-subject analysis (ANCOVA), the metabolism in the bilateral hippocampus was used as a covariate of interest, and age and sex were used as covariates of no-interest. Results demonstrated that lower hippocampal iFC is associated with higher FDG-metabolism in the angular gyrus (-48,-64,40; cluster size=157, p-value FDR corrected=0.028) and the precuneus (0,-49,52; cluster size=141, p-value FDR corrected=0.028) (Figure e-2 Supplement). There was no positive association between hippocampal iFC and FDG-metabolism in voxel-wise approach.

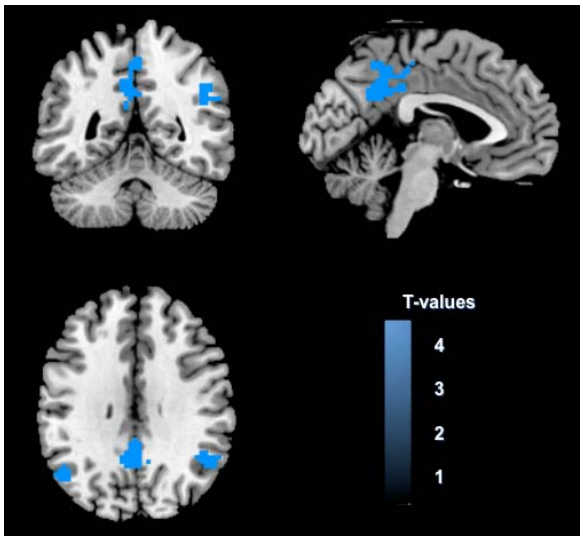

Figure e-2 Supplement: Lower hippocampal (HP) functional connectivity is linked with higher FDG-metabolism within the angular gyrus and precuneus in patients with AD-dementia (ANCOVA with covariates of no-interest including age, sex, and HP grey matter volume; $p<0.05$, FDR corrected).

This finding clearly supports our previous finding based on ROI approach meaning that higher hippocampus metabolism is associated with lower hippocampus connectivity with the precuneus. It extends our previous finding, since it demonstrated specificity of this association for the precuneus except of the angular gyrus. Interestingly, angular gyrus – as the precuneus – is part of the posterior DMN, suggesting that hippocampus metabolism is inversely associated with hippocampus connectivity with the cortical DMN. Since the hippocampus gets most of its cortical input from the DMN, this suggestion is perfectly in line with the general idea of the hippocampus disconnection hypothesis i.e. reduced cortical input contributes to disinhibition-like changes in the hippocampus.

Supplement 5:

To control the effect of global grey matter regression on the association between hippocampus metabolism and connectivity, we performed the preprocessing steps suggested by Behzadi and colleagues[29]: Based on our previously derived averaged BOLD time series of anatomically defined white matter (WM) and cerebral spinal fluid (CSF), we derived first principal component from CSF and WM time series for each patient with AD-dementia by the use of principal component analysis. We call this measure Comp-noise. The idea for this procedure is that non-neuronal noise of grey matter is similar with non-neuronal noise of non-grey matter. Then, we run first-level fixed effect models of seed-based iFC analysis as described previously but with the use of Comp-noise as nuisance variable instead of global grey matter signal. Finally, for each AD-dementia patient and whole hippocampus mask, new ß-maps were averaged and resulting hippocampus connectivity scores were further analyzed via correlation analysis as described in the manuscript. We got almost identical results for the association between hippocampus connectivity and metabolism in patients with AD-dementia as for the previous analysis with global grey matter regression i.e. r= - 0.273, p=0.051 (previous results: r= - 0.275, p=0.050; Figure 2 B2). This finding suggests that the inverse association between hippocampus connectivity and metabolism in patients with AD-dementia is not dependent on global grey matter signal regression. Particularly, it demonstrates no positive association between hippocampus metabolism and connectivity.

These results are supported by a recent study based on a large sample of over 800 subjects; this study revealed that, global brain signal control is nearly equivalent to control for global grey matter signal and variably relates to WM and CSF signals, suggesting the use of grey matter regression with an increasing interpretational accuracy of nuisance noise control[30].

Journal of Alzheimer's Disease 51 (2016) 313–326
DOI 10.3233/JAD-150823
IOS Press

Increased Intrinsic Activity of Medial-Temporal Lobe Subregions is Associated with Decreased Cortical Thickness of Medial-Parietal Areas in Patients with Alzheimer's Disease Dementia

Lorenzo Pasquini[a,d,1,*], Martin Scherr[a,b,d,f,1], Masoud Tahmasian[a,c,d], Nicholas E. Myers[d,e], Marion Ortner[b], Alexander Kurz[b], Hans Förstl[b], Claus Zimmer[a], Timo Grimmer[b], Atae Akhrif[g], Afra M. Wohlschläger[a,d], Valentin Riedl[a,c,d] and Christian Sorg[a,b,d]
[a]*Department of Neuroradiology, Technische Universität München, Munich, Germany*
[b]*Department of Psychiatry, Technische Universität München, Munich, Germany*
[c]*Department of Nuclear Medicine of Klinikum rechts der Isar, Technische Universität München, Munich, Germany*
[d]*TUM-Neuroimaging Center, Technische Universität München, Munich, Germany*
[e]*Department of Experimental Psychology, Oxford University, Oxford, UK*
[f]*Department of Neurology, Christian Doppler Klinik, Paracelsus Medical University Salzburg, Salzburg, Austria*
[g]*Department of Child and Adolescent Psychiatry and Psychotherapy, University of Würzburg, Würzburg, Germany*

Accepted 1 December 2015

Abstract. In Alzheimer's disease (AD), disrupted connectivity between medial-parietal cortices and medial-temporal lobes (MTL) is linked with increased MTL local functional connectivity, and parietal atrophy is associated with increased MTL memory activation. We hypothesized that intrinsic activity in MTL subregions is increased and associated with medial-parietal degeneration and impaired memory in AD. To test this hypothesis, resting-state-functional and structural-MRI was assessed in 22 healthy controls, 22 mild cognitive impairment patients, and 21 AD-dementia patients. Intrinsic activity was measured by power-spectrum density of blood-oxygenation-level-dependent signal, medial-parietal degeneration by cortical thinning. In AD-dementia patients, intrinsic activity was increased for several right MTL subregions. Raised intrinsic activity in dentate gyrus and cornu ammonis 1 was associated with cortical thinning in posterior cingulate cortices, and at-trend with impaired delayed recall. Critically, increased intrinsic activity in the right entorhinal cortex was associated with ipsilateral posterior cingulate degeneration. Our results provide evidence that in AD, intrinsic activity in MTL subregions is increased and associated with medial-parietal atrophy. Results fit a model in which medial-parietal degeneration contributes to MTL dysconnectivity from medial-parietal cortices, potentially underpinning disinhibition-like changes in MTL activity.

Keywords: Alzheimer's disease, atrophy, functional magnetic resonance imaging, hippocampus, medial-parietal cortex, medial-temporal lobe, neurodegeneration, neuroimaging, physiopathology, resting-state activity

[1]These authors contributed equally to this work.

*Correspondence to: Lorenzo Pasquini, Department of Neuroradiology, Klinikum rechts der Isar, Technische Universität München, Ismaningerstrasse 22, 81675 Munich, Germany. Tel.: +49 89 4140 4783; E-mail: lorenzo.pasquini@tum.de.

INTRODUCTION

Medial-temporal lobe (MTL) pathophysiology plays a central role in Alzheimer's disease (AD) [1–4]. Based on the high degree of 'normal' MTL-parietal cortex interactions via prominent structural and functional connectivity, MTL pathophysiology has been suggested to interact with parietal cortex pathophysiology in AD [5–8]. In particular, the current study suggests that intrinsic activity in MTL subregions is increased in AD, with increases being associated with degeneration in medial-parietal cortices.

The MTLs are characterized by the hippocampal-entorhinal system, which subserves navigation and memory functions via highly coordinated oscillatory dynamics among subregions [9]. The hippocampal-entorhinal system includes a main excitatory feedforward loop of subregions, starting from lower layers of entorhinal cortex (EC) to dentate gyrus (DG), cornu ammonis (CA) 3, CA1, and finally to upper layers of EC [10]. This loop interacts extensively with two cortical systems, whereas one of these two systems is mainly constituted by posterior cingulate cortex and precuneus i.e., medial-parietal cortices [11].

In AD, MTL pathophysiology is characterized by tau-based pathological changes, structural degradation and substantial cell loss; amyloid-β-based pathology is less prominent—at least in early stages of the disease [1, 4]. Tau-based pathological changes and substantial cell loss start typically in the transition zone between EC and adjacent temporal cortices, then spreading to limbic (including MTLs) and, later, to cortical regions [1]. Start of MTL changes is commonly accompanied by the start of first clinical symptoms such as impaired memory [1]. During memory processes, MTL activity particularly in the hippocampus, is paradoxically increased in disease stages of mild cognitive impairment (MCI) [12]. Such activity increase seems to be dysfunctional since both hyperactivity and memory performance normalize after anti-epileptic medication [13]. Beyond memory related activity, intrinsic activity within the MTL (i.e., local intrinsic functional connectivity), is progressively increased in MCI and dementia stages of AD, with coherence increases being linked with impaired memory function [6, 14–16].

MTL pathophysiology of AD seems to be linked with both cortical pathology and MTL dysconnectivity from the cortex. In patients with MCI, increased hippocampus activation during memory processing is associated with cortical thinning in parietal lobes [17], and in cognitive normal older adults, the amount of cortical amyloid-β pathology measured by *in vivo* PET correlates with decreased functional connectivity of the perirhinal cortex within the MTL [18]. The MTLs are part of the so-called default mode network, which is characterized by functional connectivity of intrinsic activity in MTLs, medial-prefrontal, medial-parietal and lateral-parietal cortices [19]. In patients with AD-dementia, intrinsic functional connectivity between hippocampus and medial-parietal parts of the default mode network is reduced, and such decrease is associated with both hippocampus increased local intrinsic functional connectivity and glucose metabolism [6, 7]. Furthermore, in a longitudinal study in patients with early AD, baseline hippocampus atrophy was associated with decreasing cingulum bundle integrity (the cingulum bundle is a white matter tract connecting the MTLs with medial-parietal parts of the default mode network), and cingulum bundle integrity itself was linked to decreasing medial-parietal glucose metabolism along disease progression, supporting a consistent interaction between MTL and medial-parietal pathophysiology in AD [5].

Based on these studies, we suggest increased MTL intrinsic activity in early AD. Such activity increases might be of disinhibition-like nature due to both local and remote factors. Candidates for local factors are pathological alterations like tau- or amyloid-β pathology, whereas both tau and amyloid-β have been demonstrated – at least in animal models of AD – to induce epileptiform discharges at local network level [20–22]. Candidates for remote factors are pathological changes in medial-parietal cortical regions and related MTL dysconnectivity, which may include dysfunctional signals (e.g., discharges or signal loss) [23] that in turn contribute to misbalanced excitation and inhibition of MTL's main excitatory loop from EC to hippocampus and back. The current study tested several aspects of this model. First, we hypothesized that in early AD, MTL subregions, which build up the main excitatory loop, have increased intrinsic activity. Second, we expected intrinsic activity increases to be associated with cortical degeneration in medial-parietal regions of the default mode network. Finally, we suggested that MTL intrinsic activity increases are linked with patients' memory impairment.

MATERIALS AND METHODS

Overview

We used structural MRI and resting-state-fMRI with both whole-brain and partial-brain field-of-view in healthy controls (HC) and patients with MCI and AD-dementia. Partial-brain fMRI data were of increased spatial resolution (in comparison to whole-brain fMRI) with a limited field-of-view focused on the MTL and medial-parietal cortices. Imaging data have been analyzed previously but with a focus on local and global intrinsic functional connectivity within the hippocampus and larger default mode network [6]. In contrast to the previous analysis, the current study focuses on intrinsic activity within MTL subregions (i.e., subregions constituting the hippocampus but also adjacent regions such as entorhinal cortex) and its relation to medial-parietal atrophy of the default mode network. By the use of automated brain parcellation of each subject's structural MRI data, regions-of-interest were defined in MTLs and medial-parietal cortices of the default mode network, whereas the default mode network was defined by the analysis of whole brain resting-state-fMRI data. Outcome measures were (1) the power spectrum density of low frequency fluctuations (PSD of LFF) in the blood-oxygenation-level-dependent (BOLD) signal of partial-brain fMRI data [24] for intrinsic activity in MTL subregions and (2) cortical thickness for structural degeneration of medial-parietal cortices. ANOVA was used for group comparisons in both PSD of LFF and cortical thickness, and Spearman correlation coefficients to analyze the link between intrinsic activity and both cortical thinning and memory performance (i.e., delayed recall scores). Across-subject analyses were controlled for MTL subregions' atrophy to ensure the functional nature of potential PSD changes and for multiple comparisons to account for errors in inferences due to simultaneous multiple testing.

Participants

22 HC (16 females, age 56–85), 22 MCI patients (11 females, ages 48–80) and 21 AD-dementia patients (13 females, ages 57–83) participated in this study (Table 1). The study was approved and registered by the medical ethical board of Technische Universität München (TUM) in line with Human Research Committee guidelines of TUM. All participants provided informed consent in accordance with the standard protocol approvals. Patients were recruited from the Memory Clinic of the Department of Psychiatry, controls by word-of-mouth advertising. Examination of every participant included medical history, neurological examination, informant interview (Clinical Dementia Rating, CDR) [25], neuropsychological assessment (Consortium to establish a registry for Alzheimer's disease, CERAD battery) [26], structural MRI and blood tests (for patients only). MCI patients (CDR-global = 0.5) met criteria for MCI including reported and neuropsychologically assessed cognitive impairments, largely intact activities of daily living, and excluded dementia [27]. AD patients fulfilled criteria for mild dementia (CDR-global = 1) and the National Institute of Neurological and Communicative Disorders and Stroke and the Alzheimer's Disease and Related Disorders Association (NINCIDS-ADRDA) criteria for AD [28]. Exclusion criteria for entry into the study were other neurological, psychiatric, or sys-

Table 1
Demographic and neuropsychological data

Mean (SD)	AD	MCI	HC	*F*	*p*-value
Number *n*	21	22	22		
Age (years)	72.3 (8.6)	65.3 (8.7)	66.3 (9.0)	7.00	0.16
Education (years of school)	9.3 (1.6)	9.9 (1.7)	10.1 (1.7)	0.94	0.40
% Female	61.9	50.0	72.7	–	0.31
CERAD					
Verbal Fluency	10.9 (4.9)	15.7 (5.6)	23.3 (1.7)	31.33	<0.001
Boston Naming Test	11.4 (3.7)	14.0 (1.1)	14.9 (0.3)	11.15	<0.001
Word List Learning	10.6 (3.0)	16.3 (3.4)	24.2 (2.1)	87.82	<0.001
Constructional Praxis	8.4 (1.9)	9.9 (1.2)	10.8 (0.6)	12.36	<0.001
World List Delayed Recall	1.9 (1.6)	4.0 (2.6)	9.1 (1.2)	56.10	<0.001
World list Recognition	7.7 (1.7)	8.0 (1.6)	9.9 (0.3)	9.07	<0.001
MMSE	22.4 (4.7)	27.3 (1.3)	29.6 (0.7)	35.6	<0.001

AD, Alzheimer's disease; MCI, mild cognitive impairment; HC, healthy controls; group comparisons: ANOVA for all measures except gender (Kruskal-Wallis-Test); CERAD, Consortium to Establish a Registry for Alzheimer's Disease; MMSE, Mini Mental State Examination.

temic diseases (e.g., stroke, depression, alcoholism) or clinically remarkable structural MRI alterations (e.g., stroke lesions) potentially related to cognitive impairment. 9 AD patients/8 MCI patients/6 healthy controls were treated for hypertension (Beta-blockers, ACE-inhibitors, and Calcium channel blockers), 4/5/3 for hypercholesterolemia (statins), 2/2/0 had diabetes mellitus, 6/3/0 received antidepressant medication (Mirtazapine, Citalopram), and 21/0/0 received cholinesterase inhibitors.

MRI data acquisition

All participants underwent structural MRI, 10 min of whole-brain resting-state-fMRI and 6 min of partial-brain resting-state-fMRI. For resting-state-fMRI, subjects were instructed to keep their eyes closed and not to fall asleep. We verified that subjects stayed awake by interrogating via intercom immediately after each scan. MRI was performed on a 3T MRI scanner using 8-channel phased-array head coil (Achieva, Philips, Netherland). Whole-brain resting-state-fMRI used a gradient echo EPI sequence (TE = 35 ms; TR = 2000 ms; flip angle = 82°; FoV = 220 × 220 mm^2; matrix = 80 × 80; 32 slices; slice thickness = 4 mm; 0 mm interslice gap). Partial-brain resting-state-fMRI used a gradient echo EPI sequence (TE = 35 ms; TR = 2000 ms; flip angle = 82°; FoV = 220 × 196.4 mm^2; matrix = 112 × 96; 26 slices; slice thickness = 2 mm; 0.2 mm interslice gap) and we used a limited field-of-view centered on MTL to increase spatial resolution of the data (see reference [6] for more details). To optimally cover MTL, the field-of-view orientation of resting-state-fMRI scans was systematically adapted for each individual. T1-weighted anatomical data were obtained by using a magnetization-prepared rapid acquisition gradient echo sequence (TE = 4 ms, TR = 9 ms, TI = 100 ms, flip angle = 5°, FoV = 240 × 240 mm^2, matrix = 240 × 240, 170 slices, voxel size = 1.0 × 1.0 × 1.0 mm^3).

Parcellation and volumetry of MTL and parietal subregions

For each participant, structural MRI data were parcellated in an automated mode as implemented by FreeSurfer software (http://surfer.nmr.mgh.harvard.edu) (see Supplementary Material for more details). FreeSurfer provides a highly automated structural MRI image-processing pipeline resulting in regional parcellation of subcortical and cortical regions including MTL (i.e., entorhinal cortex and hippocampus subregions), and isocortex [29]. FreeSurfer provides volumetric and thickness estimates for parcellated regions [30]. Manually based segmentation and volumetry of MTL subregions in patients with MCI and AD are comparable with FreeSurfer-based procedures [31]. FreeSurfer segmentation was thoroughly inspected for each subject. Quality checks included extensive visual inspection of pial and white matter boundaries along the cortical mantle as well as location and extend of segmented medial-parietal and MTL regions-of-interest for each subject. Furthermore, we compared both volumetry of MTL subregions and cortical thickness of medial-parietal regions-of-interest, with estimates derived from existing studies involving both automatic and manual segmentation procedures in healthy subjects and patients (see also Supplementary Tables 1 and 2). None of the subjects failed for these criteria and was excluded from the analysis.

Figure 1A and B show the current study's regions-of-interest based on FreeSurfer analysis. MTL regions-of-interest included bilateral parahippocampal cortices (PHC), EC, DG-CA4, CA2-CA3, CA1, subiculum, and presubiculum [32]. In the following, we abbreviate DG-CA4 and CA2-CA3 with DG and CA3, respectively. Medial-parietal regions-of-interest included bilateral dorsal posterior cingulate cortex (PCC), ventral PCC, and precuneus. These areas are part of the medial posterior default mode network, which is primarily affected by earliest changes in AD such as amyloid plaque deposition, hypometabolism, and atrophy [33, 34]. For each subject, overlap with the default mode network was verified by comparing individual segmented medial-parietal regions with individual default mode networks. More specifically, we used subjects' previously defined individual posterior default mode network maps (see reference [6]) and compared them with individually segmented ventral and dorsal PCC and precuneus (example in Fig. 1B). Individual default mode maps were derived from group-independent component analysis of whole-brain resting-state-fMRI data and back reconstructed from the group map into individual subject space. Overlap was counted as relevant when the network covered more than 75% of segmented areas, with none of the subjects failing this criterion.

FMRI data analysis: Preprocessing and PSD of LFF

Preprocessing. After discarding the first three volumes of each person's partial-brain fMRI scans,

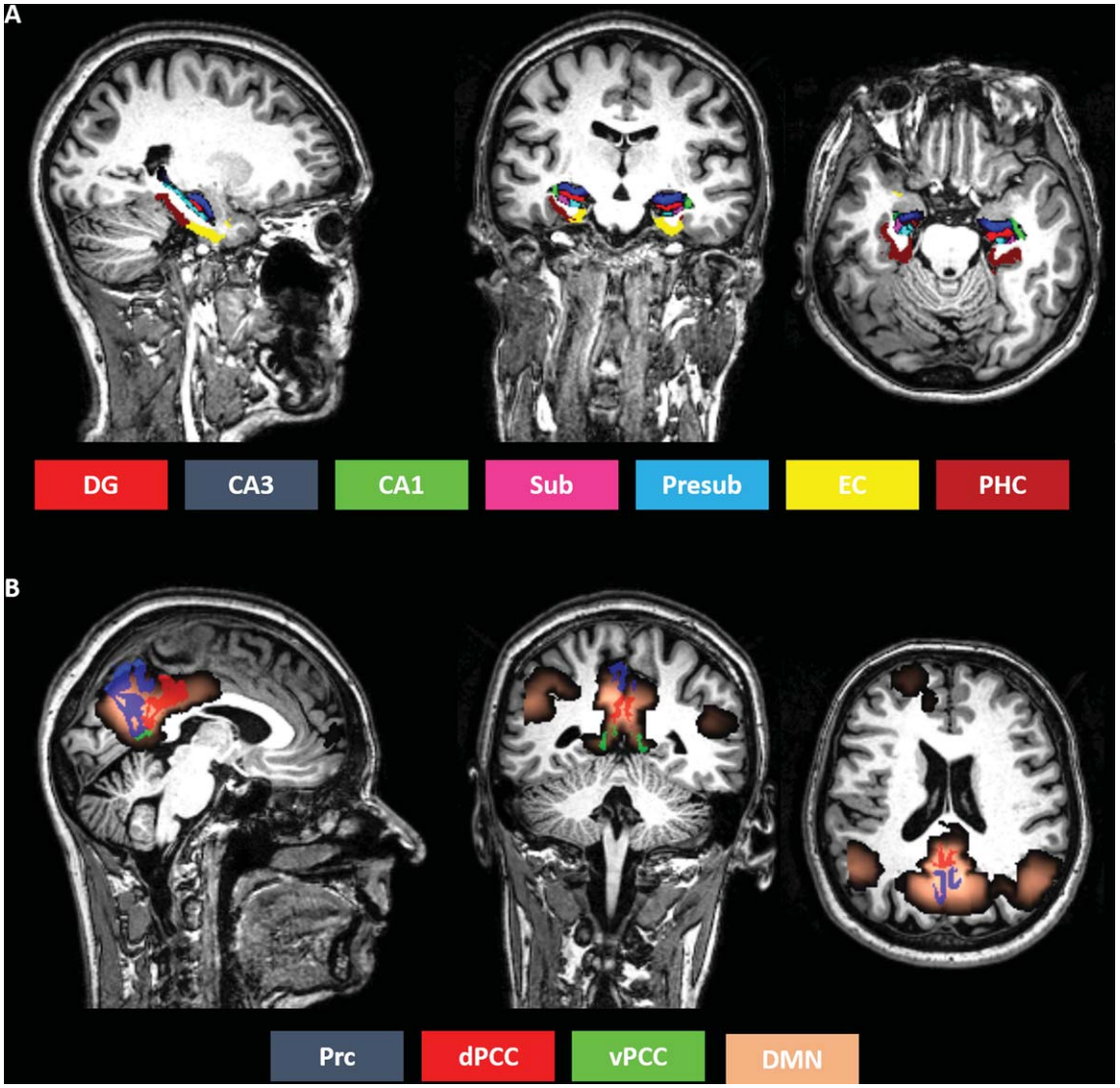

Fig. 1. Parcellation of medial-temporal lobe and medial-parietal regions-of-interest. FreeSurfer software was used to parcellate each single subject's structural MRI data in medial-temporal lobe subregions (A) and medial-parietal regions overlapping with medial-parietal portions of the default mode network (B). The segmented regions constitute the regions-of-interest of the current study. CA, cornu ammonis; DG, dentate gyrus; DMN, default mode network; dPCC, dorsal posterior cingulate cortex; EC, entorhinal cortex; PHC, parahippocampal cortex; Prc, precuneus; Presub, presubiculum; Sub, subiculum; vPCC, ventral PCC.

data were motion corrected, spatially smoothed ($3 \times 3 \times 3$ mm^3 Gaussian kernel), and co-registered with anatomical data. To control for motion-induced artifacts, point-to-point head motion was estimated for each participant [35]. Excessive head motion (cumulative translation or rotation >3 mm or 3° and mean point-to-point translation or rotation >0.15 mm or 0.1°) was applied as initial exclusion criterion. None of the participants had to be excluded. ANOVA and related *post-hoc* *t*-test yielded no significant differences between groups regarding translational and rotational head movements of any direction. In the same way, root mean square of the translational ad rotational head movement parameters was not different across groups. Furthermore, we replicated our analysis of PSD of LFF on "scrubbed" fMRI data, which were censored for movement-induced artifacts via exclusion of volumes potentially contaminated by movement [35]. Censoring was based on the root mean square of the translational

and rotational head movement parameters reflecting volume-to-volume head displacement. We identified volumes were the root mean square of translational and rotational head movement parameters exceeded a specific threshold (0.25 mm + 2 standard deviations of all subjects) and removed them from further analyses [36] (see Supplementary Material for more details and results, Supplementary Figure 1).

Outcome measure PSD of LFF. For each subject, movement parameters in six directions (linear and rotational), the global grey matter, white matter, and cerebrospinal fluid signal were extracted from partial-brain resting-state-fMRI data by linear regression. As the global grey matter signal is thought to reflect a combination of physiological processes (including cardiac and respiratory fluctuations) and scanner drift, it was extracted as a nuisance signal [37]. To get time series for grey matter, white matter, and cerebrospinal fluid, each individual's segmented T1-weighted image was segmented to define corresponding tissues. Time courses of each voxel within each region-of-interest were extracted and bandpass-filtered (0.009 to 0.09 Hz). To derive a representative time course of the region-of-interest, the BOLD signal of all voxels of the region-of-interest at a single time point was multiplied with the probability of corresponding voxels to belong to the specific region-of-interest (based on the probabilistic maps provided by FreeSurfer). Weighted time courses were averaged across voxels in the concerned region-of-interest. The power spectrum density was subsequently calculated for each time course using the Welch's method (TR: 0.5 Hz; windows: 8; overlap: 50%) [24]. To control for atrophy, we regressed out individual volumes of MTL subregions from the corresponding spectra for each subject via regression analysis. For quantification, the spectra were divided into three frequency bands (0.00–0.03; 0.03–0.06 and 0.06–0.09 Hz) and the integral calculated following the approach of Malinen et al. [24]. A frequency band specific approach was chosen since a recent study indicated selective changes across different frequency bands of intrinsic activity in early AD [38].

Cortical thickness asymmetry index

To foreshadow results, we found mainly right-sided MTL subregions of increased intrinsic activity in dementia patients. We suggested that such asymmetric activity increase in MTL might be associated with asymmetric medial-parietal cortex atrophy. To evaluate the specificity of the relationship between increased intrinsic MTL activity and medial-parietal cortex degeneration in AD, we investigated whether asymmetric inter-hemispheric cortical thinning in medial-parietal regions could account for lateralized increased PSD of LFF in right MTL subregions. Therefore, we defined an Asymmetry Index (AsI) for thickness of medial-parietal region-of-interests:

$$\mathrm{AsI} = (\mathrm{RCTr} - \mathrm{RCTl})/(\mathrm{RCTr} + \mathrm{RCTl})$$

where RCTr is the relative cortical thickness of the right region-of-interest and RCTl is the relative cortical thickness of the homologous left region-of-interest. Relative cortical thickness measures where derived by dividing the cortical thickness of a region-of-interest with its volume. AsI ranges between 1 and –1, with positive values indicating a right >left asymmetry and negative values indicating a right <left asymmetry.

Statistical analysis

Comparison between patients and control regarding PSD of LFF in MTL subregions were performed in a one-way ANOVA model with subsequent *post-hoc t*-tests ($p < 0.05$, FWE corrected for multiple comparisons). Spearman correlation ($p < 0.05$) was used to relate PSD of LFF in MTL subregions to both cortical thickness of medial-parietal regions-of-interest and delayed recall scores in patients with AD-dementia only. Correlation analysis was restricted to MTL subregions with increased PSD in patients.

RESULTS

Progressively reduced volumes in MTL subregions and cortical thinning in medial-parietal areas in patients

Cortical thickness of medial-parietal regions-of-interest and volumes of MTL subregions of healthy controls were comparable with thickness and volume estimates from previous studies using FreeSurfer and comparable to volumes from manual segmentations of the EC and PHC (Supplementary Tables 1 and 2) [32, 39, 40]. Both progressive volume loss of MTL subregions and cortical thinning of medial-parietal areas were present in MCI and AD (Supplementary Tables 1 and 2) and in line with previous studies [41–43].

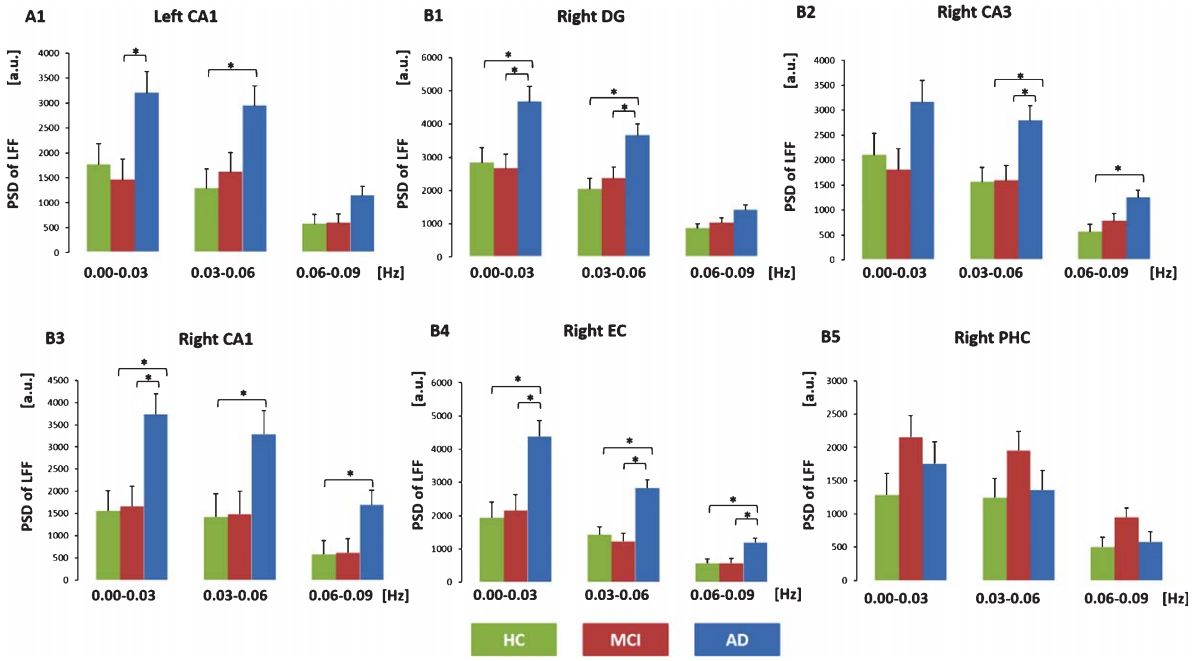

Fig. 2. Power spectrum density (PSD) of low frequency fluctuations (LFF) in the BOLD signal of medial-temporal lobe subregions in healthy controls, patients with mild cognitive impairment and Alzheimer's disease dementia. Mean and standard deviation of PSD of LFF in the BOLD signal for six medial-temporal lobe subregions (A1, B1–B5) shown for patients with AD-dementia (blue), patients with MCI (red) and HC (green). Asterisks indicate significant group differences (ANOVA, *post-hoc t*-test, $p < 0.05$ FWE corrected). AD, Alzheimer's disease; a.u., arbitrary units; CA, cornu ammonis; DG, dentate gyrus; EC, entorhinal cortex; HC, healthy aged matched controls; MCI, mild cognitive impairment; Presub, presubiculum; PSD of LFF, power spectrum density of blood-oxygenation-level-dependent signal low frequency fluctuations; Sub, subiculum.

Increased PSD of LFF in MTL subregions in patients with AD

For each subject, PSD of LFF was calculated for 14 MTL regions-of-interest by the use of extracted time series of BOLD signal with power spectra being divided into three frequency bands (0.00–0.03; 0.03–0.06 and 0.06–0.09 Hz) and adjusted for corresponding atrophy levels. Comparison between patients and controls were performed by a one-way ANOVA ($p < 0.05$ family wise error corrected for multiple comparisons; Fig. 2). We found increased PSD of LFF in AD patients compared to healthy controls and MCI patients in the left CA1 and right DG, CA3, CA1, and EC (Fig. 2 A1, B1–B5). For right CA1 and EC all frequency bands were concerned; for right CA3 the two highest frequency bands were concerned; for right DG and left CA1 the two lowest frequency bands were concerned. We did not find any significant changes of PSD in MCI patients. One should note that performing all these group comparisons but without controlling for subregions volume yields consistently stronger group differences for MTL subregions PSD, indicating relevant effects of subregional volume loss on subregional activity increases. For example, we found an increased number of MTL subregions with significant group differences in PSD (right DG 0.06–0.09 Hz AD versus HC; right CA3 0.06–0.09 Hz AD versus MCI) as indicated by Supplementary Figure 2. Furthermore, in right parahippocampal cortex or left DG there was no PSD difference across groups, indicating that observed increase of PSD is specific for mentioned MTL subregions and not a general phenomenon in AD.

To control for potential movement-induced effects, we implemented a second analysis with alternative movement control based on "censoring" procedures (see Supplementary Material). Results of control analyses are consistent with the current findings, demonstrating robustness against movement effects (Supplementary Figure 1).

Increased PSD of LFF in MTL subregions correlates with thinning of the medial-parietal cortex

To investigate the link between MTL increased intrinsic activity and medial-parietal degeneration, we correlated PSD of LFF and cortical thickness of medial-parietal regions, restricted to MTL subregions of significantly increased PSD in AD (Fig. 3A; Spearman correlation, $p < 0.05$). In AD, increased PSD of LFF of right CA1 and DG correlated with cortical thinning of right and left ventral PCC, respectively, but the relationship was not significant after multiple-comparison correction controlling for family wise error.

To test for more specific links between cortical degeneration and increased MTL intrinsic activity, we investigated whether lateralized increases in intrinsic MTL activity correspond with asymmetrically pronounced medial-parietal degeneration. First, we found positive Asymmetry Index (AsI) for the ventral PCC, indicating stronger right-sided degeneration in the vPCC (AsI [SD] = 0.09 [0.14]; $p < 0.05$ FWE corrected), while dorsal PCC showed negative AsI, indicating stronger left sided degeneration (AsI [SD] = –0.05 [0.06]; $p < 0.05$ FWE corrected). Second, we found that increased PSD of LFF in the right EC correlated negatively with cortical thickness AsI of the ventral PCC (Fig. 3B, Spearman correlation, $p < 0.05$ uncorrected). This result suggests

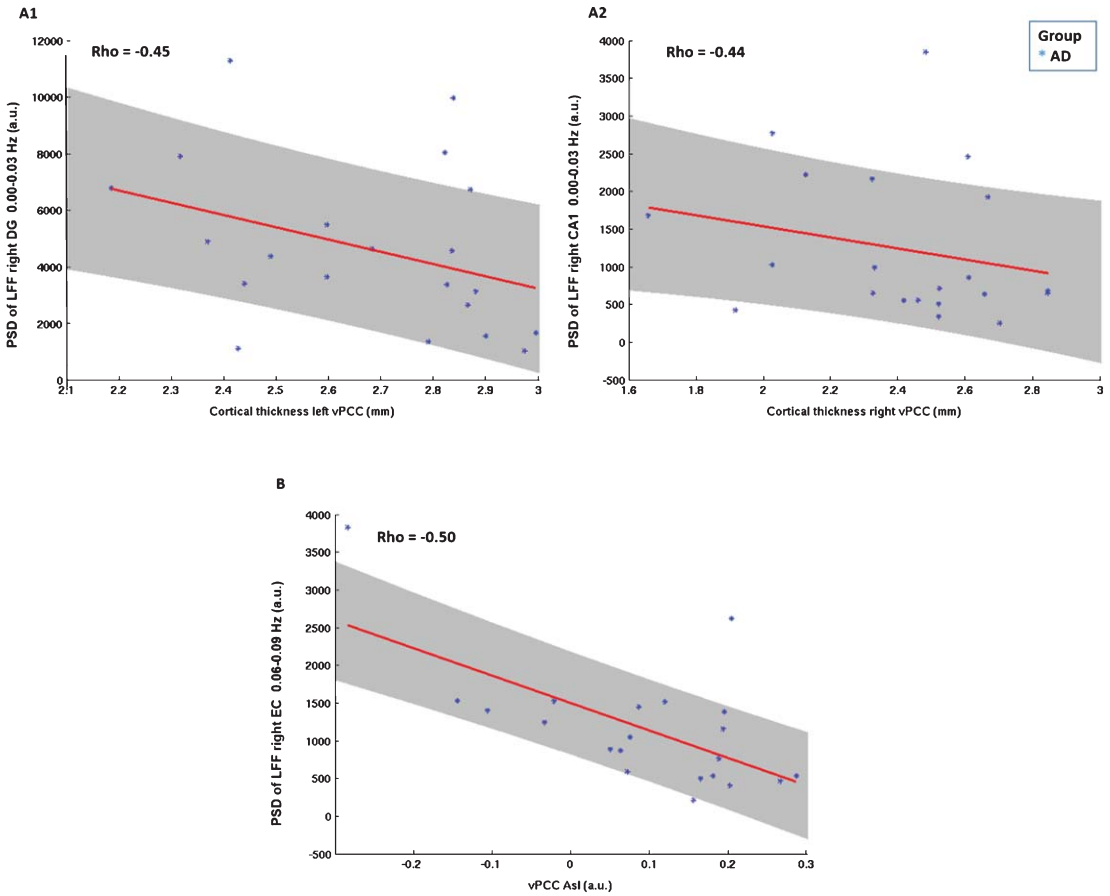

Fig. 3. Increased PSD of LFF in intrinsic activity of specific medial-temporal lobe subregions is associated with cortical thinning of medial-parietal areas. A1-A2) Increased PSD of LFF from medial-temporal lobe subregions negatively correlates with cortical thickness of medial-parietal areas in patients with AD-dementia (Spearman correlation, $p < 0.05$). B) The Asymmetry Index (AsI) of cortical degeneration reflects the asymmetry of cortical thickness between homologous left and right parietal regions-of-interest. AsI >0 reflects right>left atrophy and AsI <0 vice versa. Increased PSD of LFF from the right entorhinal cortex (0.06–0.09 Hz) negatively correlates with the Asymmetry Index in the ventral PCC in patients with AD, suggesting a link between right increased intrinsic activity in EC and relatively stronger ipsilateral degeneration of PCC (Spearman correlation, $p < 0.05$). AD, Alzheimer's disease; AsI, Asymmetry Index; a.u. arbitrary units; CA, cornu ammonis; DG, dentate gyrus; EC, entorhinal cortex; PSD of LFF, power spectrum density of blood-oxygenation-level-dependent signal low frequency fluctuations; Rho, Spearman correlation coefficient; vPCC, ventral posterior cingulate cortex.

Table 2
Correlation of PSD of LFF increases in medial-temporal lobe subregions with delayed recall scores in patients with AD-dementia

Spearman Correlation	Delayed recall
Left CA1 0.00–0.03 Hz	–0.48*
Left CA1 0.03–0.06 Hz	–0.59*
Right DG 0.00–0.03 Hz	–0.39#
Right DG 0.03–0.06 Hz	–0.42#
Right CA3 0.03–0.06 Hz	–0.40#
Right CA3 0.06–0.09 Hz	–0.30
Right CA1 0.00–0.03 Hz	–0.16
Right CA1 0.03–0.06 Hz	–0.25
Right CA1 0.06–0.09 Hz	–0.41#
Right EC 0.00–0.03 Hz	–0.02
Right EC 0.03–0.06 Hz	–0.31
Right EC 0.06–0.09 Hz	–0.20

#$p < 0.10$; *$p < 0.05$; CA, cornu ammonis; DG, dentate gyrus; EC entorhinal cortex.

that the stronger degeneration of right vPCC, the higher increased intrinsic activity of right EC. Further medial-parietal regions with significant negative AsI (i.e., dorsal PCC) did not correlate with raised intrinsic MTL activity.

Increased MTL intrinsic activity and reduced delayed recall in AD

We additionally investigated the relationship between memory impairments and PSD of LFF in patients with AD. Delayed recall scores from the CERAD battery were significantly lower in patients with AD-dementia (Table 1) and were used as a memory measure. Correlation analyses were restricted to MTL subregions with increased PSD of LFF and to AD-dementia patients. We found negative correlations between delayed recall and PSD of LFF of several MTL subregions with significant effects ($p < 0.05$) for the left CA1 (frequency bands 0.00–0.03 Hz and 0.03–0.06 Hz) and at-trend results ($p < 0.10$) for right DG (frequency bands 0.00–0.03 Hz and 0.03–0.06 Hz), CA3 (frequency band 0.03–0.06 Hz) and CA1 (frequency band 0.06–0.09 Hz) (Table 2). Relationship between left CA1 and delayed recall was not significant after multiple-comparison correction controlling for family wise error.

DISCUSSION

Power spectrum density of low frequency fluctuations in the BOLD signal of the left CA1 and right DG, CA3, CA1, and EC was increased in patients with AD-dementia. For right DG and CA1, increased intrinsic activity was associated with reduced cortical thickness in the ventral PCC and, at-trend, with impaired delayed recall. Particularly, increased intrinsic activity in the right EC was associated with ipsilateral PCC degeneration, suggesting a specific link between dysfunctional intrinsic MTL activity and medial-parietal degeneration. Results provide first evidence for both increased intrinsic activity in MTL subregions and its link with degeneration in medial-parietal cortices in AD. Data suggest that medial-parietal degeneration may contribute to disinhibition-like changes in MTL activity, possibly via parietal-MTL dysconnectivity.

Intrinsic activity is increased in MTL subregions

PSD of LFF was increased in the left and right CA1, right CA3, DG, and EC of patients with AD compared to MCI and healthy controls (Fig. 2). Findings were controlled for multiple testing, regional atrophy, and head movement, indicating robustness against these effects (Supplementary Figure 1). Particularly, adjustment for atrophy indicates the functional nature of observed PSD increases. Interestingly, PSD increases were more prominent in the right hemisphere (Fig. 2B1–5), concerning all subregions of MTL's main excitatory loop from EC to DG, CA3, and CA1 back to EC [10]. This lateralized but total effect suggests that increase of MTL subregions intrinsic activity may be an all-or-nothing effect concerning all parts of excitatory MTL loop. In line with this finding, we found in the same patients, increased local functional connectivity of intrinsic hippocampus activity within MTL [6, 14, 15] and previous studies reported increased local functional connectivity among MTL subregions in patients with MCI and AD [6, 14–16], which may indicate a 'coherent' increase of activity across MTL subregions.

While in right CA1 and EC, PSD increases in AD patients' intrinsic activity were found for all frequency bands (0.00–0.03; 0.03–0.06 and 0.06–0.09 Hz), in right CA3 the two highest and in right DG and left CA1 the two lowest frequency bands were affected (Fig. 2). This result suggests specific effects on frequency bands of intrinsic MTL subregions activity in AD. Currently, though several studies report frequency-band specific effects on regional and network-specific intrinsic activity for several brain disorders such as Parkinson's disease or chronic pain [24, 44], consensus about the function of different frequency bands in intrinsic BOLD fluctuations is missing. A recent study in early AD,

combined functional connectivity of intrinsic activity at rest and effective connectivity of attention-related activity during flankers task, and found frequency-band specific impairments in patients for the relation between lower frequent functional connectivity at rest (e.g., 0.001–0.03 Hz) and effective bottom-up connectivity to prefrontal areas during attention [38]. Given this background, our result gives reason to suggest that in AD, frequency-band specific increase in MTL subregions intrinsic activity might be relevant for distinct processes in task-related activity such as memory. Future studies are necessary, which combine resting-state and memory-related fMRI in order to investigate such relationship.

We did not find increased PSD of LFF in MTL subregions of patients with MCI, albeit previous studies have reported changes in both task-related activity and coherence of intrinsic activity within the MTL of patients with MCI [6, 14, 15, 17]. The lack of such finding might be due to several factors. First, in the same MCI patients, we found increased local hippocampus functional connectivity but significant less than in AD-dementia patients [6, 14, 15]. This result might indicate that while coherence of intrinsic activity is already increased in MCI, intrinsic activity of single subregions is still at normal levels. This finding suggests that coherence of intrinsic activity in the whole MTL subregions is more sensitive to MTL impairments than the power of intrinsic activity in single subregions. Second, we might fail to detect changes in MTL intrinsic activity in MCI due to potential heterogeneity of our MCI sample. Since MCI patients' characterization was based on clinical-neuropsychological testing without the use of additional biomarkers such as positron emission tomography or liquor diagnostics, our sample could include other neurodegenerative diseases than AD, lowering power of our approach in MCI patients.

Increased PSD of several MTL subregions negatively correlated with delayed recall in AD patients. A significant effect was found for the left CA1 of AD patients, and a trend for such correlation was found for right DG, CA3, and CA1 (Table 2). Correlations did not survive correction for multiple comparisons, increasing the risk for false positive findings. Though being of weak significance, this result contains a reference that increased intrinsic activity in patients' MTL subregions might be relevant for impaired memory performance. Interestingly, in a previous study with the same patients we found an analogous link between memory impairment and hippocampus raised local functional connectivity within the MTL [6]. This finding suggests that both intrinsic functional connectivity within the whole MTL and intrinsic activity of single MTL subregions, albeit reflecting different processes, are functionally meaningful measures of MTL activity at rest with both being related to memory performance.

In summary, we conclude that MTL subregions intrinsic activity is increased in AD; furthermore, data suggest that subregions of the main excitatory loop of the MTL might be affected as a whole and that their increased activity might contribute to impaired delayed recall in patients.

Link between increased intrinsic activity of MTL subregions and cortical thinning of medial-parietal cortices

We found that increased PSD of LFF of both the right DG and CA1 was negatively correlated with cortical thickness in ventral PCC (Fig. 3A). This finding fits previous results which link MTL activity/local functional connectivity increases and parietal degradation/impaired parietal-hippocampal connectivity [6, 7, 14, 17]. For example, in the same patients we found a link between raised local and eased global hippocampal functional connectivity in AD and MCI [6, 14]. In a sample of MCI patients whose cognitive impairment is comparable with that of the current AD sample, hippocampus hyperactivity during memory performance was associated with cortical thinning in parietal areas, in line with our results [17]. Similarly, a recent study demonstrated that in patients with mild AD, hippocampus glucose metabolism is higher when reductions in functional connectivity between hippocampus and medial posterior cortex are stronger [7].

Increased PSD of MTL subregions was largely lateralized to the right side (Fig. 2B1–5). We found further that such lateralized PSD increases link with asymmetric medial-parietal cortical degeneration (Fig. 3B). In more detail, significant asymmetry in cortical thickness was present in the ventral PCC, with relative higher cortical thickness in the right hemisphere compared to the left in patients. This result is in line with previous findings of right weighted thickness asymmetry in the PCC in healthy younger subjects and is even more pronounced in older adults [45–47]. Critically, in AD patients, we found that the smaller thickness asymmetry in the PCC, the higher right EC intrinsic activity (Fig. 3B). This result indicates that relative stronger degenerative processes in the right PCC compared to the left

PCC are associated with increased right EC activity. Having in mind that PCC and EC [48] are highly connected, this finding suggests a specific link between right hemispheric medial-parietal degeneration and increased right EC intrinsic activity.

Models of MTL pathophysiology in AD

When considering the bigger picture, our findings can be placed within a model, which we like to call MTL dysconnectivity hypothesis (precursors of this idea can be found in [2, 6, 14, 49]). This hypothesis states that in AD, due to foregoing medial-parietal pathophysiology, disrupted medial-parietal input contributes to disinhibition-like changes in the EC-hippocampus circuit with detrimental consequences for MTL physiology and function. In this model, cortical pathology is driven by amyloid-β pathology, which starts years or decades before substantial MTL changes [1, 3, 50] and which affects preferentially the default mode network [51, 52]. MTL pathophysiology is driven by tau-pathology [4, 53], which is assumed to be facilitated by remote medial-parietal dysconnectivity. Dysconnectivity, in turn, consists of missing or discharging signaling [23], and may contribute to misbalanced excitation/inhibition relationship within main MTL circuits with resulting disinhibition-like changes in MTL subregions. Our data can be interpreted in light of such a model, as we report increased intrinsic activity in MTL subregions, which affects all main regions of the right excitatory MTL circuit and which is associated with medial-parietal degeneration.

However, our findings could also be explained by alternative mechanisms driving pathological increases of intrinsic activity in MTL subregions. First, local versus remote factors: One should note that beside MTL dysconnectivity, local MTL pathology might also contribute to increased intrinsic activity. For instance, recent studies in rodents demonstrated amyloid-β-plaque-induced hyperactivity within the hippocampus [20, 21, 54]. Tau-pathology affects the hippocampus in very early AD and is associated with local network hyper-excitability in mice corresponding with seizure frequency [22]. Our data support such suggested influence of local pathology on intrinsic MTL activity, since we found that strength of group differences in MTL subregions intrinsic activity between controls and AD patients was reduced when accounting for subregions volume as co-variate-of-no-interest (Supplementary Figure 2). This group difference reduction indicates that subregions volume loss in patients (i.e., local substance loss due to assumed tau-associated pathology) is associated with subregions intrinsic activity. These data suggest that local *and* remote factors are relevant for increased intrinsic activity in the MTL circuit. Second, interaction between MTL and parietal pathophysiology: Based on our data (i.e., cross-sectional approach with analysis of correlation between MTL activity increase and parietal atrophy), we cannot exclude that MTL changes precedes medial-parietal degradation (see for example [5]) or that MTL pathology occurs independently from medial-parietal degeneration [4, 52]. For example, Villain and colleagues showed that baseline MTL atrophy is associated with the rate of cingulum degradation linking MTL and medial-parietal cortices, suggesting MTL pathological changes as cause for remote degeneration ('classical hippocampus disconnection hypothesis'). Future longitudinal studies are necessary to carefully reveal the direction of effects between MTL and medial-parietal pathophysiology. In particular, future studies should relate characteristic measures for medial-parietal pathology as amyloid load with more specific measures for MTL dysconnectivity based e.g. on diffusion tensor imaging or on MTL intrinsic functional connectivity to medial-parietal brain areas.

In summary, our findings can be related to three models of MTL pathophysiology in AD-MTL dysconnectivity, local factor model, and hippocampus disconnection-which are probably not exclusive but rather complementary mechanisms involved in the degenerative process. Longitudinal multimodal studies, which integrate local and remote factors of MTL pathophysiology, are necessary to complete our picture about MTL changes in AD.

Limitations

Our study has several limitations. First, albeit strongly hypothesis driven, our approach is of cross-sectional nature, so no causation can be inferred from our findings regarding degenerative processes in AD. Second, MCI is an etiologically heterogeneous syndrome, it is possible that some of the current MCI patients did not suffer from AD. Although AD is the most frequent cause underlying MCI [55], results of patients with MCI should be interpreted carefully. Third, patients with AD-dementia were treated with cholinesterase inhibitors, which may influence BOLD activity and consequently correspondent differences in intrinsic activity [56]. Even if our results are consistent with both previous findings in dementia

[6, 7, 14, 15, 17], they have to be interpreted carefully. Forth, the use of FreeSurfer-based anatomical parcellation is an objective method to identify subregions of interest particularly in the MTL. However, FreeSurfer-based MTL segmentation has not yet been validated in aging and neurodegenerative populations and manual segmentation is still considered as the golden standard for MTL subregional segmentation and volumetry [57, 58]. Fifth, our approach suffers from very general problems when comparing BOLD signals across groups of controls and patients, since observed group differences might stem from non-neuronal sources such as altered neurovascular coupling or movement artifacts [36, 59]. While differences in neurovascular coupling across groups are hard to control for, we accounted extensively for potential movement-induced artifacts. However, novel approaches enabling the computation of PSD of LFF on unequally sampled time points are needed when frame censoring is used to control for head movement artifacts.

CONCLUSION

In AD patients, intrinsic activity of MTL subregions is increased which is associated with medial-parietal cortex thinning. Medial-parietal degradation might contribute to disinhibition-like changes in the MTL.

ACKNOWLEDGMENTS

This work was supported by the German Federal Ministry of Education and Research (BMBF 01EV0710 to A.M.W., 01ER0803 to C.S.), the Alzheimer Forschungs-Initiative (AFI 08860 to V.R., 12819 to C.S.), the Wellcome Trust (to N.E.M.), and the Kommission für Klinische Forschung of the Klinikum rechts der Isar der Technischen Universität München (KKF 8765162 to C.S). We are grateful to the participants of the study and the staff of the Departments of Psychiatry and Neuroradiology for their help in recruitment and data collection.

Authors' disclosures available online (http://j-alz.com/manuscript-disclosures/15-0823r2).

SUPPLEMENTARY MATERIAL

The supplementary material is available in the electronic version of this article: http://dx.doi.org/10.3233/JAD-150823.

REFERENCES

[1] Braak H, Braak E (1991) Neuropathological stageing of Alzheimer-related changes. *Acta Neuropathol* **82**, 239-259.

[2] Hyman BT, Van Hoesen GW, Damasio AR, Barnes CL (1984) Alzheimer's disease: Cell-specific pathology isolates the hippocampal formation. *Science* **225**, 1168-1170.

[3] Jack CR Jr, Knopman DS, Jagust WJ, Petersen RC, Weiner MW, Aisen PS, Shaw LM, Vemuri P, Wiste HJ, Weigand SD, Lesnick TG, Pankratz VS, Donohue MC, Trojanowski JQ (2013) Tracking pathophysiological processes in Alzheimer's disease: An updated hypothetical model of dynamic biomarkers. *Lancet Neurol* **12**, 207-216.

[4] Crary JF, Trojanowski JQ, Schneider JA, Abisambra JF, Abner EL, Alafuzoff I, Arnold SE, Attems J, Beach TG, Bigio EH, Cairns NJ, Dickson DW, Gearing M, Grinberg LT, Hof PR, Hyman BT, Jellinger K, Jicha GA, Kovacs GG, Knopman DS, Kofler J, Kukull WA, Mackenzie IR, Masliah E, McKee A, Montine TJ, Murray ME, Neltner JH, Santa-Maria I, Seeley WW, Serrano-Pozo A, Shelanski ML, Stein T, Takao M, Thal DR, Toledo JB, Troncoso JC, Vonsattel JP, White CL, 3rd, Wisniewski T, Woltjer RL, Yamada M, Nelson PT (2014) Primary age-related tauopathy (PART): A common pathology associated with human aging. *Acta Neuropathol* **128**, 755-766.

[5] Villain N, Fouquet M, Baron JC, Mezenge F, Landeau B, de La Sayette V, Viader F, Eustache F, Desgranges B, Chetelat G (2010) Sequential relationships between grey matter and white matter atrophy and brain metabolic abnormalities in early Alzheimer's disease. *Brain* **133**, 3301-3314.

[6] Pasquini L, Scherr M, Tahmasian M, Meng C, Myers NE, Ortner M, Muhlau M, Kurz A, Forstl H, Zimmer C, Grimmer T, Wohlschlager AM, Riedl V, Sorg C (2015) Link between hippocampus' raised local and eased global intrinsic connectivity in AD. *Alzheimers Dement* **15**, 475-484.

[7] Tahmasian M, Pasquini L, Scherr M, Meng C, Forster S, Mulej Bratec S, Shi K, Yakushev I, Schwaiger M, Grimmer T, Diehl-Schmid J, Riedl V, Sorg C, Drzezga A (2015) The lower hippocampus global connectivity, the higher its local metabolism in Alzheimer disease. *Neurology* **84**, 1956-1963.

[8] Villain N, Desgranges B, Viader F, de la Sayette V, Mezenge F, Landeau B, Baron JC, Eustache F, Chetelat G (2008) Relationships between hippocampal atrophy, white matter disruption, and gray matter hypometabolism in Alzheimer's disease. *J Neurosci* **28**, 6174-6181.

[9] Buzsaki G, Moser EI (2013) Memory, navigation and theta rhythm in the hippocampal-entorhinal system. *Nat Neurosci* **16**, 130-138.

[10] Buzsaki G (2006) *Rhythms Of The Brain*, Oxford University Press.

[11] Ranganath C, Ritchey M (2012) Two cortical systems for memory-guided behaviour. *Nat Rev Neurosci* **13**, 713-726.

[12] Sperling RA, Dickerson BC, Pihlajamaki M, Vannini P, LaViolette PS, Vitolo OV, Hedden T, Becker JA, Rentz DM, Selkoe DJ, Johnson KA (2010) Functional alterations in memory networks in early Alzheimer's disease. *Neuromolecular Med* **12**, 27-43.

[13] Bakker A, Krauss GL, Albert MS, Speck CL, Jones LR, Stark CE, Yassa MA, Bassett SS, Shelton AL, Gallagher M (2012) Reduction of hippocampal hyperactivity improves cognition in amnestic mild cognitive impairment. *Neuron* **74**, 467-474.

[14] Das SR, Pluta J, Mancuso L, Kliot D, Orozco S, Dickerson BC, Yushkevich PA, Wolk DA (2013) Increased functional connectivity within medial temporal lobe in mild cognitive impairment. *Hippocampus* **23**, 1-6.

[15] Gour N, Ranjeva JP, Ceccaldi M, Confort-Gouny S, Barbeau E, Soulier E, Guye M, Didic M, Felician O (2011) Basal functional connectivity within the anterior temporal network is associated with performance on declarative memory tasks. *Neuroimage* **58**, 687-697.

[16] Wang Z, Yan C, Zhao C, Qi Z, Zhou W, Lu J, He Y, Li K (2011) Spatial patterns of intrinsic brain activity in mild cognitive impairment and Alzheimer's disease: A resting-state functional MRI study. *Hum Brain Mapp* **32**, 1720-1740.

[17] Putcha D, Brickhouse M, O'Keefe K, Sullivan C, Rentz D, Marshall G, Dickerson B, Sperling R (2011) Hippocampal hyperactivation associated with cortical thinning in Alzheimer's disease signature regions in non-demented elderly adults. *J Neurosci* **31**, 17680-17688.

[18] Song Z, Insel PS, Buckley S, Yohannes S, Mezher A, Simonson A, Wilkins S, Tosun D, Mueller S, Kramer JH, Miller BL, Weiner MW (2015) Brain amyloid-beta burden is associated with disruption of intrinsic functional connectivity within the medial temporal lobe in cognitively normal elderly. *J Neurosci* **35**, 3240-3247.

[19] Buckner RL, Andrews-Hanna JR, Schacter DL (2008) The brain's default network: Anatomy, function, and relevance to disease. *Ann N Y Acad Sci* **1124**, 1-38.

[20] Palop JJ, Mucke L (2010) Amyloid-beta-induced neuronal dysfunction in Alzheimer's disease: From synapses toward neural networks. *Nat Neurosci* **13**, 812-818.

[21] Busche MA, Chen X, Henning HA, Reichwald J, Staufenbiel M, Sakmann B, Konnerth A (2012) Critical role of soluble amyloid-beta for early hippocampal hyperactivity in a mouse model of Alzheimer's disease. *Proc Natl Acad Sci U S A* **109**, 8740-8745.

[22] DeVos SL, Goncharoff DK, Chen G, Kebodeaux CS, Yamada K, Stewart FR, Schuler DR, Maloney SE, Wozniak DF, Rigo F, Bennett CF, Cirrito JR, Holtzman DM, Miller TM (2013) Antisense reduction of tau in adult mice protects against seizures. *J Neurosci* **33**, 12887-12897.

[23] Stargardt A, Swaab DF, Bossers K (2015) The storm before the quiet: Neuronal hyperactivity and Abeta in the presymptomatic stages of Alzheimer's disease. *Neurobiol Aging* **36**, 1-11.

[24] Malinen S, Vartiainen N, Hlushchuk Y, Koskinen M, Ramkumar P, Forss N, Kalso E, Hari R (2010) Aberrant temporal and spatial brain activity during rest in patients with chronic pain. *Proc Natl Acad Sci U S A* **107**, 6493-6497.

[25] Morris JC (1993) The Clinical Dementia Rating (CDR): Current version and scoring rules. *Neurology* **43**, 2412-2414.

[26] Morris JC, Mohs RC, Rogers H, Fillenbaum G, Heyman A (1988) Consortium to establish a registry for Alzheimer's disease (CERAD) clinical and neuropsychological assessment of Alzheimer's disease. *Psychopharmacol Bull* **24**, 641-652.

[27] Gauthier S, Reisberg B, Zaudig M, Petersen RC, Ritchie K, Broich K, Belleville S, Brodaty H, Bennett D, Chertkow H, Cummings JL, de Leon M, Feldman H, Ganguli M, Hampel H, Scheltens P, Tierney MC, Whitehouse P, Winblad B, International Psychogeriatric Association Expert Conference on mild cognitive i (2006) Mild cognitive impairment. *Lancet* **367**, 1262-1270.

[28] McKhann G, Drachman D, Folstein M, Katzman R, Price D, Stadlan EM (1984) Clinical diagnosis of Alzheimer's disease: Report of the NINCDS-ADRDA Work Group under the auspices of Department of Health and Human Services Task Force on Alzheimer's Disease. *Neurology* **34**, 939-944.

[29] Fischl B, van der Kouwe A, Destrieux C, Halgren E, Segonne F, Salat DH, Busa E, Seidman LJ, Goldstein J, Kennedy D, Caviness V, Makris N, Rosen B, Dale AM (2004) Automatically parcellating the human cerebral cortex. *Cereb Cortex* **14**, 11-22.

[30] Fischl B, Dale AM (2000) Measuring the thickness of the human cerebral cortex from magnetic resonance images. *Proc Natl Acad Sci U S A* **97**, 11050-11055.

[31] Sanchez-Benavides G, Gomez-Anson B, Sainz A, Vives Y, Delfino M, Pena-Casanova J (2010) Manual validation of FreeSurfer's automated hippocampal segmentation in normal aging, mild cognitive impairment, and Alzheimer Disease subjects. *Psychiatry Res* **181**, 219-225.

[32] Van Leemput K, Bakkour A, Benner T, Wiggins G, Wald LL, Augustinack J, Dickerson BC, Golland P, Fischl B (2009) Automated segmentation of hippocampal subfields from ultra-high resolution *in vivo* MRI. *Hippocampus* **19**, 549-557.

[33] Drzezga A, Becker JA, Van Dijk KR, Sreenivasan A, Talukdar T, Sullivan C, Schultz AP, Sepulcre J, Putcha D, Greve D, Johnson KA, Sperling RA (2011) Neuronal dysfunction and disconnection of cortical hubs in non-demented subjects with elevated amyloid burden. *Brain* **134**, 1635-1646.

[34] Greicius MD, Srivastava G, Reiss AL, Menon V (2004) Default-mode network activity distinguishes Alzheimer's disease from healthy aging: Evidence from functional MRI. *Proc Natl Acad Sci U S A* **101**, 4637-4642.

[35] Van Dijk KR, Sabuncu MR, Buckner RL (2012) The influence of head motion on intrinsic functional connectivity MRI. *Neuroimage* **59**, 431-438.

[36] Satterthwaite TD, Elliott MA, Gerraty RT, Ruparel K, Loughead J, Calkins ME, Eickhoff SB, Hakonarson H, Gur RC, Gur RE, Wolf DH (2013) An improved framework for confound regression and filtering for control of motion artifact in the preprocessing of resting-state functional connectivity data. *Neuroimage* **64**, 240-256.

[37] Birn RM, Diamond JB, Smith MA, Bandettini PA (2006) Separating respiratory-variation-related fluctuations from neuronal-activity-related fluctuations in fMRI. *Neuroimage* **31**, 1536-1548.

[38] Neufang S, Akhrif A, Riedl V, Forstl H, Kurz A, Zimmer C, Sorg C, Wohlschlager AM (2014) Predicting effective connectivity from resting-state networks in healthy elderly and patients with prodromal Alzheimer's disease. *Hum Brain Mapp* **35**, 954-963.

[39] Pruessner JC, Kohler S, Crane J, Pruessner M, Lord C, Byrne A, Kabani N, Collins DL, Evans AC (2002) Volumetry of temporopolar, perirhinal, entorhinal and parahippocampal cortex from high-resolution MR images: Considering the variability of the collateral sulcus. *Cereb Cortex* **12**, 1342-1353.

[40] Insausti R, Juottonen K, Soininen H, Insausti AM, Partanen K, Vainio P, Laakso MP, Pitkanen A (1998) MR volumetric analysis of the human entorhinal, perirhinal, and temporopolar cortices. *AJNR Am J Neuroradiol* **19**, 659-671.

[41] Li C, Wang J, Gui L, Zheng J, Liu C, Du H (2011) Alterations of whole-brain cortical area and thickness in mild cognitive impairment and Alzheimer's disease. *J Alzheimers Dis* **27**, 281-290.

[42] Hanseeuw BJ, Van Leemput K, Kavec M, Grandin C, Seron X, Ivanoiu A (2011) Mild cognitive impairment: Differential atrophy in the hippocampal subfields. *Am J Neuroradiol* **32**, 1658-1661.

[43] La Joie R, Perrotin A, de La Sayette V, Egret S, Doeuvre L, Belliard S, Eustache F, Desgranges B, Chetelat G (2013) Hippocampal subfield volumetry in mild cognitive impairment, Alzheimer's disease and semantic dementia. *Neuroimage Clin* **3**, 155-162.

[44] Zhang J, Wei L, Hu X, Zhang Y, Zhou D, Li C, Wang X, Feng H, Yin X, Xie B, Wang J (2013) Specific frequency band of amplitude low-frequency fluctuation predicts Parkinson's disease. *Behav Brain Res* **252**, 18-23.

[45] Luders E, Narr KL, Thompson PM, Rex DE, Jancke L, Toga AW (2006) Hemispheric asymmetries in cortical thickness. *Cereb Cortex* **16**, 1232-1238.

[46] Plessen KJ, Hugdahl K, Bansal R, Hao X, Peterson BS (2014) Sex, age, and cognitive correlates of asymmetries in thickness of the cortical mantle across the life span. *J Neurosci* **34**, 6294-6302.

[47] Zhou D, Lebel C, Evans A, Beaulieu C (2013) Cortical thickness asymmetry from childhood to older adulthood. *Neuroimage* **83**, 66-74.

[48] Kahn I, Andrews-Hanna JR, Vincent JL, Snyder AZ, Buckner RL (2008) Distinct cortical anatomy linked to subregions of the medial temporal lobe revealed by intrinsic functional connectivity. *J Neurophysiol* **100**, 129-139.

[49] Yassa MA, Muftuler LT, Stark CE (2010) Ultrahigh-resolution microstructural diffusion tensor imaging reveals perforant path degradation in aged humans *in vivo*. *Proc Natl Acad Sci U S A* **107**, 12687-12691.

[50] Bateman RJ, Xiong C, Benzinger TL, Fagan AM, Goate A, Fox NC, Marcus DS, Cairns NJ, Xie X, Blazey TM, Holtzman DM, Santacruz A, Buckles V, Oliver A, Moulder K, Aisen PS, Ghetti B, Klunk WE, McDade E, Martins RN, Masters CL, Mayeux R, Ringman JM, Rossor MN, Schofield PR, Sperling RA, Salloway S, Morris JC, Dominantly Inherited Alzheimer N (2012) Clinical and biomarker changes in dominantly inherited Alzheimer's disease. *N Engl J Med* **367**, 795-804.

[51] Myers N, Pasquini L, Gottler J, Grimmer T, Koch K, Ortner M, Neitzel J, Muhlau M, Forster S, Kurz A, Forstl H, Zimmer C, Wohlschlager AM, Riedl V, Drzezga A, Sorg C (2014) Within-patient correspondence of amyloid-beta and intrinsic network connectivity in Alzheimer's disease. *Brain* **137**, 2052-2064.

[52] Jacobs HI, Van Boxtel MP, Jolles J, Verhey FR, Uylings HB (2012) Parietal cortex matters in Alzheimer's disease: An overview of structural, functional and metabolic findings. *Neurosci Biobehav Rev* **36**, 297-309.

[53] Jack CR Jr, Wiste HJ, Knopman DS, Vemuri P, Mielke MM, Weigand SD, Senjem ML, Gunter JL, Lowe V, Gregg BE, Pankratz VS, Petersen RC (2014) Rates of beta-amyloid accumulation are independent of hippocampal neurodegeneration. *Neurology* **82**, 1605-1612.

[54] Palop JJ, Mucke L (2009) Epilepsy and cognitive impairments in Alzheimer disease. *Arch Neurol* **66**, 435-440.

[55] Petersen RC, Caracciolo B, Brayne C, Gauthier S, Jelic V, Fratiglioni L (2014) Mild cognitive impairment: A concept in evolution. *J Intern Med* **275**, 214-228.

[56] Pa J, Berry AS, Compagnone M, Boccanfuso J, Greenhouse I, Rubens MT, Johnson JK, Gazzaley A (2013) Cholinergic enhancement of functional networks in older adults with mild cognitive impairment. *Ann Neurol* **73**, 762-773.

[57] Wenger E, Martensson J, Noack H, Bodammer NC, Kuhn S, Schaefer S, Heinze HJ, Duzel E, Backman L, Lindenberger U, Lovden M (2014) Comparing manual and automatic segmentation of hippocampal volumes: Reliability and validity issues in younger and older brains. *Hum Brain Mapp* **35**, 4236-4248.

[58] Cherbuin N, Anstey KJ, Reglade-Meslin C, Sachdev PS (2009) *In vivo* hippocampal measurement and memory: A comparison of manual tracing and automated segmentation in a large community-based sample. *PLoS One* **4**, e5265.

[59] D'Esposito M, Deouell LY, Gazzaley A (2003) Alterations in the BOLD fMRI signal with ageing and disease: A challenge for neuroimaging. *Nat Rev Neurosci* **4**, 863-872.

Pasquini, Scherr et al.

Supplemental Information for

"Increased intrinsic activity of medial-temporal lobe subregions is associated with decreased cortical thickness of medial-parietal areas in patients with Alzheimer's disease dementia"

by Lorenzo Pasquini, Martin Scherr et al.

- Cortical thickness of medial-parietal regions

Supplementary Methods

Parcellation of structural MRI data based on FreeSurfer.

In each participant's structural MRI data, the medial-temporal lobes (MTL) and medial-parietal areas were parcellated in an automated mode as implemented by FreeSurfer Version 5.1.0 (http://surfer.nmr.mgh.harvard.edu). FreeSurfer provides a highly automated structural MRI image-processing pipeline resulting in regional volumetric measures based on geometrical brain reconstruction. Such reconstruction and volumetric segmentation includes removal of non-brain tissue using a hybrid watershed/surface deformation procedure [1], automated Talairach transformation, segmentation of subcortical white matter and deep grey matter volumetric structures [2, 3], intensity normalization [4], tessellation of the grey/white matter boundary, automated topology correction [5, 6], and surface deformation following intensity gradients to optimally place the grey/white and grey/cerebrospinal fluid borders at the location where the greatest shift in intensity defines the transition to the other tissue class [7-9]. Once brain models are completed, registration to a spherical atlas is performed, applying individual cortical folding patterns to match brain geometry across subjects [10]. After that, parcellation of the cerebral cortex into units based on gyral and sulcal structure is realized [11, 12]. In addition, the parcellation of the MTL includes a prior-distribution that makes predictions about neuroanatomical labels in individual subject's structural image. This prior is based on a generalization of probabilistic atlases [13, 14], and has been implemented by learning algorithms

from manual segmentations of the hippocampal formation in MRI images of a number of training subjects.

Control for head movement.

Previous studies in resting-state-functional MRI [15-17] demonstrated that even when study groups were not different regarding head movement parameters, group differences in the power spectrum of the blood-oxygenation-level-dependent (BOLD) signal may be due to movement artifacts [15]. To investigate potential associations between head motion and intrinsic activity of MTL subregions, we first analyzed the correlation between individual head motion's time course and the time course of MTL subregion's activity for each subject. MTL subregion's activity was derived from the seed-based approach using regions-of-interest based on FreeSurfer segmentation. Head motion time course was estimated by the root mean square of image translational and rotational head movement parameters at each time point [16]. Pearson's correlation was used to estimate association between MTL subregions' activity and head movement. Finally, Pearson's correlation coefficients were Fisher z-transformed and analyzed for group differences by the use of ANOVA and post hoc t-tests. Based on this analysis, we did not find any significant correlation between MTL subregions' activity and head movement for each group as well as no differences between groups except for the right cornu ammonis 2-3 ($R= 0.03$, $p<0.05$ uncorrected for multiple comparisons). This result indicates that MTL subregion's activity was not associated with head movements, suggesting that group differences for MTL subregion's PSD of LFF are unrelated to movement artifacts.

To additionally control for potential effects of head movement on group differences in intrinsic activity of MTL subregions, we performed frame censoring via exclusion of volumes potentially contaminated by movement artifacts [15-17]. There is an ongoing discussion on which frame censoring method might be optimal to remove head movement artifacts from resting-state functional MRI data [15-17]. In more detail, to estimate whether individual head motion affects our main finding of increased PSD of LFF in MTL subregions in Alzheimer's disease, frames where subject's root mean square of the translational and rotational head movement parameters exceeded a specific threshold (0.25mm + 2SD of all subjects) [15] were excluded from subsequent analyses. At least 15% of subject's data had to be retained to be included in further analyses. None of the subjects had to be excluded. Group differences in PSD of LFF based on censored data did not substantially differ from previous findings (Figure S1).

Supplementary Results

Cortical thickness of medial-parietal areas and volumes of medial-temporal subregions derived from FreeSurfer segmentation.

We used FreeSurfer to segment the MTL and medial-parietal areas. Segmented MTL subregions were used to derive the PSD of LFF of the intrinsic BOLD signal; segmented parietal regions were used to derive the cortical thickness as a measure for structural integrity. Within the scope of sanity checking, we found volumes of MTL subregions of healthy controls in line with the volumes expected by FreeSurfer segmentation (Table S1) [13] and with previous works using manual segmentation [13, 18, 19]. Except for the right and left cornu ammonis 1, volumes of MTL subregions were significantly reduced in patients compared to healthy controls, particularly

in patients with Alzheimer's disease, in line with well-known progressive atrophy of the MTL along Alzheimer's disease progression (Table S1) [20-23]. Moreover, cortical thickness of medial-parietal regions in healthy controls were in the range as expected [24] and significantly reduced in patients [25], particularly in patients with Alzheimer's disease (Table S2). This finding is in line with progressive cortical degeneration of medial-parietal regions along Alzheimer's disease stages [26].

Supplementary References

[1] Segonne F, Dale AM, Busa E, Glessner M, Salat D, Hahn HK, Fischl B (2004) A hybrid approach to the skull stripping problem in MRI. Neuroimage 22, 1060-1075.

[2] Fischl B, Salat DH, Busa E, Albert M, Dieterich M, Haselgrove C, van der Kouwe A, Killiany R, Kennedy D, Klaveness S, Montillo A, Makris N, Rosen B, Dale AM (2002) Whole brain segmentation: automated labeling of neuroanatomical structures in the human brain. Neuron 33, 341-355.

[3] Fischl B, Salat DH, van der Kouwe AJ, Makris N, Segonne F, Quinn BT, Dale AM (2004) Sequence-independent segmentation of magnetic resonance images. Neuroimage 23 Suppl 1, S69-84.

[4] Sled JG, Zijdenbos AP, Evans AC (1998) A nonparametric method for automatic correction of intensity nonuniformity in MRI data. IEEE Trans Med Imaging 17, 87-97.

[5] Fischl B, Liu A, Dale AM (2001) Automated manifold surgery: constructing geometrically accurate and topologically correct models of the human cerebral cortex. IEEE Trans Med Imaging 20, 70-80.

[6] Segonne F, Pacheco J, Fischl B (2007) Geometrically accurate topology-correction of cortical surfaces using nonseparating loops. IEEE Trans Med Imaging 26, 518-529.

[7] Dale AM, Fischl B, Sereno MI (1999) Cortical surface-based analysis. I. Segmentation and surface reconstruction. Neuroimage 9, 179-194.

[8] Dale AM, Sereno MI (1993) Improved Localizadon of Cortical Activity by Combining EEG and MEG with MRI Cortical Surface Reconstruction: A Linear Approach. J Cogn Neurosci 5, 162-176.

[9] Fischl B, Dale AM (2000) Measuring the thickness of the human cerebral cortex from magnetic resonance images. Proc Natl Acad Sci U S A 97, 11050-11055.

[10] Fischl B, Sereno MI, Tootell RB, Dale AM (1999) High-resolution intersubject averaging and a coordinate system for the cortical surface. Hum Brain Mapp 8, 272-284.

[11] Desikan RS, Segonne F, Fischl B, Quinn BT, Dickerson BC, Blacker D, Buckner RL, Dale AM, Maguire RP, Hyman BT, Albert MS, Killiany RJ (2006) An automated labeling system for subdividing the human cerebral cortex on MRI scans into gyral based regions of interest. Neuroimage 31, 968-980.

[12] Fischl B, van der Kouwe A, Destrieux C, Halgren E, Segonne F, Salat DH, Busa E, Seidman LJ, Goldstein J, Kennedy D, Caviness V, Makris N, Rosen B, Dale AM (2004) Automatically parcellating the human cerebral cortex. Cereb Cortex 14, 11-22.

[13] Van Leemput K, Bakkour A, Benner T, Wiggins G, Wald LL, Augustinack J, Dickerson BC, Golland P, Fischl B (2009) Automated Segmentation of Hippocampal Subfields From Ultra-High Resolution In Vivo MRI. Hippocampus 19, 549-557.

[14] Ashburner J, Neelin P, Collins DL, Evans A, Friston K (1997) Incorporating prior knowledge into image registration. Neuroimage 6, 344-352.

[15] Satterthwaite TD, Elliott MA, Gerraty RT, Ruparel K, Loughead J, Calkins ME, Eickhoff SB, Hakonarson H, Gur RC, Gur RE, Wolf DH (2013) An improved framework for

confound regression and filtering for control of motion artifact in the preprocessing of resting-state functional connectivity data. Neuroimage 64, 240-256.

[16] Van Dijk KR, Sabuncu MR, Buckner RL (2012) The influence of head motion on intrinsic functional connectivity MRI. Neuroimage 59, 431-438.

[17] Power JD, Barnes KA, Snyder AZ, Schlaggar BL, Petersen SE (2012) Spurious but systematic correlations in functional connectivity MRI networks arise from subject motion. Neuroimage 59, 2142-2154.

[18] Insausti R, Juottonen K, Soininen H, Insausti AM, Partanen K, Vainio P, Laakso MP, Pitkanen A (1998) MR volumetric analysis of the human entorhinal, perirhinal, and temporopolar cortices. AJNR Am J Neuroradiol 19, 659-671.

[19] Pruessner JC, Kohler S, Crane J, Pruessner M, Lord C, Byrne A, Kabani N, Collins DL, Evans AC (2002) Volumetry of temporopolar, perirhinal, entorhinal and parahippocampal cortex from high-resolution MR images: considering the variability of the collateral sulcus. Cereb Cortex 12, 1342-1353.

[20] Frisoni GB, Ganzola R, Canu E, Rub U, Pizzini FB, Alessandrini F, Zoccatelli G, Beltramello A, Caltagirone C, Thompson PM (2008) Mapping local hippocampal changes in Alzheimer's disease and normal ageing with MRI at 3 Tesla. Brain 131, 3266-3276.

[21] Mueller SG, Schuff N, Yaffe K, Madison C, Miller B, Weiner MW (2010) Hippocampal atrophy patterns in mild cognitive impairment and Alzheimer's disease. Hum Brain Mapp 31, 1339-1347.

[22] Lim HK, Hong SC, Jung WS, Ahn KJ, Won WY, Hahn C, Kim IS, Lee CU (2013) Automated segmentation of hippocampal subfields in drug-naive patients with Alzheimer disease. AJNR Am J Neuroradiol 34, 747-751.

[23] Hanseeuw BJ, Van Leemput K, Kavec M, Grandin C, Seron X, Ivanoiu A (2011) Mild Cognitive Impairment: Differential Atrophy in the Hippocampal Subfields. American Journal of Neuroradiology 32, 1658-1661.

[24] Dickerson BC, Bakkour A, Salat DH, Feczko E, Pacheco J, Greve DN, Grodstein F, Wright CI, Blacker D, Rosas HD, Sperling RA, Atri A, Growdon JH, Hyman BT, Morris JC, Fischl B, Buckner RL (2009) The cortical signature of Alzheimer's disease: regionally specific cortical thinning relates to symptom severity in very mild to mild AD dementia and is detectable in asymptomatic amyloid-positive individuals. Cereb Cortex 19, 497-510.

[25] Li C, Wang J, Gui L, Zheng J, Liu C, Du H (2011) Alterations of whole-brain cortical area and thickness in mild cognitive impairment and Alzheimer's disease. J Alzheimers Dis 27, 281-290.

[26] Putcha D, Brickhouse M, O'Keefe K, Sullivan C, Rentz D, Marshall G, Dickerson B, Sperling R (2011) Hippocampal hyperactivation associated with cortical thinning in Alzheimer's disease signature regions in non-demented elderly adults. J Neurosci 31, 17680-17688.

Supplementary Figures

Figure S1.

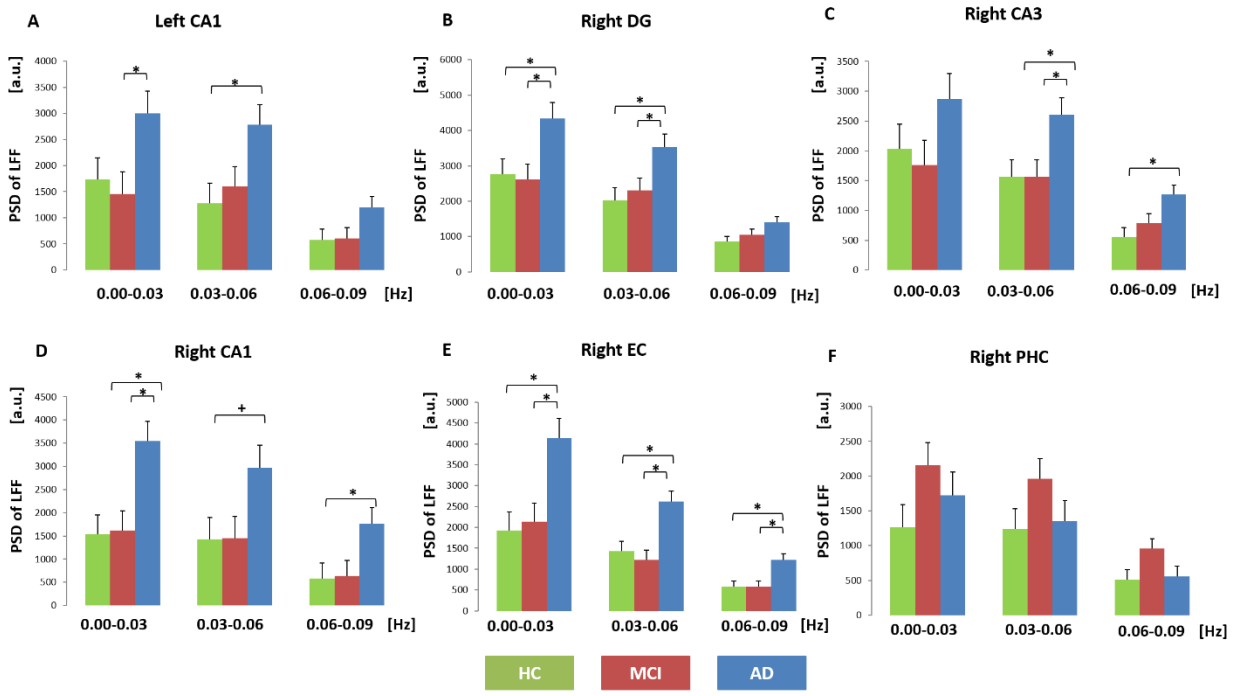

Figure S1. Power spectrum density (PSD) of low frequency fluctuations (LFF) in the BOLD signal of MTL subregions in healthy controls, patients with mild cognitive impairment and Alzheimer's disease dementia after frame censoring. Mean and standard deviation of PSD of LFF in the BOLD signal for six MTL subregions (A-F) after application of frame censoring of fMRI data shown for patients with AD-dementia (blue), patients with MCI (red) and HC (green). Asterisk over balks indicate significant group differences (post-hoc t-test, $p<0.05$ family wise error corrected for multiple comparisons). Plus symbol '+' above the balk indicates statistical trend (post-hoc t-test, $p<0.10$ family wise error corrected for multiple comparisons). AD, Alzheimer's disease; a.u., arbitrary units; CA, cornu ammonis; DG, dentate gyrus; EC, entorhinal cortex; HC, aged matched healthy controls; MCI, mild cognitive impairment; Presub,

presubiculum; PSD of LFF, power spectrum density of blood-oxygenation-dependent-signal's low frequency fluctuations; Sub, subiculum.

Figure S2.

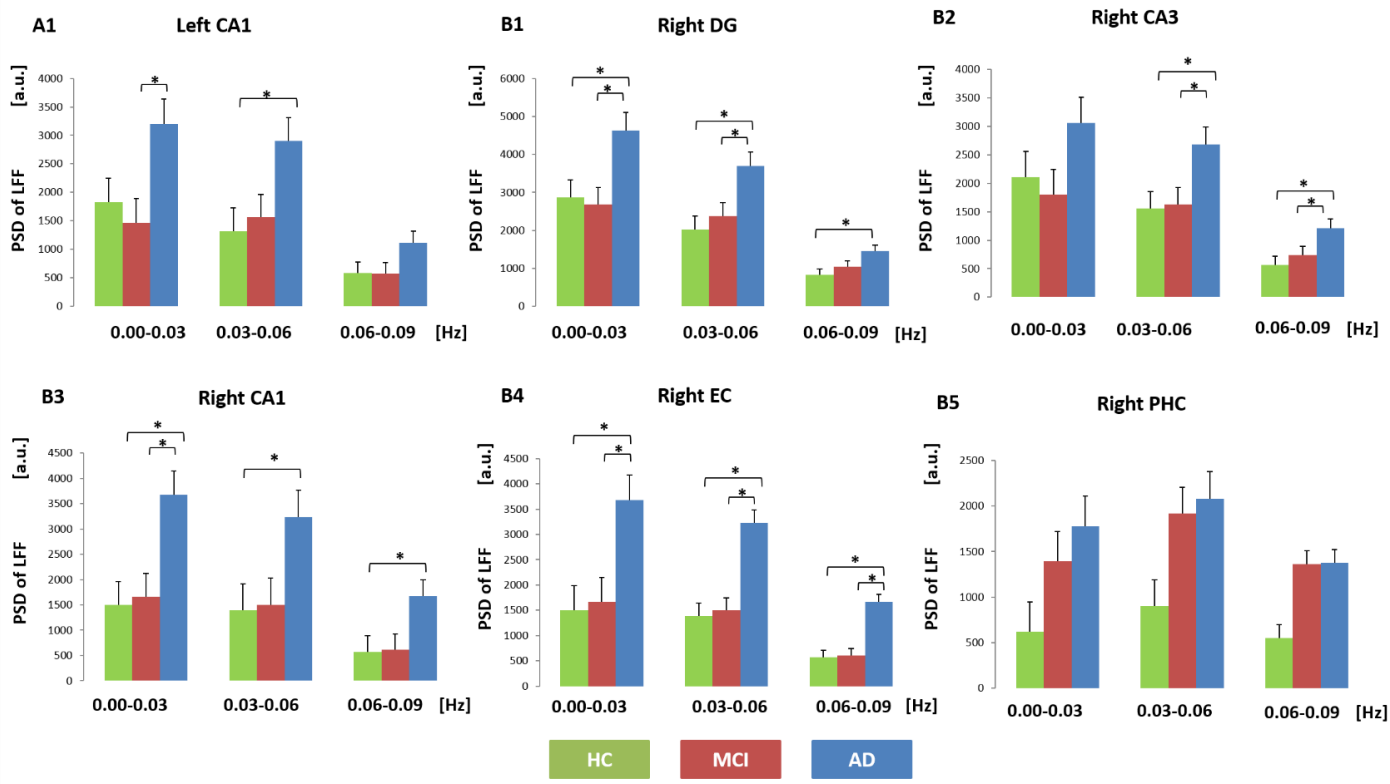

Figure S2. Power spectrum density (PSD) of low frequency fluctuations (LFF) in the BOLD signal of medial-temporal lobe subregions in healthy controls, patients with mild cognitive impairment and Alzheimer's disease dementia without control for medial-temporal subregional volumes. Mean and standard deviation of PSD of LFF in the BOLD signal for six medial-temporal lobe subregions (A1, B1-B5) shown for patients with AD-dementia (blue), patients with MCI (red) and HC (green). Results are not controlled for MTL subregional volume loss (see Fig. 1). Asterisks indicate significant group differences (ANOVA, post-hoc t-test, $p<0.05$ FWE corrected). AD, Alzheimer's disease; a.u., arbitrary units; CA, cornu ammonis; DG, dentate gyrus; EC, entorhinal cortex; HC, healthy aged matched controls; MCI, mild cognitive impairment; Presub, presubiculum; PSD of LFF, power spectrum density of blood-oxygenation-level-dependent signal low frequency fluctuations; Sub, subiculum.

Supplementary Tables

Table S1. Volumes of medial-temporal lobe regions-of-interests.

Groups (n)	AD (21)	MCI (22)	HC (22)	F	p-value
Left DG	475.6 (17.9)	520.8 (17.4)	564.1 (17.4)	4.95	0.010
Left CA3	873.2 (32.7)	954.3 (32.0)	1010.6 (32.0)	3.54	0.034
Left CA1	308.7 (9.7)	317.2 (9.5)	332.9 (9.5)	0.88	0.418
Left Sub	491.5 (20.7)	530.5 (20.2)	588.2 (20.2)	5.64	0.006
Left Presub	327.1 (14.3)	380.0 (14.0)	412.5 (14.0)	8.73	<0.001
Left EC	1327.3 (74.1)	1578.6 (72.4)	1601.7 (72.4)	3.14	0.050
Left PHC	1537.8 (63.6)	1915.3 (62.2)	1985.8 (62.2)	7.65	0.001
Right DG	475.7 (17.9)	520.8 (17.4)	564.1 (17.4)	6.28	0.003
Right CA3	873.2 (32.7)	954.3 (32.0)	1010.6 (32.0)	4.55	0.014
Right CA1	308.7 (9.7)	317.2 (9.5)	332.9 (9.5)	1.63	0.203
Right Sub	490.4 (18.6)	539.8 (18.2)	587.4 (18.2)	6.94	0.002
Right Presub	327.1 (14.3)	380.0 (14.0)	412.5 (15.0)	9.26	<0.001
Right EC	1327.3 (74.1)	1578.6 (72.4)	1601.7 (72.4)	4.28	0.018
Right PHC	1537.8 (63.5)	1925.3 (62.2)	1985.8 (62.2)	`14.55	<0.001

Group comparisons are based on ANOVA ($p<0.05$). AD, Alzheimer's disease; CA, cornu ammonis; DG, dentate gyrus; EC, entorhinal cortex; HC, healthy controls. MCI, mild cognitive impairment; PHC, parahippocampal cortex; Presub, presubiculum; Sub, subiculum. Average volumes in mm^3 for respective MTL subregions in healthy controls derived from appropriate previous study for comparison [Supplementary References]: DG=526 [13]; CA3=935 [13]; CA1=340 [13]; Sub = 537 [13]; Presub = 431 [13]; EC = 1558 [18]; PHC = 2675 [19].

Table S2. Cortical thickness of medial-parietal regions

Cortical thickness of medial-parietal regions: Mean (SD) in mm					
Groups (n)	AD (21)	MCI (22)	HC (22)	F	p-value
Left dPCC	2.67 (0.24)	2.73 (0.25)	2.88 (0.25)	5.15	0.009
Left vPCC	1.90 (0.29)	2.02 (0.34)	2.14 (0.27)	3.29	0.044
Left Prc	2.25 (0.19)	2.30 (0.21)	2.45 (0.12)	8.00	0.001
Right dPCC	2.55 (0.21)	2.74 (0.19)	2.89 (0.14)	18.74	<0.001
Right vPCC	2.41 (0.31)	2.49 (0.31)	2.70 (0.19)	6.68	0.002
Right Prc	2.23 (0.21)	2.21 (0.16)	2.36 (0.13)	4.49	0.015

Group comparisons are based on ANOVA ($p<0.05$). AD, Alzheimer's disease; dPCC, dorsal posterior cingulate cortex; HC, healthy controls; MCI, mild cognitive impairment; Prc, precuneus; vPCC, ventral posterior cingulate cortex. Previous average estimates of cortical thickness for parietal areas vary between 2.02-2.38 mm in healthy controls depending on the concerned area; see Supplementary Reference [24].